

Molekulare Erkennungs- und Selbstorganisations-  
phänomene von funktionalisierten Resorc[4]arenen  
und Octahydroxypyridin[4]arenen

Dissertation zur Erlangung des  
naturwissenschaftlichen Doktorgrades  
der Fakultät für Chemie  
der Universität Bielefeld

vorgelegt von  
Dipl. Chem. Björn-Uwe Decker  
Bielefeld 2004

*Für meine Familie*

*„Die angenehmste aller Verbindungen ist die zwischen Wirt und Gast“*  
*Aischylos (525-456 v. Chr.): Choephoren*

Die vorliegende Arbeit wurde auf Anregung und unter Anleitung von

Herrn Universitätsprofessor Dr. J. Mattay

an der Fakultät für Chemie an der Universität Bielefeld in der Zeit von Januar 2001 bis November 2004 durchgeführt.

Mein besonderer Dank gilt Herrn Professor Dr. J. Mattay für die Aufnahme in den Arbeitskreis, die interessante Themenstellung, die fachliche Anregung und die Schaffung hervorragender Rahmenbedingungen zur Durchführung dieser Arbeit.

Herrn Prof. Dr. Anselmetti danke ich für die Übernahme des Koreferates.

Für die vielfältige Unterstützung, die mir von unterschiedlichster Seite zu Teil geworden ist, möchte ich mich an dieser Stelle bedanken.

Mein besonderer Dank gilt meinen Eltern und meiner Familie ohne deren langjährige Unterstützung diese Dissertationsschrift vermutlich nicht zustande gekommen wäre.

Dem gesamten Arbeitskreis OC I danke ich für die stets entspannte und humorvolle Atmosphäre. Ganz besonders hervorheben möchte ich Herrn Dr. Ceno Agena, der mich mit seinem Wissen und großer Geduld in die Chemie der Calixarene eingeführt hat. Frau Dr. Juliane Grota danke ich für die, auch in schwierigen Zeiten, gute Stimmung im Laboralltag. Herrn Dr. Christian Schiel und der gesamten Kieler Fraktion danke ich für die Unterstützung in allen chemischen Belangen und die überaus angenehme und unterhaltsame Zeit innerhalb und außerhalb des Labors. Herrn Dipl.-Chem. Michael Klaes und Herrn Dipl.-Chem. Christian Schäfer, sowie allen anderen jüngeren und aktuellen Arbeitsgruppenmitglieder, danke ich für zahlreiche Diskussionen und Anregungen rund um die Chemie, aber auch privater Natur.

Herrn Thomas Geisler und Herrn Dieter Barth danke ich für deren Unterstützung in Belangen des Laboralltags und der Synthese von Vorstufen.

Herrn Dr. Matthias Letzel bin ich für informative Gespräche und die Lösung zahlreicher Probleme rund um die Massenspektrometrie dankbar. Ihm und seinem Team danke darüber hinaus für die Durchführung aller massenspektrometrischen Experimente.

Herrn Peter Mester bin ich für zahllose NMR-Messungen dankbar.

Herrn Dr. Ulrich Neuert danke ich für die Hilfestellung bei der Beseitigung alltäglicher Soft- und Hardwareprobleme.

Herrn Mark Schmidtmann und Frau Beate Neumann danke ich für die Anfertigung von Röntgenstrukturanalysen.

Dem gesamten Lagerteam danke ich für die Bereitstellung von Rohstoffen auch zu den unmöglichsten Zeiten.

Dankbar bin ich auch für die Forschungstätigkeiten, die mir im Rahmen des SFB 613 ermöglicht wurden. Ganz besonders möchte ich hier die Zusammenarbeit mit Herrn Dipl.-Chem. Rainer Eckel, Herrn Dr. Alexander Rozhenko und Herrn Dipl.-Phys. Martin Michelswirth hervorheben.

Bedanken möchte ich mich für die produktive aber auch stets unterhaltsame Zusammenarbeit mit Frau Daniela Maag, Herrn Oliver Tasic und Herrn Dipl.-Chem. Björn Schnatwinkel im Rahmen ihrer Blockpraktika.

Herrn Dipl.-Chem. Timo Hagemeister danke ich für das Ertragen meiner Person in zahlreichen Praktika während des Studiums, für tolle Monate in Dublin, das langjährige Zusammenleben in der „Männer-WG“ und stundenlange Diskussion fernab des Unialltags.

Meinem gesamten Freundes- und Bekanntenkreis danke ich dafür, dass sie mir immer wieder gezeigt haben, dass es auch ein Leben nach der Chemie gibt.

# Inhaltsverzeichnis

1	Vorwort.....	1
2	Einleitung .....	2
2.1	Einführung in die Chemie der Resorcarenne.....	2
2.1.1	Nomenklatur .....	3
2.1.2	Die räumliche Gestalt .....	3
2.1.3	Synthese und Funktionalisierung.....	5
2.1.4	Selbstorganisierte Resorcaren-Systeme .....	7
2.2	Selbstorganisierte Systeme basierend auf Pyridinarenen .....	9
2.2.1	Selbstorganisierte Dimerisierung.....	10
2.2.2	Komplexbildung durch Octahydroxypyridin[4]arene .....	12
2.2.3	Untersuchung des gelartigen Pyridinaren/Naphthyridin Systems .....	15
2.3	Untersuchungen an Resorcaren-Monoschichten.....	20
2.3.1	Studium photoinduzierter Struktur- und Bindungsänderungen mit fs-zeitaufgelöstem ESCA.....	20
2.3.2	Einzelmolekülkraftspektroskopie mit Resorc[4]arenen .....	23
3	Zusammenfassung und Ausblick .....	28
4	Summary.....	32
5	Anhang Publikationen .....	36

# 1 Vorwort

Die Komplex- und Supramolekulare Chemie gehören heute zu den wohl interessantesten Forschungsbereichen der präparativen Organischen Chemie. Die Natur dient als Vorbild für eine große Anzahl komplex funktionalisierter Einheiten, die hierarchisch über multiple, nicht kovalente Wechselwirkungen zu großen Aggregaten organisiert sind.<sup>1,2</sup> Bereits um den Wechsel zum 20. Jahrhundert wurden mit den Arbeiten von EMIL FISCHER<sup>3</sup> zum Schlüssel-Schloss-Prinzip, PAUL EHRLICH<sup>4</sup> zu molekularen Rezeptoren und ALFRED WERNER<sup>5</sup> zur Koordinationschemie erste Grundsteine für diese modernen Disziplinen gelegt. Doch erst inspiriert durch CRAM, LEHN und PEDERSEN, die 1987 den Nobelpreis „Für die Entwicklung und Verwendung von Molekülen mit strukturspezifischer Wechselwirkung von hoher Selektivität“ erhielten, entwickelte sich Jahrzehnte später ein breites Forschungsgebiet, das sich mit Selbstorganisation, Molekularer Erkennung, Wirt-Gast-Verbindungen und nanostrukturierten Materialien beschäftigt. Einen wichtigen Baustein stellen in diesem Zusammenhang die Calixarene dar. Ausschlaggebend hierfür sind ihre leichte Zugänglichkeit, ihre kelchartige dreidimensionale Struktur und die Möglichkeit zur vielfältigen, kovalenten Modifikation. Darüber hinaus bilden sie durch ihre cyclische Struktur einen Hohlraum, der bereits den reversiblen Einschluss von Gastmolekülen suggeriert. Calixarene sind deshalb ideale Ausgangsverbindungen für die Synthese unterschiedlichster Wirtverbindungen und Bausteine für die Konstruktion größerer, molekularer Systeme mit definierter Struktur und Funktion. Die potentiellen Anwendungen reichen vom Einsatz als hochspezifische Liganden für die Analytik, die Sensortechnik und die medizinische Diagnostik, über die Konstruktion künstlicher Enzyme, bis hin zur Herstellung neuer Materialien für die nicht lineare Optik oder für ultradünne Schichten.

---

<sup>1</sup> J.-M. Lehn, *Supramolecular Chemistry*, VCH, Weinheim, 1995.

<sup>2</sup> F. Vögtle, *Supramolekulare Chemie*, Teubner, Stuttgart, 1989.

<sup>3</sup> E. Fischer, *Ber. Dt. Chem. Ges.* **1894**, 27, 2985-2993.

<sup>4</sup> P. Ehrlich, *Klinisches Jahrbuch* **1897**, 6, 299-326.

<sup>5</sup> A. Werner, *Ber. Dt. Chem. Ges.* **1907**, 40, 15-69.

## 2 Einleitung

Der Name Calixarene wurde 1978 von GUTSCHE<sup>6</sup> für cyclische Oligomere eingeführt, die durch Kondensation von Formaldehyd mit *p*-Alkylphenolen unter alkalischen Bedingungen zugänglich sind. Die kelchartige Gestalt der stabilsten Konformation des Tetramers war ausschlaggebend für die Namensgebung [*calix* (lat.) = Kelch] der Calixarene.<sup>7</sup>

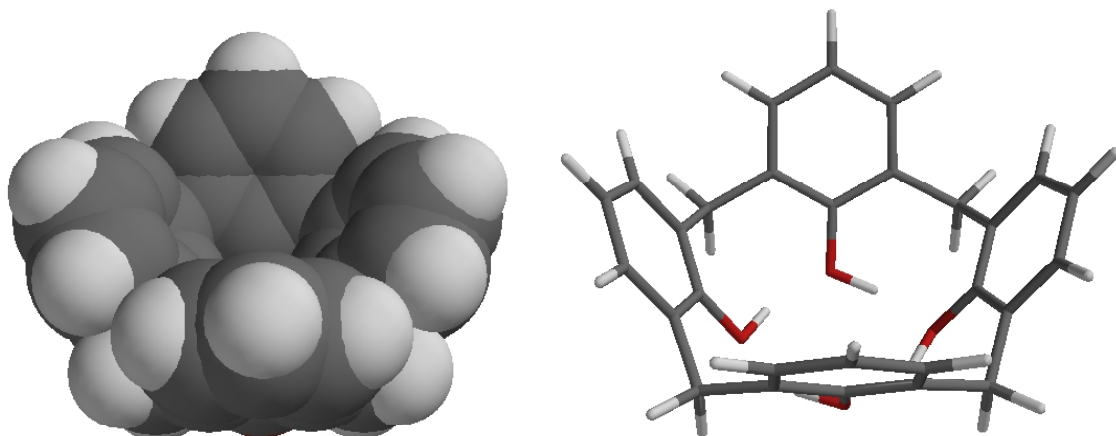


Abbildung 1: Kalotten- und Stab-Modell eines Calix[4]arens.

### 2.1 Einführung in die Chemie der Resorcarene

Eine wichtige Unterart der Calixarene stellen die Resorcarene dar. Sie sind wie die Phenolderivate leicht in guten Ausbeuten zugänglich. Die Synthese kann durch direkte säurekatalysierte Kondensation von Resorcin mit einer großen Anzahl von Aldehyden durchgeführt werden. BAYER<sup>8</sup> berichtete bereits 1872 von einem hochschmelzenden, kristallinen Kondensationsprodukt, das er durch die schwefelsäurekatalysierte Reaktion von Resorcin mit Benzaldehyd erhielt. Endgültig konnte die cyclische, tetramere Struktur aber erst 1968 von ERDTMAN und HÖGBERG<sup>9</sup> mittels Röntgenstrukturanalyse belegt werden. In diese Zeit fallen auch die Arbeiten von PEDERSEN<sup>10</sup> zur Synthese der Kronenether und ihrem Komplexierungsverhalten, wodurch auch den „cyclischen phenolischen Mehrkernverbindungen“ eine immer wichtigere Bedeutung zukam.

<sup>6</sup> C.D. Gutsche, R. Muthukrishnan, *J. Org. Chem.* **1978**, 43, 4905-4906.

<sup>7</sup> V. Böhmer, *Angew. Chem.* **1995**, 107, 785-818; *Angew. Chem., Int. Ed. Engl.* **1995**, 34, 713-745.

<sup>8</sup> A. Bayer, *Ber. Dtsch. Chem. Ges.* **1872**, 5, 1094-1100.

<sup>9</sup> H. Erdtman, S. Höglberg, S. Abrahamson, B. Nilsson, *Tetrahedron Lett.* **1968**, 14, 1679-1682.

<sup>10</sup> C.J. Pedersen, *J. Am. Chem. Soc.* **1967**, 89, 7017-7036.

## 2.1.1 Nomenklatur

Resorcarene gehören formal zur Substanzklasse der  $1_n$ -Metacyclophane, die das Grundgerüst der Calixarene bilden. GUTSCHE<sup>11</sup> hat eine Namensgebung vorgeschlagen, die sich bis heute durchgesetzt hat, da sich die systematische IUPAC-Nomenklatur in der Praxis als entschieden zu umständlich erweist.

Als Calixarene werden die Phenol enthaltenden Cyclen bezeichnet. Die Benennung der nicht Phenol enthaltenden Calixarene wird systematisch modifiziert, indem sie nach den auftretenden Aromaten benannt werden. So werden beispielsweise die Resorcin enthaltenden tetrameren Makrocyclen als Calixresorcin[4]arene, Calixresorc[4]arene oder einfach als Resorc[4]arene bezeichnet.

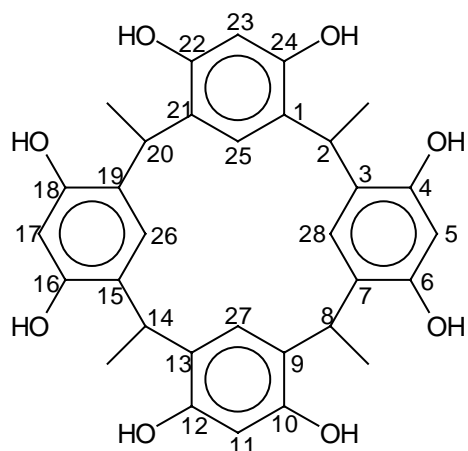


**Abbildung 2:** Nummerierung des 2,8,14,20-Tetramethylresorc[4]arens nach GUTSCHE.

Die jeweilige Ringgröße, bezogen auf die miteinander verknüpften, aromatischen Einheiten, wird dabei in eckigen Klammern beschrieben. Entsprechend werden beispielsweise die aus 2,6-Dihydroxypyridin oder Pyrogallol erhaltenen, cyclischen Produkte als 4,6,10,12,16,18,22,24-Octahydroxypyridin[4]arene bzw. Pyrogallo-[4]arene bezeichnet.

## 2.1.2 Die räumliche Gestalt

Aus der dreidimensionalen Gestalt der Resorc[4]arene ergibt sich theoretisch eine große Anzahl möglicher isomerer Strukturen. Diese kann generell durch die

<sup>11</sup> C.D. Gutsche, *Calixarenes*, The Royal Society of Chemistry, Cambridge, England, 1989.

Kombination zweier stereochemischer Elemente, der Konfiguration und der Konformation, definiert werden.<sup>12</sup>

Die relative Konfiguration der Substituenten an der Methinbrücke, die die aromatischen Einheiten miteinander verknüpft, wird durch die Abkürzungen *rccc*, *rcct*, *rctt* und *rtct* beschrieben.

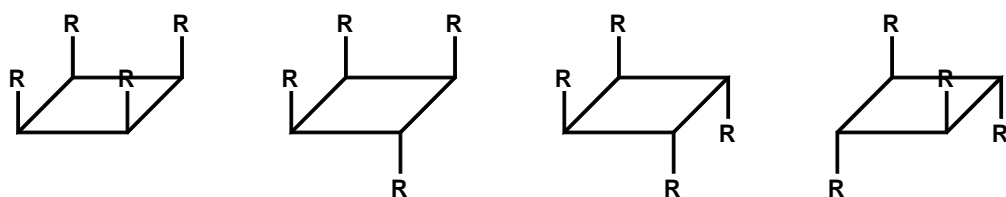


**Abbildung 3:** Relative Konfiguration der Reste R an den Methinbrücken: *rccc*, *rcct*, *rctt* und *rtct*.

Sie beschreiben die relative Anordnung dreier Reste R bezogen auf einen beliebigen vierten in der Reihenfolge der Bindung an den Resorcaryencyclus. Die Reste können entweder *axial* oder *equatorial* orientiert sein. Daraus folgt, dass die weiteren Reste bezogen auf die Referenz *r* entweder auf der gleichen Seite (*cis*, *c*) oder auf der anderen Seite (*trans*, *t*) liegen können. Die größtmögliche Zahl an *c*-Nennungen wird dabei am Anfang des Kürzels genannt.

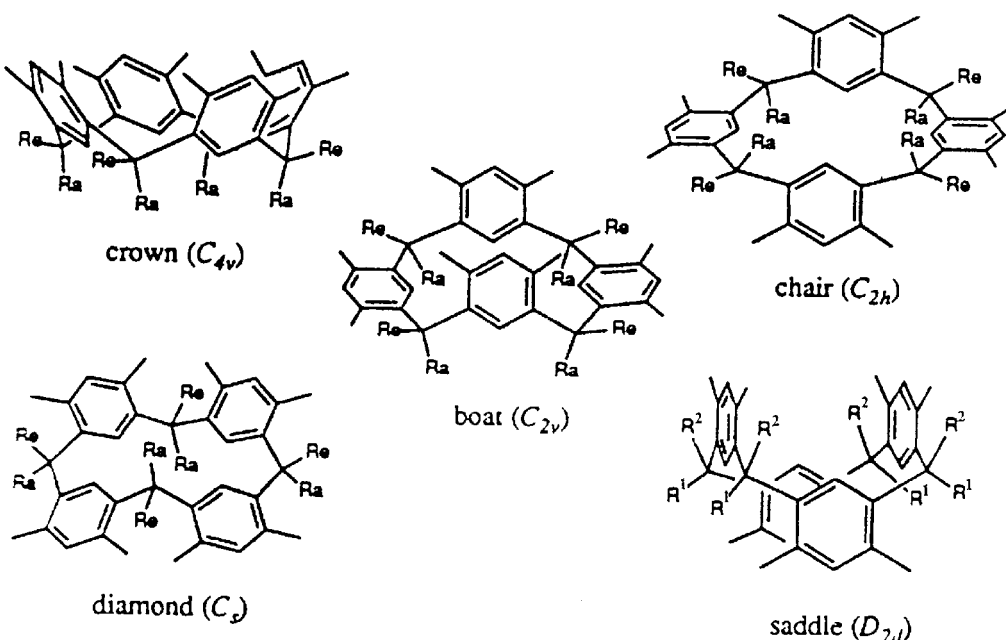


**Abbildung 4:** Konformationen der Resorc[4]arene (a = axial, e = equatorial).

<sup>12</sup> P. Timmerman, W. Verboom, D.N. Reinhoudt, *Tetrahedron* **1996**, 52, 2663-2704.

Aus der Konfiguration ergeben sich theoretisch fünf verschiedene, extreme Anordnungen für den macrocyclischen Ring: Die *crown*-, *boat*-, *chair*-, *diamond*- und *saddle*-Konformation.

Um eine schnelle Orientierung am Resorcarenengerüst zu ermöglichen, werden zwei weitere Begriffe eingeführt. Der *Obere Rand* beschreibt den Bereich der Hydroxygruppen und der *Untere Rand* den Bereich der Bindungsebene, wobei auch die vom Aldehyd eingeführten Reste einbezogen werden.

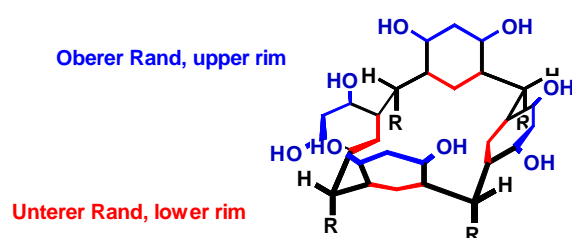


**Abbildung 5:** Oberer und Unterer Rand der Resorc[4]arene.

### 2.1.3 Synthese und Funktionalisierung

Das Interesse, das die Calixarene in den letzten Jahren zunehmend erlangten, beruht zum großen Teil auf ihrer leichten Zugänglichkeit. So können Resorcarene durch einfache Eintopfsynthesen in mittleren bis hohen Ausbeuten synthetisiert werden, ohne dass Verdünnungsbedingungen erforderlich sind. Unter sauren Bedingungen cyclisieren Resorcin und eine Reihe seiner 2-substituierten Derivate mit einer Vielzahl an aromatischen und aliphatischen Aldehyden.

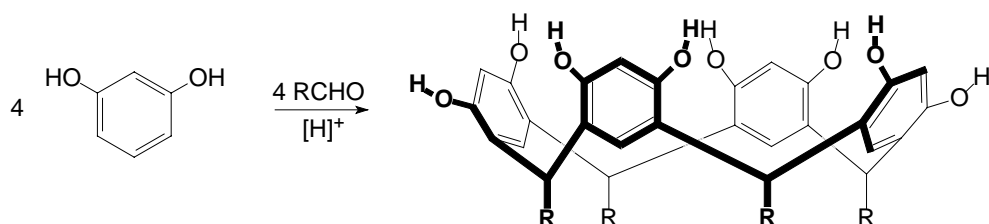


**Abbildung 6:** Synthese der Resorc[4]arene.

Durch leichte Variation der Reaktionsbedingungen für die verschiedenen Aldehyde werden die meisten Cyclisierungsprodukte in Ausbeuten von 40-95% erhalten. Der

Mechanismus der Cyclisierung ist ausführlich von WEINELT und SCHNEIDER<sup>13</sup> diskutiert worden. Im Falle aliphatischer Aldehyde entstehen die entsprechenden *rccc*-Resorc[4]arene als die thermodynamisch stabilsten Produkte. Werden aromatische Aldehyde eingesetzt, entstehen häufig Mischungen aus *rccc*- und *rctt*-Isomeren.

Resorcarene können am *Oberen* und *Unteren Rand* funktionalisiert werden. Am *Oberen Rand* können hier die Sauerstoff- bzw. Kohlenstoffatome selektiv involviert werden. Die Anwesenheit zweier elektronenschiebender Hydroxygruppen am aromatischen Ring der Resorc[4]arene führt zu einer starken Aktivierung für eine elektrophile aromatische Substitution. Dies ist allerdings nur an der doppelten *ortho*-Position zu den beiden Hydroxygruppen möglich. So führt beispielsweise die Reaktion mit *N*-Bromsuccinimid (NBS) ausschließlich zu dem am *Oberen Rand* vierfach bromierten Derivat.<sup>14</sup> Andere Positionen des Resorc[4]arengerüsts werden auf diese Art nicht angegriffen. Eine Substitution an der doppelten *meta*-Position ist nicht bekannt.

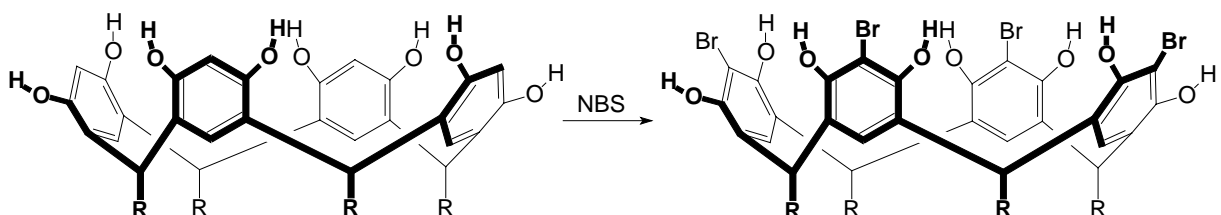


**Abbildung 7:** Vierfachbromierung eines Resorc[4]arens.

Das so erhaltene Tetrabromid dient als Plattform für eine große Reihe an weiteren Derivatisierungsmöglichkeiten.

Eine zweite Variante zur Funktionalisierung am *Oberen Rand* bieten die Hydroxygruppen. Eine vollständige Veresterung oder Veretherung ist problemlos in guten Ausbeuten möglich. Eine wichtige Derivatisierung stellt hier die Reaktion mit Bromchlormethan zu den entsprechenden Cavitanden dar.

<sup>13</sup> F. Weinelt, H.-J. Schneider, *J. Org. Chem.* **1991**, 56, 5527-5535.

<sup>14</sup> J. Moran, S. Karbch, D.J. Cram, *J. Am. Chem. Soc.* **1982**, 104, 5826-5828.

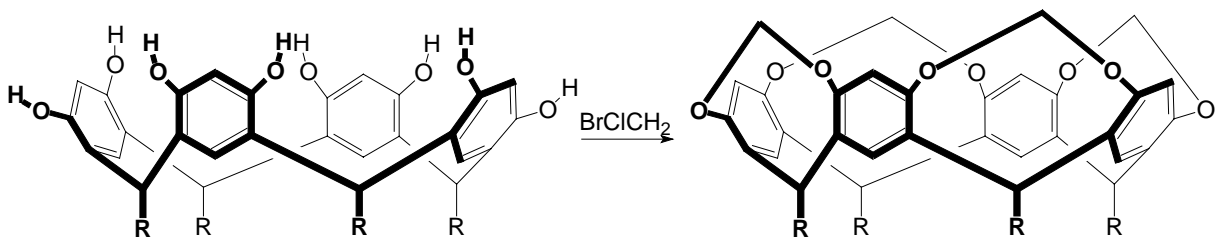


**Abbildung 8:** Darstellung von Cavitanden.

Der Begriff Cavitand (*cavity* (engl.) = Hohlraum) wurde 1982 von CRAM eingeführt.<sup>14</sup> Durch die Verbrückung der benachbarten Hydroxygruppen wird das Resorc[4]aren in der *crown*-Konformation fixiert und bildet so einen starren Hohlraum, in den kleine Moleküle oder Ionen eingelagert werden können. Ein weiterer Vorteil dieser Derivatisierung liegt darin, dass die phenolischen Hydroxygruppe chemisch blockiert werden.

Die Möglichkeit zur Funktionalisierung am *Unteren Rand* des Resorc[4]arenggerüsts wird durch den Aldehyd eingeführten Rest vorgegeben.

#### 2.1.4 Selbstorganisierte Resorcaren-Systeme

Vor rund 20 Jahren publizierte CRAM<sup>15</sup> die erste Synthese eines sogenannten Carceranden. Diese molekularen Kapseln werden durch kovalente Kopf-an-Kopf Verknüpfung zweier Cavitanden gebildet und können als molekulare Container Gastmoleküle in ihren sphärischen Hohlraum permanent einschließen. Auf diesem Weg konnten einige hochreaktive Spezies wie beispielsweise Cyclobutadien<sup>16</sup> oder 1,2-Didehydrobenzol<sup>17</sup> bei Raumtemperatur erzeugt und untersucht werden. Einen neuen Ansatz zum reversiblen Aufbau solch komplexer Systeme bietet hier die Supramolekulare Chemie. Solche Systeme haben den Vorteil, dass „falsche“ Bindungen korrigiert werden können und auf diesem Weg automatisch der thermodynamisch stabilste Zustand erreicht wird. Das erste Beispiel für eine über Wasserstoffbrücken stabilisierte Kapsel ist REBEKS<sup>18</sup> sogenannter „Tennisball“. Er entsteht durch Dimerisierung zweier selbstkomplementärer Bisglucourylderivate.

<sup>15</sup> D.J. Cram, *Science* **1983**, 219, 1177-1183.

<sup>16</sup> D.J. Cram, M.E. Tanner, R. Thomas, *Angew. Chem.* **1991**, 103, 1048-1051; *Angew. Chem., Int. Ed. Engl.* **1991**, 30, 1024-1027.

<sup>17</sup> R. Warmuth, *Angew. Chem.* **1997**, 109, 1406-1409; *Angew. Chem., Int. Ed. Engl.* **1997**, 36, 1347-1350.

<sup>18</sup> R. Wyler, J. de Mendoza, J. Rebek, *Angew. Chem.* **1993**, 105, 1820-1821; *Angew. Chem., Int. Ed. Engl.* **1993**, 32, 1699-1701.

Aber auch Calix- und Resorcaredenderivate eignen sich zum gezielten Design solcher selbstorganisierter Systeme. Calixarene, basierend auf Glycoluryl<sup>19</sup> und Harnstoffbausteinen<sup>20</sup> oder imidverbrückte<sup>21</sup> und C<sub>2v</sub>-symmetrisch acetylierte Resorc[4]arene,<sup>22</sup> zeigen die Bildung homodimerer Kapseln. Ein in Bezug auf Selbstorganisations- und Komplexierungseigenschaften gut untersuchtes System stellen die auf Tetrapyridin- und Tetracarbonsäurecavitanen basierenden Heterodimere dar.<sup>23</sup>

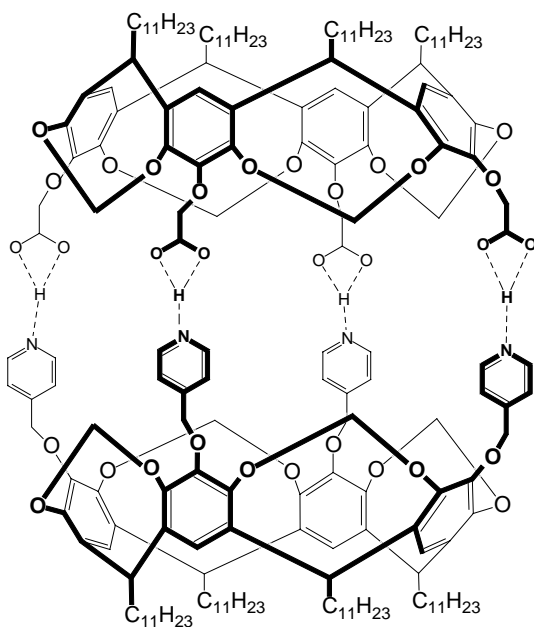


**Abbildung 9:** Heterodimerer molekularer Container, gebildet aus Tetrapyridin- und Tetracarbonsäurecavitan.

Eine weitere, in Hinblick auf Struktur und Thermodynamik gut charakterisierte, dimere Kapsel wurde erstmals von SHERMAN *et al.* beschrieben.<sup>24</sup> Durch die Zugabe von vier Äquivalenten 1,8-Diazabicyclo[5.4.0]undec-7-en (DBU) dimerisieren zwei Tetraphenolcavitanen unter Deprotonierung jeweils zweier Hydroxygruppen. Die reversible Verknüpfung erfolgt durch vier geladene Wasserstoffbrücken.

<sup>19</sup> B.M. O'Leary, T. Szabo, N. Svenstrup, C.A. Schalley, A. Lützen, M. Schäfer, J. Rebek, *J. Am. Chem. Soc.* **2001**, 123, 11519-11533.

<sup>20</sup> O. Mogck, V. Böhmer, W. Vogt, *Tetrahedron* **1996**, 52, 8489-8496.

<sup>21</sup> J. Scheerder, J.P.M. van Duynhoven, J.F.J. Engbersen, D.N. Reinhoudt, *Angew. Chem.* **1996**, 108, 1172-1175; *Angew. Chem., Int. Ed. Engl.* **1996**, 35, 1090-1093.

<sup>22</sup> T. Heinz, D.M. Rudkevich, J. Rebek, *Nature* **1998**, 394, 764-766.

<sup>23</sup> K. Kobayashi, K. Ishii, S. Sakamoto, T. Shirasaka, K. Yamaguchi, *J. Am. Chem. Soc.* **2003**, 125, 10615-10624.

<sup>24</sup> R. G. Chapman, J. C. Sherman, *J. Am. Chem. Soc.* **1995**, 117, 9081-9082.

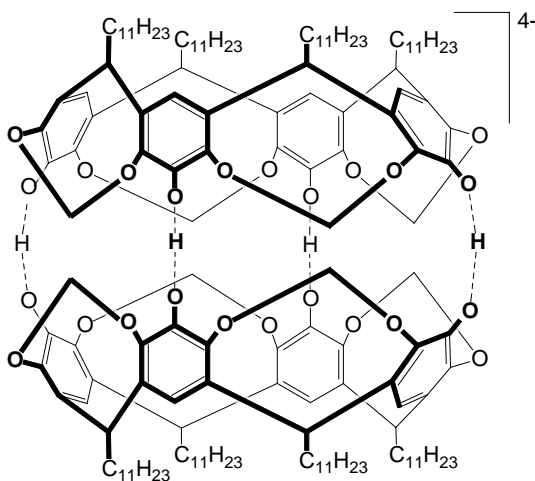


**Abbildung 10:** Dimer aus zwei Tetrahydroxycavitanden nach Deprotonierung mit DBU.

Auch dieser molekulare Container bietet die Möglichkeit zum reversiblen, hochselektiven Einschluss einer großen Anzahl an Gastmolekülen.<sup>25</sup>

## 2.2 Selbstorganisierte Systeme basierend auf Pyridinarenen

Einen relativ neuen Typ von Calixarenen stellen die Octahydroxypyridin[4]arene dar. Sie wurden erstmals von MATTAY *et al.*<sup>26</sup> durch direkte, saure Kondensation von 2,6-Dihydroxypyridin mit einer Reihe von aliphatischen und elektronenarmen, aromatischen Aldehyden zugänglich gemacht.

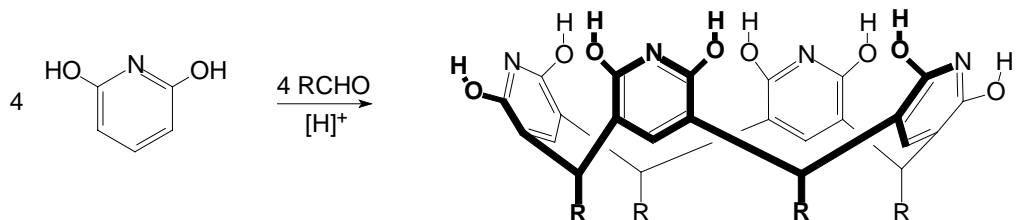


**Abbildung 11:** Synthese von Octahydroxypyridin[4]arenen.

Auf diesem Weg konnte in einer einfachen, einstufigen Synthese eine neue Substanzklasse dargestellt werden, die sich durch ihr Substitutionsmuster am Oberen Rand auszeichnet. Die Hydroxygruppen und Stickstoffatome der 2,6-Dihydroxypyridineinheiten bieten die Option zur Ausbildung von über Wasserstoffbrücken selbstorganisierten Systemen mit geeigneten Partnern.

<sup>25</sup> R.G. Chapman, J.C. Sherman, *J. Am. Chem. Soc.* **1998**, 120, 9818-9826.

<sup>26</sup> T. Gerkensmeier, C. Näther, J. Mattay, *Chem. Eur. J.* **2001**, 7, 465-474.

## 2.2.1 Selbstorganisierte Dimerisierung

Das Octahydroxy-2,8,14,20-tetra-(*iso*-butyl)-pyridin[4]aren (**1**) zeigt im Kristall eine über Wasserstoffbrücken verknüpfte dimere Struktur (Abbildung 12). Zur Optimierung des Donor-Akzeptor-Verhaltens sind die monomeren Einheiten um  $30^\circ$  gegeneinander verdreht. So wechselwirken acht Hydroxygruppen mit den jeweils gegenüberliegenden Stickstoffatomen. Auch die verbleibenden Hydroxygruppen können nun als Donor und Akzeptor dienen, indem sie eine Wasserstoffbrücke mit einer weiteren, gegenüberliegenden Hydroxygruppe ausbilden. Auf diese Weise wird die dimere Struktur über 12 Wasserstoffbrückenkontakte stabilisiert.

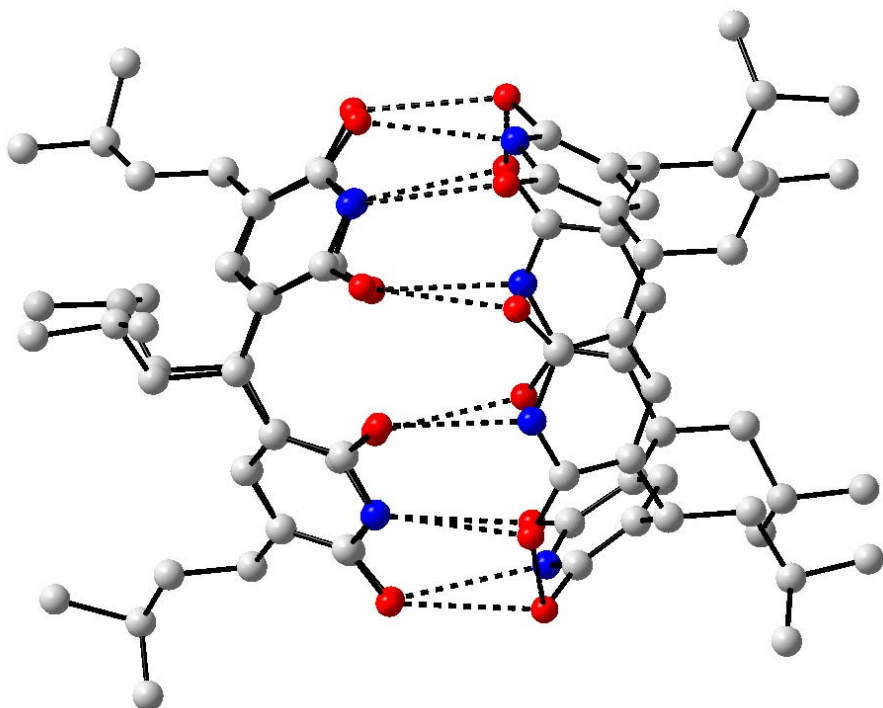
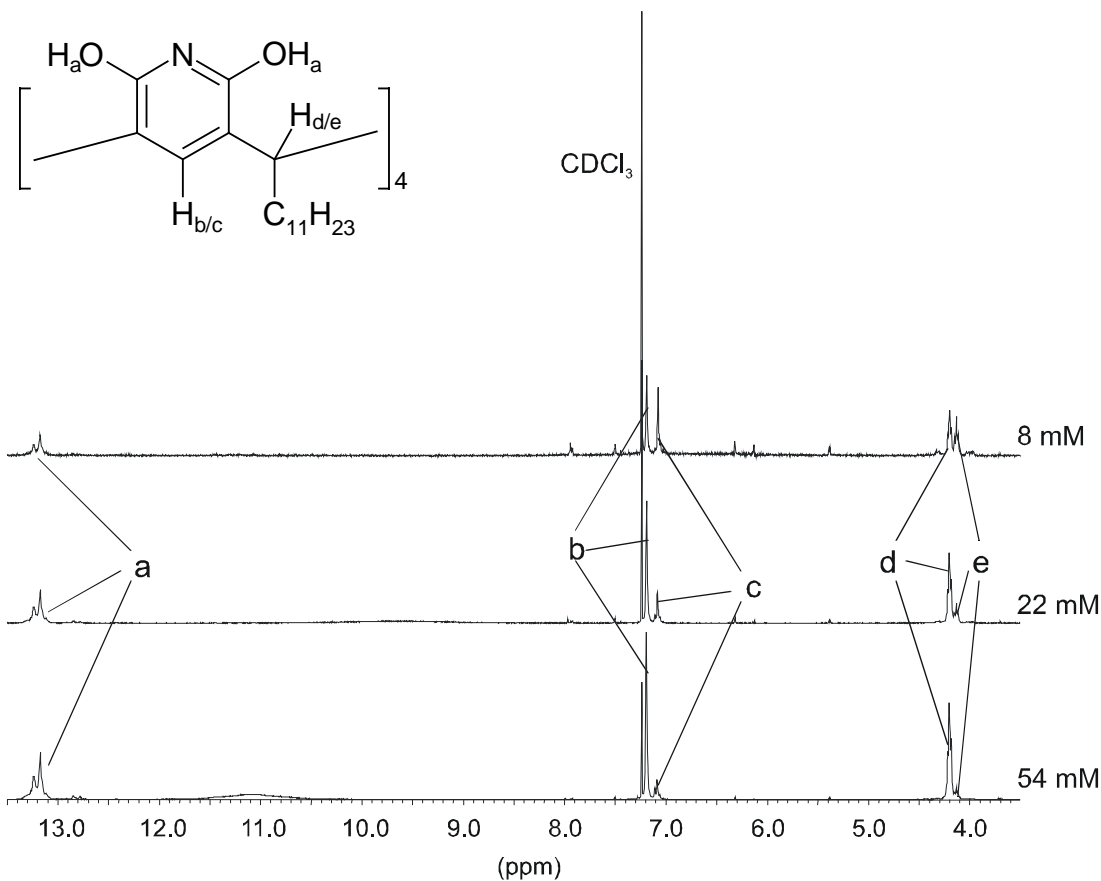


Abbildung 12: Kristallstruktur des dimeren Octahydroxy-2,8,14,20-tetra-(*iso*-butyl)-pyridin[4]arens (**1**).

Auch in Lösung zeigen die Octahydroxypyridin[4]arene die Ausbildung dimerer Strukturen.<sup>27</sup> Dies wurde am Beispiel des Octahydroxy-2,8,14,20-tetra-(*n*-undecyl)-pyridin[4]arens (**2**)  $^1\text{H}$ - und  $^{13}\text{C}$ -NMR-spektroskopisch untersucht. In deuteriertem Chloroform zeigt **2** konzentrationsabhängig zwei Sätze von Signalen (Abbildung 13).

<sup>27</sup> M.C. Letzel, B. Decker, A.B. Rozhenko, W.W. Schoeller, J. Mattay, *J. Am. Chem. Soc.* **2004**, 126, 9669-9674 (A1).



**Abbildung 13:** Konzentrationsabhängige  $^1\text{H}$ -NMR-Spektren von **2** in Chloroform-d<sub>1</sub>.

Bei einer relativ hohen Konzentration von 100 mM zeigt sich nur ein Satz von  $^1\text{H}$ -NMR-Signalen für das dimere Pyridin[4]aren **2**. Es wird ein Singulett bei 7.19 ppm für die aromatischen Protonen (Abbildung 13, b) und ein Triplet bei 4.20 ppm für die Methinprotonen (Abbildung 13, d) detektiert. Wasserstoffbrücken können durch ein Signal im Bereich von 13.1 ppm bis 13.4 ppm (Abbildung 13, a) und ein weiteres breites Signal von 8.50 ppm bis 11.0 ppm belegt werden. Das  $^{13}\text{C}$ -NMR-Spektrum zeigt auch nur einen Satz von Signalen für eine  $C_4$ -symmetrische Spezies. Dies deutet auf eine um  $30^\circ$  verdrehte Struktur hin, wie sie auch im Kristall beobachtet wird (Abbildung 12).

Mit abnehmender Pyridinarenkonzentration kann die zunehmende Bildung des Monomers beobachtet werden. Für die aromatischen und die Methinprotonen werden die  $^1\text{H}$ -NMR-Signale leicht ins höhere Feld verschoben (Abbildung 13, c und e). Die Signale der Wasserstoffbrücken (Abbildung 13, a) verschwinden völlig. Im  $^{13}\text{C}$ -NMR-Spektrum zeigt sich eine Symmetrieveränderung von  $C_4$  zu  $C_{4v}$ . Dies deutet auf die Bildung eines Monomers mit vierfacher Pyridindioltautomerie und perfekter crown-Konformation hin. Der gleiche Effekt kann auch durch die Zugabe von polaren

Reagenzien, wie etwa Triflouressigsäure, erzielt werden, wodurch alle Wasserstoffbrücken zerstört werden.

Durch direkte Integration kann aus den  $^1\text{H-NMR}$ -Spektren die aktuelle Konzentration der monomeren und dimeren Spezies bestimmt werden. Auf diesem Weg ergibt sich aus konzentrationsabhängigen Messungen eine Assoziationskonstante von  $K_{\text{ass}} = (146 \pm 8) \text{ M}^{-1}$ .

Ein weitere Möglichkeit, die Dimerisierung von Octahydroxypyridin[4]arenen zu verfolgen, bietet die Dampfdruckosmose (VPO). Messungen in Chloroform ergeben eine durchschnittliche Masse der in Lösung vorliegenden Spezies von  $(2230 \pm 92) \text{ g/mol}$ . Dieser Wert ist in guter Übereinstimmung mit dem theoretischen Wert für das Dimer von  $2219 \text{ g/mol}$ . Messungen in THF ergeben einen kleineren Wert von  $(1443 \pm 78) \text{ g/mol}$ . Dieses Ergebnis deutet darauf hin, dass in diesem polareren Lösungsmittel eine Mischung aus dimeren und monomeren Spezies vorliegt.

## 2.2.2 Komplexbildung durch Octahydroxypyridin[4]arene

Selbstorganisierte, dimere Kapseln basierend auf Octahydroxypyridin[4]arenen sollten die Möglichkeit zum Einschluss von Gastmolekülen bieten. Als erstes Beispiel wurde hier die Komplexierung von Carbonsäuren und einigen ihrer Derivate untersucht.

Pyridin[4]arene zeigen unter ESI-MS-Bedingungen die Bildung von Dimeren. Nach Zugabe geringer Mengen verschiedener Carbonsäuren wird neben der protonierten, dimeren Spezies auch die Bildung von protonierten Komplexkationen aus zwei Pyridinarenen **2** und einem entsprechenden Carbonsäuremolekül beobachtet.

Ein Vergleich homologer Carbonsäuren zeigt ein großenabhangiges Verhalten für die Bildung dieser 2:1 Komplexe. Propionsäure ist hierbei das größte Molekül für das eine Komplexbildung beobachtet wird. Unter Zugabe von größeren Addukten, wie Buttersäure, 2-Methylbuttersäure oder 2,2-Dimethylbuttersäure, werden keine Komplexe gebildet. Diese Beobachtung deutet darauf hin, dass die kleineren Carbonsäuren in die dimere Pyridinarenenkapsel eingebaut werden, die größeren aber zu groß für den gebildeten Hohlraum sind (Abbildung 14).

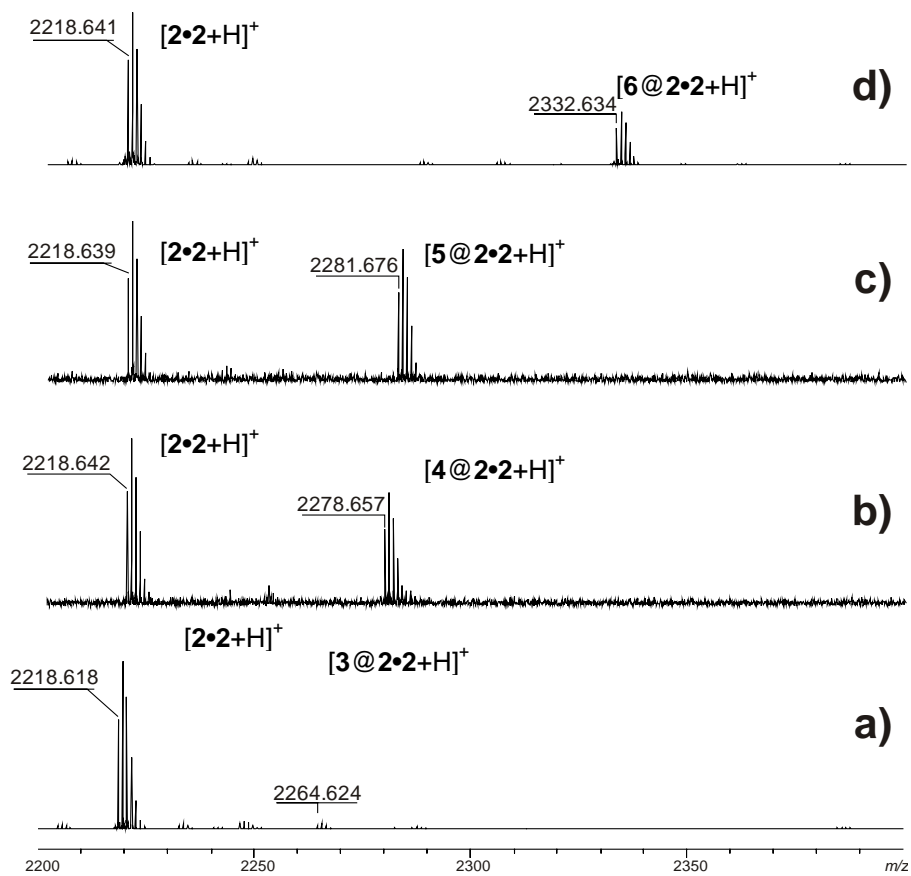


**Abbildung 14:** FT-ICR-MS (ESI) Massenspektrum der Dimerenregion des Pyridin[4]arens **2** mit verschiedenen Carbonsäuren a) Ameisensäure (**3**), b) Essigsäure (**4**), c) Essigsäure-d<sub>3</sub> (**5**) und d) Trifluoressigsäure (**6**).

In Lösung kann die Bildung solcher 2:1 Komplexe mit Hilfe von <sup>19</sup>F-NMR-Spektroskopie in deuteriertem Chloroform verfolgt werden. Als Sonde dienen hier die Fluoratome der Trifluoressigsäure (TFA, **6**).

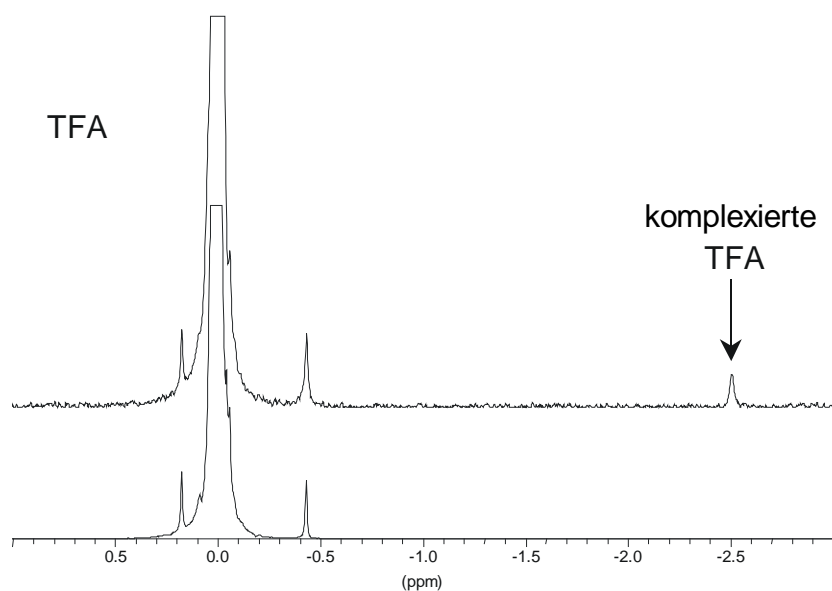


**Abbildung 15:** <sup>19</sup>F-NMR-Spektrum von **2** (46 mM) mit TFA-Konzentrationen von 30 mM (oben) und 160 mM (unten) in Chloroform-d<sub>1</sub>.

Bei einer konstanten Pyridinarenkonzentration von 46 mM wird hierbei neben den typischen TFA-Signalen für Konzentrationen von bis zu 150 mM ein tiefeldverschobenes  $^{19}\text{F}$ -NMR-Signal für in die Kapsel eingeschlossene Trifluoressigsäure detektiert. Der überwiegende TFA-Anteil liegt über den gesamten Konzentrationsbereich allerdings unkomplexiert vor. Für höhere TFA-Konzentrationen kann das Signal für komplexierte Trifluoressigsäure nicht mehr detektiert werden. Grund hierfür ist die Zerstörung der dimeren Pyridinarenkapseln durch den Einfluss des Wasserstoffbrücken zerstörenden Reagenzes.

Weitere Möglichkeiten zur Untersuchung solcher Einschlusverbindungen bieten moderne theoretische Methoden. So wurden sowohl die protonierten, als auch die unprotonierten Komplexe mittels Berechnungen auf dem DFT-Näherungsniveau (B3-LYP/3-21G\*) betrachtet. Die Ergebnisse zeigen eine gute Übereinstimmung mit den praktisch durchgeführten ESI-MS-Experimenten. Diese Methode bietet so eine Möglichkeit zur Bestimmung neuer, potentieller Komplexpartner, die in die Kavität dimerer Pyridin[4]arene eingebaut werden können.

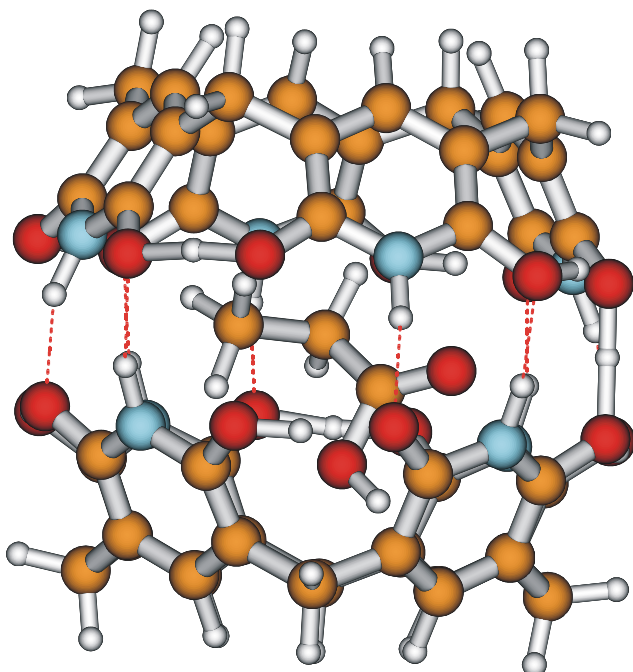


**Abbildung 16:** Berechnete Struktur des Pyridinarendimer-Propionsäure-Komplexes.

Eine weitere interessante Eigenschaft der amphiphilen Pyridin[4]arene stellt die Ausbildung zweidimensionaler Monoschichten dar. Dies ermöglicht die Stabilisierung von Goldclustern definierter Größe in organischen Lösungsmitteln durch Chemisorption und/oder elektrostatische Wechselwirkungen.<sup>28</sup>

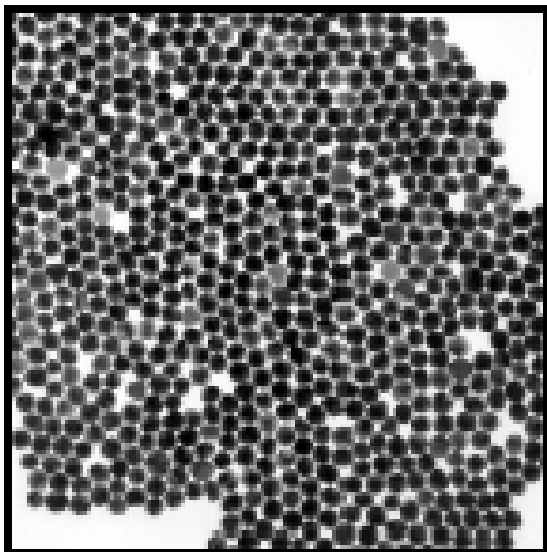


**Abbildung 17:** TEM-Aufnahme selbstorganisierter, durch **2** komplexierter Goldpartikel ( $35 \pm 3$  nm).

Durch **2** komplexierte Goldpartikel zeigen die selbstorganisierte Ausbildung einer lokal hochgeordneten, zweidimensionalen Struktur.

### 2.2.3 Untersuchung des gelartigen Pyridinaren/Naphthyridin Systems

Die ersten Versuche zur Bildung selbstorganisierter 1:4 Komplexe basierend auf Pyridinaren **2** mit 2,6-Diaminopyridin und verschiedenen Pyridin- oder Benzoësäurederivate waren nicht erfolgreich. Interessante Effekte konnten hingegen mit dem 2-Amino-*N*<sup>3</sup>-(*n*-undecyl)-1,8-naphthyridin-3-carboxamid (**7**) beobachtet werden.

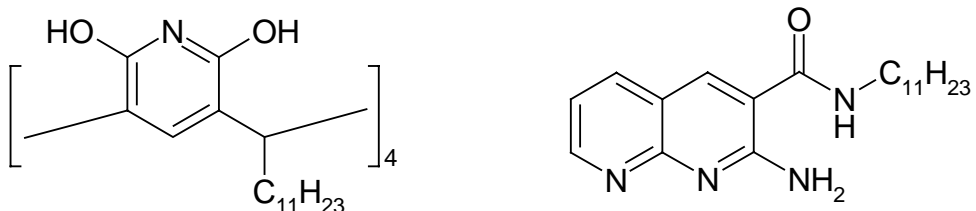


**Abbildung 18:** Gelbildende Komponenten Pyridinaren **2** und Naphthyridin **7**.

---

<sup>28</sup> B. Kim, R. Balasubramanian, W. Perez-Segarra, B. Decker, J. Mattay, A. Wei, *Supramol. Chem.* **2004**, im Druck (A2).

In einem molaren Mischungsverhältnis von 1:4 und Konzentrationen im millimolaren Bereich zeigen die beiden Komponenten in einem geeigneten Lösungsmittel ein gelartiges Erstarren.<sup>29</sup> Nach der Definition von FLORY<sup>30</sup> ist ein Gel eine kolloidale Dispersion, die (1.) eine kontinuierliche Struktur mit makroskopischen Dimensionen besitzt, die auf der Zeitskala des analytischen Experiments erhalten bleibt und die sich (2.) in ihren rheologischen Eigenschaften wie ein Feststoff verhält. Um die Eigenschaften von Gelen zu beschreiben, haben sich in den letzten Jahren eine Reihe von effizienten Methoden durchgesetzt.<sup>31,32</sup> Als Beispiele seien hier die Rheologie, Mikroskopie, Röntgen- und Neutronenbeugung, aber auch verschiedene spektroskopische Methoden wie beispielsweise NMR, UV oder Fluoreszenz genannt.

Rheologische Experimente eignen sich zur Beschreibung der makroskopischen Eigenschaften eines Gels. Die Viskosität wurde temperaturabhängig für verschiedene Konzentrationen und Verhältnisse der beiden Komponenten untersucht. Das Gel zeigt ein thixotropes Verhalten, d.h. durch eine mechanische Belastung wird die zähe Substanz flüssiger. Nach kurzer Zeit ohne äußeren Einfluss erhöht sich die Viskosität jedoch wieder. Eine weitere interessante Eigenschaft des Gels ist seine Thermoreversibilität. Durch Erwärmen kann die Viskosität erniedrigt werden, erneutes Abkühlen führt aber wieder zu einer Viskositätserhöhung. Aufgrund dieser Ergebnisse kann für die vorliegenden Aggregate eine bandartige, mikroskopische Struktur postuliert werden. Faserförmige Aggregate liegen in einer verknoteten und ineinander verschlungenen Form vor. Durch einen äußeren mechanischen oder thermischen Einfluss können diese faserförmigen Aggregate aber entschlungen oder Quervernetzungen gebrochen werden, wodurch dann die Viskosität sinkt.

TEM (Transmissions Elektronen Mikroskopie) erlaubt weitere Rückschlüsse auf den strukturellen Aufbau des Gels. Zu diesem Zweck wird eine Probe des Gels schockgefroren und mittels Gefrierbruch, Anätzen und Beschatten mit einem Metall der Elektronenmikroskopie zugänglich gemacht.

---

<sup>29</sup> T. Gerkensmeier, B. Decker, M. Schwertfeger, W. Buchheim, J. Mattay, *Eur. J. Org. Chem.* **2002**, 2120-2125 (A3).

<sup>30</sup> P.J. Flory, *Faraday Discuss. Soc.* **1974**, 57, 7-18.

<sup>31</sup> P. Terech, R.G. Weiss, *Chem. Rev.* **1997**, 97, 3133-3159.

<sup>32</sup> L.A. Estroff, A.D. Hamilton, *Chem. Rev.* **2004**, 104, 1201-1217.

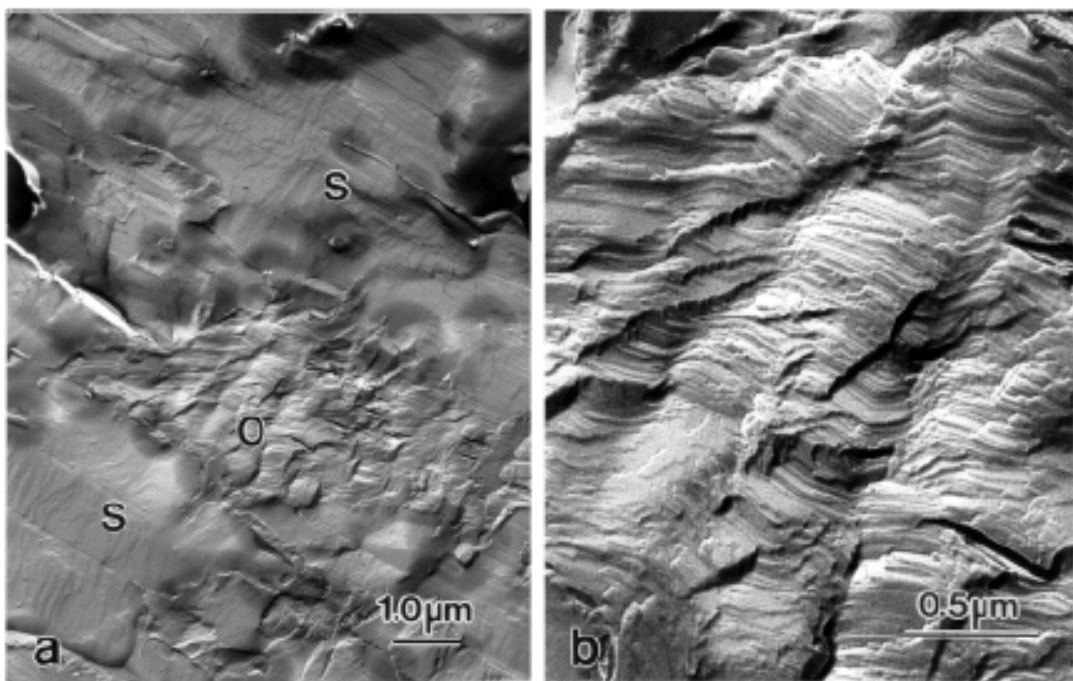


**Abbildung 19:** TEM-Aufnahmen einer gefriergebrochenen 1:4 Mischung von Pyridinaren **2** und Naphthyridin **7** in 1,2-Dichlorbenzol.

Abbildung 19 zeigt TEM-Aufnahmen des gefriergebrochenen Gels. In Abbildung 19 a können zwei Domänen voneinander unterschieden werden. Durch **S** sind Lösungsmittelbereiche gekennzeichnet. **O** zeigt einen Bereich, in dem geordnete Strukturen auftreten. In Abbildung 19 b ist ein solcher Bereich vergrößert dargestellt. Es bildet sich eine periodische, lamellare Struktur mit einheitlichen Abständen von etwa 5 nm. Solche langgestreckten, geordneten Aggregate können allerdings nicht für die rheologischen Eigenschaften des Gels verantwortlich sein. Sie müssen durch die schwer durchzuführende Probenpräparation für die TEM-Aufnahmen zustande gekommen sein.

Mit Hilfe von Lichtstreuungsexperimenten wurde das Wachstum der das Gel aufbauenden Aggregate untersucht.<sup>33</sup> Die zeitaufgelöste, statische Lichtstreuung ist eine klassische Methode zur Bestimmung von Molmassen. Darüber hinaus sind Informationen über Form und Wechselwirkung der fraglichen Partikel zugänglich, bis hin zu Überstrukturen.

---

<sup>33</sup> T. Witte, B. Decker, J. Mattay, K. Huber, *J. Am. Chem. Soc.* **2004**, 126, 9276-9282 (A4).

Nach der Methode von BERRY<sup>34</sup> lassen die experimentellen Daten Aussagen über den Trägheitsradius  $R_g$  und die durchschnittliche, relative molare Masse  $M_w$  der vorliegenden Partikel zu. Durch zeitabhängige Messungen kann somit deren Wachstum beobachtet werden. Aus dem Verhältnis zwischen Größe und Masse der Partikel kann man Informationen über deren Form erhalten. Nach einem Modell für das diffusionskontrollierte Wachstum der Aggregate kommen prinzipiell Stäbe, Knäuel und Kugeln als mögliche Strukturen in Frage.<sup>35</sup> Unter der Annahme, dass das Wachstum der in Lösung vorhandenen Partikel durch Anlagerung von kleinen, monomeren Einheiten erfolgt, ergibt sich nach BURCHARD<sup>36</sup> eine nicht zufällig verzweigte Struktur für das Polykondensat des ABC-Typs.<sup>37</sup> An den Verzweigungspunkten der linearen Partikelstruktur werden drei verschiedene Endgruppen, A, B und C, postuliert, an denen das Wachstum fortgesetzt werden kann. A kann dabei nur mit B oder C reagieren, B und C können als Endgruppe dagegen nur mit A das Wachstum fortsetzen.

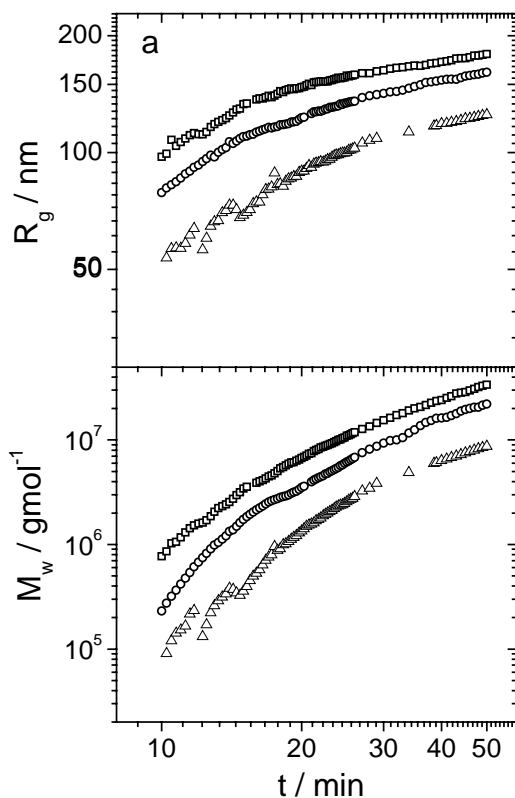


**Abbildung 20:** Zeitliche Entwicklung von  $R_g$  und  $M_w$  von 1:4 Mischungen von **2** und **7** verschiedener Konzentration.

Für den Wachstumprozess der gelbildenden Überstruktur des Pyridinarens **2** mit dem Naphthyridin **7** in 1,2-Dichlorbenzol kann nun ein Modell postuliert werden. Monomere aggregieren zu faserartigen Filamenten, welche die Möglichkeit besitzen, Verzweigungspunkte auszubilden. Jeder Verzweigungspunkt initiiert das Wachstum mindestens zweier weiterer Filamente.

<sup>34</sup> G.C. Berry, *J. Chem. Phys.* **1966**, 44, 4550-4564.

<sup>35</sup> D.A. Weitz, J.S. Huang, M.Y. Lin, J. Sung, *Phys. Rev. Lett.* **1985**, 54, 1416-1419.

<sup>36</sup> W. Burchard, *Advances in Polymer Science* 48, Springer: Berlin, Heidelberg, **1983**.

<sup>37</sup> W. Burchard, *Macromolecules* **1972**, 5, 604-610.

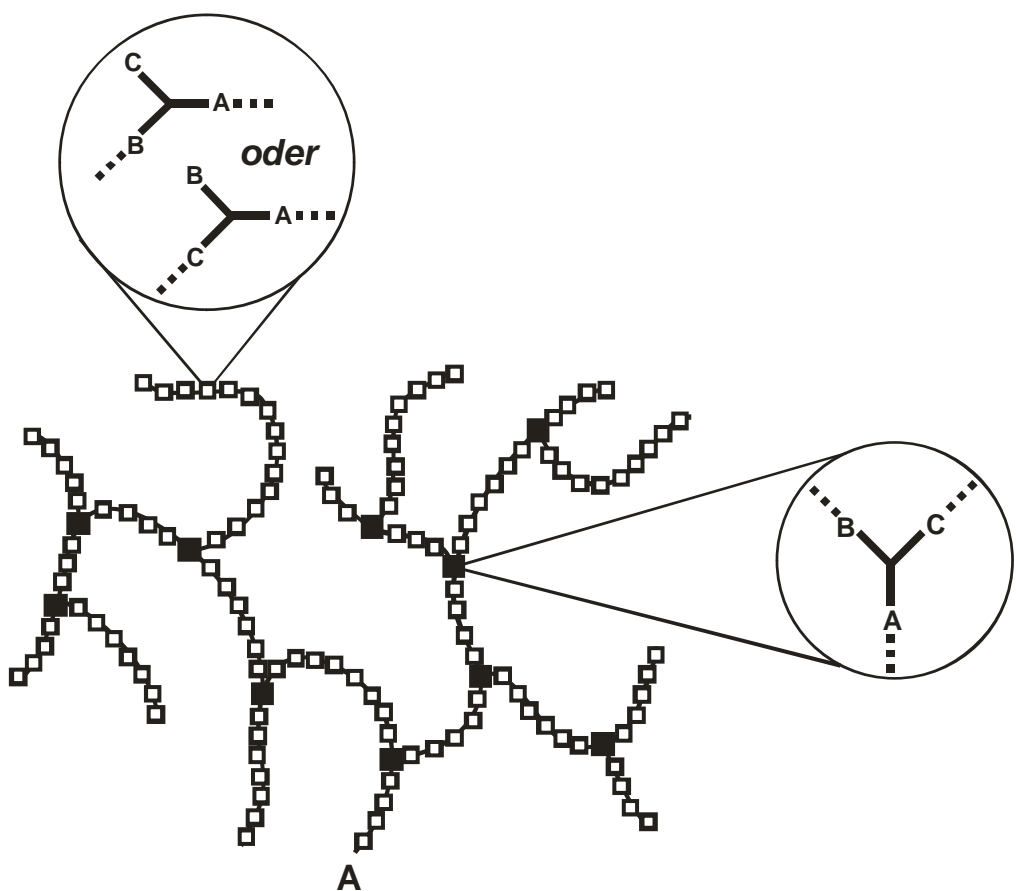


**Abbildung 21:** Schematische Darstellung eines ABC-Polykondensates.

Eine vergleichbare Struktur wurde bisher erst für zwei weitere Gelsysteme, die nicht auf Polymeren basieren, postuliert.<sup>38,39</sup> Im Rahmen der durchgeführten Experimente ist es erstmals gelungen, den Selbstorganisationsprozess einer nichtlinearen Struktur mit Hilfe zeitaufgelöster Lichtstreuung zu verfolgen und Ähnlichkeiten zu einem gut etablierten Verzweigungsmodell aus der Polymerforschung herauszustellen.

<sup>38</sup> X.Y. Liu, P.D. Sawant, *Applied Physics Letters* **2001**, 79, 3518-3520.

<sup>39</sup> X.Y. Liu, P.D. Sawant, W.B. Tan, I.B.M. Noor, C. Pramesti, B.H. Chen, *J. Am. Chem. Soc.* **2002**, 124, 15055-15063.

## 2.3 Untersuchungen an Resorcaren-Monoschichten

### 2.3.1 Studium photoinduzierter Struktur- und Bindungsänderungen mit fs-zeitaufgelöstem ESCA

Die physikalische Methode des ESCA (Electron Spectroscopy for Chemical Analysis), sowie pump and probe Spektroskopie, sind jeweils gut eingeführte und erfolgreiche Methoden der Oberflächenanalytik bzw. der Femtosekundenchemie. In Bielefeld steht eine Quelle zur Verfügung, die im Hinblick auf die Untersuchung sehr komplexer Systeme für eine optimale Kombination von spektraler Selektivität und zeitlicher Auflösung entwickelt worden ist.<sup>40</sup> Mit ihr sollen nichtreversible, dynamische Prozesse an organischen Molekülschichten mittels zeitaufgelöstem ESCA studiert werden. Calixarene dienen hier aufgrund ihrer Möglichkeiten in der Wirt-Gast-Chemie und ihrer vielfältigen chemischen Variabilität als Modellsystem. Dauerhaft sollen lichtinduzierte transiente Änderungen von Wirt-Gast Systemen in Echtzeit beobachtet werden. Nach Anregung durch einen UV- oder Vis-Puls (pump) kann die chemische Umgebung eines Sonden- oder Markeratoms, das in das System eingebaut ist, nach einer definierten und variablen Zeit mit einem extremen ultravioletten (EUV) Puls (probe) abgefragt werden.

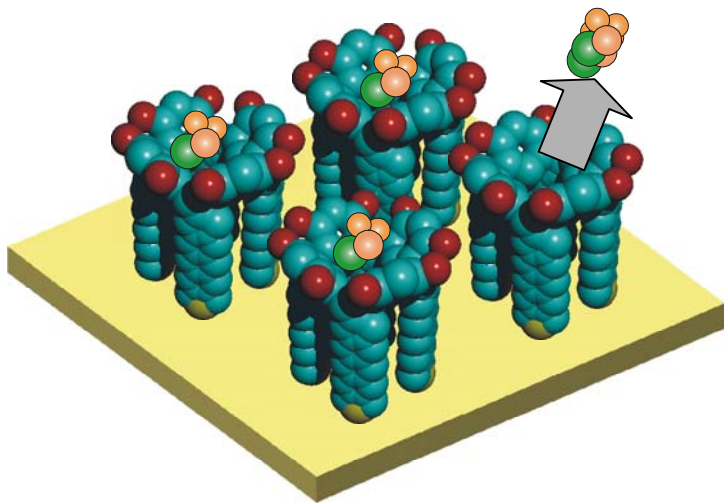


**Abbildung 22:** Selbstorganisiert auf Oberflächen aufgebrachte Calixarene als Modellsystem für das Studium der Dynamik der Wirt-Gast Wechselwirkung.

Zu diesem Zweck wurde ein achtfach iodfunktionalisiertes Resorc[4]aren **8** synthetisiert, das sich durch seine Sulfidfunktionalisierung am *Unteren Rand* zur Bildung von SAMs (Self Assembled Monolayers) auf glatten Goldoberflächen

<sup>40</sup> M. Drescher, P. Siffalovic, M. Spieweck, U. Heinzmann, *J. Electron Spectrosc. Relat. Phenom.* **2002**, 127, 103-108.

eignet.<sup>41</sup> Die acht Iodatome am *Oberen Rand* können durch einen UV-pump Puls dissoziiert und durch den EUV-probe Puls in der Änderung ihrer chemischen Umgebung untersucht werden.

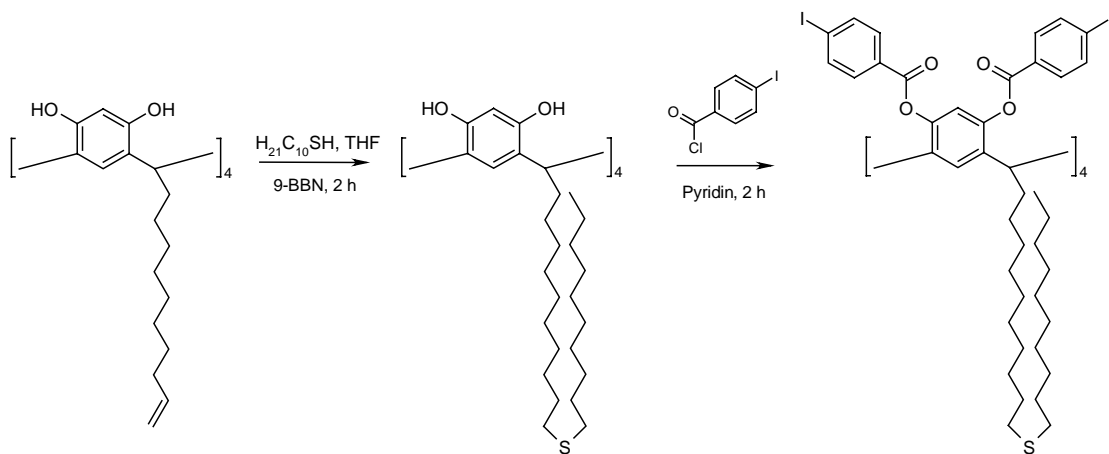


**Abbildung 23:** Synthese des Octaiodids **8**.

Die Präparation der SAMs erfolgte durch etwa 16stündige Inkubation bei 60 °C der Goldsubstrate in einer 1 mM Ethanol/Chloroform (1/1) Lösung des Octaiodids **8**.<sup>42</sup> Die so hergestellten SAMs wurden mittels XPS (X-ray Photoelectron Spectroscopy), Ellipsometrie, AFM (Atomic Force Microscopy) und statischem ESCA charakterisiert.

XPS ermöglicht eine quantitative Bestimmung der elementaren Zusammensetzung auf einer Oberfläche. Eine Analyse der Signalläden unter Berücksichtigung ihres Ionisierungswirkungsgrades führt direkt zu einem C : O : I-Verhältnis von 1 : 0.15 : 0.07.

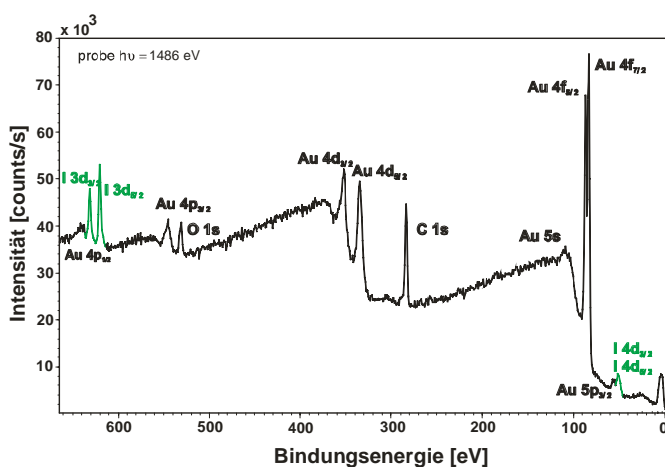


**Abbildung 24:** XPS-Spektrum von **8** auf einem Goldsubstrat.

<sup>41</sup> P. Siffalovic, M. Michelswirth, P. Bartz, B. Decker, C. Agena, C. Schäfer, S. Molter, R. Ros, M. Bach, M. Neumann, D. Anselmetti, J. Mattay, U. Heinzmann, M. Drescher, *J. Biotech.* **2004**, *112*, 139-149 (A5).

<sup>42</sup> E.U. Thoden van Velzen, D.N. Reinhoudt, *J. Am. Chem. Soc.* **1995**, *117*, 6853-6862.

Dies ist in guter Übereinstimmung mit dem theoretischen Verhältnis von 1 : 0.10 : 0.05. Eine quantitative Analyse des Schwefels der Sulfidgruppe war aufgrund der geringen Signalintensität nicht möglich.

AFM bietet die Möglichkeit, Informationen über die Filmhöhe zu erlangen. Durch Behandlung des beschichteten Substrats mit UV-Licht durch ein 25 µm Gitter kann die Oberfläche durch Zerstörung des organischen Materials strukturiert werden. Auf diesem Weg ergibt sich eine Schichthöhe von 2.85 nm. Dieser Wert ist in guter Übereinstimmung mit literaturbekannten Werten anderer Resorcaren-SAMs.<sup>43,44</sup> Ellipsometrie erlaubt Aussagen über die Dichte des Films. Aus der gemessenen Schichthöhe von 2.85 nm ergibt sich ein effektiver Brechungsindex von 1.45. Dieser Wert ist typisch für Sulfidfilme mit einer hohen Dichte.<sup>45</sup>

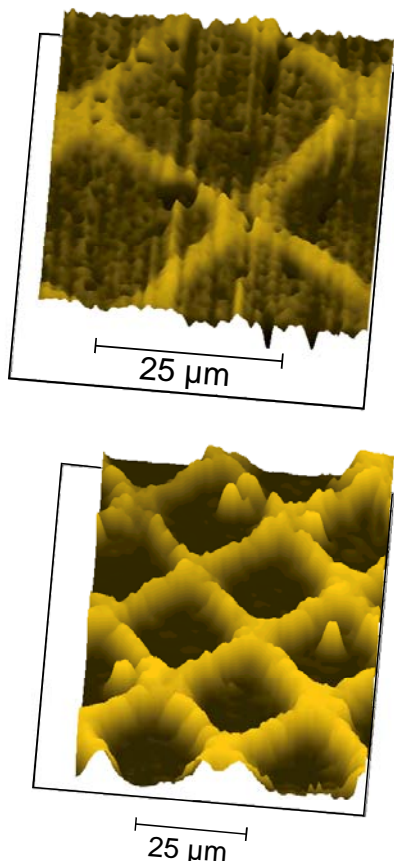


**Abbildung 25:** AFM (oben) und Ellipsometrie (unten) – Profile.

An den so präparierten Molekülschichten konnte nun der photoinduzierte Bruch der Iod-Benzol Bindung mittels statischem ESCA beobachtet werden. Die präparierten Octaiodidschichten wurden zunächst mit der frequenzverdreibachten Strahlung des Femtosekundenlasersystems bei 4.6 eV Photonenergie (266 nm) untersucht. Abbildung 26 zeigt die statischen ESCA-Spektren vor und nach der Belichtung. Die atomare Signatur des Iods in Form der 4d-Photolinien ist nach der Bestrahlung verschwunden, während der Rest des Spektrums unverändert bleibt. Dies deutet auf einen selektiven Bruch der Iodbindung ohne Schädigung des Resorcarengerüsts hin. Das letztlich vollständige Verschwinden des Iodsignals unterstützt die angestrebte Platzierung der Iodbenzolgruppen an der Oberseite der Molekülschicht, so dass die dissozierten Atome die Oberfläche in das Vakuum verlassen können.

<sup>43</sup> S.A. Levi, P. Guatteri, F.C.J.M. van Veggel, G.J. Vansco, E. Dalcanale, D.N. Reinhoudt, *Angew. Chem.* **2001**, 113, 1945-1948; *Angew. Chem., Int. Ed. Engl.* **2001**, 40, 1892-1896.

<sup>44</sup> E. Menozzi, R. Pinalli, E.A. Speets, B.J. Ravoo, E. Dalcanale, D.N. Reinhoudt, *Chem. Eur. J.* **2004**, 10, 2199-2206.

<sup>45</sup> C.D. Bain, E.B. Troughton, Y.-T. Tao, J. Evall, G.M. Whitesides, R.G. Nuzzo, *J. Am. Chem. Soc.* **1989**, 111, 321-325.

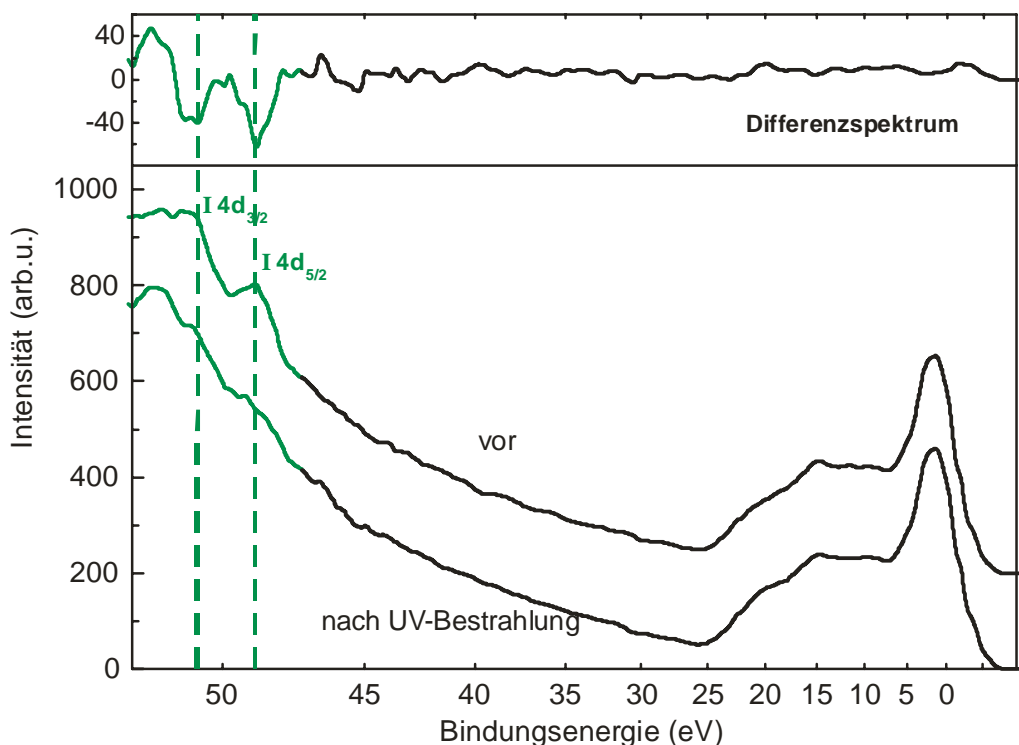


**Abbildung 26:** Statisches ESCA-Spektrum der Photodissoziation von Iodatomen des Octaiodid-Films.

Erste Experimente zur zeitlichen Verfolgung dieses Dissoziationsprozesses wurden bereits durchgeführt. Hier stellt aber der Multiphotonenuntergrund aus dem Goldsubstrat ein bisher nicht gelöstes Problem dar.

### 2.3.2 Einzmolekülkraftspektroskopie mit Resorc[4]arenen

Moderne Rastersondenmikroskopische Methoden, wie etwa AFM, eignen sich zur dreidimensionalen, strukturellen Charakterisierung und Modifizierung von Oberflächen im Nanometermaßstab. Mit denselben Geräten sind auch Messungen von Kräften im Piconewtonbereich unter physiologischen Bedingungen möglich. Die Kombination dieser beiden Eigenschaften eröffnet die Option zur Beobachtung nicht-kovalenter Wechselwirkungen auf molekularer Ebene. Es wurden bereits eine Reihe solcher Wechselwirkungen in biologischen Systemen, wie beispielsweise Biotin-(Strept)avidin,<sup>46</sup> Antikörper-Antigen,<sup>47</sup> DNA-Protein<sup>48</sup> oder zwischen komplementären DNA-Strängen,<sup>49</sup> untersucht. Eine noch geringe Anzahl neuerer Arbeiten beschäftigt sich mit der Wechselwirkung in chemisch synthetisierten Supramolekularen

<sup>46</sup> E.-L. Florin, V.T. Moy, H.E. Gaub, *Science* **1994**, 264, 415-417.

<sup>47</sup> F. Schwesinger, R. Ros, T. Strunz, D. Anselmetti, H.-J. Güntherodt, A. Honegger, L. Jermutus, L. Tiefenauer, A. Plückthun, *Proc. Natl. Acad. Sci. USA* **2000**, 97, 9972-9977.

<sup>48</sup> F.W. Bartels, B. Baumgarth, D. Anselmetti, R. Ros, A. Becker, *J. Struct. Biol.* **2003**, 143, 145-152.

<sup>49</sup> G.U. Lee, L.A. Chrisey, R.J. Colton, *Science* **1994**, 266, 771-773.

Systemen. Die ersten Beispiele stellen hier das Cyclodextrin-Ferrocen-<sup>50</sup> und das Kronenether-Ammonium-System<sup>51</sup> dar.

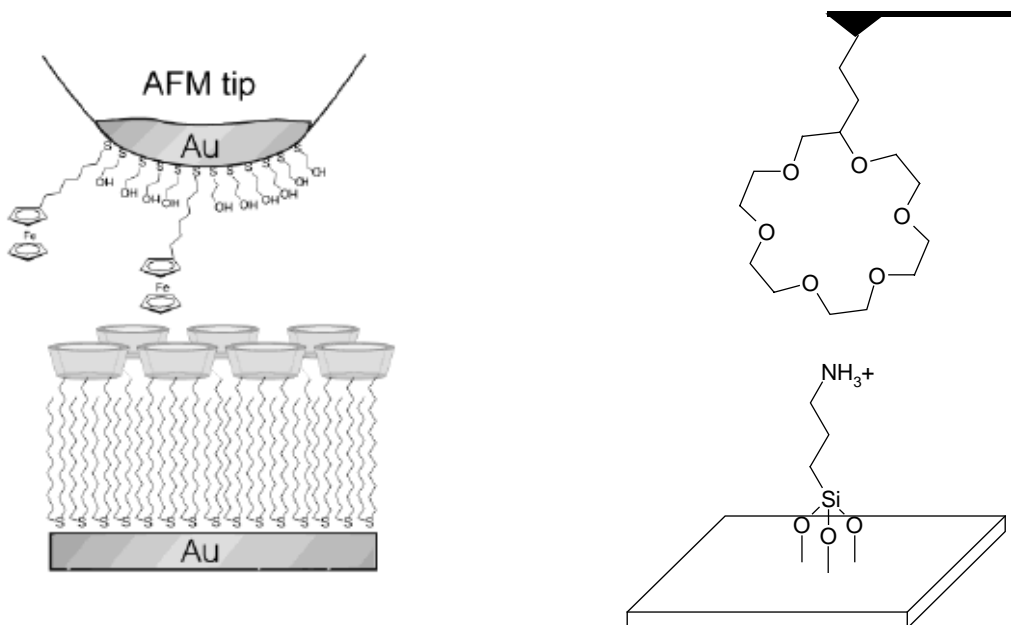


**Abbildung 27:** Schematischer Aufbau einzelmolekülkraftspektroskopischer Untersuchungen der Cyclodextrin-Ferrocen- und Kronenether-Ammonium-Systeme.

In beiden Beispielen konnte die Wirt-Gast Wechselwirkung nur durch eine statistische Analyse der gemessenen Verteilungshistogramme identifiziert werden. Es konnte keine Aussage bezüglich der Beladungsrate („loading rate“) gemacht werden, welche die Grundlage für eine weitere thermodynamische Auswertung darstellt.

Nicht funktionalisierte Resorc[4]arene bilden mit einer Reihe geeigneter Template, wie beispielsweise Tropylium- und Ammoniumionen, dimere<sup>52</sup> aber auch hexamere<sup>53</sup> Kapseln. In der Gasphase wurden 1:1 Komplexe mit Alkalimetallkationen und Ammoniumionen beobachtet;<sup>54</sup> diese Resultate konnten auch durch theoretische Methoden<sup>55,56</sup> erfasst werden. Komplexe von unsubstituierten Cavitanden mit Ammoniumionen sind bisher nicht untersucht worden, was auf ihr unterschiedliches

<sup>50</sup> T. Auletta, M.R. de Jong, A. Mulder, F.C.J.M. van Veggel, J. Huskens, D.N. Reinhoudt, S. Zou, S. Zapotoczny, H. Schönherr, G.J. Vansco, L. Kuipers, *J. Am. Chem. Soc.* **2004**, 126, 1577-1584.

<sup>51</sup> S. Kado, K. Yamada, K. Kimura, *Langmuir* **2004**, 20, 3259-3263.

<sup>52</sup> A. Shivanyuk, J. Rebek, *Chem. Commun.* **2001**, 2374-2375.

<sup>53</sup> A. Shivanyuk, J.C. Friese, S. Döring, J. Rebek, *J. Org. Chem.* **2003**, 68, 6489-6496.

<sup>54</sup> M.C. Letzel, C. Agena, J. Mattay, *J. Mass. Spectrom.* **2002**, 37, 63-68.

<sup>55</sup> A.B. Rozhenko, W.W. Schoeller, M.C. Letzel, B. Decker, C. Agena, J. Mattay, *J. Phys. Chem.* **2005**, eingereicht (A6).

<sup>56</sup> A.B. Rozhenko, W.W. Schoeller, M.C. Letzel, B. Decker, C. Agena, J. Mattay, *Theo. Chem.* **2005**, 7-20 (A7).

Lösungsverhalten zurückzuführen ist. Die Einzelmolekülkraftspektroskopie eröffnet hier völlig neue Möglichkeiten.<sup>57</sup>

Es wurde ein vierfach sulfidisubstituierter Cavitand **9** synthetisiert, der sich zur Herstellung von Monoschichten auf Gold eignet.<sup>58</sup>

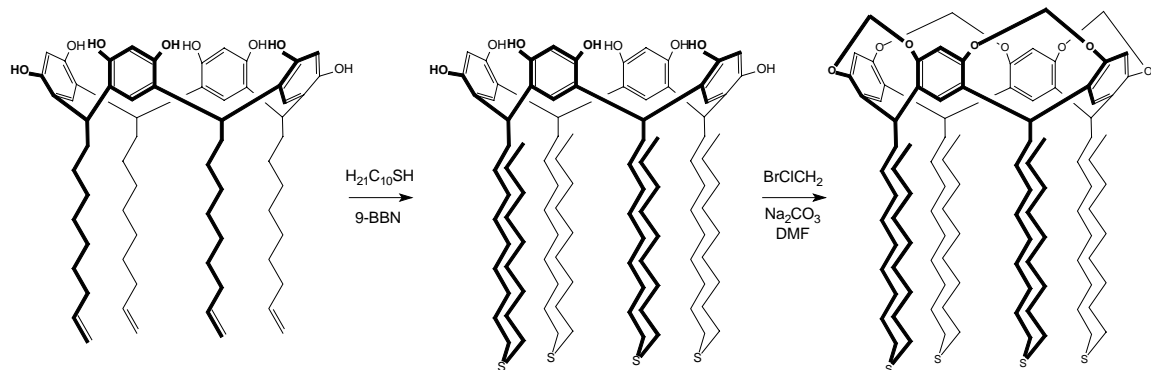


**Abbildung 28:** Darstellung von **9**.

Inkubation eines Goldsubstrats in einer 1:40 Mischung aus **9** und Didecylsulfid führt zur Bildung einer „verdünnten“ Cavitand-Monoschicht. Zur Untersuchung des Wirt-Gast Verhaltens wurden drei verschiedene Ammoniumionen (Ammonium, Trimethylammonium und Triethylammonium) kovalent über einen Polyethylenglycol(PEG)-Linker mit einer Länge von etwa 30 nm an die AFM-Spitze gebunden.

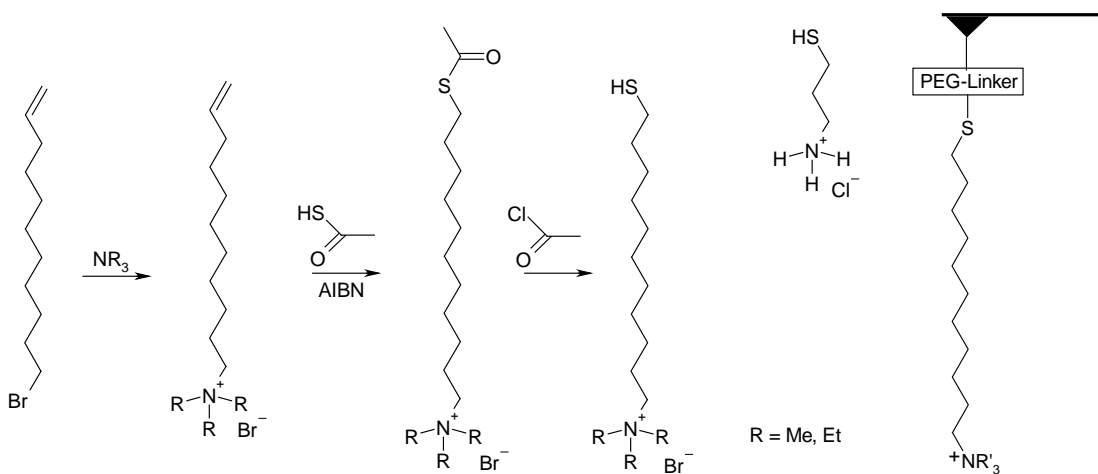


**Abbildung 29:** Darstellung der Ammoniumionen und Anbindung an die AFM-Spitze.

Auf diesem Weg erhält das System mehr sterische Flexibilität, wodurch die Komplexbildung und Identifizierung einzelner Wirt-Gast Paare, im Vergleich zu

<sup>57</sup> R. Eckel, R. Ros, B. Decker, J. Mattay, D. Anselmetti, *Angew. Chem.* **2004**, im Druck (A8).

<sup>58</sup> E.U. Thoden van Velzen, J.F.J. Engbersen, D.N. Reinhoudt, *Synthesis* **1995**, 989-997.

anderen Systemen, bei denen die Anbindung direkt an die AFM-Spitze erfolgt, erleichtert wird.

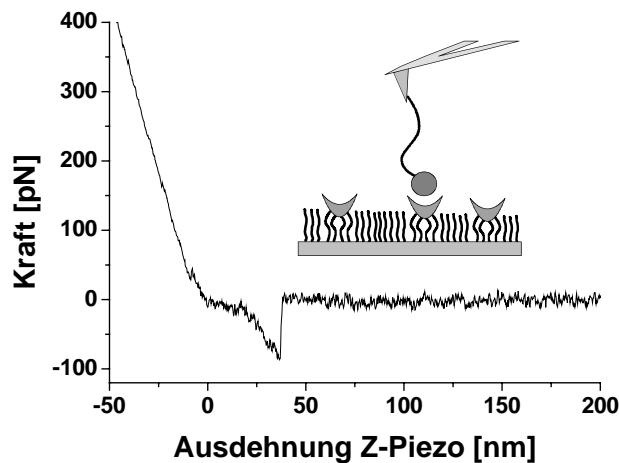


**Abbildung 30:** Schematischer Aufbau (a) und typische Kraft-Abstand Kurve (b).

Durch Auftragung der am AFM-Cantilever gemessenen Kraft gegen seine z-Piezo Position zur Cavitand-Oberfläche können einzelne Abrissereignisse identifiziert werden. Die wahrscheinlichste Abrisskraft wird durch eine statistische Auswertung von etwa 200 Messungen bestimmt.

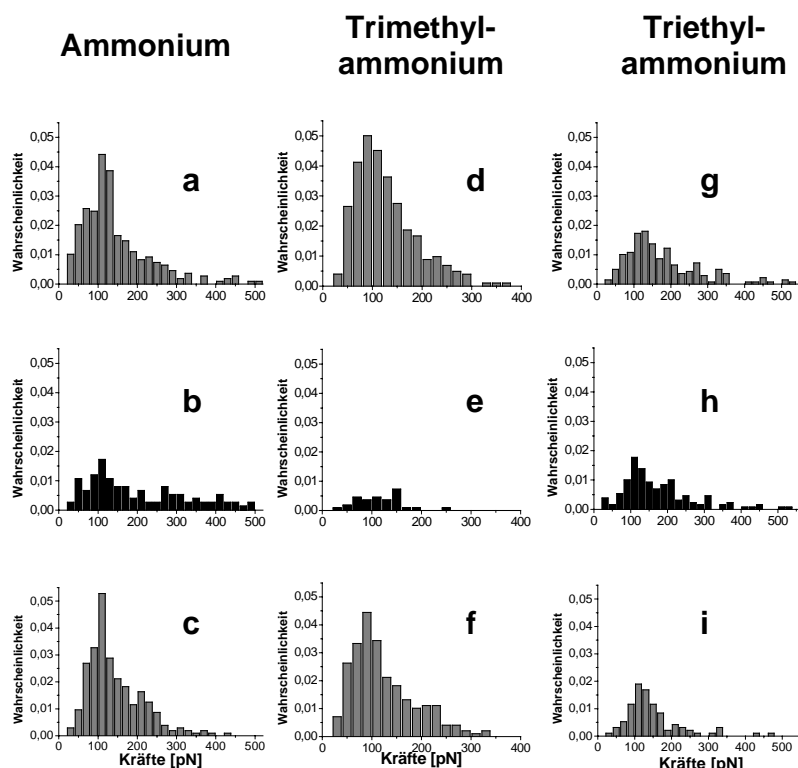


**Abbildung 31:** Einzelmolekül Konkurrenzexperimente.

Die Messungen wurden in Ethanol durchgeführt. Für das Ammonium- und das Trimethylammoniumion können den Histogrammen in Abbildung 31 die wahrscheinlichsten Abrisskräfte entnommen werden (a, d). Als Kontrollexperimente wurden die Messungen in, mit den entsprechenden Ammoniumsalzen gesättigten, Lösungen durchgeführt (b, e). Die Anzahl der auftretenden Abrisse konnte so signifikant reduziert werden, was die Spezifität der Wechselwirkungen belegt. Durch Waschen des Substrats mit Ethanol werden die freien Salze entfernt, und die Oberfläche wird reaktiviert (c, f). Das Triethylammoniumion zeigt schon in Ethanol keine spezifischen Abrisse (g). Auch der Zusatz von Tetraethylammoniumchlorid (h) zu der Lösung und anschließendes Spülen mit Ethanol (i) ändert an dem Verhalten nichts. Dies war auch zu erwarten, da der Triethylammoniumrest mit einer berechneten Größe von 0.8 nm zu groß für eine Wirt-Gast Wechselwirkung mit der Kavität (0.7 nm am *Oberen Rand*) sein sollte.

Die gemessenen Abrisskräfte sind nicht konstant, sondern abhängig von der zeitlichen Kraftentwicklung, die auf den gebildeten Komplex einwirkt. D.h., die Kraft ändert sich mit der Geschwindigkeit, mit der der Cantilever schwingt. Durch dynamische Kraftspektroskopie können so Informationen über die Kinetik der Komplexbildung und die molekulare Länge der Wechselwirkung erhalten werden.<sup>59,60</sup>

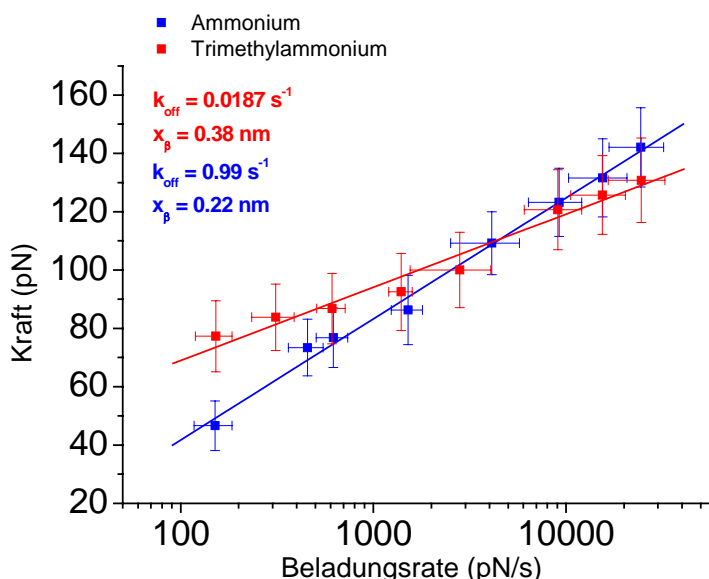


**Abbildung 32:** Abrisskräfte für Ammonium- und Trimethylammoniumionen in Abhängigkeit von der Beladungsrate.

<sup>59</sup> G.I. Bell, *Science* **1978**, 200, 618-627.

<sup>60</sup> E. Evans, K. Ritchie, *Biophys. J.* **1997**, 72, 1541-1555.

Aus der Steigung der in Abbildung 32 gezeigten Auftragung können direkt Informationen über die molekulare Länge der Wechselwirkung erhalten werden. Die Werte sind in guter Übereinstimmung mit der Größe der beiden Ionen. Das Ammoniumion hat eine Wechselwirkungslänge von  $x_\beta = (0.22 \pm 0.04)$  nm bei einer Größe von 0.3 nm. Das Trimethylammoniumion wechselwirkt auf einer Länge von  $x_\beta = (0.38 \pm 0.06)$  nm bei einer Größe von 0.6 nm. Dieser Wert zeigt, dass das Ion nicht in vollem Umfang in die Kavität eingebaut werden kann.

Durch Extrapolation der Abrisskräfte gegen Null, werden für die Off-Raten der Ammonium- und Trimethylammoniumionen Werte von  $k_{\text{off}} = 0.99 \text{ s}^{-1}$  und  $0.0187 \text{ s}^{-1}$  erhalten. Daraus ergeben sich für die jeweiligen Komplexe Lebenszeiten von  $\tau = 1.01 \text{ s}$  und  $53.5 \text{ s}$ . Unter der Annahme einer diffusionskontrollierten On-Rate von  $k_{\text{on}} = 10^5 \text{ M}^{-1}\text{s}^{-1}$  kann die Gleichgewichtskonstante ( $K_{\text{diss}} = k_{\text{off}}/k_{\text{on}}$ ) der Komplexbildung berechnet werden.<sup>61</sup> Die Freie Energie ist damit nach  $\Delta G = -RT \ln K_{\text{diss}}$  für das Ammoniumion -28 kJ/mol und für das Trimethylammoniumion -38 kJ/mol. Diese Werte sind in guter Übereinstimmung mit Freien Energien, die aus kalorimetrischen Messungen oder NMR-Titrationen für ähnliche Systeme, wie etwa Cyclodextrine<sup>62</sup> oder wasserlösliche Cavitanden,<sup>63</sup> bestimmt worden sind.

### 3 Zusammenfassung und Ausblick

Im Rahmen der vorliegenden Arbeit wurden Untersuchungen zu einer Reihe von Komplexierungs- und Selbstorganisationsphänomenen von Octahydroxypyridin[4]arenen und anderen funktionalisierten Resorc[4]arenen durchgeführt.

Ziel der ersten Syntheseversuche der Octahydroxypyridin[4]arene war die direkte Darstellung eines Resorcarendervats, das bereits im Grundkörper ein Donor-Akzeptor-Motiv am *Oberen Rand* des Kelches besitzt. Dieses sollte dem Molekül die reversible Ringerweiterung über Wasserstoffbrücken mit geeigneten Komplexpartnern ermöglichen. Die Selbstkomplementarität dieser Moleküle ermöglicht aber auch deren direkte Dimerisierung. Dies konnte sowohl in Lösung als

<sup>61</sup> F. Schwesinger, R. Ros, T. Strunz, D. Anselmetti, P. Wagner, M. Dreier, W. Huber, H.-J. Güntherodt, *Biophys. J.* **1996**, *70*, 2437-2441.

<sup>62</sup> L.A. Godinez, L. Schwartz, C.M. Criss, A.E. Kaifer, *J. Phys. Chem.* **1997**, *101*, 3376-3380.

<sup>63</sup> T. Haino, D.M. Rudkevich, A. Shivanyuk, K. Rissanen, J. Rebek, *Chem. Eur. J.* **2000**, *6*, 3797-3805.

auch in der Gasphase nachgewiesen werden. Das Dimer eröffnet die Möglichkeit zum reversiblen Einschluss von Gastmolekülen in den gebildeten Hohlraum. Als erste Beispiele hierfür wurden Carbonsäuren und einige ihrer Derivate untersucht. Gestützt werden diese Ergebnisse durch theoretische Methoden. Solche Berechnungen könnten in Zukunft die Grundlage für die Entwicklung neuer Wirt-Gast-Systeme, nicht nur auf Basis der Pyridinarene, bilden und somit ein rein intuitives „Ausprobieren“ weitgehend erübrigen.

Erste Versuche zur reversiblen Ringerweiterung der Pyridinarene durch Naphthyridinderivate waren nicht erfolgreich. Stattdessen wurde ein nicht minder interessantes, gelartiges System erhalten. Durch rheologische und elektronenmikroskopische Methoden wurden Informationen über die Struktur des Gels erhalten. So konnten langgestreckte, faserförmige Aggregate für seinen Aufbau verantwortlich gemacht werden. Zeitaufgelöste Lichtstreuungsexperimente ermöglichen die Beobachtung des Wachstums der gelbildenden Strukturen. Über die Wechselwirkungen auf molekularer Ebene kann allerdings nur spekuliert werden. Nach dem Konzept von JORGENSEN<sup>64</sup> stellt die Ausbildung eines AAD-DDA-Motivs zwischen dem Pyridinaren **2** in seiner tautomeren Pyridonform und dem Naphthyridin **7** einen möglichen Erklärungsansatz dar. Aber auch die Amidfunktion in 3-Position des Naphthyridins **7** erlaubt eine weitere Quervernetzung über Wasserstoffbrücken.

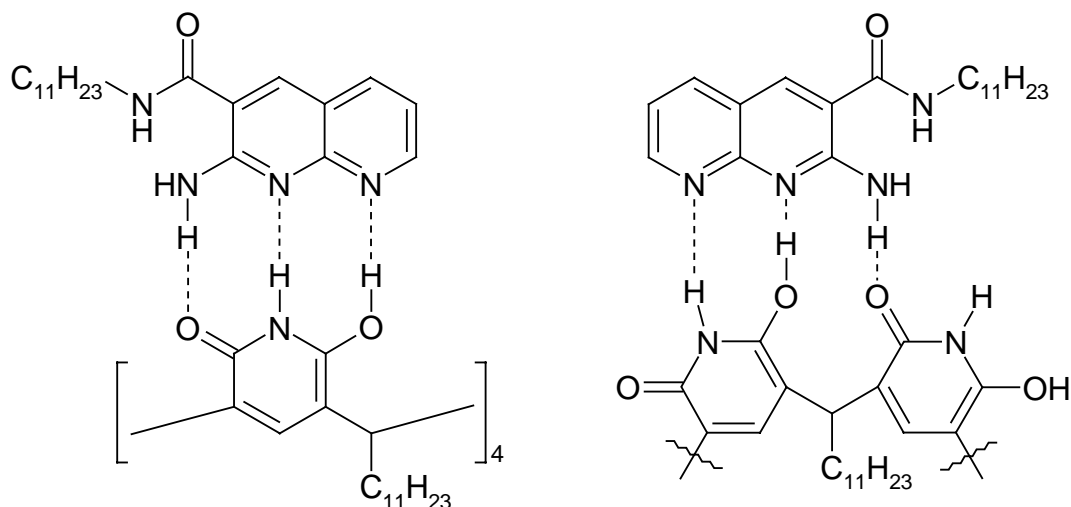


**Abbildung 33:** Mögliche ausgebildete Wasserstoffbrücken zwischen **2** und **7**.

<sup>64</sup> W.T. Jorgensen, J. Pranant, *J. Am. Chem. Soc.* **1990**, 112, 2008-2010.

Es wurde eine Reihe von Sulfidfunktionalisierten Resorc[4]arenen mit der Zielsetzung verschiedener physikalischer Anwendungen auf Oberflächen synthetisiert. Das Octaiodid **8** eignet sich zur Herstellung von monomolekularen Schichten auf Gold. Solche SAMs konnten eindeutig charakterisiert und hinsichtlich ihres Potentials für zeitaufgelöste ESCA-Experimente untersucht werden. Die Abstraktion der Iodmarkeratome hat sich dabei als geeignetes System erwiesen. Durch einen UV-Laserpuls können die Iodatome unter Erhalt des Resorcarenengerüsts selektiv entfernt werden. Die Aufbringung auf Goldsubstrate hingegen ist nicht optimal. Der Multiphotonenuntergrund des Goldes erlaubt keine zeitliche Auflösung der Experimente, da die herausgeschlagenen Elektronen sich energetisch mit den beobachteten 4d-Elektronen des Iods überlagern. Verbesserungen könnten hier durch andere Sondenatome wie beispielsweise Natrium, Arsen oder Selen erzielt werden. Dies wäre allerdings mit aufwendigen Modifikationen an der fs-ESCA-Apparatur verbunden. Die Beschichtung von Siliziumsubstraten könnte eine weitere Alternative darstellen. Silizium ist für die Herstellung von großflächigen Monoschichten gut untersucht,<sup>65</sup> und der störende Multiphotonenuntergrund könnte minimiert werden. Aktuelle Arbeiten beschäftigen sich mit der Entwicklung neuer photoschaltbarer Systeme auf Anthracenbasis,<sup>66</sup> die auch in Kürze auf Oberflächen übertragbar sein sollten.

Durch Kraftspektroskopie-Experimente konnte die nicht-kovalente Wechselwirkung zwischen der Kavität und drei verschiedenen Ammoniumionen auf der Ebene einzelner Moleküle untersucht werden. Im Rahmen dieser Arbeit ist es erstmals gelungen, auf Basis solcher Messungen, thermodynamische Daten für ein nicht biologisches, chemisch synthetisiertes Wirt-Gast-System zu erhalten. In Zukunft sollen aufwendigere homo- und heterodimere Resorcarenenkapseln untersucht werden. Als Vorbilder könnten hier die oben diskutierten Systeme von Kobayashi oder Sherman dienen. Für die Anbindung auf Goldsubstrate und über den PEG-Linker an die AFM-Spitze müssen die entsprechenden Resorcarene am *Unteren Rand* mit Sulfid- und Thiolgruppen funktionalisiert werden.

---

<sup>65</sup> J.M. Buriak, *Chem. Rev.* **2002**, 102, 1271-1308.

<sup>66</sup> C. Schäfer, J. Mattay, *Photochem. Photobiol. Sci.* **2004**, 331-333.

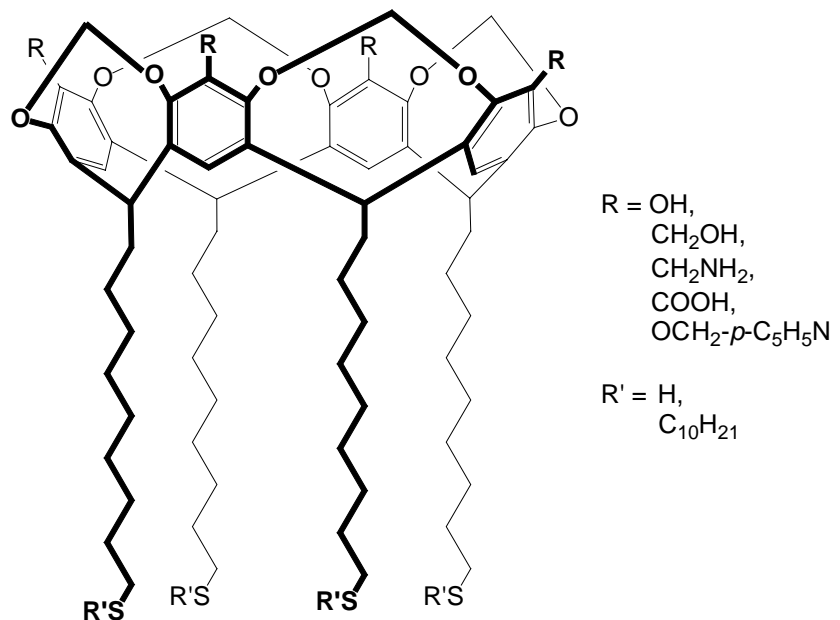


**Abbildung 34:** Beispiele synthetisierter Resorc[4]arene für zukünftige Einzelmolekülkraftspektroskopische Experimente.

In Abbildung 34 sind einige, noch nicht veröffentlichte, aber im Rahmen dieser Arbeit bereits synthetisierte, Moleküle abgebildet, die für solche Experimente in Frage kommen. Sie bilden die Basis für erste kraftspektroskopische Untersuchungen von selbstorganisierten Kapseln. Interessante Fragestellungen sind hier neben den auftretenden Kräften und der Übertragbarkeit auf bereits durch andere Methoden, wie beispielsweise NMR oder Kalorimetrie, erhaltene thermodynamische Daten, aber auch der Einfluss potentieller Komplexpartner.

## 4 Summary

The design of organic compounds that form defined structures through noncovalent association is important for the development of new molecules for information storage, catalysis, molecular transport, sensing, and the assembly of self organized structures. Calixarenes and modified calixarene systems are widely used modules in supramolecular chemistry. This interest is based on their easy generation, multiple modification facilities, and rigidity.

A new type of calix[4]arenes has been synthesized via condensation of 2,6-dihydroxypyridine and a number of aldehydes under acidic conditions. These octahydroxypyridine[4]arenes feature a donor-acceptor substitution pattern which is expected to promote self-organization processes comparable to uracil derivatives.

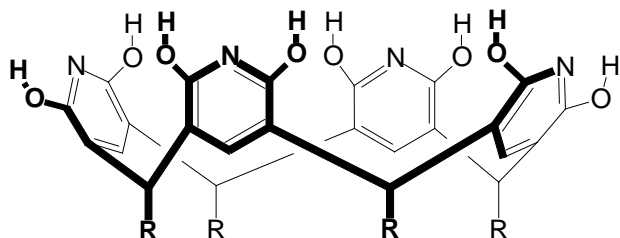


**Figure 1:** 2,6,8,12,14,18,20,24-Octahydroxy-4,10,16,22-tetra-R-pyridine[4]arene.

The self-complementary pyridinearenes show the formation of dimeric species. Their association was investigated by NMR spectroscopy, ESI mass spectrometry and VPO (vapour pressure osmometry). In chloroform-d<sub>1</sub> an association constant  $k_a = (146 \pm 8) \text{ M}^{-1}$  was determined. The capsules form a cavity which can incorporate various guest molecules, like carboxylic acids and amides. Complexation was observed by ESI FT-ICR mass spectra. Small acids as formic or acetic acid are incorporated into the cavity. Using homologous carboxylic acids of different size leads to the conclusion that there is only room for small variations. Acids that are more bulky than propionic acid are not incorporated in the capsule anymore. In solution the complexation of trifluoro acetic acid (TFA) was followed by <sup>19</sup>F NMR spectroscopy. Incorporated TFA shows an additional upfielded signal compared to the spectrum of pure TFA. The intensity of these signals is low due to the low concentration of the complex. With higher TFA concentrations all dimeric or complex species are destroyed.

Octahydroxypyridine[4]arenes are capable of mediating the self-assembly of gold nanoparticles at the aqueous interface. Their efficacy depends on the presence of associative electrolytes such as sodium chloride or citrate prior to nanoparticle extraction. Pyridinearenes extract colloidal gold nanoparticles in the presence of minimal electrolyte to the organic layer. Encapsulated particles could be transferred onto carbon-coated copper grids, and self-assembly of 2D-arrays was observed. At higher electrolyte concentrations nanoparticles remain suspended in the aqueous solution.

In apolar media the formation of gel-like aggregates of an octahydroxypyridine[4]arene and 2-aminonaphthyridine at a ratio of 1:4 was observed. This viscous liquid was investigated by means of rheology and TEM techniques. It shows shear thinning and thixotropic features, and is thermoreversible. The ratio of the components plays an important role. Only low viscosity is observed, if ratios other than 1:4 are applied. Freeze fracture TEM allows to display the topology of a surface generated by fracture and controlled sublimation of a matrix like water or suitable organic solvents from a solid specimen at adequate low temperatures. TEM electron micrographs show periodical linear structures with unit distances of 5 nm. The gel-like structure itself was not revealed in the TEM probably for reasons of segregation phenomena which covered most of the records. The aggregation process was followed by means of time-resolved multiangle light scattering, yielding a detailed record of the relative mass, the radius of gyration, and the particle scattering function of the growing aggregates. On the basis of these data, the polycondensation of ABC monomers towards non-randomly branched macromolecules could be proposed as a conclusive model for the developing aggregates. Monomers aggregate to fiber-like filaments, which form branching points. Each branching point initiates the growth of at least two other filaments. Thus, aggregation results to hyperbranched particles with striking analogies to the polymerization of glucose to amylopectin.

Various at the *lower rim* sulphide and thiol functionalized resorcarenes have been synthesized for the preparation of self-assembled monolayer films on gold substrates. Additional iodobenzoyloxy functionalization at the *upper rim* leads to molecules suitable as model systems for future time-resolved ESCA studies of molecular recognition processes. SAMs were prepared by immersing the substrates into a 1 mM solution of the resorcarene in ethanol/chloroform (7/3) for 16 h at 60 °C. Characterization by X-ray photoelectron spectroscopy, atomic force microscopy of

UV-microstructured templates and ellipsometry indicates a densely packed monolayer film with the iodobenzoyloxy groups pointing away from the surface. ESCA on the prepared templates is feasible and provides sufficient statistical accuracy. Data acquired on different positions of the substrate do not reveal any changes and thus support the homogenous preparation over several cm<sup>2</sup>. The spectral signature of the iodine marker atoms attached to the resorcarenne is clearly discernible and completely vanishes upon illumination of the film with ultraviolet radiation. In future experiments the spectral signature of selected marker atoms attached to the host (or guest) molecules can now be used to study chemical shifts as a transient probe of the local environment at the guest-host interface when a bond to a guest is formed, breaks apart or transforms in other ways in response to a photoexcitation event.

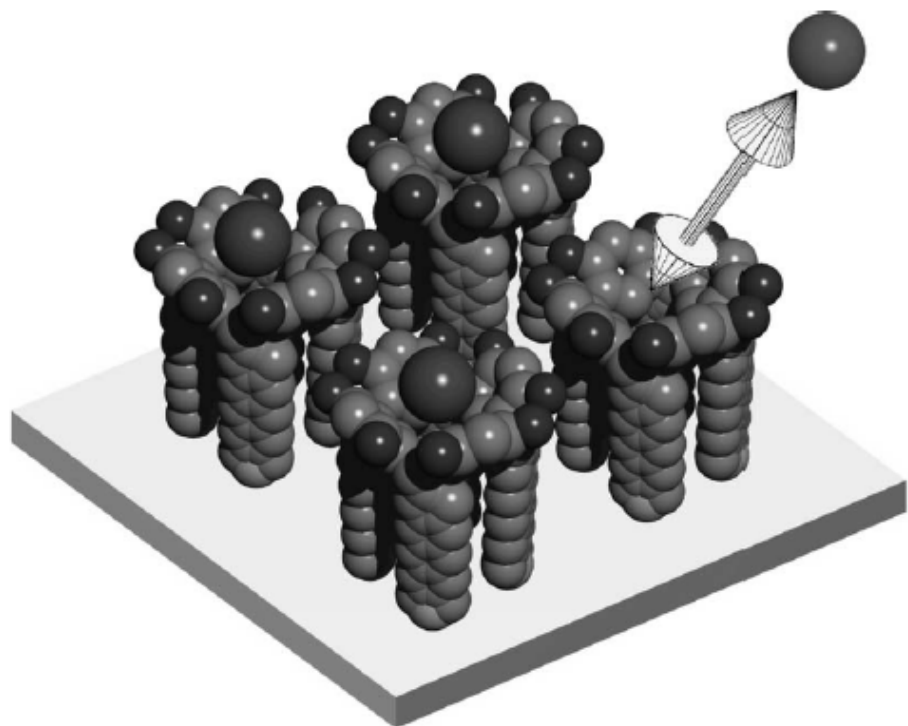


**Figure 2:** Schematic drawing of resorc[4]arene-guest interaction on a surface.

In supramolecular chemistry synthetically designed organic constituents interact non-covalently in a direct and specific way to host-guest complexes of higher complexity. The individual binding of three different ammonium ions to cavitand host molecules was investigated by mechanical single molecule force spectroscopy. This method records the deflection of an atomic force microscope cantilever to measure minute forces in the pico-Newton range under physiological conditions. The guest binding ions (ammonium, trimethyl ammonium and triethyl ammonium, carrying one chemically modified entity each) were covalently attached to the AFM tip via a flexible

polyethylene glycol linker. Diluted cavitand monolayers were prepared on gold substrates using 1:40 mixtures of at the *lower rim* sulphide functionalized cavitands and didecylsulphide. Single molecular unbinding events were observed by approaching to and retracting the functionalized AFM tip from the cavitand surface in ethanol. As a control experiment to validate the specificity of the host-guest interaction, free ammonium, tetramethyl ammonium and tetraethyl ammonium ions were added to the solvent as competing ligands. The ammonium and trimethyl ammonium residues show a specific interaction with the cavity. For the triethyl ammonium residue the behaviour is different. Its total unbinding probability is much lower, and it does not interact with the cavity in a specific way. This correlates with the fact that the triethyl ammonium residue with a calculated diameter of 0.8 nm does exceed the receptor cavity. According to the thermally driven unbinding theory the loading rate can be calculated from the experimental data. In dynamic force spectroscopy (force loading rate plots) details about the kinetics of the binding and information of concerning the length scale of the interaction can be extracted. This results to thermal off-rates, yielding  $k_{\text{off}} = (0.99 \pm 0.81) \text{ s}^{-1}$  for the ammonium and  $k_{\text{off}} = (1.87 \pm 0.75) \times 10^{-2} \text{ s}^{-1}$  for the trimethyl ammonium residue. This finding indicates that the trimethyl ammonium residue fits tighter into the receptor cavity, ensuring a rise in binding affinity as compared to ammonium. Assuming a diffusion limited association with a typical on-rate of  $k_{\text{on}} = 10^5 \text{ M}^{-1}\text{s}^{-1}$ , the equilibrium constants can be deduced, resulting to the Gibbs' free energy of  $\Delta G = -28 \text{ kJ mol}^{-1}$  for the ammonium and  $\Delta G = -38 \text{ kJ mol}^{-1}$  for the trimethyl ammonium residue, respectively. These values correspond well with calorimetric or NMR data obtained for related supramolecular systems such as cyclodextrins and water soluble cavitands. Another parameter resulting from the experimental data is the molecular length (depth of the binding pocket) of the interaction between the cavity and the corresponding ammonium residue. Values yielding  $x_\beta = (0.22 \pm 0.04) \text{ nm}$  for ammonium, and  $x_\beta = (0.38 \pm 0.06) \text{ nm}$  for trimethyl ammonium ions were extracted. These values qualitatively scale with calculated van-der-Waals diameters of 0.3 nm and 0.6 nm for the ions. This work is the first example to estimate equilibration constants and related binding energies of self-organized, chemically designed single supramolecular complexes by force spectroscopic methods. The measured single molecule kinetic reaction rates are consistent with the expected nature of a moderate-affinity guest-host interaction, whereas a clear affinity ranking between the probed host ligands was possible.

## 5 Anhang Publikationen

- A1** *Encapsulated Guest Molecules in Dimers of Octahydroxypyridine[4]arenes*  
M.C. Letzel, B. Decker, A.B. Rozhenko, W.W. Schoeller, J. Mattay, *J. Am. Chem. Soc.* **2004**, 126, 9669-9674.
- A2** *Self-Assembly of Resorcinarene-Stabilized Gold Nanoparticles: Influence of the Macroyclic Headgroup*  
B. Kim, R. Balasubramanian, W. Perez-Segarra, B. Decker, J. Mattay, A. Wei, *Supramol. Chem.* **2005**, 17, 173-180.
- A3** *Formation of Gel-Like Systems of an 2,6,8,12,14,18,20,24-Octahydroxypyridine[4]arene and an 2-Aminonaphthyridine*  
T. Gerkensmeier, B. Decker, M. Schwertfeger, W. Buchheim, J. Mattay, *Eur. J. Org. Chem.* **2002**, 2120-2125.
- A4** *Formation of Branched Calixarene-Aggregates – A Time Resolved Static Light Scattering Studie*  
T. Witte, B. Decker, J. Mattay, K. Huber, *J. Am. Chem. Soc.* **2004**, 126, 9276-9282.
- A5** *Large-Scale homogenous molecular templates for femtosecond timeresolved studies of the guest-host interaction*  
P. Siffalovic, M. Michelswirth, P. Bartz, B. Decker, C. Agena, C. Schäfer, S. Molter, R. Ros, M. Bach, M. Neumann, D. Anselmetti, J. Mattay, U. Heinzmann, M. Drescher, *J. Biotech.* **2004**, 112, 139-149.
- A6** *Calixarenes as Hosts for Ammonium Cations. A quantum chemical Study*  
A.B. Rozhenko, W.W. Schoeller, M.C. Letzel, B. Decker, C. Agena, J. Mattay, *J. Phys. Chem.* **2005**, eingereicht.
- A7** *Features of conformations of resorc[4]arenes with alkali metal ions. A quantum chemical investigation with density functional theory*  
A.B. Rozhenko, W.W. Schoeller, M.C. Letzel, B. Decker, C. Agena, J. Mattay, *Theo. Chem.* **2005**, 7-20.
- A8** *Supramolecular Chemistry at the Single Molecule Level*  
R. Eckel, R. Ros, B. Decker, C. Agena, J. Mattay, D. Anselmetti, *Angew. Chem.* **2005**, 117, 489-492; *Angew. Chem., Int. Ed. Engl.* **2005**, 44, 484-488.

## Encapsulated Guest Molecules in the Dimer of Octahydroxypyridine[4]arene

Matthias C. Letzel, Björn Decker, Alexander B. Rozhenko,  
Wolfgang W. Schoeller, and Jochen Mattay\*

*Contribution from the Fakultät für Chemie, Universität Bielefeld,  
Postfach 100131, 33501 Bielefeld, Germany*

Received February 17, 2004; E-mail: mattay@uni-bielefeld.de

**Abstract:** Recently a new type of calix[4]arenes has been synthesized via condensation of 2,6-dihydroxypyridine and a number of aldehydes. This type of pyridine[4]arenes forms capsules consisting of two single pyridine[4]arenes. These capsules can incorporate different guest molecules, like carboxylic acids and amides in this case. We proved that the guest acids really are incorporated inside the cavity of the capsules by electrospray mass spectrometry, NMR spectroscopy, and theoretical calculations.

### Introduction

2,6,8,12,14,18,20,24-Octahydroxypyridine[4]arenes were first synthesized in our group by direct acidic condensation of 2,6-dihydroxypyridine with several aliphatic and aromatic aldehydes.<sup>1</sup> Pyridine containing calixarenes have been prepared before using alternative multistep pathways.<sup>2–4</sup> But these calixarenes feature neither hydroxy groups nor substituents at the stereogenic methine center. The substitution pattern of our 2,6,8,12,14,18,20,24-octahydroxypyridine[4]arenes is expected to promote self-organization processes comparable to those of uracil derivatives if complementary molecules are present. In addition new host–guest complexes may be available by complexation of metal cations and anions as well. Both fields of research are currently under investigation.<sup>5–8</sup>

As the very first example of a hydrogen-bonded capsule, Rebek's so-called tennis ball was reported in 1993.<sup>9</sup> In the following years calixarenes and modified calixarene systems attracted great interest concerning their aggregation and self-assembling behavior. This interest is based on their easy generation, multiple modification facilities, and rigidity. Numerous hydrogen-bonded capsules have been reported in recent years.<sup>10,11</sup> Calixarenes based on self-complementary glycoluril building blocks,<sup>12</sup> urea functions,<sup>13,14</sup> and imide-bridged<sup>15</sup> or  $C_{2v}$ -symmetric derived resorcarenes<sup>16</sup> show the formation of dimeric structures. Alanine-functionalized calix[4]arenes dimerize even

in polar, protic solvents.<sup>17</sup> With suitable guests, unsubstituted resorc[4]arenes show the formation of dimeric<sup>18</sup> but also hexameric<sup>5,19,20</sup> molecular containers. Due to their structural features, resorc[4]arenes play an important role as host molecules for a variety of neutral and charged guest compounds.

Since its invention electrospray ionization (ESI) became the most powerful tool in mass spectrometry for the examination of charged host–guest compounds. By desolvating ions from solution it is expected that most of the analyte structural features are transferred into the gas-phase giving a close approximation to the solution state.

So far, ESI–MS has mainly been used in calixarene chemistry simply as an analytical method to control the result of a synthetic procedure. To our knowledge only a few investigations have been undertaken concerning the analysis of host–guest complexes with calixarenes using ESI–MS; among them are binding selectivities of alkali metal ions,<sup>21–23</sup> gas-phase inclusion of

- (1) Gerkenmeier, T.; Näther, C.; Mattay, J. *Chem. Eur. J.* **2001**, *7*, 465–474.
- (2) Newcome, G. R.; Joo, J. Y.; Frontzek, F. R. *J. Chem. Soc., Chem. Commun.* **1987**, 854–856.
- (3) Kral, V.; Gale, P. A.; Anzenbacher, P.; Jursikova, K.; Lynch, V.; Sessler, J. L. *J. Chem. Soc., Chem. Commun.* **1998**, 9–10.
- (4) Kral, V.; Sessler, J. L.; Wolf, P. A.; Wolf, R.; Shishkanova, T. V. *J. Am. Chem. Soc.* **1999**, *121*, 8771–8775.
- (5) Gerkenmeier, T.; Agena, C.; Iwanek, W.; Fröhlich, R.; Kotila, S.; Näther, C.; Mattay, J. *Eur. J. Org. Chem.* **1999**, 2257–2262.
- (6) Agena, C.; Wolff, C.; Mattay, J. *Eur. J. Org. Chem.* **2001**, *15*, 2977–2981.
- (7) Letzel, M. C.; Agena, C.; Mattay, J. *Eur. J. Mass Spectrom.* **2001**, *7*, 35–38.
- (8) Letzel, M. C.; Agena, C.; Mattay, J. *J. Mass Spectrom.* **2002**, *37*, 63–68.
- (9) Wyler, R.; de Mendoza, J.; Rebek, J. *Angew. Chem.* **1993**, *105*, 1820–1821; *Angew. Chem., Int. Ed. Engl.* **1993**, *32*, 1699–1701.
- (10) Rebek, J. *Chem. Commun.* **2000**, 637–643. Vysotsky, M. O.; Böhmer, V. *Aust. J. Chem.* **2001**, *54*, 671–677.
- (11) Hof, F.; Craig, S. L.; Nuckolls, C.; Rebek, J., Jr. *Angew. Chem.* **2002**, *114*, 1556–1578; *Angew. Chem., Int. Ed.* **2002**, *41*, 1488–1508 and references therein.
- (12) O'Leary, B. M.; Szabo, T.; Svenstrup, N.; Schalley, C. A.; Lützen, A.; Schäfer, M.; Rebek, J. *J. Am. Chem. Soc.* **2001**, *123*, 11519–11533.
- (13) Mogck, O.; Böhmer, V.; Vogt, W. *Tetrahedron* **1996**, *52*, 8489–8496. Frish, L.; Vysotsky, M. O.; Matthews, S. E.; Böhmer, V.; Cohen, Y. *J. Chem. Soc., Perkin Trans. 2*, **2002**, 88–93.
- (14) Scheerder, J.; van Duynhoven, J. P. M.; Engbersen, J. F. J.; Reinhoudt, D. N. *Angew. Chem.* **1996**, *108*, 1172–1175; *Angew. Chem., Int. Ed. Engl.* **1996**, *35*, 1090–1093.
- (15) Heinz, T.; Rudkevich, D. M.; Rebek, J. *Nature* **1998**, *394*, 764–766.
- (16) Shivanyuk, A.; Paulus, E.; Böhmer, V. *Angew. Chem.* **1999**, *111*, 3091–3094.
- (17) Brewster, R. E.; Shuker, S. B. *J. Am. Chem. Soc.* **2002**, *124*, 7902–7903.
- (18) Murayama, K.; Aoki, K. *Chem. Commun.* **1998**, 607–608. Shivanyuk, A.; Rebek, J. *Chem. Commun.* **2001**, 2374–2375.
- (19) Shivanyuk, A.; Rebek, J. *Proc. Natl. Acad. Sci. U.S.A.* **2001**, *98*, 7662–7665.
- (20) McGillivray, R. L.; Atwood, J. L. *Nature* **1997**, *389*, 469–472.
- (21) Blanda, M. T.; Farmer, D. B.; Brodbelt, J. S.; Goolsby, B. J. *J. Am. Chem. Soc.* **2000**, *122*, 1486–1491.
- (22) Goolsby, B. J.; Brodbelt, J. S.; Adou, E.; Blanda, M. *Int. J. Mass Spectrom.* **1999**, *193*, 197–204.
- (23) Allain, F.; Virelizier, H.; Moulin, C.; Jankowski, C. K.; Dozol, J. F.; Tabet, J. C. *Spectroscopy* **2000**, *14*, 127–139.

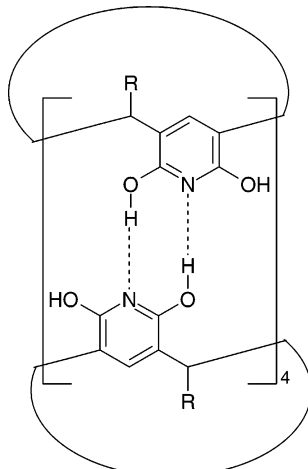


**Figure 1.** Pyridine[4]arene dimer  $[C \bullet C]$  (with  $R = C_{11}H_{23}$ ) and  $[C' \bullet C']$  (with  $R = H$  for calculated structures, Table 2).

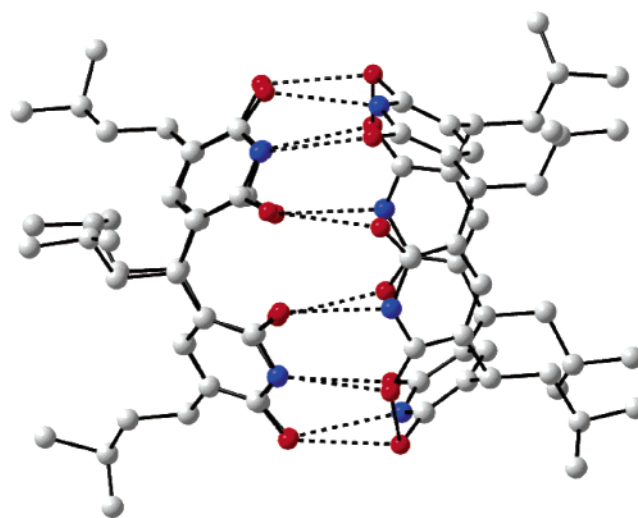


**Figure 2.** Dimer of octacydroxy-tetra-*iso*-butyl-pyridine[4]arene in the crystal structure.

neutral molecules,<sup>24</sup> and inclusion of alkylammonium ions in calixarene capsules.<sup>25–27</sup>

## Results and Discussion

**Mass Spectrometry.** Calix[4]arenes, like the one shown in Figure 1 (always called calixarene **C** in the following text), form stable dimers in the crystal structure (X-ray) as well as under electrospray conditions in the mass spectrometer. The crystal structure of the pyridine[4]arenes shows head–head dimers attracted by hydrogen bonding (Figure 2). These dimers form a cavity which may include molecules or ions if the guest fits into the cavity. This kind of guest incorporation can be observed in the ESI FT-ICR mass spectra (Figure 3). Other than the most abundant pseudomolecular ion  $[C + H]^+$ , the gas-phase dimer  $[C \bullet C + H]^+$  of the calixarene **C** is observed. The addition of small amounts of different carboxylic acids (Table 1) results in a partial incorporation of those acids into the cavity of the dimer,

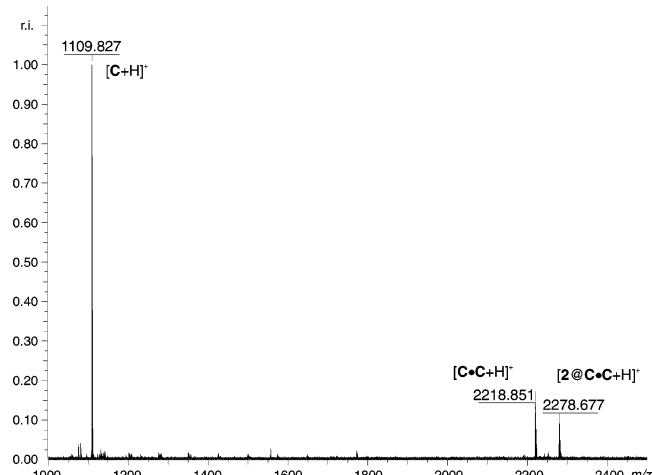


**Figure 3.** FT-ICR-MS (ESI) mass spectrum of pyridine[4]arene (**C**) with addition of 0.2% acetic acid (**2**).

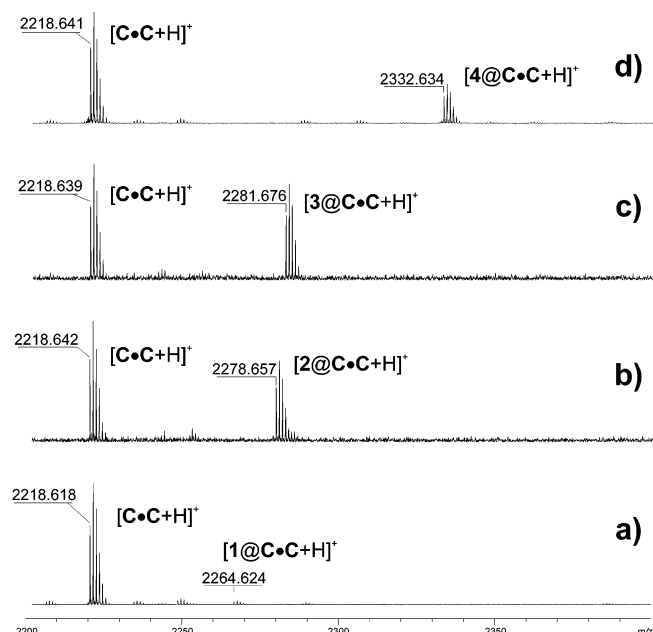


**Figure 4.** FT-ICR-MS (ESI) mass spectrum of dimer region with pyridine[4]arene (**C**) and different carboxylic acids (a) formic acid (**1**), (b) acetic acid (**2**), (c)  $d_3$ -acetic acid (**3**), and (d) trifluoroacetic acid (**4**).

as seen in Figures 3 and 4b for acetic acid, to yield  $[2@C \bullet C + H]^+$ . No adduct formation like  $[2@C + H]^+$  is observed with the monomeric species. We assume that the monomeric calixarene acid complex might not be stable enough to survive the ionization process intact. Therefore we assume that in the dimer the acid molecule is incorporated inside the calixarene cavity. If it were placed outside the cavity, we cannot see any reason this kind of complex should ride out the ionization process other than the monomer. When using homologous carboxylic acids of different size (Table 1), it turns out that there is only room for small variations: we also find incorporation of guests such as formic acid (**1**) (Figure 4a, very poor signal),  $d_4$ -acetic acid (**3**) (Figure 4c), trifluoro acetic acid (**4**) (Figure 4d), and propionic acid (**5**) (Figure 5e). Acids that are more bulky than propionic acid are not incorporated in the capsule anymore (Figure 5f–h). It can be observed that on higher acid concentrations the abundance of the dimer decreases or cannot be observed at all. This can be traced back to the fact that the acids are breaking the dimer's hydrogen bonds, cracking the dimers

(24) Nuutinen, J. M. J.; Irico, A.; Vincenti, M.; Dalcanale, E.; Pakarinen, J. M. H.; Vainiotalo, P. *J. Am. Chem. Soc.* **2000**, *122*, 10090–10100.

(25) Schalley, C. A.; Castellano, R. K.; Brody M. S.; Rudkevich, D. M.; Siuzdak, G.; Rebek, J., Jr. *J. Am. Chem. Soc.* **1999**, *121*, 4568–4579.

(26) Lippmann, T.; Wilde, H.; Pink, M.; Schäfer, A.; Hesse, M.; Mann, G. *Angew. Chem., Int. Ed. Engl.* **1993**, *32*, 1195–1197.

(27) Mansikkamäki, H.; Nissinen, M.; Schalley, C. A.; Rissanen, K. *New J. Chem.* **2003**, *27*, 88–97.

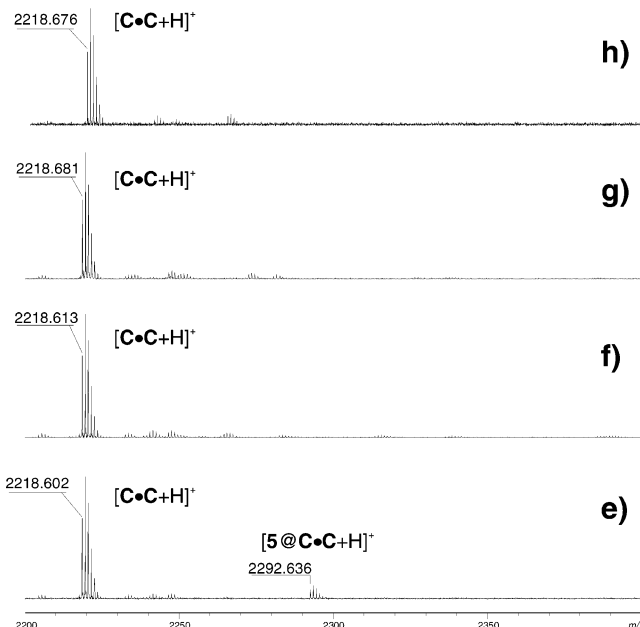


**Figure 5.** FT-ICR-MS (ESI) mass spectrum of dimer region with pyridine-[4]arene (**C**) and different carboxylic acids (e) propionic acid (**5**), (f) butyric acid (**6**), (g) 2-methyl butyric acid (**7**), and (h) 2,2-dimethyl butyric acid (**8**).

to monomers. This effect is also observed by  $^{19}\text{F}$  NMR spectroscopy.

So far we observed host–guest complexes with simple carboxylic acids in the ESI–MS. Therefore we first extended our investigation to a homologous row of different carboxylic acids to get an idea of the size limits of the cavity. Because of the problems arising from competition with the hydrogen bonding of the complex, as observed in the TFA NMR experiments (Figure 11), we also checked some amides (Table 1), which also were complexed quite well under ESI–MS conditions. Those amides were acetamide (**9**) (Figure 6a) and trifluoroacetamide (**10**) (Figure 6b), which were successfully incorporated. In Figure 6a beside the protonated dimer  $[\text{C} \cdot \text{C} + \text{H}]^+$  at  $m/z$  2218.6, also the sodiated dimer  $[\text{C} \cdot \text{C} + \text{Na}]^+$  at  $m/z$  2240.6 is observed. For the host–guest complex  $[\text{9} @ \text{C} \cdot \text{C} + \text{H}]^+$ , no corresponding sodiated species was detected. In our opinion the cavity of the sodiated dimer  $[\text{C} \cdot \text{C} + \text{Na}]^+$  is blocked by the sodium ion leaving no room for other guest molecules (Table 1). On the other hand the small proton might be located somewhere on one of the nitrogen atoms of the calixarene and is not able to block the cavity.

An MS/MS experiment with the complex  $[\text{2} @ \text{C} \cdot \text{C} + \text{H}]^+$  using excitation by infrared irradiation (IRMPD) was performed. Prior to the infrared irradiation, the parent ion  $[\text{2} @ \text{C} \cdot \text{C} + \text{H}]^+$  was isolated using a correlated sweep (Figure 7a). Infrared laser irradiation yields the monomeric fragment ion  $[\text{C} + \text{H}]^+$  and some dimer ion  $[\text{C} \cdot \text{C} + \text{H}]^+$  by loss of the guest (Figure 7b). This experiment supports our hypothesis that the complex of carboxylic acid and the monomeric pyridine[4]arene is not very stable and dissociates quickly after cleavage of the dimer complex. This might also be the case for a complex where the carboxylic acid is attached outside the dimer’s cavity as an ion molecule complex for a short time after irradiation.

We also performed some IRMPD experiments on  $[\text{10} @ \text{C} \cdot \text{C} + \text{H}]^+$  with the same results as observed for  $[\text{2} @ \text{C} \cdot \text{C} + \text{H}]^+$  (data not shown). Furthermore we were able to tune the laser

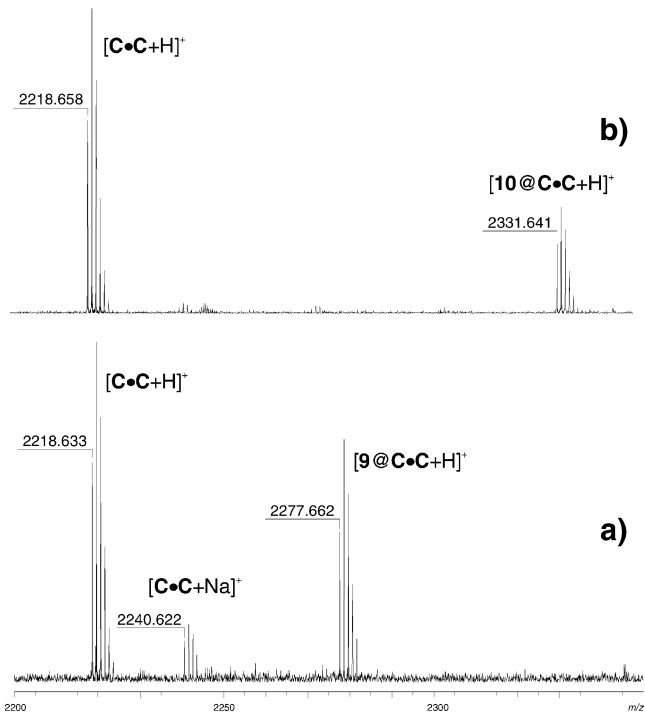


**Figure 6.** FT-ICR-MS (ESI) mass spectrum of dimer region with pyridine-[4]arene (**C**) and different carboxylic acid amides (a) acetamide (**9**) and (b) trifluoroacetamide (**10**). The signal in spectrum (a) at  $m/z$  2240.622 is the corresponding  $[\text{C} + \text{Na}]^+$  ion. Interestingly no sodium adduct is observed for the host–guest complex.

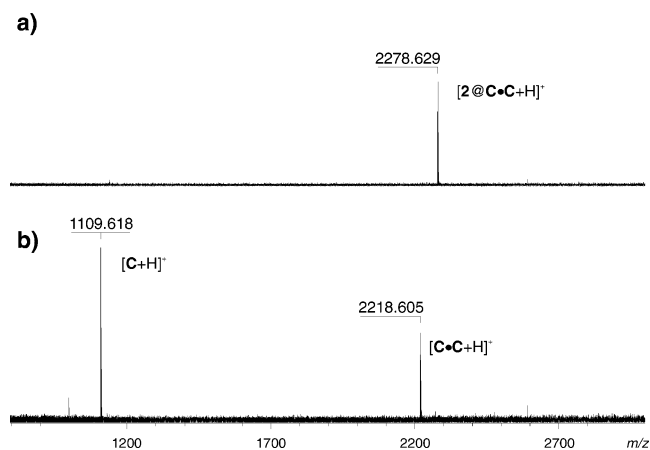


**Figure 7.** IRMPD experiment with acetic acid encapsulated in the dimer’s cavity  $[\text{2} @ \text{C} \cdot \text{C} + \text{H}]^+$ : (a) isolated  $[\text{2} @ \text{C} \cdot \text{C} + \text{H}]^+$  ion; (b) after IR irradiation (0.1 s): decomposition of the complex into the dimer  $[\text{C} \cdot \text{C} + \text{H}]^+$  without guest and the monomer  $[\text{C} + \text{H}]^+$  is observed.

**Table 1.** Guest Molecules Used in Complexation Experiments

no.	guest	no.	guest
<b>1</b>	HCOOH	<b>6</b>	$\text{CH}_3(\text{CH}_2)_2\text{—COOH}$
<b>2</b>	$\text{CH}_3\text{—COOH}$	<b>7</b>	$\text{CH}_3\text{—CH}_2\text{—CH}(\text{CH}_3)\text{—COOH}$
<b>3</b>	$\text{CD}_3\text{—COOH}$	<b>8</b>	$\text{CH}_3\text{—CH}_2\text{—C}(\text{CH}_3)_2\text{—COOH}$
<b>4</b>	$\text{CF}_3\text{—COOH}$	<b>9</b>	$\text{CH}_3\text{—CONH}_2$
<b>5</b>	$\text{CH}_3\text{—CH}_2\text{—COOH}$	<b>10</b>	$\text{CF}_3\text{—CONH}_2$

intensity in such a way that the capsule releases the guest **10** without further fragmentation to the monomer.

In summary of these results, the cavity of the pyridinearene capsule appears to be quite small, so that it is difficult to find other guest molecules that are not too volatile and fulfill the constraints given by the size of the cavity.

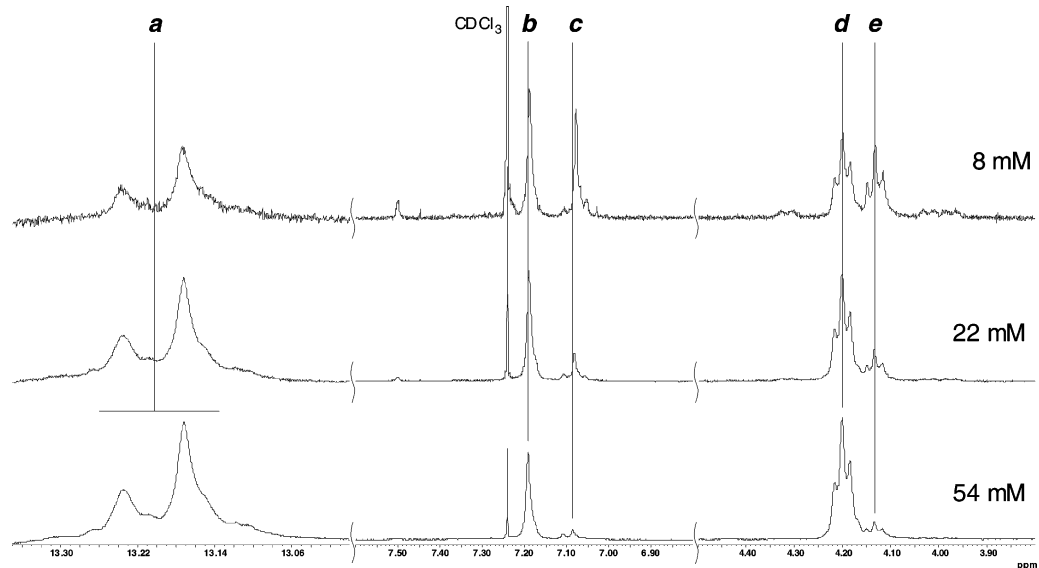


**Figure 8.**  $^1\text{H}$  NMR of the pyridine[4]arene in three different concentrations of 8, 22, and 54 mM in  $\text{CDCl}_3$ . Dimer signals are marked with **a** (H-bonding), **b** (aromatic proton), and **d** (methine proton). Monomer signals are marked with **c** (aromatic proton) and **e** (methine proton).

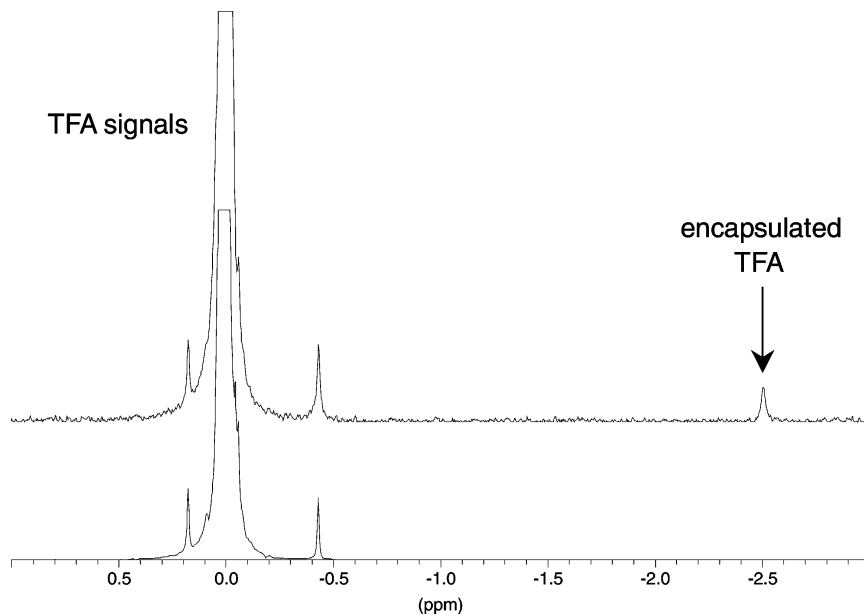


**Figure 9.**  $^{19}\text{F}$  NMR spectrum of pyridine[4]arene (**C**) (46 mM) with 30 (upper spectrum) and 160 mM (lower spectrum) TFA.

**NMR Spectroscopy.** The dimerization of pyridine[4]arenes can be followed by  $^1\text{H}$  and  $^{13}\text{C}$  NMR spectroscopy. At high concentrations (100 mM), only one set of signals is observed corresponding to the dimeric pyridine[4]arene. The  $^1\text{H}$  spectrum shows a singlet at 7.19 ppm for the aromatic protons (Figure 8, **b**) and a triplet at 4.20 ppm for the methine protons (Figure 8, **d**). The existence of H-bonding can be documented by a low-field signal at 13.1 ppm to 13.4 ppm (Figure 8, **a**) and another broad signal from 8.50 to 11.0 ppm.

The  $^{13}\text{C}$  spectrum shows only one set of signals for a  $C_4$ -symmetric species. These results indicate a dimeric structure built up by two pyridine[4]arenes twisted by  $30^\circ$  (Figure 1). The structure is already known from the crystal structure of the tetra-*iso*-butylpyridine[4]arene (Figure 2).<sup>1</sup>

With decreasing concentration, new sets of  $^1\text{H}$  and  $^{13}\text{C}$  signals arise for the monomeric species (Figure 8). The  $^1\text{H}$  spectrum shows two high field shifted signals for the aromatic protons (Figure 8, **c**) at 7.08 ppm and at 4.13 ppm for the methine

protons (Figure 8, **e**). The low field shifted dimer signals disappear with decreasing concentration. Hydroxy protons that are involved in H-bonding cannot be detected anymore. The  $^{13}\text{C}$  spectrum shows a change of symmetry from  $C_4$  to  $C_{4v}$ , indicating the existence of a monomer with perfect crown conformation. The same effect can be achieved by addition of polar additives to a highly concentrated solution of the pyridine[4]arene.

The association constant for the formation of dimeric pyridine[4]arenes was determined by  $^1\text{H}$  NMR spectroscopy, since the signals for the monomeric and dimeric species are separated and their actual concentrations could be calculated by direct integration (Figure 8).<sup>28</sup> Concentration-dependent measurements yield an association constant  $k_a = 146 \pm 8 \text{ M}^{-1}$  in chloroform.  $^1\text{H}$  NMR investigations in  $\text{CHCl}_3/\text{CDCl}_3$  give no indication for encapsulated chloroform molecules. Because

(28) Schneider, H.-J.; Yatsimirsky, A. *Principles and Methods in Supramolecular Chemistry*; Wiley: Chichester, 2000.

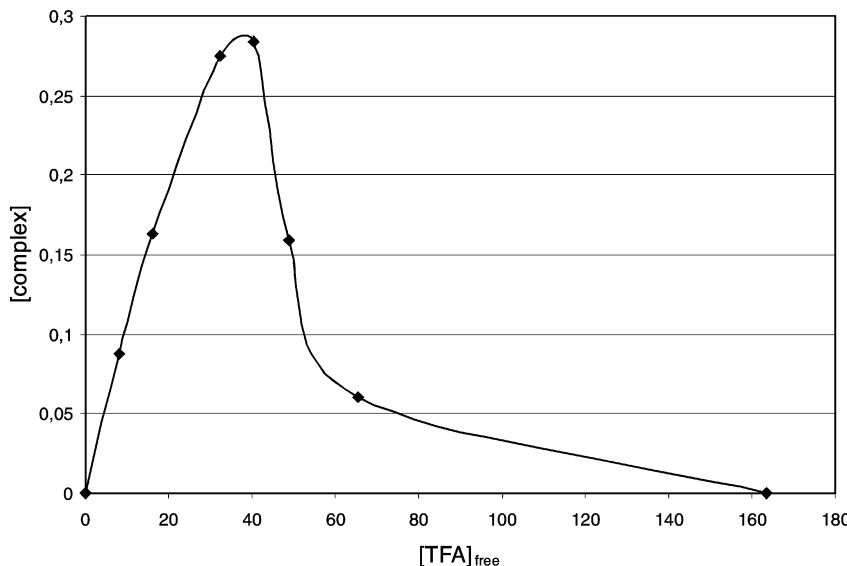


**Figure 10.** Complex formation (from  $^{19}\text{F}$  NMR integration) depending on the TFA concentration.

of its low solubility, the dimerization could not be studied in other solvents such as benzene or dichloromethane.

With further decreasing concentration, numerous new signals come up. These signals cannot be allocated to a certain species but might be the result of the tautomerism of the individual 2,6-dihydroxypyridine units.<sup>29–31</sup>

The complex studies with TFA were recorded at a constant pyridine[4]arene concentration of 46.7 mM in water-saturated deuterated chloroform. The TFA concentration was varied from 0 to 160 mM, and the complexation of TFA was confirmed by  $^{19}\text{F}$  NMR spectroscopy at 298 K.

For low TFA concentrations, the spectra exhibit an additional upfielded signal for complexed TFA compared to the spectrum of TFA in  $\text{CDCl}_3$  showing solely the typical singlet with its satellites (Figure 9). The exchange of TFA is slow compared to the  $^{19}\text{F}$  NMR time scale, and consequently the concentration of complexed TFA can be obtained by integration of the measured signals. The complex concentration is low compared to the concentration of free TFA.

For TFA concentrations up to 30 mM, a growing complex concentration is obtained. A maximum is reached for approximately 40 mM of TFA. With further growing acid concentration, the formation of dimers is decreased. In the same way the formation of the complex is reduced (Figure 10).

With higher TFA concentrations of about 150 mM, all dimeric or complex species are destroyed. Only the signal for free TFA can be detected in the  $^{19}\text{F}$  spectrum. In the  $^1\text{H}$  spectrum, the signals for the monomeric pyridine[4]arene (**C**) are observed and none for a dimer.

The  $^1\text{H}$  spectra exhibit the signals of the monomer and the dimeric species. New signals for the complex are not detected (data not shown). This may be the consequence of their low intensity compared to empty dimer or superposition of the dimer with the complex. Investigations with other complex partners such as ammonium or tropylium cations are still in progress.

**VPO Measurements.** VPO (Vapor Pressure Osmometry) experiments with the pyridine[4]arene (**C**) in chloroform lead

(29) Katritzky, A. R.; Popp, F. D.; Rowe, J. D. *J. Chem. Soc. B* **1966**, 562–564.

(30) Spinner, E.; White, J. C. B. *J. Chem. Soc. B* **1966**, 991–995.

(31) Spinner, E.; Yeoh, G. B. *Aust. J. Chem.* **1971**, 24, 2557–2573.

**Table 2.** Calculated Total Energy Values and  $\Delta E^2$  Values Calculated for Model Structures **11–20** and Free Acids

structure	complex	total charge <sup>a</sup>	total energy (dimers and complexes with acids), au	total energy (free guests), au	$\Delta E^2$ , kcal/mol
<b>11</b>	<b>C'·C'</b>	0	-3496.009 491		
<b>12</b>	<b>2@C'·C'</b>	0	-3725.163 598	-229.154 059	0.0
<b>13</b>	<b>3@C'·C'</b>	0	-3764.475 410	-268.479 463	8.5
<b>14</b>	<b>6@C'·C'</b>	0	-3803.781 566	-307.803 581	19.8
<b>15</b>	<b>7@C'·C'</b>	0	-3882.375 185	-386.448 154	51.7
<b>16</b>	<b>[C'·C' + H]<sup>+</sup></b>	+1	-3496.379 864		
<b>17</b>	<b>[2@C'·C' + H]<sup>+</sup></b>	+1	-3725.548 437	-229.154 059	-9.1
<b>18</b>	<b>[3@C'·C' + H]<sup>+</sup></b>	+1	-3764.858 193	-268.479 463	0.7
<b>19</b>	<b>[6@C'·C' + H]<sup>+</sup></b>	+1	-3804.152 474	-307.803 581	19.4
<b>20</b>	<b>[7@C'·C' + H]<sup>+</sup></b>	+1	-3882.764 320	-386.448 154	40.0

<sup>a</sup> Either the neutral capsules (total charge = 0) or the singly protonated form of the capsules (total charge = +1) were calculated. <sup>b</sup> Calculated at the B3LYP/6-311G\*\*//B3LYP/3-21G\* level of approximation without ZPE energy correction.

to an average molecular weight of  $2230 \pm 92$  g/mol. This agrees well with the theoretical mass of 2219 g/mol for the dimer. In THF, VPO measurements result in a lower average mass of  $1443 \pm 78$  g/mol. The more polar solvent should reduce the tendency of the formation of dimeric species. In this case, a mixture of monomers and dimers exists in solution.

**Theoretical Calculations.** The model structures **11–20** (Figure 1, R = H, Table 2) involving the model capsule **11** and its protonated form **16** as well as their aggregates with acids were investigated theoretically (with the GAUSSIAN-98 set of programs,<sup>32</sup> at the DFT (B3LYP<sup>33,34</sup>) level of approximation using the 3-21G\* standard Gaussian basis set for geometry optimization and the 6-311G\*\* standard Gaussian basis set for

(32) Frisch, M. J.; Trucks, G. W.; Schlegel, H. B.; Scuseria, G. E.; Robb, M. A.; Cheeseman, J. R.; Zakrzewski, V. G.; Montgomery, J. A.; Stratmann, R. E.; Burant, J. C.; Dapprich, S.; Millam, J. M.; Daniels, A. D.; Kudin, K. N.; Strain, M. C.; Farkas, O.; Tomasi, J.; Barone, V.; Cossi, M.; Cammi, R.; Mennucci, B.; Pernelli, C.; Adamo, C.; Clifford, S.; Ochterski, J.; Petersson, G. A.; Ayala, P. Y.; Cui, Q.; Morokuma, K.; Malick, D. K.; Rabuck, A. D.; Raghavachari, K.; Foresman, J. B.; Cioslowski, J.; Ortiz, J. V.; Stefov, B. B.; Liu, C.; Liashenko, A.; Piskorz, P.; Komaromi, I.; Gomperts, R.; Martin, R. L.; Fox, D. J.; Keith, T.; Al-Laham, M. A.; Peng, C. Y.; Nanayakkara, A.; Gonzalez, C.; Challacombe, M.; Gill, P. M. W.; Johnson, B. G.; Chem, W.; Wong, M. W.; Andres, J. L.; Head-Gordon, M.; Replogle, E. S.; Pople, J. A. *Gaussian* 98, revision A.1; Gaussian, Inc.: Pittsburgh, PA, 1998.

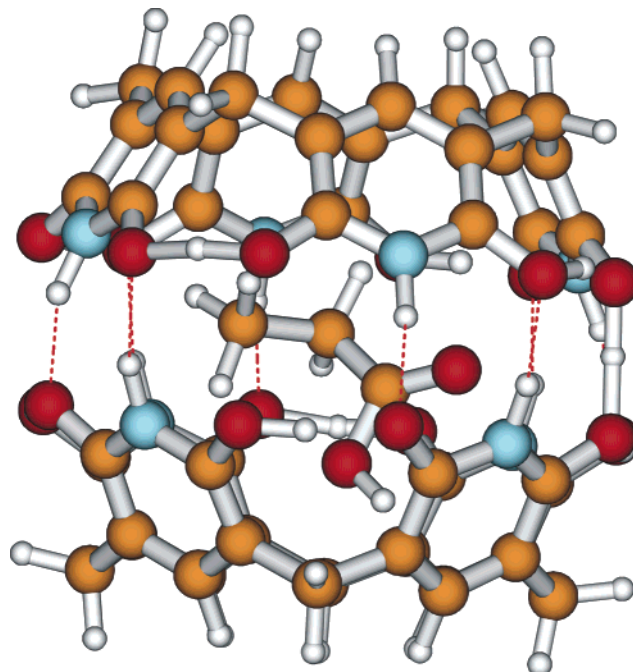


**Figure 11.** Calculated structure of  $3@C' \cdot C'$  (Table 2, structure 13).

the single-point energy calculation). As the calculated capsule structures differ significantly from the species investigated experimentally and due to the relatively low level of approximation by geometry optimization, one could hardly expect a quantitative agreement with the experimental data discussed above. Nevertheless, our calculations predict a high exothermic effect for reaction 1, where the dimer is formed from two pyridine[4]arene molecules.

The encapsulated acid is rigidly fixed and a large number of conformers are feasible. To take care of this aspect, a number of different starting structures were selected which differ by the conformation of the acid molecule, its orientation relative to the aromatic rings, and (in case of the protonated capsules) the protonation sites. All of these varieties were tested until no further lowering of the calculated total energy was achieved. Nevertheless, we cannot completely exclude the existence of other conformations with lower total energies. As we have found, the lowest total energies possess the conformations with the acid molecule lying approximately between the two pyridine[4]arene cavities. An increase of the alkyl substituent's size forces the alkyl chain of the guest molecule to be twisted still lying in this restricted volume of the cavity (see for example structure 13, Figure 11). The electronegative oxygen atoms are oriented between the electron-rich pyridine rings.



As one can see from Table 2, a formation of the host–guest aggregates (reaction 2) seems to be only possible for acetic acid

(33) Becke, A. D. *J. Chem. Phys.* **1993**, *98*, 5648–5652.

(34) Lee, C.; Yang, W.; Parr, R. G. *Phys. Rev.* **1988**, *B37*, 785–789.

and propionic acid in the presence of acid (structures 17, 18). Interestingly, the single protonation of the capsule (structure 16) makes the acid coordination more favorable by 9–12 kcal/mol.



Thus, the results of our calculations agree well with the conclusions made on the basis of the experimental FT-ICR MS data.

## Experimental Section

**Preparation of Octahydroxypyridine[4]arene C.** Octahydroxypyridine[4]arene C was prepared according to the procedure given in the literature.<sup>1</sup>

**FT-ICR Mass Spectrometry (ESI).** Mass spectra were measured on a Bruker APEX III FT-MS (7T magnet) instrument with the Apollo ESI source. A solution of pyridine[4]arene C in chloroform (20  $\mu\text{L}$ , 2 nmol/ $\mu\text{L}$ ) was added to a 0.2% solution of the acid in MeOH/CHCl<sub>3</sub> (1:1). In the case of the amides, the given amount of C was added to a solution with an amide concentration of 700 pmol/ $\mu\text{L}$ . This mixture was introduced into the ESI source by syringe injection with a flow rate of 120  $\mu\text{L}/\text{h}$ . Spectra displayed here are the result of summing up to about 100 single measurements.

**NMR Spectroscopy.** NMR spectra were measured on a Bruker DRX 500. CDCl<sub>3</sub> (with the residual CHCl<sub>3</sub>) was used as internal standard for <sup>1</sup>H and <sup>13</sup>C spectra. <sup>19</sup>F spectra are referenced to TFA. CDCl<sub>3</sub> for complexation experiments was saturated with water before use.

**Vapor Pressure Osmometry (VPO).** Vapor pressure osmometry was performed with a Gonotec Osmomat 070-SA with benzil as calibration standard. Measurements with *rcccc-octa-O-acetyl-tetra-n-undecyl-resorc[4]arene* were carried out in order to confirm the accuracy of the benzil calibration. Measurements in CHCl<sub>3</sub> were carried out at 35 °C, in THF at 45 °C. Solvents were tempered for 2 days before use in order to ensure its water saturation.

## Conclusions

It was shown by FT-ICR MS and MS/MS that pyridine[4]-arene C forms dimers in the gas phase which may contain guests such as carboxylic acids and amides of different size. Our experiments indicate that these guests are incorporated inside the cavity. This is also true in solution as can be proven by <sup>19</sup>F NMR spectroscopy.

**Acknowledgment.** Financial support by the Deutsche Forschungsgemeinschaft (DFG), the Department of Science and Research NRW (MSWF), by the Innovationsfonds (University of Bielefeld), and by the Fonds der Chemischen Industrie is gratefully acknowledged.

**Supporting Information Available:** Atomic coordinates and pictures (GIF) of the calculated structures 11–20. This material is available free of charge via the Internet at <http://pubs.acs.org>.

JA049128X

# Self-assembly of Resorcinarene-stabilized Gold Nanoparticles: Influence of the Macrocyclic Headgroup

BEOMSEOK KIM<sup>a</sup>, R. BALASUBRAMANIAN<sup>a</sup>, WALESKA PÉREZ-SEGARRA<sup>a</sup>, ALEXANDER WEI<sup>a,\*</sup>,  
BJÖRN DECKER<sup>b</sup> and JOCHEN MATTAY<sup>b</sup>

<sup>a</sup>Department of Chemistry, Purdue University, West Lafayette, IN, USA; <sup>b</sup>Department of Chemistry, University of Bielefeld, 33501 Bielefeld, Germany

Received (in Austin, USA) 9 July 2004; Accepted 12 September 2004

Gold nanoparticles can be encapsulated by various resorcinarene derivatives and assembled into monolayer films at solvent interfaces. Surface charge plays a critical role in both nanoparticle extraction and self-assembly: the degree of monolayer formation and local two-dimensional (2D) order within the nanoparticle arrays is dependent on the chemical nature of the resorcinarene headgroup as well as the presence of other electrolytes. Cluster size distribution analysis can be used to parameterize local 2D order within the arrays in a quantitative manner, based on mean cluster sizes and fractional hexagonal close-packed (hcp) cluster formation. 2D nanoparticle arrays can also be prepared in some cases using Langmuir–Blodgett techniques. These studies demonstrate that resorcinarenes with chemisorptive headgroups promote the self-assembly of well-ordered 2D arrays.

**Keywords:** Calixarenes; Nanoparticles; Encapsulation; Self-assembly

## INTRODUCTION

There is currently tremendous interest in using the principles of self-assembly for the construction of materials with structural features in the low to mid-nanometer (1–100 nm) size range [1]. Self-assembly methods have the potential for fabricating well-defined nanomaterials in large scale and at low cost, and can be performed in conjunction with high-resolution lithography for nanoscale patterning. Examples of two-dimensional (2D) and three-dimensional (3D) nanoparticle superlattices have increased dramatically in recent years [2,3]. 2D nanoparticle arrays have thus far yielded novel electronic properties such as nonlinear and

spin-dependent transport [4–6] or tunable optical phenomena such as second-harmonic generation [7] and surface-enhanced Raman scattering [8–10], whereas 3D superlattices and colloidal crystals are promising candidates for photonic band gaps at visible and near-infrared wavelengths [11,12].

An attractive feature of self-assembly is its ability to promote crystalline order in two or three dimensions, enabling ensemble properties to be correlated with tunable physical parameters such as particle size and aspect ratio, periodicity and interparticle spacing, and higher-order lattice structure. These scalable effects are the quintessence of nanoscale science and technology — quantized physical phenomena once considered the domain of atoms and molecules are now observed in many types of nanomaterials, giving rise to the concept of nanocrystals and their ordered superlattices as “artificial atoms” and “quantum dot solids” [2]. Nanosized logic circuits [13,14], chemical and biomolecular sensors [1,15–17] and ultradense data storage devices [18] have all been envisioned as technologically useful products created by the ordering of nanoscale components.

The forces that drive colloidal self-assembly depend on the physical characteristics and surface chemistry of the unit particle as well as on environmental factors. Particle size and composition determine whether long-range van der Waals (vdW) interactions play an important role in self-organization. For the very smallest nanoparticles, such vdW forces are typically at or below thermal energies ( $k_B T$ ), such that self-assembly would be mostly driven by interactions at molecular length

\*Corresponding author. E-mail: alexwei@purdue.edu

scales (e.g. surfactant chain interdigitation) [19–21]. “Programmed” nanoparticle self-assembly mediated by molecular recognition has been demonstrated in several instances [22–28] with at least one example of ordered superlattice formation reported recently [29]. As particle size increases, self-organization is often determined by a more complex balance of vdW interactions, electrostatic forces and/or short-range steric repulsion; at still greater (mesoscopic) length scales, interfacial surface energies and solvophobic interactions become significant [30].

Not surprisingly, methods for assembling colloidal particles into ordered superlattices vary considerably, depending on the nature of the particles used and the media in which they are dispersed. Surfactant-coated nanocrystals with weak vdW interactions can be deposited at submonolayer concentrations onto air–water interfaces and compressed into close-packed 2D arrays in a Langmuir–Blodgett trough [7,19,20,31–33] or organized into 3D superlattices by molecular crystal growth techniques [34–36]. Stable dispersions of nanoparticles and colloids with greater long-range vdW interactions can self-assemble into 2D arrays by simple dropcasting techniques onto wettable surfaces [21,37–43]. Air–liquid and liquid–liquid interfaces are especially useful for tuning particle interactions, and permit self-assembled films to be transferred onto solid surfaces with a high degree of fidelity. Several examples of highly ordered 2D colloidal arrays have been prepared by Langmuir monolayer transfer [33,44,45].

With respect to metal nanoparticles, the vast majority of studies on nanoscale self-assembly have focused on particles in the low nanometer size range ( $d < 10 \text{ nm}$ ). Metal colloids in the mid-nanometer (10–100 nm) size range also have important optical or magnetic properties, but their strong interaction potentials promote kinetic aggregation and often result in poorly organized structures. This is essentially a problem in dispersion control; if repulsive interactions are sufficiently strong to offset particle self-attraction at close range, it should be possible to achieve conditions for thermodynamically controlled self-organization irrespective of particle size.

In order to tap the potential of nanomaterials in the relatively unexplored 10–100 nm size range, we have developed surfactants derived from C-undecylcalix[4]resorcinarene [46] to enhance both the dispersion of colloidal metal particles in various solvents and their self-assembly into well-defined nanostructures with tunable properties [10,47–55]. These compounds possess at least two salient features that contribute to their superior qualities as nanoparticle dispersants: (i) large, multivalent headgroups for robust adsorption onto the nanoparticle surface, and (ii) several

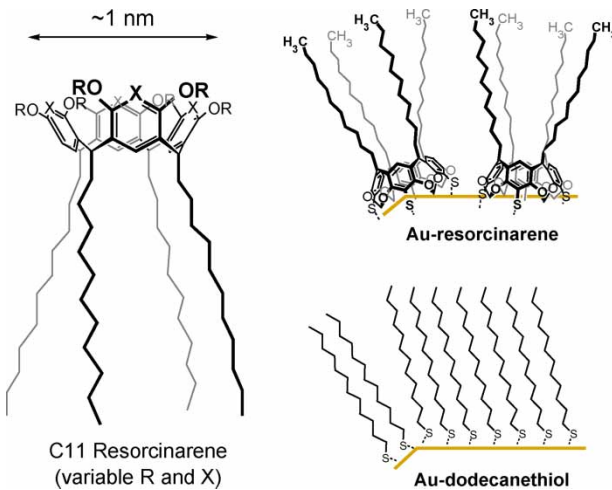


FIGURE 1 Resorcinarenes as nanoparticle surfactants. Resorcinarene monolayers support chains at intermediate packing densities (*upper right*) and retain a high degree of conformational entropy at the nanoparticle surface. Single-chain surfactants tend to assemble into monolayers with high packing densities (*lower right*) and limited potential for entropic steric repulsion.

hydrocarbon chains per molecule spaced several angstroms apart (see Fig. 1). The latter ensures a high degree of configurational freedom per chain in the surfactant layer, which translates into effective steric repulsion associated with the loss of entropy. This is particularly important for nanoparticles with planar facets or a large radius of curvature; single-chain surfactants on these particles tend to form densely packed monolayers with minimal entropic repulsive potential (see Fig. 1, *lower right*), which translates into poor kinetic control during nanoscale self-assembly [47,52].

In the course of these studies, we demonstrated that colloidal Au particles as large as 170 nm could be dispersed at the air–water interface and organized into monoparticulate films when encapsulated by resorcinarene tetrathiol **1** [50,52]. These were deposited onto planar substrates and analyzed by transmission electron microscopy (TEM), which confirmed the formation of hexagonally close-packed 2D arrays with good local order. The Au nanoparticle arrays exhibited size-tunable optical properties including surface-enhanced Raman scattering (SERS), a highly sensitive form of surface spectroscopy with exciting potential for chemical and biomolecular sensing [10]. The SERS activities of the 2D arrays was observed to be both reproducible and stable over a period of months, attributable to the thermodynamic stability of the arrays themselves.

In this article we investigate the surfactant properties of several resorcinarene-like derivatives (**1–8**) for nanoparticle dispersion and self-assembly (see Fig. 2). By varying the chemical functionality

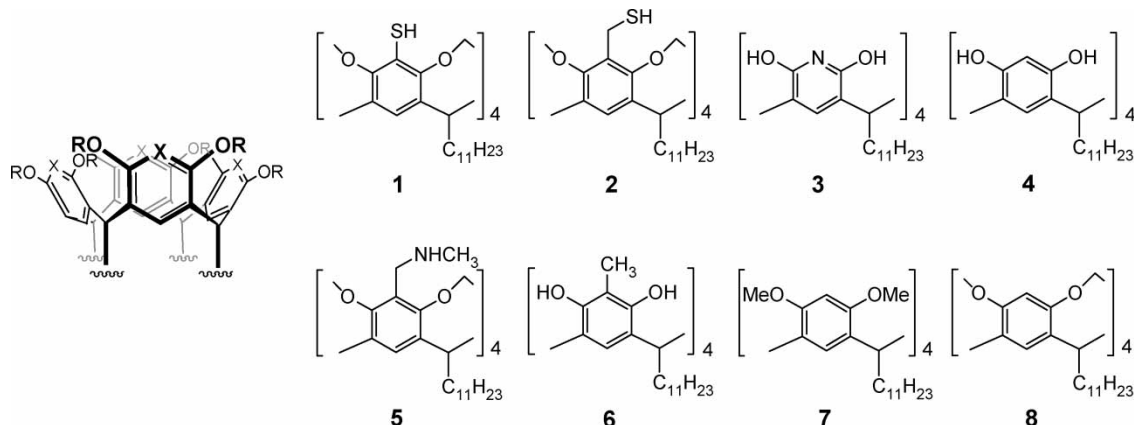


FIGURE 2 Tetra-C-undecylresorcinarene derivatives and related analogs. 1: X = C-SH, R = -CH<sub>2</sub>-; 2: X = C-CH<sub>2</sub>SH, R = -CH<sub>2</sub>-; 3: X = N, R = H; 4: X = CH, R = H; 5: X = C-CH<sub>2</sub>NHCH<sub>3</sub>, R = -CH<sub>2</sub>-; 6: X = C-CH<sub>3</sub>, R = H; 7: X = CH, R = OCH<sub>3</sub>; 8: X = CH, R = -CH<sub>2</sub>-.

on the resorcinarene headgroups while keeping the hydrocarbon chains constant, we are able to evaluate chemisorption effects on nanoparticle extraction and self-organization at the air–water interface. This work complements a recent study on the influence of adsorbed electrolyte in the self-assembly and local 2D ordering of nanoparticle arrays stabilized by resorcinarene **1** [56]. Both studies demonstrate the importance of surface charge for nanoparticle self-organization at aqueous interfaces.

## RESULTS AND DISCUSSION

### Extraction and Self-assembly of Resorcinarene-stabilized Au Nanoparticles

Aqueous suspensions of colloidal Au nanoparticles ( $35 \pm 3$  nm,  $\sim 10^{11}$  particles/mL) were first conditioned with an ion-exchange resin to reduce electrolyte concentrations to a minimum. Resorcinarene-encapsulated nanoparticles were prepared by mixing the conditioned Au nanoparticle suspension with an equal portion of a 1 mM solution of resorcinarene in THF, to produce a homogeneous pink solution (see Materials and Methods for additional details). Addition and vigorous mixing of toluene resulted in a separation of organic and aqueous layers; in many cases, a dark bluish film could be observed at the solvent interface, signifying the formation of a densely packed nanoparticle film. After removing the organic layer, the films were transferred onto carbon-coated Cu grids for TEM analysis.

Resorcinarene derivatives **1–4** were all capable of mediating the self-assembly of Au nanoparticles at the aqueous interface, but their efficacy depended on the condition of the aqueous

medium prior to nanoparticle extraction (see Fig. 3). In particular, the presence of associative electrolytes such as NaCl and sodium citrate (Na<sub>3</sub>Cit) played an important role in determining the efficiency of extraction. For example, Au nanoparticles suspended in solutions with minimal electrolyte ( $I \ll 1$  mM) were extracted to the aqueous interface by tetraarylthiol derivative **1** and octahydroxy derivative **4**, but only partially extracted by tetraazzaresorcinarene analog **3**. However, Au nanoparticles treated with tetrabenzylthiol derivative **2** were not confined to the solvent interface, but were transferred completely into the organic phase [48,49]. Raising the NaCl and Na<sub>3</sub>Cit concentrations to millimolar levels ( $I = 8.95$  mM) had a dramatic effect. In the case of tetrabenzylthiol **2**, a large fraction of encapsulated nanoparticles were not transferred into the organic layer but remained confined at the solvent interface, whereas in the case of tetraaza analog **3**, the nanoparticles were not extracted at all but remained suspended in aqueous solution. In comparison, resorcinarenes **1** and **4** remained essentially constant in their extraction efficiencies.

Two assumptions can be made based on the above observations. First, adsorbed electrolytes are not completely displaced by the resorcinarene surfactants, such that the encapsulated nanoparticles are rendered amphiphatic by the residual surface charge [56]. This confines the nanoparticles to the aqueous interface and promotes their self-organization into 2D arrays, as noted in several other self-assembly studies involving functionalized latex and silica particles [44,57–60]. Second, the resorcinarenes adsorb onto the nanoparticle surfaces primarily through chemisorption rather than electrostatic interactions. In the cases of tetraazzaresorcinarene analog **3** and octahydroxy derivative **4**, both

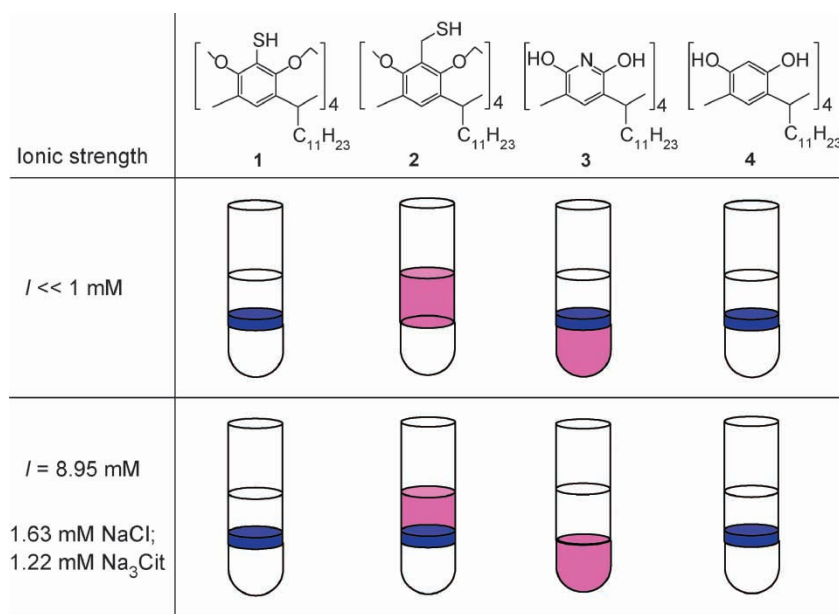


FIGURE 3 Illustrations of nanoparticle extractions by resorcinarenes **1–4**, in the absence and presence of aqueous electrolyte. Self-assembled nanoparticle films at the aqueous interface appeared dark blue.

of these are expected to adsorb as anions in the absence of strong acids<sup>†‡</sup> [61,62]. It is worth noting that while pyridinearene **3** can extract colloidal gold nanoparticles in the presence of minimal electrolyte, attempts to extract nanoparticles using tetra(*N*-methylamino)methylresorcinarene **5** under identical conditions were unsuccessful. Furthermore, exposing extracted nanoparticles encapsulated in **3** to 0.1 M HCl resulted in their redispersion to the aqueous medium. This demonstrates that the Lewis basicity of the headgroup is important for surface adsorption.

Nanoparticles encapsulated by tetra-C-methylresorcinarene **6** or octa-O-methyl ether derivative **7** could be extracted to the aqueous interface but were not well dispersed, suggesting that the surfactant layer was not sufficiently robust against desorption to prevent rapid kinetic aggregation (see Fig. 4). We have previously shown octamethyl ether **7** to be an effective surfactant for entrapping and dispersing neutral gold nanoparticles (generated as aerosols) in hydrocarbon solutions, but this surfactant layer could be easily displaced by competing adsorbates [47]. Finally, cavitand **8** showed little ability to extract colloidal Au nanoparticles from aqueous solution and was deemed to be a poor encapsulating agent, in line with previous observations using aerosol-generated gold nanoparticles [47].

### Characterization of 2D Nanoparticle Arrays

Au nanoparticle films were transferred onto carbon-coated Cu grids using Langmuir–Schaefer conditions for TEM analysis (see Fig. 4). Nanoparticles encapsulated by resorcinarenes **1–3** were observed to assemble into 2D arrays with good local order, demonstrative of thermodynamic self-organization. In comparison, nanoparticles encapsulated by **4** produced monoparticulate films with less order, and those encapsulated by resorcinarenes **6** and **7** resulted in multilayers. The latter experiments correlate with a loss of dispersion control, most likely related to the weaker adsorption of these surfactants to the nanoparticle surface. Surfactant desorption compromises short-range steric repulsion, permitting self-assembly to be dominated by kinetic aggregation. Overall, these results confirm that resorcinarenes with good chemisorption properties are important for promoting nanoparticle self-organization at aqueous interfaces.

In order to better characterize the quality of local 2D order within the self-assembled nanoparticle arrays, the TEM images were subjected to a quantitative method of analysis based on cluster size distributions [56]. Radial distribution ( $g(r)$ ) functions were derived from digitally processed TEM images, and used to generate lattice parameters for the determination of hexagonal close-packed

<sup>†</sup>While the  $pK_a$  values of compound **3** have not been measured, it is known that 2,6-dihydroxypyridine exists in monoanionic form between pH 4.2 and 15.

<sup>‡</sup>The  $pK_a$  values of a water-soluble version of **4** have been measured by pH titration, with the first ionization occurring at pH 6.95: see Ref. [62].

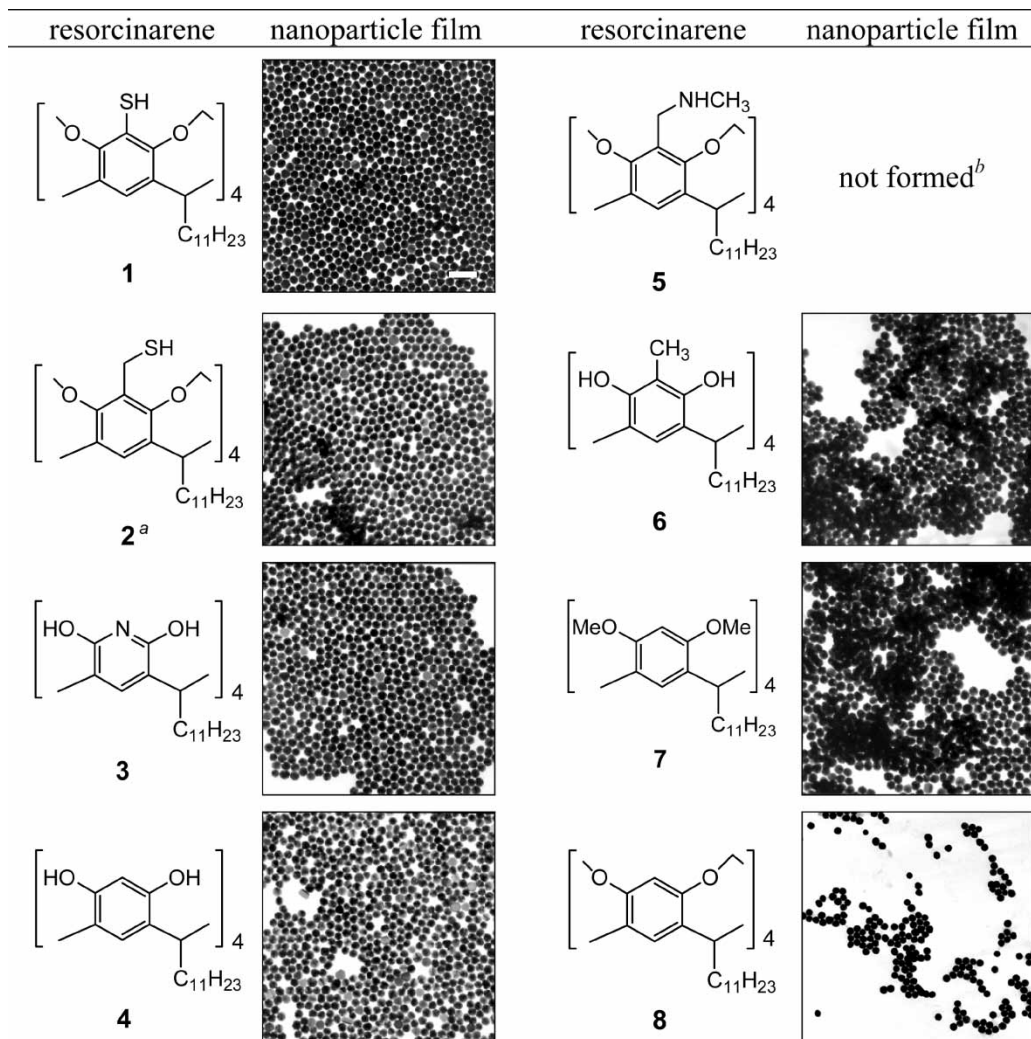


FIGURE 4 Self-assembly of resorcinarene-encapsulated Au nanoparticles ( $35 \pm 3$  nm) upon extraction to aqueous interfaces. Nanoparticle films were transferred onto carbon-coated Cu grids for TEM analysis. Scale bar = 100 nm. <sup>a</sup>Nanoparticles were extracted from aqueous suspensions containing electrolyte ( $I = 8.95$  mM). <sup>b</sup>Nanoparticles remained dispersed in aqueous solution.

(hcp) arrays (see Fig. 5). Cluster size distributions were restricted to nonoverlapping domains to prevent redundancy in particle count [56]. This method enables 2D order to be described in quantitative terms, using number-averaged and weight-averaged cluster sizes ( $M_n$  and  $M_w$ , respectively) and fractional hcp values ( $f_{\text{hcp}}$ ) as figures of merit.

Cluster size distribution analyses were performed on self-assembled nanoparticle films, formed upon extraction to the aqueous interface by resorcinarenes 1–3. The 2D order within these films was determined to be comparable, with  $M_n$  and  $f_{\text{hcp}}$  in the range of 20 and 0.60, respectively (see Table I)<sup>1</sup>. In comparison, analysis of nanoparticle films formed with resorcinarene 4 produced significantly smaller values for  $M_n$  and  $f_{\text{hcp}}$  (15.1 and 0.43, respectively). A similar loss in 2D order has been observed when

nanoparticles were extracted by 1 from solutions containing additional NaCl and Na<sub>3</sub>Cit [56]. Both results suggest that while surface-bound electrolytes can be useful for confining surfactant-encapsulated nanoparticles to aqueous interfaces, they are also capable of promoting kinetic aggregation and can have an unpredictable effect on self-assembly.

#### Nanoparticle Arrays by Langmuir–Blodgett Compression

Resorcinarene-stabilized nanoparticles have excellent dispersion characteristics in organic solvents, suggesting the possibility of using Langmuir–Blodgett techniques for creating 2D nanoparticle arrays [7,31–33]. In particular, nanoparticles encapsulated by tetrabenzylthiol 2 can be fully

<sup>1</sup>It is worth mentioning that  $f_{\text{hcp}}$  serves as a lower limit when calculated with the assumption of nonoverlapping clusters. Values in the range of 0.70 are obtained if partially overlapping clusters (up to 30%) are allowed.

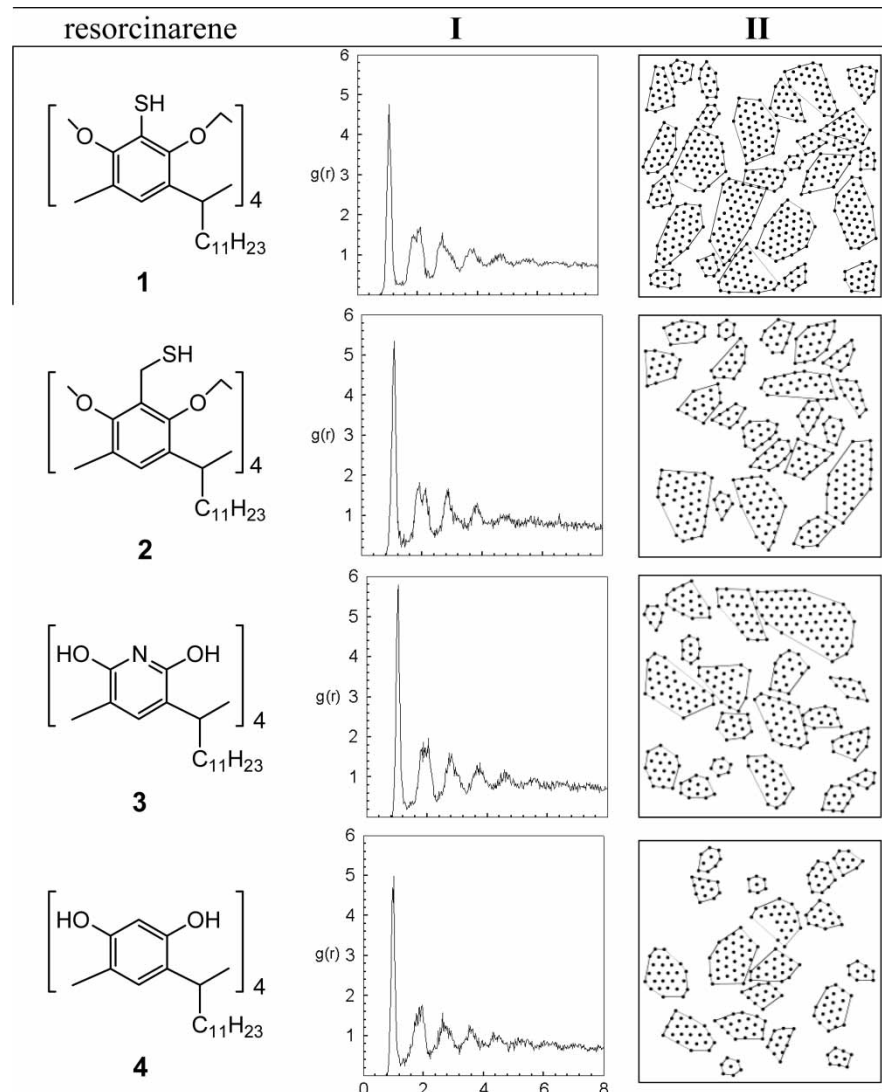


FIGURE 5 Cluster size distribution analysis of resorcinarene-encapsulated Au nanoparticle arrays, based on TEM images in Fig. 4. Column I: radial distribution functions derived from digitized images. Column II: nonoverlapping hcp clusters within self-assembled nanoparticle films. Domain boundaries are drawn to guide the eye.

extracted into the organic phase, and redeposited onto air–water interfaces [48]. However, when 35-nm Au particles encapsulated by **2** were extracted into toluene and condensed onto an aqueous interface,

only multilayered films were produced. This suggests that as the residual film is concentrated, kinetic aggregation driven by the nanoparticles' vdW attractions supersedes reversible self-organization at the solvent interface.

To ascertain whether particle size was responsible for poor kinetic control, the same procedure was repeated using toluene extracts of 9.2-nm Au particles. These were indeed amenable to monolayer film formation, and could be subjected to surface compression to maximize the overall packing (see Fig. 6). However, cluster size distribution analysis revealed no improvement in 2D order; the  $M_n$  and  $f_{hcp}$  values of the arrays obtained after Langmuir–Blodgett compression were no greater than those formed by self-organization under amphiphatic conditions (see Table I). TEM images of 9.2-nm particle films obtained in the absence of surface compression (not shown) revealed that the particles

TABLE I Cluster size distribution analysis of resorcinarene-stabilized nanoparticle arrays

Compound	Particle size (nm)	Particle count ( $N^*$ )	hcp clusters (nonoverlapping)		
			$M_n$	$M_w$	$f_{hcp}$
<b>1<sup>†</sup></b>	$35 \pm 3$	901	21.4	28.5	0.64
<b>2</b>	$35 \pm 3$	601	17.1	21.9	0.60
<b>2<sup>‡</sup></b>	$9.2 \pm 0.8$	852	18.4	22.6	0.52
<b>3</b>	$35 \pm 3$	616	18.7	26.8	0.58
<b>4</b>	$35 \pm 3$	640	15.1	17.9	0.43

\*Number of centroids taken from TEM image (cf. Fig. 5). <sup>†</sup>Data taken from Ref. [56]. <sup>‡</sup>Formed after compression in a Langmuir–Blodgett trough (cf. Fig. 6).

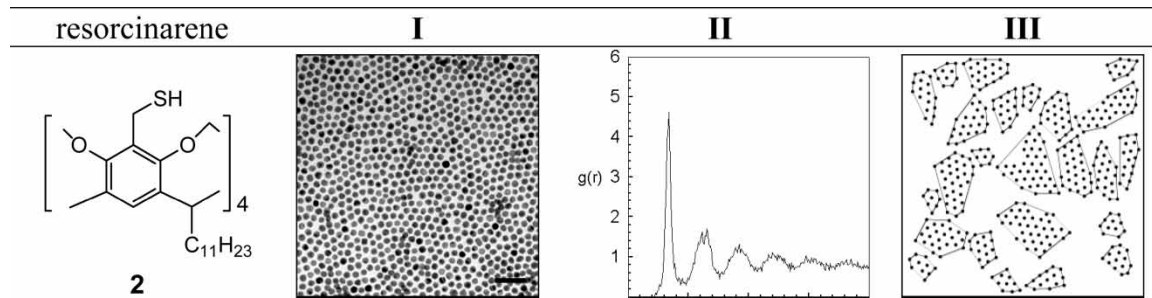


FIGURE 6 TEM image and cluster size distribution analysis of 2D arrays of 9.2-nm Au particles encapsulated by **2**, transferred after compression in a Langmuir–Blodgett trough. I: TEM image of nanoparticle film (scale bar = 50 nm); II: radial distribution functions derived from digitized images; III: nonoverlapping hcp clusters within self-assembled nanoparticle films.

were already assembled into close-packed domains, an indication that vdW forces continued to provide the dominant driving force for nanoparticle self-assembly. Thus, while resorcinarene **2** substantially enhances the dispersion of Au nanoparticles, additional repulsion potential is needed to achieve self-assembly conditions with complete thermodynamic control.

## MATERIALS AND METHODS

Resorcinarene derivatives **1**, **2**, **4–8** and tetraazaresorcinarene analog (pyridine[4]arene) **3** were synthesized as reported previously or by a slight modification of published procedures<sup>§,||</sup> [63–65]. Colloidal Au particle suspensions were purchased from British Biocell International (EM.GC10, *ca.*  $5.7 \times 10^{12}$  particles/mL; EM.GC40, *ca.*  $9 \times 10^{10}$  particles/mL) and characterized by TEM (Philips EM-400, 80 keV); the average particle sizes were  $9.2 \pm 0.8$  nm ( $N = 846$ ) and  $35 \pm 3$  nm ( $N = 1165$ ), respectively. Carbon-coated Cu TEM grids were purchased from Ted Pella, Inc. and used as supplied. The resorcinarene-encapsulated nanoparticles were handled in silanized glassware (SiliClad, Gel-Est) to minimize electrostatic surface adsorption. High-purity water with measured resistivity above  $18\text{ M}\Omega\text{ cm}$  was obtained using an ultrafiltration system (Milli-Q, Millipore) equipped with an additional 0.22- $\mu\text{m}$  membrane filter.

Aqueous suspensions of colloidal Au particles were treated with a mixed-bed ion-exchange resin (Amberlite MB-3, Mallinckrodt) for 30 min to remove excess electrolyte<sup>#</sup>. In a typical experiment, resorcinarene-encapsulated nanoparticles were prepared by vigorously mixing colloidal suspensions (1 mL) with 1 mM solution of surfactant in freshly distilled

THF (1 mL) in a silanized glass tube, which resulted in a homogeneous pink solution. In the case of nanoparticles encapsulated with resorcinarene **2**, NaCl and Na<sub>3</sub>Cit were reintroduced in controlled amounts (1.63 and 1.22 mM, respectively) prior to extraction. Addition and vigorous mixing of toluene (1 mL) resulted in a separation of organic and aqueous layers, with amphiphatic nanoparticle films spontaneously assembled at the solvent interface. The organic layer was removed by pipette, and the aqueous layer and particles were washed twice more with toluene (1 mL each) to extract THF and excess surfactant. The Au nanoparticle films were drawn up in a silanized glass pipette, then drained and carefully redeposited onto a clean air–water interface in a silanized test-tube and allowed to stand at room temperature for 60 min. The nanoparticle film was then transferred onto carbon-coated Cu TEM grids by Langmuir–Schaefer transfer using a pair of forceps, and dried in air.

## Nanoparticle Films by Langmuir–Blodgett Compression

An aqueous suspension of 9.2-nm Au particles (3.5 mL) was mixed with an equal portion of a 1 mM solution of resorcinarene **2** in THF, then extracted with toluene (17 mL). Encapsulated particles were treated with methanol (6 mL) and centrifuged at 6000 g for 20 min, then redispersed in 0.3 mL toluene with the aid of an ultrasonic cleaning bath (4 × 5-s exposures). Nanoparticle dispersions were drawn up in a silanized glass pipette, then slowly redeposited onto a clean air–water interface in a Langmuir–Blodgett trough (Nima Technologies, 611M), allowing time for the evaporation of toluene. The resulting Au nanoparticle film was slowly compressed (barrier speed = 1 mm/min) until

<sup>§</sup>Compounds **1**, **2** and **6**: see Ref. [50]; compounds **4** and **7**: see Ref. [47].

<sup>||</sup>Compound **3**; Compound **5**; Compound **8**.

<sup>#</sup>Additional experimental details can be found in Ref. [56].

the theoretical area for a monolayer was achieved. The film was transferred onto a carbon-coated Cu TEM grid using a pair of forceps, and dried in air.

### Acknowledgements

We gratefully acknowledge financial support from the National Science Foundation (BES-0228143, CHE-0243496 and ECS-0210445) and the Deutsche Forschungsgemeinschaft (SFB 613).

### References

- [1] Shipway, A. N.; Katz, E.; Willner, I. *Chem. Phys. Chem.* **2000**, 1, 18.
- [2] Collier, C. P.; Vossmeyer, T.; Heath, J. R. *Annu. Rev. Phys. Chem.* **1998**, 49, 371.
- [3] Pileni, M. P. *J. Phys. Chem. B* **2001**, 105, 3358.
- [4] Andres, R. P.; Bielefeld, J. D.; Henderson, J. I.; Janes, D. B.; Kolagunta, V. R.; Kubiak, C. P.; Mahoney, W. J.; Osifchin, R. G. *Science* **1996**, 273, 1690.
- [5] Parthasarathy, R.; Lin, X.-M.; Jaeger, H. M. *Phys. Rev. Lett.* **2001**, 87, 186807.
- [6] Black, C. T.; Murray, C. B.; Sandstrom, R. L.; Sun, S. *Science* **2000**, 290, 1131.
- [7] Collier, C. P.; Saykally, R. J.; Shiang, J. J.; Henrichs, S. E.; Heath, J. R. *Science* **1997**, 277, 1978.
- [8] Moody, R. L.; Vo-Dinh, T.; Fletcher, W. H. *Appl. Spectrosc.* **1987**, 41, 966.
- [9] Tessier, P. M.; Velev, O. D.; Kalambur, A. T.; Rabolt, J. F.; Lenhoff, A. M.; Kaler, E. W. *J. Am. Chem. Soc.* **2000**, 122, 9554.
- [10] Wei, A.; Kim, B.; Sadtler, B.; Tripp, S. L. *Chem. Phys. Chem.* **2001**, 2, 743.
- [11] Moroz, A. *Phys. Rev. Lett.* **1999**, 83, 5274.
- [12] Braun, P. V.; Wiltzius, P. *Curr. Opin. Colloid Interface Sci.* **2002**, 7, 116.
- [13] Feldheim, D. L.; Keating, C. D. *Chem. Soc. Rev.* **1998**, 27, 1.
- [14] Smith, C. G. *Science* **1999**, 284, 274.
- [15] Wohltjen, H.; Snow, A. W. *Anal. Chem.* **1998**, 70, 2856.
- [16] Krasteva, N.; Besnard, L.; Guse, B.; Bauer, R. E.; Mullen, K.; Yasuda, A.; Vossmeyer, T. *Nano Lett.* **2002**, 2, 551.
- [17] Genov, D. A.; Sarychev, A. K.; Shalaev, V. M.; Wei, A. *Nano Lett.* **2004**, 4, 153.
- [18] Chou, S. Y.; Krauss, P. R.; Kong, L. *J. Appl. Phys.* **1996**, 79, 6101.
- [19] Heath, J. R.; Knobler, C. M.; Leff, D. V. *J. Phys. Chem. B* **1997**, 101, 189.
- [20] Gelbart, W. M.; Sear, R. P.; Heath, J. R.; Chaney, S. *Faraday Discuss.* **1999**, 112, 299.
- [21] Motte, L.; Pileni, M. P. *J. Phys. Chem. B* **1998**, 102, 4104.
- [22] Mirkin, C. A.; Letsinger, R. L.; Mucic, R. C.; Storhoff, J. J. *Nature* **1996**, 382, 607.
- [23] Storhoff, J. J.; Mirkin, C. A. *Chem. Rev.* **1999**, 99, 1849.
- [24] Alivisatos, A. P.; Johnsson, K. P.; Peng, X.; Wilson, T. E.; Loweth, C. J.; Bruchez, M. P. Jr.; Schultz, P. G. *Nature* **1996**, 382, 609.
- [25] Cusack, L.; Rizza, R.; Gorelov, A.; Fitzmaurice, D. *Angew. Chem., Int. Ed. Engl.* **1997**, 36, 848.
- [26] Liu, J.; Mendoza, S.; Roman, E.; Lynn, M. J.; Xu, R.; Kaifer, A. E. *J. Am. Chem. Soc.* **1999**, 121, 4304.
- [27] Simard, J.; Briggs, C.; Boal, A. K.; Rotello, V. M. *Chem. Commun.* **2000**, 1943.
- [28] Frankamp, B. L.; Uzun, O.; Ilhan, F.; Boal, A.; Rotello, V. M. *J. Am. Chem. Soc.* **2002**, 124, 892.
- [29] Kanehara, M.; Oumi, Y.; Sano, T.; Teranishi, T. *J. Am. Chem. Soc.* **2003**, 125, 8708.
- [30] Bowden, N. B.; Weck, M.; Choi, I. S.; Whitesides, G. M. *Acc. Chem. Res.* **2001**, 34, 231.
- [31] Dabbousi, B. O.; Murray, C. B.; Rubner, M. F.; Bawendi, M. G. *Chem. Mater.* **1994**, 6, 216.
- [32] Meldrum, F. C.; Kotov, N. A.; Fendler, J. H. *Chem. Mater.* **1995**, 7, 1112.
- [33] Brown, J. J.; Porter, J. A.; Daglian, C. P.; Gibson, U. J. *Langmuir* **2001**, 17, 7966.
- [34] Murray, C. B.; Kagan, C. R.; Bawendi, M. G. *Science* **1995**, 270, 1335.
- [35] Thomas, P. J.; Kulkarni, G. U.; Rao, C. N. R. *J. Phys. Chem. B* **2001**, 105, 2515.
- [36] Talapin, D. V.; Shevchenko, E. V.; Kornowski, A.; Gaponik, N.; Haase, M.; Rogach, A. L.; Weller, H. *Adv. Mater.* **2001**, 13, 1868.
- [37] Harfenist, S. A.; Wang, Z. L.; Alvarez, M. M.; Vezmar, I.; Whetten, R. L. *J. Phys. Chem.* **1996**, 100, 13904.
- [38] Wang, Z. L.; Harfenist, S. A.; Vezmar, I.; Whetten, R. L.; Bentley, J.; Evans, N. D.; Alexander, K. B. *Adv. Mater.* **1998**, 10, 808.
- [39] Maye, M. M.; Zheng, W.; Leibowitz, F. L.; Ly, N. K.; Zhong, C. J. *Langmuir* **2000**, 16, 490.
- [40] Puntes, V. F.; Krishnan, K. M.; Alivisatos, P. *Appl. Phys. Lett.* **2001**, 78, 2187.
- [41] Lin, X. M.; Jaeger, H. M.; Sorensen, C. M.; Klabunde, K. J. *J. Phys. Chem. B* **2001**, 105, 3353.
- [42] Brown, L. O.; Hutchison, J. E. *J. Phys. Chem. B* **2001**, 105, 8911.
- [43] Yamamuro, S.; Farrell, D.; Humfeld, K. D.; Majetich, S. A. *MRS Symp. Proc.* **2001**, 636, D108.
- [44] Kondo, M.; Shinozaki, K.; Bergström, L.; Mizutani, N. *Langmuir* **1995**, 11, 394.
- [45] Goldenberg, L. M.; Wagner, J.; Stumpe, J.; Paulke, B. R.; Görnitz, E. *Langmuir* **2002**, 18, 5627.
- [46] Aoyama, Y.; Tanaka, Y.; Sugahara, S. *J. Am. Chem. Soc.* **1989**, 111, 5397.
- [47] Stavens, K. B.; Pusztay, S. V.; Zou, S.; Andres, R. P.; Wei, A. *Langmuir* **1999**, 15, 8337.
- [48] Balasubramanian, R.; Xu, J.; Kim, B.; Sadtler, B.; Wei, A. *J. Dispersion Sci. Technol.* **2001**, 22, 485.
- [49] Balasubramanian, R.; Kim, B.; Tripp, S. L.; Wang, X.; Lieberman, M.; Wei, A. *Langmuir* **2002**, 18, 3676.
- [50] Kim, B.; Tripp, S. L.; Wei, A. *J. Am. Chem. Soc.* **2001**, 123, 7955.
- [51] Wei, A.; Kim, B.; Pusztay, S. V.; Tripp, S. L.; Balasubramanian, R. *J. Inclusion Phenom. Macrocycl. Chem.* **2001**, 41, 83.
- [52] Kim, B.; Tripp, S. L.; Wei, A. *MRS Symp. Proc.* **2001**, 676, Y61.
- [53] Pusztay, S. V.; Wei, A.; Stavens, K. B.; Andres, R. P. *Supramol. Chem.* **2002**, 14, 289.
- [54] Tripp, S. L.; Pusztay, S. V.; Ribbe, A. E.; Wei, A. *J. Am. Chem. Soc.* **2002**, 124, 7914.
- [55] Tripp, S. L.; Dunin-Borkowski, R. E.; Wei, A. *Angew. Chem., Int. Ed. Engl.* **2003**, 42, 5591.
- [56] Kim, B.; Carignano, M. A.; Tripp, S. L.; Wei, A. *Langmuir* **2004**, 20, 9360.
- [57] Pieranski, P. *Phys. Rev. Lett.* **1980**, 45, 569.
- [58] Beck, C.; Hartl, W.; Hempelmann, R. *Angew. Chem., Int. Ed. Engl.* **1999**, 38, 1297.
- [59] Hansen, P. H. F.; Bergström, L. *J. Colloid Interface Sci.* **1999**, 218, 77.
- [60] Hansen, P. H. F.; Malmsten, M.; Bergenståhl, B.; Bergström, L. *J. Colloid Interface Sci.* **1999**, 220, 269.
- [61] Spinner, E.; White, J. C. B. *J. Chem. Soc. B* **1966**, 991.
- [62] Kobayashi, K.; Asakawa, Y.; Kato, Y.; Aoyama, Y. *J. Am. Chem. Soc.* **1992**, 114, 10307.
- [63] Gerkensmeier, T.; Mattay, J.; Näther, C. *Chem. Eur. J.* **2001**, 7, 465.
- [64] Boerrigter, H.; Verboom, W.; Reinhoudt, D. N. *J. Org. Chem.* **1997**, 62, 7148.
- [65] Román, E.; Peinador, C.; Mendoza, S.; Kaifer, A. E. *J. Org. Chem.* **1999**, 64, 2577.

# Formation of Gel-Like Systems of an 2,6,8,12,14,18,20,24-Octahydroxy-pyridine[4]arene and an 2-Aminonaphthyridine

Thorsten Gerkensmeier,<sup>[a]</sup> Björn Decker,<sup>[a]</sup> Marcus Schwertfeger,<sup>[b]</sup> Wolfgang Buchheim,<sup>[b]</sup> and Jochen Mattay<sup>\*[a]</sup>

Dedicated to Professor Waldemar Adam on the occasion of his 65th birthday

**Keywords:** Calixarenes / Gels / Hydrogen bonds / Aggregation / Supramolecular chemistry

2,6,8,12,14,18,20,24-Octahydroxypyridine[4]arenes are capable of forming complexes with suitable partner molecules. In apolar media the formation of gel-like aggregates of an octahydroxypyridine[4]arene and an 2-aminonaphthyridine at a ratio of 1:4 was observed. This viscous liquid was investigated by means of rheology and TEM techniques and was

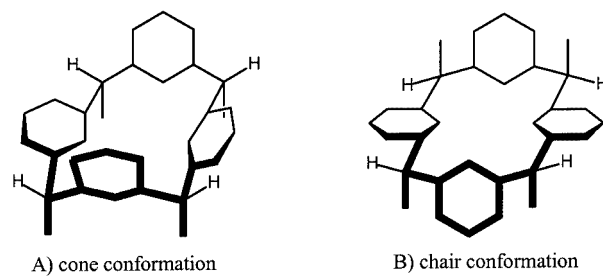
characterized as shear thinning and thermoreversible gel-like solution which is strongly affected by changes in the stoichiometry of the complex partners.

(© Wiley-VCH Verlag GmbH, 69451 Weinheim, Germany, 2002)

## Introduction

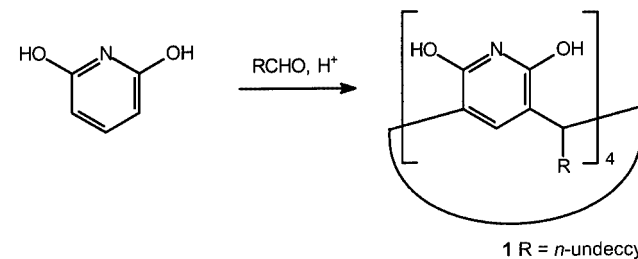
Calixarenes are still one of the important building blocks of supramolecular aggregates. Many projects within this field concern the complexation of both organic and inorganic compounds. The complexation of organic molecules is often controlled by molecular recognition phenomena and therefore the stoichiometry and the shape of the complex is crucial. One tool to achieve this selectivity is multivalent hydrogen bonding,<sup>[1a]</sup> and recently the groups of Hanabusa<sup>[1b]</sup> and McPherson<sup>[1c]</sup> have used this concept for designing novel organogel systems. The number and the stability of calixarene aggregates previously reported gives an idea of the importance of these macrocycles to this research area.<sup>[2–9]</sup> However, not all complexation phenomena lead to structurally well-defined aggregates but more likely result in less ordered structures of large size. Among these are micelles, layers, sticks and stripes. The microstructures often cause rheologic effects such as increased viscosity, which can be measured as a macroscopic material property. Other methods of determining the properties and the structural nature of viscous solutions and gels are various electron microscopy techniques,<sup>[10]</sup> light, small-angle X-ray or neutron scattering.

Very recently the synthesis of a new member of the calixarene family derived from 2,6-dihydroxypyridine and aldehydes was developed.<sup>[11]</sup> In general, these compounds are accessible as *rccc*-configured, cone-shaped molecules in medium yields (Scheme 1).



Scheme 1. Cone conformation (A) of a *rccc*-configured and chair conformation (B) of an *rctt*-configured calix[4]arene isomer

Only long-chain aldehydes, at least like hexanal, lead to highly soluble pyridine[4]arenes, that can be handled even in apolar solvents (Scheme 2). Short-chain aldehydes gener-



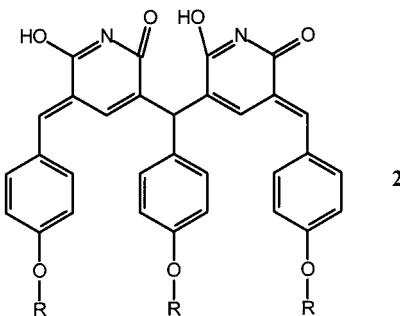
Scheme 2. Acid-catalysed synthesis of pyridine[4]arenes from 2,6-dihydroxypyridine and aliphatic aldehydes

[a] Organische Chemie I, Fakultät für Chemie, Universität Bielefeld,  
Postfach 100131, 33501 Bielefeld, Germany  
E-mail: mattay@uni-bielefeld.de

[b] Bundesanstalt für Milchforschung,  
Hermann-Weigmann-Straße 1, 24103 Kiel, Germany

ally yield nearly insoluble calixarenes which have to be acetylated or benzoylated to be analysed.

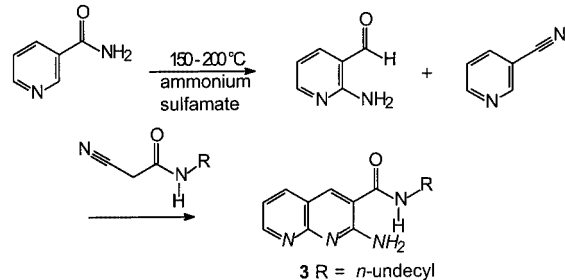
A number of aldehydes has been successfully applied in this reaction. However, some restrictions of the use of aldehydes are found. From alkene-carboxaldehydes only traces or no calixarene at all were isolated. Electron-deficient aromatic aldehydes mostly favour the *rctt*-configured isomer while electron-rich aromatic aldehydes lead to a methylidene-pyridinone substructure **2**.



The motivation for the synthesis of this kind of calixarenes was to find a new building block for self-organizing systems. Since 2,6-dihydroxypyridines feature uracil mimics, a number of complementary molecules for multiple hydrogen bonding should be accessible for complexation studies.

## Results

The use of apolar media should support the formation of hydrogen bonds, therefore solutions of 2,6,8,12,14,18,20,24-octahydroxy-4,10,16,24-tetra-*n*-undecylpyridine[4]arene (**1**) as receptor molecule in toluene were applied for complexation studies. These conditions may also lead to homodimer formation, which has to be taken into consideration when discussing heteromolecular complexes. The first substrate checked, was 2,6-diaminopyridine. Upon mixing hot solutions of the calixarene and the diaminopyridine, a colourless, insoluble precipitate was obtained which turned black within a few hours. Attempts to analyse the precipitate by MS and NMR techniques were not successful. Whether the driving force of the formation of this insoluble precipitate is simply an acid-base interaction or the desired multivalent hydrogen bonding or both is not clear. In order to obtain more soluble complexes, we were looking for very apolar substituted partner molecules. Therefore we took a closer look at 2-aminonaphthyridine-3-carboxamides. These compounds have a hydrogen donor and two acceptor binding sites at the naphthyridine unit and should be complementary to the hydroxypyridone substructure of the pyridine[4]arenes, which is expected to be the dominant tautomer in the 2,6-dihydroxypyridine.<sup>[12–14]</sup> According to a procedure of Majewicz and Caluwe 2-aminopyridine-3-carboxaldehyde was prepared.<sup>[15,16]</sup> The reaction with malonamidonitriles according to the preparation of Fenlon affords the 2-aminonaphthyridine-3-carboxamides (Scheme 3).<sup>[17]</sup>



Scheme 3. Synthesis and binding sites (in italics) of the 2-amino-*N*<sup>3</sup>-R-1,8-naphthyridin-3-carboxamide **3**

For our tests we chose *rccc*-octahydroxy-tetraundecylpyridine[4]arene **1** and 2-amino-*N*<sup>3</sup>-undecynaphthyridine-3-carboxamide (**3**). Both compounds are quite soluble in apolar media like toluene and dichloromethane. We mixed hot solutions of the pyridine[4]arene **1** and the naphthyridine **3** in toluene at a molar ratio of 1:2, 1:3 and 1:4 and tried to find evidence for complex formations by means of Maldi-MS and UV/Vis absorption spectroscopy. In all cases only the molecular mass of one of the components was detected by Maldi-MS. On the other hand UV/Vis spectroscopy showed a small decrease of absorption of the naphthyridine upon addition of the calixarene partner, however, too small to be used for a detailed analysis. We assume that there is no defined complex present due to the following observation. While 1:2 and 1:3 mixtures of **1** and **3** do not differ much, both presenting a clear, somewhat coloured solution of low viscosity, the 1:4 mixture forms a viscous solution upon cooling to at least 5 °C. Warming up to room temperature the solution becomes an easy moving fluid again. This process appeared to be reversible. In THF and 1,4-dioxane no thickening or gelation effect was observed for 1:4 mixtures. We decided to characterise the viscous solution by means of rheology and, if possible, by freeze fracture transmission electron microscopy. The rheologic experiments were carried out with the 1:3 and 1:4 mixtures.

## Rheology Studies

For reasons, that are going to be explained in the TEM part, 1,2-dichlorobenzene was applied as a solvent for the rheology experiments. Two solutions with given concentrations were prepared. The compounds were weighed and dissolved in hot 1,2-dichlorobenzene. Solution 1 contained the calixarene **1** and naphthyridine **3** in a molar ratio of 1:3 and was a clear liquid of low viscosity, whereas solution 2 contained **1** and **3** in a molar ratio of 1:4 and was a translucent fluid, that became viscous upon cooling to 5 °C. If this solution was stirred, the gel-like substance reversibly turned into a fluid. At first the results for the 1:3 ratio will be discussed. The temperature dependence is shown in Figure 1.

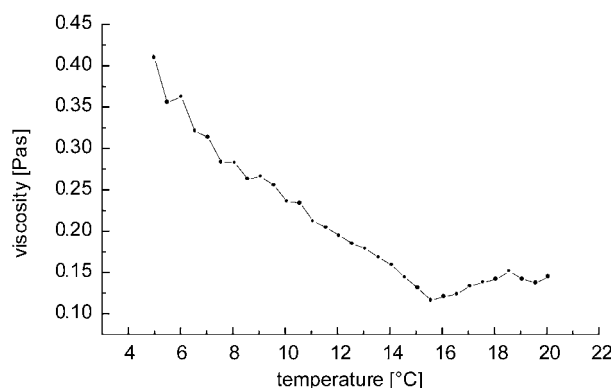


Figure 1. Temperature dependence of the 1:3 mixture of calixarene **1** and naphthyridine **3** at a shear rate of 0.2 [1/s]

Although the viscosity of the solution is comparatively low, a distinct decrease can be noted upon warming up to room temperature. Further interesting features of viscous liquids concern shear thinning or shear thickening. Shear thinning describes the decrease of viscosity upon mechanical stress whereas shear thickening describes just the opposite behaviour. The corresponding time-dependent effects are known as thixotropy and rheopecty. These effects take place, if special microstructures are present. Figure 2 shows the viscosity of the 1:3 mixture depending on the shear rate and time.

These experiments clearly revealed shear thinning and thixotropic features. The viscosity is dominantly controlled by the actual shear rate and by the time of shearing. On the other hand, the viscosity itself is relatively low. If the composition of the mixture changes from 1:3 to 1:4 viscosity of the solution drastically increases. The general features

of thermoreversibility, shear thinning and thixotropy remain, i.e. the 1:4 mixture generally shows the same behaviour. However, especially for low shear rates the viscosity turns out to be high. The temperature as well as the shear rate takes strong influence on the viscosity of the solution (Figure 3).

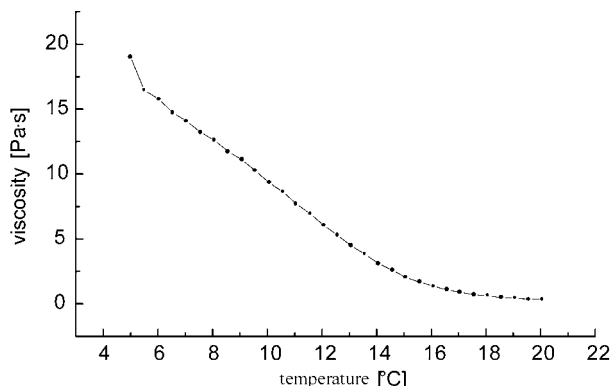


Figure 3. Temperature dependence of the 1:4 mixture of **1** and **3** at a shear rate of 0.2 [1/s]

Temperature changes have a strong influence on the viscosity of the viscous gel-like solution. Between 5 and 15 °C a nearly linear decrease is observed. This effect is reversible as well.

Figure 4 shows the shear rate dependence of the viscosity at 5 °C. Note the strong decrease of viscosity under mechanical stress and the fast recovering of the system if low shearing rates are applied. It is also important, that no viscoelasticity was observed and for that reason the gel-like mixture does not show a yield value.

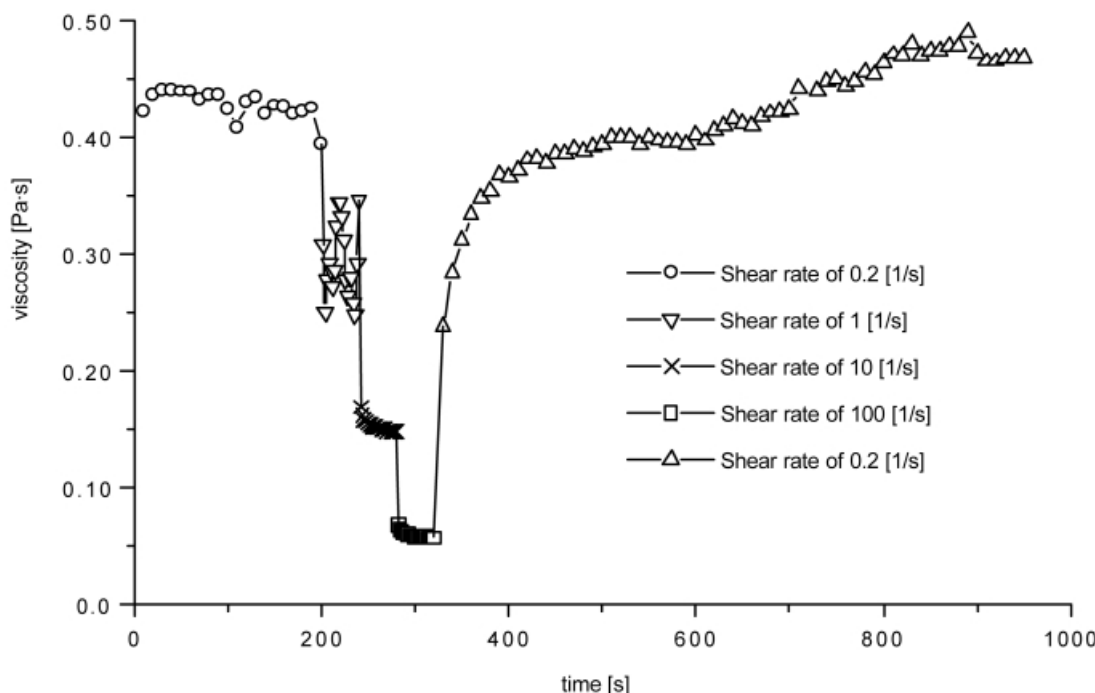


Figure 2. Shear-rate dependence of the viscosity of the 1:3 mixture of **1** and **3** at 5 °C

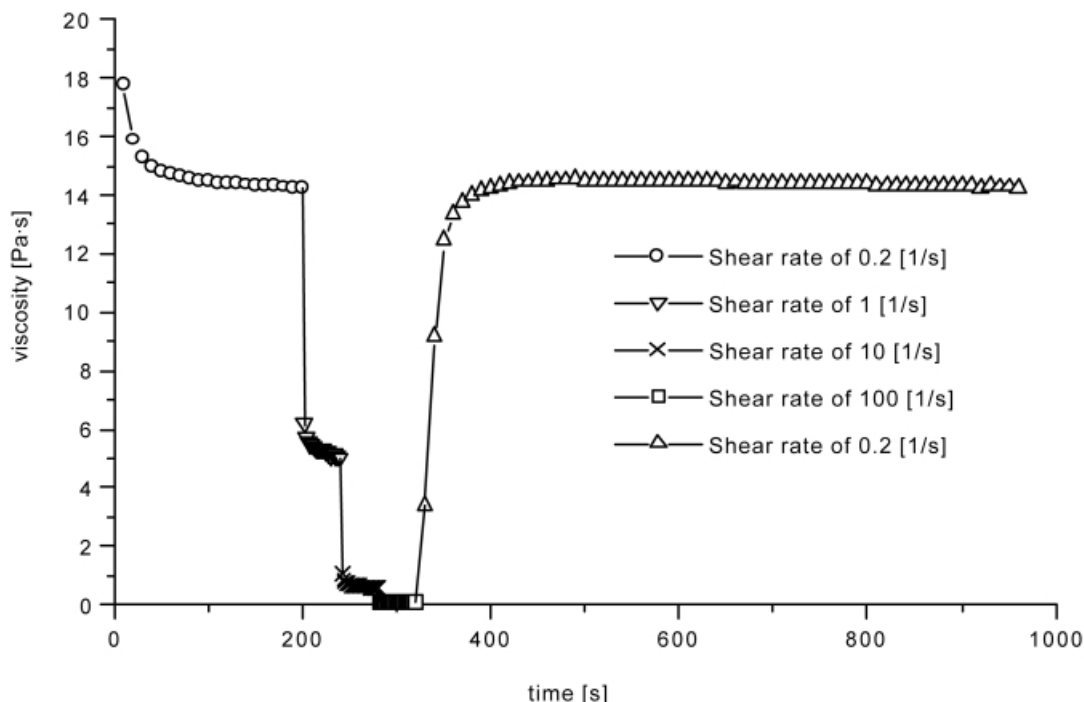


Figure 4. Shear rate dependence of the viscosity of **1** and **3** (1:4 ratio) at 5 °C

Rheologic experiments are important tools in characterising fluids. Yet, they only allow very limited insights into the structural details that are responsible for the rheologic behaviour. One method that has been successfully applied in the past is freeze fracture transmission electron microscopy.<sup>[18]</sup>

#### Freeze Fracture Transmission Electron Microscopy

Freeze fracture TEM allows to display the topology of a surface generated by fracture and controlled sublimation of a matrix like water or suitable organic solvents from a solid specimen at adequate low temperatures. Since gels and similar systems are elastic or rather viscous fluids, they must be cryofixed in advance. Our first approach was a solution of the components in toluene, but unfortunately the viscous toluene solution is not well suited for the freeze fracture procedure. The quick freezing must allow the formation of an amorphous solid. Crystallization of the solvent leads to separation of the components and destruction or deformation of sensible microstructures. Toluene tends to crystallize upon freezing in melting freon.<sup>[18]</sup> Therefore we were looking for alternative solvents that allow the formation of the viscous gel-like solution and which are suitable for the freeze fracture procedure. We chose 1,2-dichlorobenzene because it allows the thickening effect and has a rather high melting point supporting amorphous freezing.

It is known, that various factors may affect the result of a freeze fracture preparation. One problem we faced was the separation phenomenon of the components upon cryofixation. The segregation of solvent and dissolved compounds may lead to the formation of an irregular network structure, that might be misinterpreted as an original struc-

ture. However, in our experiments we observed areas consisting of partly lamellar or partly hexagonal-like ordered planes (Figure 5). Careful examination of highly magnified electron micrographs showed periodical linear structures with unit distances of about 5 nm. Yet, the nature of the structure is unknown. It is not possible that these lamellar ordered aggregates are responsible for the rheologic effects, since their density is too high to be maintained throughout the solution at the actual molar concentration. However, they may be the reason for the degrading of the gel-like system. If most of the calixarene and naphthyridine needed to build up the thickening microstructure is concentrated in the dense but relatively small lamellar structures, the viscosity will be lowered.

The viscous solution is stable for many weeks if stored in the refrigerator at 5 °C or at lower temperature. At room temperature the shear thinning properties are irreversibly lost within one day and the system becomes an easy moving solution. No defined structures except one of the partner molecules are identified by Maldi-MS.

#### Conclusions

The complexation experiment between the pyridine[4]arene **1** and the naphthyridine **3** in apolar solvents leads to aggregates of lesser order that has an impact on the rheologic properties of the solution. The gel-like viscous liquid shows shear thinning and thixotropic features and is thermoreversible. The ratio of the components plays an important role. No viscous solution formation is observed, if ratios other than 1:4 are applied. The viscosity is not stable at

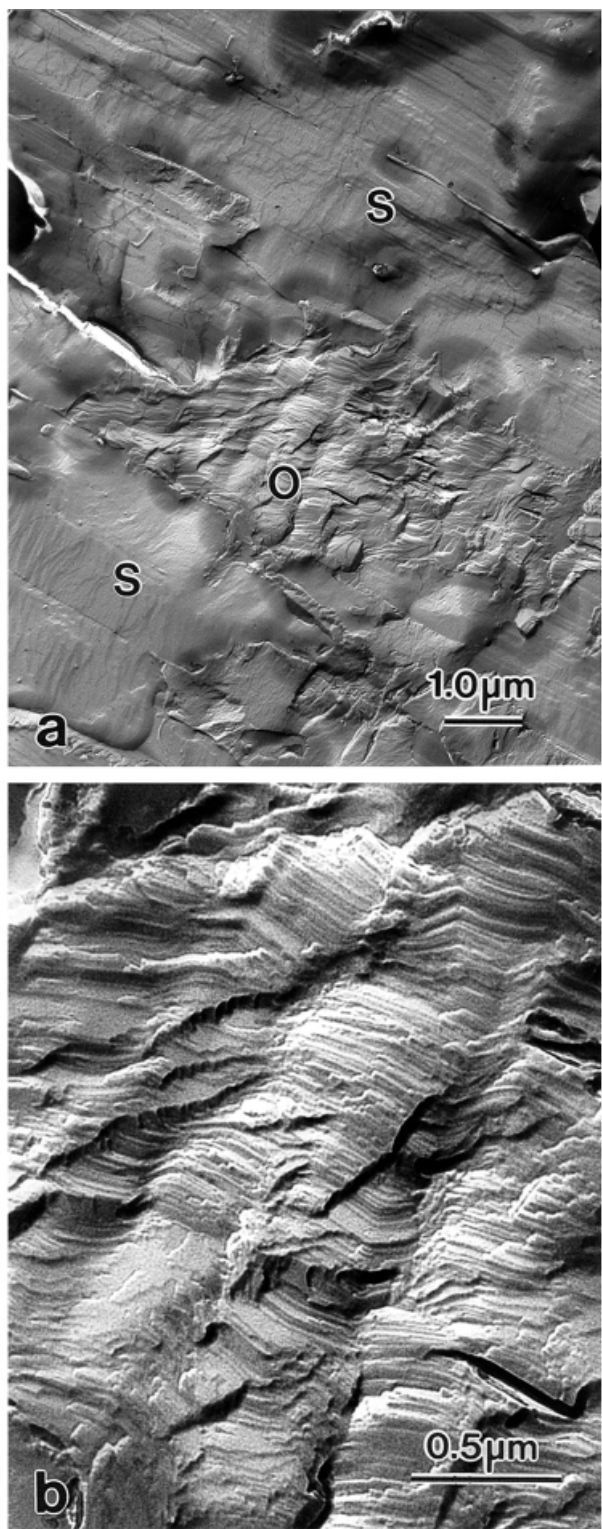


Figure 5. TEM electron micrograph of a freeze-etched 1:4 mixture of **1** and **3** in 1,2-dichlorobenzene: a: overview (O: area with ordered structure; S: solvent); b: detailed view of area O

room temperature. Eventually the thickening structure may rearrange into different aggregates which were observed by TEM. This aggregate contains dense layers of parallel molecular piles. The gel-like structure itself was not revealed in

the TEM probably for reasons of segregation phenomena which covered most of the TEM records.

## Experimental Section

**General:** All chemicals and solvents were used in p.a. quality. The gel-like systems were prepared by the freeze fracture/freeze etch method:<sup>[19]</sup> Small particles (approx. 2  $\mu$ L) were attached to gold specimen supports and immediately cryofixed by immersion into melting freon 22 (113 K), subsequently stored in liquid nitrogen. The freeze fracture preparation was carried out in a Balzers BA 360 M apparatus (cleavage temperature 173 K; etching time 10 min; shadowing the sample with 2 nm platinum at an angle of 45°, fortification of this layer with 20 nm of carbon). The cleaning of the replica film was achieved by repeated washing with chloroform. TEM was performed with a Philips EM 301 transmission electron microscope operating at 60 kV. Rheologic experiments were performed with a Physica UDS 200 apparatus; solvent 1,2-dichlorobenzene. Solution 1 contained 11.2 mg/ml calixarene ( $1 \cdot 10^{-2}$  mol/L) and 10.7 mg/ml naphthyridine ( $3 \cdot 10^{-2}$  mol/L). Solution 2 contained 5.5 mg/ml calixarene ( $5 \cdot 10^{-3}$  mol/L) and 7.1 mg/ml naphthyridine ( $2 \cdot 10^{-2}$  mol/L).

**rccc-4,6,10,12,16,18,22,24-Octahydroxy-2,8,14,20-tetra-n-undecylpyridine[4]arene or rccc-2,8,14,20-Tetraundecyl-5,11,17,23-tetraazapentacyclo[19.3.1.1<sup>3,7</sup>.1<sup>9,13</sup>.1<sup>15,19</sup>]octacosa-1(25),3,5,7(28),9,11,13(27),15(26),16,18,21,23-dodecaen-4,6,10,12,16,18,22,24-octol (1):** A suspension of 2,6-dihydroxypyridine (8.0 g, 54.4 mmol) in glycol monoisopropyl ether (40 mL) and concd. hydrochloric acid (20 mL) was mixed with *n*-dodecanal (10.0 g, 54.4 mmol) and was heated to reflux under argon. After clearing of the solution, a wax-like yellow to red precipitate was formed within 5 h. Heating was continued for 7 d. After cooling, the raw product was filtered off, taken up in acetone (250 mL) and treated with ultrasound for 30 min. The resulting amorphous pale-yellow powder was separated and washed with acetone and ethanol. After drying and recrystallization from chloroform/ethanol, 7.15 g (6.4 mmol, 47%) of pale-yellow leafy crystals were obtained and identified as **1**. M.p. 170–172 °C. <sup>1</sup>H NMR (500 MHz, CDCl<sub>3</sub> + CF<sub>3</sub>COOD, 25 °C):  $\delta$  = 0.89 (t, <sup>3</sup>J = 7.1 Hz, 12 H, CH<sub>3</sub>), 1.10–1.50 (m, 72 H, CH<sub>2</sub>), 2.14 (dt, <sup>3</sup>J = 8.0, 7.2 Hz, 8 H, CHCH<sub>2</sub>CH<sub>2</sub>), 4.27 (t, <sup>3</sup>J = 8.1 Hz, 4 H, CH<sub>methine</sub>), 7.44 (s, 4 H, CH<sub>pyridine</sub>) ppm. <sup>13</sup>C NMR (75 MHz, CDCl<sub>3</sub>, 25 °C):  $\delta$  = 14.1 (CH<sub>3</sub>), 22.1 (CH<sub>2</sub>CH<sub>3</sub>), 27.7 (CHCH<sub>2</sub>), 29.4, 29.55, 29.63, 29.70, 29.73, 29.75, 31.94 (CH<sub>2</sub>, partial overlap), 109.8 (COHC), 117.0 (CCOH<sub>pyridinediol tautomer</sub>), 136.1 (CH<sub>pyridinediol tautomer</sub>), 124.0 (C=OC), 153.5 (COH), 157.8 (COH<sub>pyridinediol tautomer</sub>), 163.3 (C=O) ppm. UV/Vis (CH<sub>2</sub>Cl<sub>2</sub>):  $\lambda$  (lg  $\epsilon$ ) = 240 (4.21), 328 (4.65) nm. IR:  $\tilde{\nu}$  = 3458, 3116, 2923, 2851, 1633, 1593, 1466, 1400, 1370, 1303, 1211, 867, 608, 538 cm<sup>-1</sup>. ESI-MS (toluene/methanol): *m/z* (%) = 1109.8 (100) [M<sup>+</sup>], 1167.9 (8), 1184.9 (5). MALDI-TOF-MS (matrix of 2,6-dihydroxybenzoic acid, ions positive): 1109 [M<sup>+</sup>]. HMRMS for C<sub>68</sub>H<sub>109</sub>N<sub>4</sub>O<sub>8</sub>: calcd. 1109.8246; found 1109.8238.

**2-Amino-N<sup>3</sup>-(n-undecyl)-1,8-naphthyridine-3-carboxamide (3):** *N*<sup>1</sup>-Dodecylcyanoacetamide (1.85 g, 7.30 mmol) and pyridine (2 mL) were added to a suspension of 2-aminonicotinic aldehyde (1.00 g, 7.29 mmol) in ethanol (40 mL). Heating under reflux for 24 h followed by cooling to 5 °C yield a yellow precipitate which was recrystallised from chloroform/ethanol to give **3** (1.99 g, 62%) as yellow needles. M.p. 148–149 °C – <sup>1</sup>H NMR (300 MHz, CDCl<sub>3</sub>, 25 °C):  $\delta$  = 8.82 (dd, <sup>3</sup>J = 4.5, <sup>4</sup>J = 2.01, 1 H, 7-H), 8.17 (s, 1 H, 4-H), 7.87 (dd, <sup>3</sup>J = 8.0, <sup>3</sup>J = 2.0 Hz, 1 H, 5-H), 7.12 (dd, <sup>3</sup>J =

4.4, 7.9 Hz, 1 H, 6-H), 6.65–6.75 (br., 3 H, NH, NH<sub>2</sub>), 3.45 (dt, <sup>3</sup>J = 5.5, <sup>2</sup>J = 7.3 Hz, 2 H, NCH<sub>2</sub>), 1.6–1.75 (br., 2 H, NCH<sub>2</sub>CH<sub>2</sub>), 1.2–1.5 (m, 18 H, CH<sub>2</sub>), 0.88 (t, <sup>3</sup>J = 6.9 Hz, 3 H, CH<sub>3</sub>) ppm. <sup>13</sup>C NMR (75 MHz, CDCl<sub>3</sub>, 25 °C): δ = 167.0 (C=O), 158.5 (C-2), 157.0 (C-10), 154.6 (C-7), 137.2 (C-5), 137.1 (C-4), 118.5 (C-6), 116.7 (C-9), 116.4 (C-3), 40.2 (NCH<sub>2</sub>), 31.9 (NCH<sub>2</sub>CH<sub>2</sub>), 29.7, 29.6, 29.59, 29.56, 29.53, 29.35, 29.32, 27.0 (CH<sub>2</sub>, dodecyl residue), 22.7 (CH<sub>2</sub>CH<sub>3</sub>), 14.1 (CH<sub>3</sub>) ppm. UV/Vis (acetone): λ (lg ε) = 238 (4.42), 268 (3.78), 363 (3.74) nm. IR: ν = 3389, 3150, 2920, 2847, 1643, 1558, 1516, 1479, 1432, 1208, 805.6 cm<sup>-1</sup>. HRMS for C<sub>21</sub>H<sub>32</sub>N<sub>4</sub>O: calcd. 356.25760; found 356.25670; for C<sub>20</sub><sup>13</sup>CH<sub>32</sub>N<sub>4</sub>O: calcd. 357.26096; found 357.26030.

## Acknowledgments

We are indebted to Dr. H. Luftmann at the University of Münster, who performed all MALDI-MS measurements, to Dr. Wolff at the University of Kiel for the NMR measurements, to the Innovationsfonds des Landes NRW, and to the Fonds der Chemischen Industrie for financial support.

- [<sup>1</sup>] [<sup>1a</sup>] D. M. Rudkevich, *Chem. Eur. J.* **2000**, *6*, 2679–2686. [<sup>1b</sup>] K. Hanabusa, T. Miki, Y. Taguchi, T. Koyama, H. Shirai, *J. Chem. Soc., Chem. Commun.* **1993**, 1382–1384. [<sup>1c</sup>] M. Tata, V. T. John, Y. Y. Waguestack, G. L. McPherson, *J. Am. Chem. Soc.* **1994**, *116*, 9464–9470.  
[<sup>2</sup>] T. Gerkensmeier, W. Iwanek, C. Agena, R. Fröhlich, S. Kotila, C. Näther, J. Mattay, *Eur. J. Org. Chem.* **1999**, 2257–2262.

- [<sup>3</sup>] I. Higler, L. Grave, E. Breuning, W. Verboom, F. de Jong, T. M. Fyles, D. N. Reinhoudt, *Eur. J. Org. Chem.* **2000**, 1727–1734.  
[<sup>4</sup>] S. K. Körner, F. C. Tucci, D. M. Rudkevich, T. Heinz, J. Rebek, Jr., *Chem. Eur. J.* **2000**, *6*, 187–195.  
[<sup>5</sup>] R. H. Vreekamp, W. Verboom, D. N. Reinhoudt, *J. Org. Chem.* **1996**, *61*, 4282–4288.  
[<sup>6</sup>] K. Koh, K. Araki, S. Shinkai, *Tetrahedron Lett.* **1994**, *35*, 8255–8258.  
[<sup>7</sup>] J. J. Gonzalez, P. Prados, J. de Mendoza, *Angew. Chem. Int. Ed.* **1999**, *38*, 525–528; *Angew. Chem.* **1999**, *111*, 546–549.  
[<sup>8</sup>] O. Mogck, M. Pons, V. Böhmer, W. Vogt, *J. Am. Chem. Soc.* **1997**, *119*, 5706–5712.  
[<sup>9</sup>] L. R. MacGillivray, J. L. Atwood, *Nature* **1997**, *389*, 469–472.  
[<sup>10</sup>] J. H. van Esch, B. L. Feringa, *Angew. Chem.* **2000**, *112*, 2351–2354.  
[<sup>11</sup>] T. Gerkensmeier, C. Näther, J. Mattay, *Chem. Eur. J.* **2001**, *7*, 465–474.  
[<sup>12</sup>] A. R. Katritzky, F. D. Popp, J. D. Rowe, *J. Chem. Soc. B* **1966**, 562–564.  
[<sup>13</sup>] E. Spinner, J. C. B. White, *J. Chem. Soc. B* **1966**, 991–995.  
[<sup>14</sup>] E. Spinner, G. B. Yeoh, *Aust. J. Chem.* **1971**, *24*, 2557–2573.  
[<sup>15</sup>] I. Cardinaud, A. Gueiffier, J.-C. Debouzy, J.-C. Milhavet, J. P. Chapat, *Heterocycles* **1993**, *36*, 2513–2522.  
[<sup>16</sup>] T. G. Majewicz, P. Caluwe, *J. Org. Chem.* **1974**, *39*, 720.  
[<sup>17</sup>] E. E. Fenlon, T. J. Murray, M. H. Baloga, S. C. Zimmerman, *J. Org. Chem.* **1993**, *58*, 6625–6628.  
[<sup>18</sup>] W. Buchheim in *Electron Microscopy*, vol. 2 (Ed.: Y. Ben-Shaul), Tal Internat. Publishing Comp., Israel, **1976**, pp. 122–124.  
[<sup>19</sup>] W. Buchheim, *Food Microstruct.* **1982**, *1*, 189–208.

Received January 24, 2002  
[O02033]

## Formation of Branched Calixarene Aggregates—A Time-Resolved Static Light Scattering Study

Thomas Witte,<sup>‡</sup> Björn Decker,<sup>§</sup> Jochen Mattay,<sup>§</sup> and Klaus Huber<sup>\*</sup>,<sup>‡</sup>

*Contribution from the Fakultät für Naturwissenschaften, Department Chemie, Physikalische Chemie, Universität Paderborn, Warburger Strasse 100, D-33098 Paderborn, Germany, and Fakultät für Chemie, Organische Chemie I, Universität Bielefeld, Postfach 100131, D-33501 Bielefeld, Germany*

Received February 6, 2004; E-mail: huber@chemie.uni-paderborn.de

**Abstract:** Mixtures of a calix[4]arene and a naphthyridine derivative dissolved in 1,2-dichlorobenzene form thermoreversible aggregates. The aggregation process was followed by means of time-resolved multiangle light scattering at two different mixing ratios, 1:3 and 1:4, yielding a detailed record of the relative mass, the radius of gyration, and the particle scattering function of the growing aggregates. On the basis of these data, a conclusive model of the structure is presented for the developing aggregates: monomers aggregate to wormlike filaments which form branching points. Formation of branching points proceeds in a frequency and distribution which is similar to the polycondensation of ABC monomers toward non-randomly branched macromolecules (Burchard, W. *Macromolecules* **1977**, *10*, 919–927). Thus, aggregation results in hyperbranched-like particles with striking analogies to the polymerization of glucose to amylopectin.

### Introduction

For small molecules, the highest degree of order certainly is achieved in a three-dimensional pattern, denoted as crystal formation. From the thermodynamic point of view, this corresponds to a first-order phase transition. Although it is the most prominent example, crystallization is far from being the only process to generate ordered structures. Meanwhile, a large number of self-assembly processes have been discovered and investigated. These self-assembly processes generate supramolecular aggregates as countless and diverse as polymer science did and still does in the field of covalently linked molecules.<sup>1,2</sup> Although supramolecular structures are much less stable in general than macromolecules are, this instability is a strength rather than a weakness in many biological processes.<sup>3</sup> The inherent reversibility of these processes enables biological systems to respond in a highly flexible manner to ever-changing conditions. Therefore, such reversible processes may become an example for technical applications.

Despite characteristic differences between supramolecular structures and covalently linked polymers, analogies between the two classes of structures are striking and highly inspiring.<sup>4</sup> These analogies suggest application of many of the physico-

chemical concepts originally developed in polymer science also to the interpretation of the behavior of supramolecular structures. One of the first examples is the successful application of the concept of wormlike chains<sup>5–7</sup> to the aggregates of amphiphilic molecules.<sup>8–12</sup> Another example<sup>13</sup> is the interpretation of dilute solution viscosity measurements in terms of a model analogous to the A–B-type polycondensation,<sup>14</sup> controllable by means of the addition of monofunctional monomers. Finally, exponents from intrinsic viscosity versus molar mass plots were successfully used by Foglman et al.<sup>15</sup> to extract information on the shape of aggregates.

Significant progress became possible through the use of time-resolved static light scattering (TR-SLS), which enabled an *in situ* recording of the growth process of aggregates. The first publications on this method reported on the investigation of ionic

<sup>‡</sup> Universität Paderborn.

<sup>§</sup> Universität Bielefeld.

- (1) Among others, the following reviews give an excellent introduction into the field: (a) Fuhrhop, J.-H.; Helfrich, W. *Chem. Rev.* **1993**, *93*, 1565–1582. (b) Terech, P.; Weiss, R. G. *Chem. Rev.* **1997**, *97*, 3133–3159.
- (2) (a) Lehn, J.-M. *Supramolecular Chemistry: Concepts and Perspectives*; VCH: Weinheim, Germany, 1995. (b) Lehn, J.-M. In *Supramolecular Science: Where It Is and Where It Is Going*; Ungaro, R., Dalcanale, E., Eds.; Kluwer: Dordrecht, The Netherlands, 1999.
- (3) Alberst, B.; Bray, D.; Lewis, J.; Raff, M.; Roberts, K.; Watson, J. D. *The Molecular Biology of the Cell*, 3rd ed.; Garland Publishers Inc.: New York and London, 1994.

- (4) (a) Brunsved, L.; Fomer, B. J. B.; Meijer, E. W.; Sijbesma, R. P. *Chem. Rev.* **2001**, *101*, 4071–4097. (b) Ciferri, A. *Macromol. Rapid Commun.* **2002**, *23*, 511–529.
- (5) Kratky, O.; Porod, G. *Recl. Trav. Chim.* **1949**, *68*, 1106–1122.
- (6) Pedersen, J. S.; Schurtenberger, P. *Macromolecules* **1996**, *29*, 7602–7612.
- (7) Pötschke, D.; Hickl, P.; Ballauff, M.; Astrand, P.-O.; Pedersen, J. S. *Macromol. Theory Simul.* **2000**, *9*, 345–353.
- (8) (a) Imae, T.; Kamya, R.; Ikeda, S. *J. Colloid Interface Sci.* **1985**, *108*, 215–225. (b) Imae, T.; Ikeda, S. *J. Phys. Chem.* **1986**, *90*, 5216–5223.
- (9) Denkinger, P.; Kunz, M.; Burchard, W. *Colloid Polym. Sci.* **1990**, *268*, 513–527.
- (10) Jerke, G.; Pedersen, J. S.; Egelhaaf, S. U.; Schurtenberger, P. *Phys. Rev. E* **1997**, *56*, 5772–5788.
- (11) von Berlepsch, H.; Harnau, L.; Reineker, P. *J. Phys. Chem. B* **1998**, *102*, 7518–7522.
- (12) Magid, L. *J. Phys. Chem. B* **1998**, *102*, 4064–4074.
- (13) Sijbesma, R. P.; Beijer, F. H.; Brunsfeld, L.; Folmer, B. J. B.; Hirschberg, J. H. K. K.; Lange, R. F. M.; Lowe, J. K. L.; Meijer, E. W. *Science* **1997**, *278*, 1601–1604.
- (14) Flory, P. J. *Principles of Polymer Chemistry*; Cornell University Press: Ithaca, NY, 1953.
- (15) Foglman, E. A.; Yount, W. C.; Xu, J.; Craig, S. L. *Angew. Chem.* **2002**, *114*, 4198–4200.

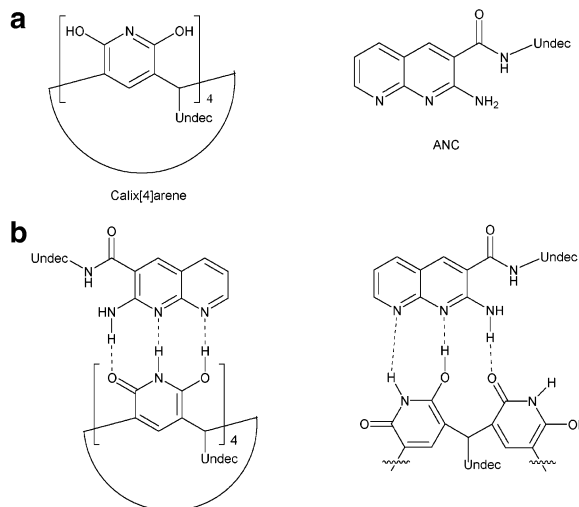


**Figure 1.** (a) Molecular structure of calix[4]arene and ANC. (b) Possible hydrogen bonding of aggregates between octahydroxypyridine[4]arenes and 2-amino-1,8-naphthyridines following the AAD-DDA pattern (note the octahydroxypyridine[4]arene in its tautomeric hydroxypyridone form).

dyestuffs<sup>16–18</sup> in dilute aqueous solution. Again, the model of wormlike chains turned out to be extremely valuable. Aside from correctly reproducing the particle shape, the wormlike chain model made it possible to discuss light scattering results without referring to mass data. This could be achieved by transforming mass values into contour lengths by means of the so-called mass per unit length.<sup>16</sup> However, as could also be demonstrated, this application has to be performed with great care because the onset of branching may be misinterpreted as an increased flexibility of the fibers.<sup>17</sup> Meanwhile, dilute solutions of a so-called dendron rod–coil molecule in 2-propanol, also investigated by TR-SLS, provided another system of reversible wormlike aggregates.<sup>19</sup>

Motivated by this progress, we were tempted to apply TR-SLS to the self-assembly of a completely different system. This system is composed of two components, 2,6,8,12,14,18,20,24-octahydroxy-4,10,16,24-tetra-*n*-undecylpyridine[4]arene (calix[4]arene) and 2-amino-*N*<sup>3</sup>-(*n*-undecyl)-1,8-naphthyridine-3-carboxamide (ANC). Formulas of both components are shown in Figure 1a. The present investigation succeeds earlier work which aimed at a controlled molecular aggregation<sup>20</sup> and which included systems involving naphthyridines.<sup>21</sup> Due to their AAD pattern<sup>22</sup> of hydrogen donor (D) and acceptor (A) groups, 2-amino-1,8-naphthyridines perfectly complement the DDA motif of octahydroxypyridine[4]arenes in their tautomeric hydroxypyridone form.<sup>23</sup> Following this idea, both components should form complexes especially at a 1:4 ratio of the calixarene macrocycle and naphthyridine, respectively (Figure 1b). Indeed, this was experimentally shown earlier<sup>24</sup> in apolar solvents such as toluene and 1,2-dichlorobenzene.

- (16) Inglés, S. E.; Katzenstein, A.; Schlenker, W.; Huber, K. *Langmuir* **2000**, *16*, 3010–3018.
- (17) Katzenstein, A.; Huber, K. *Langmuir* **2002**, *18*, 7049–7056.
- (18) Herzog, B.; Huber, K.; Stegemeyer, H. *Langmuir* **2003**, *19*, 5223–5232.
- (19) de Gans, B. J.; Wiegand, S.; Zubarev, E. R.; Stupp, S. I. *J. Phys. Chem. B* **2002**, *106*, 9730–9736.
- (20) Zimmerman, S. C.; Duerr, B. F. *J. Org. Chem.* **1992**, *57*, 2215–2217.
- (21) (a) Kelly, T. R.; Bridger, G. J.; Zhao, C. J. *Am. Chem. Soc.* **1990**, *112*, 8024–8034. (b) Murray, T. J.; Zimmerman, S. C. *J. Am. Chem. Soc.* **1992**, *114*, 4010–4011. (c) Brammer, S.; Lüning, U.; Kühl, C. *Eur. J. Org. Chem.* **2002**, *4054*–4062.
- (22) Jorgensen, W. L.; Pranata, J. *J. Am. Chem. Soc.* **1990**, *112*, 2008–2010.
- (23) Gerkensmeier, T.; Näther, C.; Mattay, J. *Chem. Eur. J.* **2001**, *7*, 465–474.

By now, a few other examples of calix[*n*]arene-based gelation have appeared in the literature. Xu et al.<sup>25</sup> reported on a calix[4]arene species to which Pd(II) cations had to be added as a second component in order to induce formation of a stable “metallogel” in DMSO. However, addition of a second component is not always a necessary prerequisite for gelation. As has been shown by Shinkai et al.,<sup>26</sup> calix[*n*]arenes with *n* = 8 are capable of forming gels in apolar solvents by themselves. In their case, less than 1% of the calix[8]arene was required in order to induce a thermoreversible sol–gel process. Finally, we would like to draw attention to a class of water-soluble calix[*n*]arenes.<sup>27,28</sup> They turned out to spontaneously form gels both in their acidic forms or as salts,<sup>28</sup> or after addition of lanthanides to their aqueous solutions.<sup>27,28</sup> As determined by dynamic light scattering, their size reached hydrodynamically effective radii as large as 225 nm, with the sodium salts persistently larger than the corresponding acids.<sup>27</sup> Calix[*n*]arenes also form supramolecules via inclusion of *trans*-β-carotenoid, which further aggregate to larger particles. The respective hydrodynamic radii were only 100–150 nm and thus smaller than those without the *trans*-β-carotenoid inclusion.<sup>27</sup>

For the system presently under investigation, shear thinning and thixotropy were observed for mixtures of calix[4]arene and ANC in molar ratios of 1:3 and 1:4. Rheological effects were much larger with the ratio 1:4. With the mixing ratio 1:4 of calix[4]arene and ANC, thermoreversible gelation could be achieved at *T* = 5 °C with concentrations of the mixture as low as 12.6 g L<sup>-1</sup>.<sup>24</sup> In the present paper, we are aiming at the primary structures of the calix[4]arene/ANC aggregates preceding gelation by means of TR-SLS. In line with the preceding paper,<sup>24</sup> our experiments will be restricted to the calix[4]arene/ANC ratios 1:3 and 1:4. To make the features of single growing aggregates accessible to scattering experiments, an appropriate concentration and temperature regime had to be established first. To the best of our knowledge, we succeeded for the first time in extending the investigation of self-assembly processes by TR-SLS to the formation of nonlinear structures, and we point out similarities to a branching model well established in polymer science.

## Experiments and Data Evaluation

Scattering intensities are recorded at 19 different angles *θ*, resulting in angular-dependent scattering curves.<sup>29</sup> In these curves, the scattering intensity of the aggregating particles in excess to the solvent scattering is expressed as the difference between the Rayleigh ratio of the respective calix[4]arene/ANC solutions, *R*<sub>θ</sub>(CA), and the solvent background, *R*<sub>θ</sub>(SB),  $\Delta R_\theta = R_\theta(\text{CA}) - R_\theta(\text{SB}) = \Delta R(q)$ . The variable of these curves is the magnitude of the scattering vector *q*,

$$q = (4\pi n_0/\lambda) \sin(\theta/2) \quad (1)$$

- (24) Gerkensmeier, T.; Decker, B.; Schwertfeger, M.; Buchheim, W.; Mattay, J. *Eur. J. Org. Chem.* **2002**, 2120–2125.
- (25) (a) Xing, B.; Choi, M.-F.; Zhou, Z.; Xu, B. *Chem. Commun.* **2002**, 362–363. (b) Xing, B.; Choi, M.-F.; Zhou, Z.; Xu, B. *Langmuir* **2002**, *18*, 9654–9658.
- (26) Aoki, M.; Nakashima, K.; Kawabata, H.; Tsutsui, S.; Shinkai, S. *J. Chem. Soc., Perkin Trans. 2* **1993**, 347–354.
- (27) Steed, J. W.; Johnson, C. P.; Banes, C. L.; Juneja, R. K.; Atwood, J. L.; Reilly, S.; Hollis, R. L.; Smith, P. H.; Clark, D. L. *J. Am. Chem. Soc.* **1995**, *117*, 11426–11433.
- (28) Makha, M.; McKinnon, I. R.; Raston, C. L. *J. Chem. Soc., Perkin Trans. 2* **2002**, 1801–1806.
- (29) Becker, A.; Schmidt, M. *Macromol. Chem., Macromol. Symp.* **1991**, *50*, 249–260.

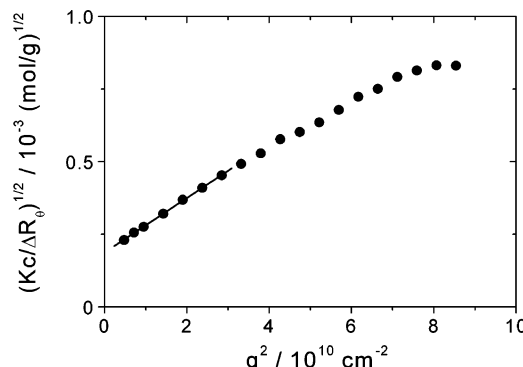


**Figure 2.** Data evaluation of a single curve at  $t = 45$  min selected from Figure 3. The scattering curve is selected from an aggregation run of a 1:4 calix[4]arene/ANC mixture with  $c = 7.61$  g L $^{-1}$ . The mean square radius of gyration,  $R_g^2$ , is given by the slope of the curve and the relative weight-averaged molecular weight,  $M_w$ , by the limit at  $q \rightarrow 0$ . Curve fitting is restricted to  $6.89 \times 10^{-3} \leq q \leq 1.69 \times 10^{-2}$  nm $^{-1}$ , corresponding to the linear part of the curve.

with  $n_0$  the refractive index of the solvent and  $\lambda$  the wavelength of the laser light source. Data evaluation of the scattering curves uses the inverse reduced scattering intensities  $Kc/\Delta R(q)$ , with  $K$  the contrast factor and  $c$  the weight in concentration of the solid (calix[4]arene with ANC) in grams per liter. In the limit of infinitely small  $c$  and  $q$ , the reduced intensity  $Kc/\Delta R(q)$  yields the weight-averaged molar mass,  $M_w$ , and the z-averaged square radius of gyration,  $R_g^2$ , of the dissolved solid particles according to<sup>30,31</sup>

$$\frac{1}{M_w} = \lim_{\substack{c \rightarrow 0 \\ q \rightarrow 0}} \left[ \frac{Kc}{\Delta R(q)} \right] \quad (2)$$

$$R_g^2 = \lim_{\substack{c \rightarrow 0 \\ q \rightarrow 0}} \left[ 3M_w \frac{\partial(Kc/\Delta R(q))}{\partial q^2} \right] \quad (3)$$

However, an extrapolation to  $c = 0$  in eqs 2 and 3 is not possible in an aggregating system. The particle scattering factor corresponding to a normalized scattering curve was calculated by dividing the original curve by its limit at  $q \rightarrow 0$ ,  $Kc/\Delta R(q) = 1/M_w$ ,

$$P_z(q) = \frac{\Delta R_\theta/Kc}{\Delta R_0/Kc} \quad (4)$$

The aggregation process is followed by measuring scattering curves at variable aggregation time  $t$ . The onset of aggregation,  $t = 0$ , is defined by the mixing of the two components calix[4]arene and ANC in solution.

Detailed information about the experimental procedure and the data evaluation are given in the Supporting Information.

## Results and Discussion

**Evolution of Particle Size.** Solutions of calix[4]arene/ANC in the present investigation led to aggregation processes which could be followed by means of TR-SLS for at least 60 min. The power of this method is illustrated in Figure 3, representing a selection of scattering curves from a single run. Each curve results in a value for the relative mass,  $M_w$ , and the size,  $R_g$ . Figures 4 and 5 show the development of the radius of gyration,  $R_g$ , and the relative weight-averaged molar mass,  $M_w$ , as functions of time for the 1:4 and 1:3 mixtures, respectively. For both mixing ratios, the growth process is accelerated if the

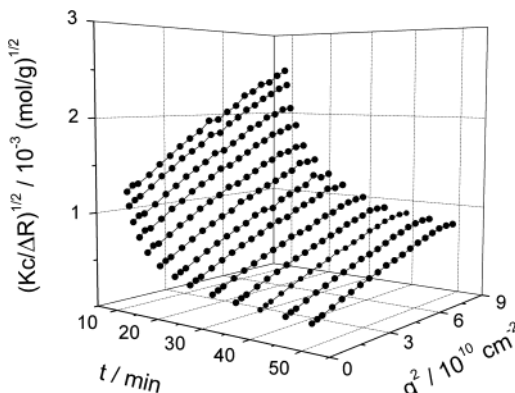


**Figure 3.** Berry plot of a selection of scattering curves for a 1:4 calix[4]-arene/ANC mixture with  $c = 7.61$  g L $^{-1}$ .

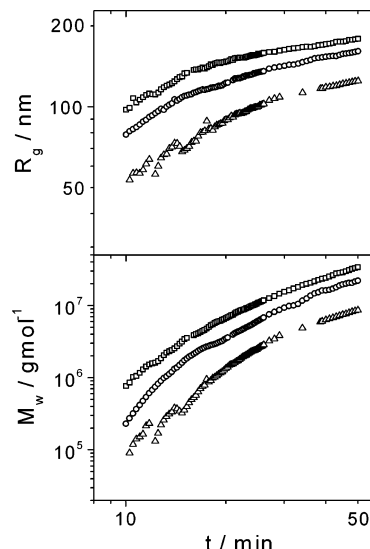


**Figure 4.** Development of the radius of gyration,  $R_g$ , and the relative weight-averaged molar mass,  $M_w$ , as a function of time for the 1:4 mixtures at  $c = 7.61$  (□), 6.97 (○), and 6.34 g L $^{-1}$  (△).

concentration of the calix[4]arene/ANC mixture is increased. Aggregation of all 1:4 mixtures is faster, leading to larger particles than aggregation in solutions of the corresponding 1:3 mixtures does. Although this is represented in a double logarithmic plot, no clear-cut power laws became discernible in Figures 4 and 5.

However, focusing on the initial and final stages of the respective aggregation processes, limiting exponents can be discussed for  $R_g \propto t^{\alpha_t}$ . At the onset of aggregation, exponents were close to  $\alpha_t = 0.75$  for 1:4 mixtures and  $\alpha_t = 1.4$  for 1:3 mixtures. In the case of the final stage, located at aggregation times of  $t \geq 30$  min, exponents were found to be  $0.19 \leq \alpha_t \leq 0.26$  for the 1:4 mixtures and  $0.33 \leq \alpha_t \leq 0.52$  for the 1:3 mixtures.

Those limiting exponents can be compared with the growth laws of two prominent model processes for fractal aggregates, diffusion-limited cluster aggregation (DLCA) and reaction-limited cluster aggregation (RLCA). In these model processes, not only do monomers add to aggregates but particles at any degree of aggregation, denoted as clusters, stick to any other cluster. Both processes may serve as possible models for the aggregation of calix[4]arene and ANC. Noticeably, the exponents at the final stages of the aggregation do not even get close to the theoretical value,  $\alpha_t \propto 1/d_f = 1/1.8$ , which corresponds

(30) (a) Zimm, B. *J. Chem. Phys.* **1948**, *16*, 1093–1099. (b) Zimm, B. *J. Chem. Phys.* **1948**, *16*, 1099–1116.

(31) Berry, G. C. *J. Chem. Phys.* **1966**, *44*, 4550–4564.

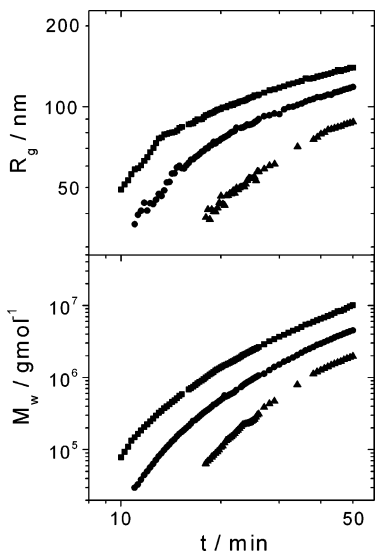


**Figure 5.** Development of the radius of gyration,  $R_g$ , and the apparent weight-averaged molar mass,  $M_w$ , as a function of time for the 1:3 mixtures at  $c = 6.53$  (■), 6.00 (●), and  $5.45 \text{ g L}^{-1}$  (▲).

to the respective inverse fractal or Hausdorff dimension expected for DLCA.<sup>32,33</sup> Exponents at the initial stages were significantly larger than 1/1.8. If at all, the only structural hint is provided by the initial exponents from the 1:4 mixtures being close to 1, which may indicate an initial formation of linear objects with an almost constant growth rate. Finally, the curves in Figure 4 do not support the exponential growth (not shown explicitly) of  $R_g \propto e^{ct}$  predicted for the RLCA.<sup>33,34</sup>

Further insight into the mechanism of particle formation is expected to be obtained if the radius of the growing particles is related to the respective increase of the relative particle mass. Such a relation is shown in Figure 6, where the  $z$ -averaged root-mean-squared radius of gyration,  $R_g$ , is plotted versus the apparent weight-averaged mass,  $M_w$ , for all three concentrations of both mixtures. In the case of self-similar systems, such a plot leads to a power law of

$$R_g \propto M_w^{\alpha_g} \quad (5)$$

The most prominent examples are rods ( $\alpha_g = 1.0$ ), polymeric coils<sup>14</sup> ( $\alpha_g = 0.5\text{--}0.6$ ), and spheres ( $\alpha_g = 0.33$ ). For clusters from DLCA<sup>32,33</sup> and from RLCA,<sup>33,34</sup> exponents of  $\alpha_g \approx 0.57$  and 0.48, respectively, are predicted. For the calix[4]arene/ANC system, a single power law could be identified only at the lowest concentrations respectively, resulting in  $\alpha_g = 0.19$  for the 1:4 mixture and  $\alpha_g = 0.24$  for the 1:3 mixture. At higher concentrations, at least two regimes became distinguishable, indicating two stages of the growth process with the corresponding exponents extending over a range of  $0.12 < \alpha_g < 0.21$  for the 1:4 mixtures and  $0.18 < \alpha_g < 0.31$  for the 1:3 mixtures. Thus, all experimental slopes are much smaller than  $\alpha_g$  of any of the above-mentioned self-similar systems.

Yet, only distributions of clusters resulting from DLCA or RLCA can unambiguously be ruled out as possible model

- (32) Weitz, D. A.; Huang, J. S.; Lin, M. Y.; Sung, J. *Phys. Rev. Lett.* **1984**, *53*, 1657–1660.
- (33) Weitz, D. A.; Huang, J. S.; Lin, M. Y.; Sung, J. *Phys. Rev. Lett.* **1985**, *54*, 1416–1419.
- (34) Lin, M. Y.; Lindsay, H. M.; Weitz, D. A.; Ball, R. C.; Klein, R.; Meakin, P. *Phys. Rev. A* **1990**, *41*, 2005–2020.

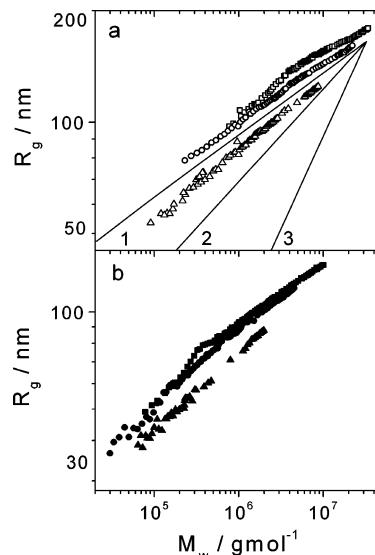


**Figure 6.** (a) Radii of gyration,  $R_g$ , versus the apparent mass,  $M_w$ , for the 1:4 mixture at  $c = 7.61$  (□), 6.97 (○), and  $6.34 \text{ g L}^{-1}$  (△). The curves describe trends of  $R_g$  versus  $M_w$  for particle formation of spheres (1), coils (2), and rods (3), where the average values include the monomer fraction, respectively. (b) Radii of gyration,  $R_g$ , versus the apparent mass,  $M_w$ , for the 1:3 mixtures at  $c = 6.53$  (■), 6.00 (●), and  $5.45 \text{ g L}^{-1}$  (▲). For the higher concentrations, at least two linear regimes became distinguishable.

systems. The three other examples for self-similar systems have to be considered more carefully. If the calix[4]arene/ANC aggregates consist of growing rods, coils, or spheres, growth may occur at the expense of monomers, which gradually attach to the aggregates. In such cases, the  $M_w$  values available from eq S5 (Supporting Information) and used in eq 5 correspond to overall mass values, which include the monomers. This is due to the fact that evaluation of  $M_w$  by means of eq S5 is based on a constant overall concentration,  $c$ , corresponding to the original weight in quantity. On the other hand, power laws require averaged mass data which exclusively refer to the aggregates. Such aggregate mass values could be calculated from eq S5 only if separate concentrations were measurable for the mass fractions of monomers and of aggregates, respectively, at all intermediate stages<sup>18</sup> of the aggregation process. Unfortunately, such data are not available.

To account explicitly for a decreasing amount of monomers, we calculated  $R_g$  versus  $M_w$  curves which include the respective monomer fractions for all three self-similar systems. For simplicity, we assumed that monodisperse rods, coils, or spheres are formed. Consideration of a polydispersity for the developing aggregates would only result in a parallel shift of the trends and would be of no relevance for our qualitative discussion. Monomer length and monomer weight were adopted to generate systems comparable in size to the present aggregates. Details are given in the Supporting Information. The calculated systems still form self-similar particles but are not self-similar as a whole due to the coexistence of the monomers. As a consequence, those systems no longer lead to unique exponents  $\alpha_g$ . However, we are still able to compare trends in the size and mass regime under consideration. Corresponding trends are expressed in terms of intermediate exponents, which are  $\alpha_g \approx 0.50$  (rods), 0.25 (coils), and 0.17 (spheres). These intermediate exponents are half of the exponents of the corresponding power laws in the “particle-only” limit. As is demonstrated in Figure 6, neither the theoretical trend for rods nor coils is small enough to

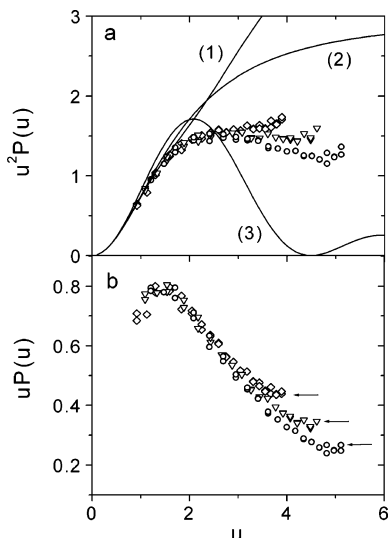


**Figure 7.** (a) Kratky plot of three scattering curves for a 1:4 mixture with  $c = 7.61 \text{ g L}^{-1}$  at  $t = 15$  ( $\diamond$ ),  $25$  ( $\nabla$ ), and  $45$  min ( $\circ$ ). All curves show an upturn in the scattering curve for  $q > 2.5 \times 10^{-2} \text{ nm}^{-1}$ . (b) Holtzer plot of the same data as in (a). The scattering factor approaches a power law of  $P(q) \propto q^{-1}$  for  $q > 2.5 \times 10^{-2} \text{ nm}^{-1}$ , typical for rodlike structures (indicated by arrows).

reproduce the observed experimental curves. Thus, comparison with experiments may provide a first hint for the formation of compact particles. In the section to follow, we take advantage of the fact that we can discuss results without referring to mass values. As will be outlined, this is achieved by a procedure which transforms  $M_w$  data into  $L_w$  and in which the above-mentioned problem caused by the use of overall concentrations is canceled.

**Particle Shape.** To get additional information on the shape of the growing particles, particle scattering factors are analyzed in a final step. If a dimensionless and normalized variable  $u$ ,

$$u = qR_g \quad (6)$$

is used instead of  $q$ , all scattering curves of a self-similar system fall on top of each other. Examples of such systems are polymer coils, rods, and spheres. In Figure 7, theoretical curves of these systems are compared with three experimental curves. The experimental curves were recorded at three different times during the growth of the 1:4 mixture with  $c = 7.61 \text{ g L}^{-1}$ . Three major aspects become apparent: (i) None of the three models generates a scattering curve comparable to those of the calix[4]arene/ANC aggregates. (ii) All experimental curves form a single trend, indicating similar shapes for all intermediates. Noticeably, the experimental curves represented as Kratky plots,  $u^2P(u)$  versus  $u$ , exhibit a shallow maximum at  $u \approx 2.5$ . Such maxima are typical for rather compact structures such as branched macromolecules. (iii) All curves in Figure 7a show an upturn in the scattering curve for  $q > 2.5 \times 10^{-2} \text{ nm}^{-1}$ .

We first pay attention to the maximum value observed in Figure 7a with the Kratky plot. This maximum is compatible with various types of branched structures. An overview of the scattering behavior of the most prominent branching models was given by Burchard<sup>35</sup> in 1983, comprising (i) stars with numbers of rays equal in length;<sup>36</sup> (ii) stars with  $f$  rays having

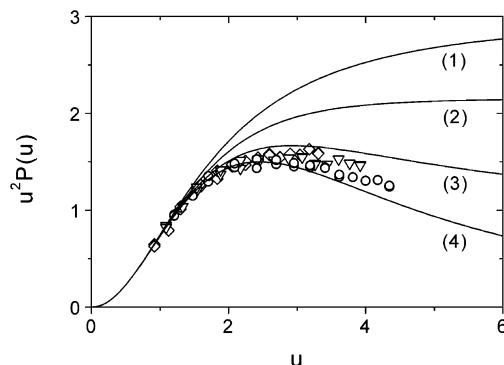


**Figure 8.** Kratky plot for an  $f$ -functional randomly branched polycondensate of the  $A_f$  type with  $C = 1$  (1), and three curves of the non-randomly branched  $ABC$  polycondensation model<sup>40</sup> for  $C = 0.3$  (2),  $C = 0.1$  (3), and  $C = 0$  (4). Theoretical curves are compared with the same selection of scattering curves used in Figure 7 (1:4 mixture of calix[4]arene/ANC with  $c = 7.61 \text{ g L}^{-1}$ ). The  $q$  regime is restricted to  $q < 2.5 \times 10^{-2} \text{ nm}^{-1}$ , corresponding to  $u < 3.33$ ,  $u < 3.94$ , and  $u < 4.37$ , respectively.

a distribution of their length;<sup>37</sup> (iii) randomly branched polycondensates of the  $A_f$  type with a functionality  $f$  of the monomer;<sup>38</sup> (iv) non-randomly branched polycondensates of the  $ABC$  type<sup>39</sup> where  $A$  can only react with  $B$  or  $C$ , including the special case of  $B = C$ ;<sup>40</sup> and (v) a loosely branched microgel denoted as soft sphere.<sup>41</sup> For non-randomly branched structures (iv), the term “hyperbranched” is used alternatively.

As pointed out by Burchard,<sup>40</sup> distinction among some of the models becomes possible by means of the Kratky representation of the particle scattering behavior. Whereas star branched molecules and nonrandom polycondensates exhibit a maximum value in this plot, random polycondensates and linear chains do not. To interpret our scattering data in terms of branching models, we compared experiments with theoretical predictions based on two models as a “first guess”. The comparison is outlined in Figure 8, which includes a selection of experimental scattering curves as  $u^2P(u)$  together with the model curve of the randomly branched  $A_f$  type and three non-randomly branched  $ABC$  polycondensates. The three  $ABC$  types differ in the branching parameter  $C$  defined by eq S14 (Supporting Information). Variation of the parameter  $C$  is achieved by varying the reactivity  $\beta$  of the  $B$  groups and the reactivity  $\gamma$  of the  $C$  groups with the  $A$  groups, respectively. It has to be emphasized that  $\beta = \gamma$  corresponds to the nonrandom  $ABB$  type. In Figure 8, two different values for the  $C$  parameter and the limit of large extent of reaction of the  $A$  groups for  $C = 0$  were calculated. In Figure 9, a sketch of an  $ABC$  polycondensate is shown. Details of the calculations are given in the Supporting Information. In fact, description of the experimental curves by the  $ABC$  type with  $0 < C < 0.1$  is fairly good as long as we exclude the  $q$  regime of  $q > 2.5 \times 10^{-2} \text{ nm}^{-1}$ , which is characterized by an upturn in the Kratky plot. The height of the maximum in the Kratky representation led to a further differentiation. Regular stars with monodisperse rays have lower maximum values than nonrandom polycondensates and stars with a length distribution of the arms. They can thus be excluded as potential candidates for the aggregates under the present investigation.

(37) Burchard, W. *Macromolecules* **1974**, *7*, 835–841.

(38) Kajiwara, K.; Burchard, W.; Gordon, M. *Br. Polym. J.* **1970**, *2*, 110–115.

(39) Burchard, W. *Macromolecules* **1972**, *5*, 604–610.

(40) Burchard, W. *Macromolecules* **1977**, *10*, 919–927.

(41) Burchard, W.; Kajiwara, K.; Nerger, D. *J. Polym. Sci. Part B: Polym. Phys.* **1982**, *20*, 157–171.

(35) Burchard, W. *Light scattering from polymers; Advances in Polymer Science* 48; Springer: Berlin/Heidelberg, 1983.  
(36) Benoit, H. J. *J. Polym. Sci.* **1953**, *11*, 507–510.

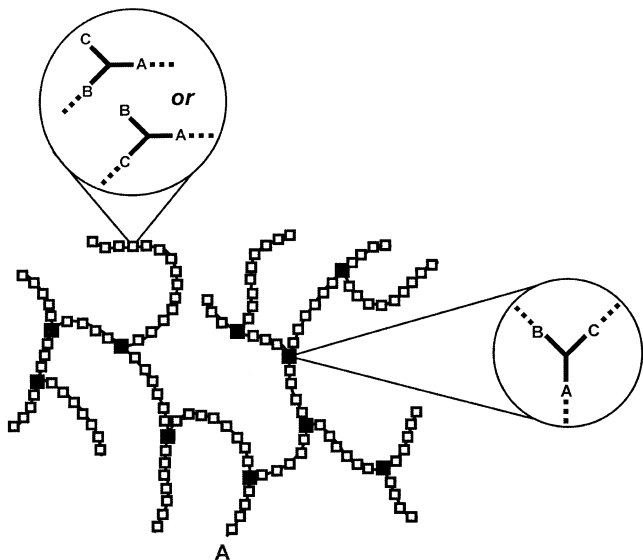


**Figure 9.** Sketch of an ABC polycondensate. The branching points consist of three reacted groups, whereas the linear segments exhibit two reacted groups only.

Finally, we direct our attention to the high  $q$  regime of the experimental scattering curves in Figure 7. As is demonstrated in Figure 7b, the upturn of the Kratky plots turns into the onset of a plateau if the so-called bended-rod plot ( $uP(u)$  versus  $u$ ) is used. A plateau of  $qP(q)$  corresponds to a power law of  $P(q) \propto q^{-1}$ , which is typical for rodlike structures<sup>42,43</sup> and semiflexible chains.<sup>44</sup> Under the assumption that this plateau is significant, we estimated the corresponding heights by multiplying the original scattering data at  $2.75 \times 10^{-2} < q < 2.92 \times 10^{-2} \text{ nm}^{-1}$  by the magnitude of the scattering vector,  $q$ . According to eq 7, this gives access to a mass per unit length,  $M_L$ , via<sup>45</sup>

$$\frac{\Delta R_\theta}{Kc} = \pi M_L = \pi \frac{M_w}{L_w} \quad (7)$$

where  $L_w$  is the weight-averaged contour length of the particles.

Prior to any application of eq 7, two aspects have to be emphasized: (i) Branching does not affect the unambiguous determination of the contour length.<sup>17</sup> If branching occurs, all linear segments contribute to the overall contour length,  $L_w$ . (ii) Theoretically, the  $q^{-1}$  power law of particle scattering factors is reached at  $u > 1$  for monodisperse rods and at  $u > 2$  for polydisperse rods. Assuming the contour lengths,  $L_w$ , of the rodlike constituents to be twice as large as the aggregate radius,  $R_g$  ( $L_w = 2R_g$ ), at the most, a lower particle size limit  $R_{g(\text{low})}$  for the applicability of eq 7 can be estimated. This estimation has to be related to the high  $q$  regime accessible to the present instrument ( $2.75 \times 10^{-2} < q < 2.92 \times 10^{-2} \text{ nm}^{-1}$ ) and is based on  $u = 2 = qR_{g(\text{low})} = qL_w/\sqrt{12}$ , yielding  $R_{g(\text{low})} = 2/q \approx 80 \text{ nm}$  and  $L_w = 300 \text{ nm}$ . On the basis of these arguments, we restricted application of eq 7 to scattering curves with  $R_g > 100 \text{ nm}$ . In fact, all scattering curves selected according to this criterion exhibited an onset of a  $q^{-1}$  power law. Only in the case of  $c = 5.45 \text{ g L}^{-1}$  of the 1:3 mixture, all radii remained

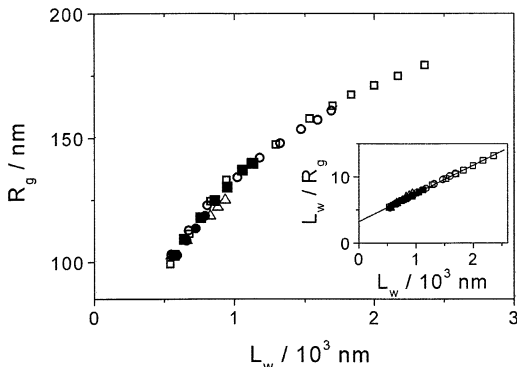


**Figure 10.** Radii of gyration,  $R_g$ , versus the overall contour length,  $L_w$ , for 1:4 mixtures with  $c = 7.61$  (□),  $6.97$  (○), and  $6.34 \text{ g L}^{-1}$  (△) and for 1:3 mixtures with  $c = 6.53$  (■) and  $6.00 \text{ g L}^{-1}$  (●). Inset: Same data plotted as  $L_w/R_g$  versus  $L_w$ . Data can be extrapolated to  $L_w/R_g = 3.21$ , indicating rodlike aggregates.

below this size limit and could not be used for calculating  $M_L$  values.

Although not shown explicitly, the apparent values for  $M_L$  extracted according to eq 7 exhibit a gradual increase with  $L_w$ . As was demonstrated earlier,<sup>18</sup> this reflects either an increase of the cross section of the fiber-like constituents or an increase of an apparent mass per unit length due to an increasing number of linear aggregates (with a large scattering power) at the expense of a gradual loss of monomers (with a very low scattering power) at a constant overall value of  $c$  in eqs 2 and S5. The resulting mass per unit length lies within a range of  $1500 < M_L < 15000 \text{ g mol}^{-1} \text{ nm}^{-1}$ . Assuming a density of  $1 \text{ g mL}^{-1}$ , this results in fiber cross sections  $D$  of  $1.8 < D < 5.6 \text{ nm}$ . Because the monomers contribute to  $c$ , the estimated  $M_L$  range establishes a lower limit. Yet, these values are realistic and point to fiber cross sections which comprise several monomeric strands.

Once values for the mass per unit length are established, they can be transformed into weight-averaged contour lengths,  $L_w$ , by inserting mass values into eq 7. These contour lengths can be related to the particle size (Figure 10) in much the same way as was done for the relative molar mass,  $M_w$ , in Figure 6a,b. Yet, contrary to  $M_w$ , the contour length  $L_w$  is not affected by the use of overall concentrations in eqs 2 and S5, and remaining deviations from the true values for  $L_w$  can arise only from the influence of interparticle excluded volume effects, which are considered to be negligible in the present case.

Most strikingly,  $R_g$  data of all concentrations and mixtures now fall on a single line. This success confirms the onset of a  $q^{-1}$  decrease of  $P(q)$  at  $q > 2.75 \times 10^{-2} \text{ nm}^{-1}$  and at the same time can be considered to be a justification for the applicability of eq 7. As a consequence, the same topological features can be assumed for all mixing ratios and solute concentrations. An additional hint about the structure of the constituents can be extracted from an alternative representation of the data in Figure 10. This representation is initiated by the fact that, for rodlike particles,  $L/R_g = \sqrt{12}$ . In fact, a plot of  $L_w/R_g$  versus  $L_w$  yields a straight line, which can be extrapolated to 3.21, indicating rodlike aggregates to be the initial aggregates or constituents.

By combining the two structural features just established, the following model is proposed for the aggregates. On large length scales, the aggregates behave like hyperbranched polymers. On

(42) Neugebauer, T. *Ann. Phys.* **1943**, *42*, 509–533.

(43) Holtzer, A. *J. Polym. Sci.* **1955**, *17*, 432–434.

(44) Kojima, R. *J. Phys. Soc. Jpn.* **1973**, *34*, 1029–1038.

(45) Schmidt, M.; Paradossi, G.; Burchard, W. *Makromol. Chem. Rapid Commun.* **1985**, *6*, 767–772.

decreasing the length scale, the focus turns toward linear segments between branching points, which correspond to rather stiff fibers.

The character of hyperbranching became transparent by the scattering curves at  $q < 2.5 \times 10^{-2} \text{ nm}^{-1}$ . In this  $q$  regime, the respective experiments could be well described by the Gaussian limit of the *ABC* polycondensate, with  $R_g$  and  $C$  in eq S13 being the only fit parameters. We have to emphasize that, in this limit, all intraparticle distances of the model obey a Gaussian distance distribution. This feature certainly gets increasingly unrealistic with decreasing intraparticle distances and increasing chain stiffness. The character of stiff fiber-like constituents is supported by the onset of  $P(q) \propto q^{-1}$  for  $q > 2.75 \times 10^{-2} \text{ nm}^{-1}$  and by a ratio of  $R_g/L_w \approx 1/\sqrt{12}$  in the limit of small aggregates.

### Conclusions

At this stage we can only speculate about the details of intermolecular interactions which cause the aggregation process under consideration. However, due to the typical dependence of the aggregates on the solvent polarity, we assume an interaction according to the AAD-DDA pattern<sup>22</sup> (Figure 1b). Since the 2-amino-1,8-naphthyridine has an amide function in its 3-position, an additional cross-linking between small assemblies should be possible, leading to aggregates of high molecular weight. Furthermore, the arrangement of four naphthyridine units at the upper rim of the calixarene might cause severe steric hindrance, resulting in a rearrangement under formation of cross-linked aggregates. Further studies to elucidate the oriented bond formation between neighboring constituents of these calixarene aggregates by experimental and theoretical methods are in progress.

However, we succeeded in following the time-resolved aggregation process of calix[4]arene/ANC in 1,2-dichlorobenzene by TR-SLS. Aside from demonstrating the power of TR-SLS in the field of aggregation, we were able to offer a structural model for the calix[4]arene-based aggregation in solution. Without referring to a specific particle shape, we could use the onset of a  $qP(q)$  plateau to attribute contour lengths,  $L_w$ , to the particles. All radii of aggregating intermediates fall on a single curve if plotted versus this total contour length,  $L_w$ , independent of the concentrations and compositions of calix[4]arene/ANC mixtures. Angle-dependent scattering curves compared best with

a model curve for a non-randomly branched *ABC* polycondensate with a branching parameter of  $0 < C < 0.1$ . This corresponds to non-randomly branched polymers with a large extent of reaction  $\alpha$ . On the basis of these findings, we postulate the following scheme of particle formation for the calix[4]arene/ANC aggregates in 1,2-dichlorobenzene: Monomers aggregate to fiber-like filaments, which form branching points. Each branching point initiates the growth of at least two other filaments. It is noteworthy that a strikingly similar structure was proposed recently for two different low-molecular-weight gels.<sup>46,47</sup> In the present system, the branching points occur in a frequency and distribution which is similar to those for nonrandom *ABC* polycondensates in macromolecular chemistry. Unlike the original model, which is based on a Gaussian distance distribution between any two segments, the bridges between two branching points are very stiff. Although resolution of the actual aggregation mechanism requires a detailed analysis of all scattering curves in terms of the respective model parameters of the *ABC*-type polycondensate, it is noteworthy that aggregates of calix[4]arene/ANC mixtures reveal striking analogies to the polymerization of glucose to amylopectin<sup>48,49</sup> or to the formation of a hyperbranched polyester.<sup>50</sup>

**Acknowledgment.** This work is dedicated to the memory of Professor Walther H. Stockmayer. Many helpful discussions with Professor Walther Burchard are gratefully acknowledged. The authors are indebted to Matthias Fornefeld for assistance in the laboratory.

**Supporting Information Available:** Experimental procedures and data evaluation, formulas for the calculation of the  $R_g$  versus  $M_w$  curves of monomer/aggregate mixtures, and equations of the scattering factor for the *ABC*-type polycondensates. This material is available free of charge via the Internet at <http://pubs.acs.org>.

JA0493291

- (46) Liu, X. Y.; Sawant, P. D. *Appl. Phys. Lett.* **2001**, *79*, 3518–3520.
- (47) Liu, X. Y.; Sawant, P. D.; Tan, W. B.; Noor, I. B. M.; Pramesti, C.; Chen, B. H. *J. Am. Chem. Soc.* **2002**, *124*, 15055–15063.
- (48) Hanselmann, R.; Burchard, W.; Ehrat, M.; Widmer, H. M. *Macromolecules* **1996**, *29*, 3277–3282.
- (49) Galinsky, G.; Burchard, W. *Macromolecules* **1997**, *30*, 4445–4453.
- (50) De Luca, E.; Richards, R. W.; Grillo, I.; King, S. M. *J. Polym. Sci. Part B: Polym. Phys.* **2003**, *41*, 1352–1361.



Available online at [www.sciencedirect.com](http://www.sciencedirect.com)



Journal of Biotechnology 112 (2004) 139–149

JOURNAL OF  
**Biotechnology**

[www.elsevier.com/locate/jbiotec](http://www.elsevier.com/locate/jbiotec)

## Large-scale homogeneous molecular templates for femtosecond time-resolved studies of the guest–host interaction

P. Siffalovic <sup>a,\*</sup>, M. Michelswirth <sup>a</sup>, P. Bartz <sup>a</sup>, B. Decker <sup>b</sup>, C. Agena <sup>b</sup>, C. Schäfer <sup>b</sup>, S. Molter <sup>c</sup>, R. Ros <sup>c</sup>, M. Bach <sup>d</sup>, M. Neumann <sup>d</sup>, D. Anselmetti <sup>c</sup>, J. Mattay <sup>b</sup>, U. Heinzmann <sup>a</sup>, M. Drescher <sup>a</sup>

<sup>a</sup> *Molekül und Oberflächenphysik, Fakultät für Physik, Universität Bielefeld, 33615 Bielefeld, Germany*

<sup>b</sup> *Organische Chemie I, Fakultät für Chemie, Universität Bielefeld, 33615 Bielefeld, Germany*

<sup>c</sup> *Experimentelle Biophysik, Fakultät für Physik, Universität Bielefeld, 33615 Bielefeld, Germany*

<sup>d</sup> *Elektronenspektroskopie, Fachbereich Physik, Universität Osnabrück, 49069 Osnabrück, Germany*

Received 15 December 2003; received in revised form 31 March 2004; accepted 1 April 2004

### Abstract

Self-assembled monolayer films based on iodobenzoyloxy-functionalized resorc[4]arenes were prepared on gold substrates to serve as model systems for future time-resolved studies of molecular recognition, a mechanism of outstanding importance in bioorganic systems. The film properties were tested using X-ray photoelectron spectroscopy (XPS), atomic force microscopy (AFM) and imaging ellipsometry. An apparatus for time-resolved electron spectroscopy utilizing femtosecond soft X-ray pulses is capable of detecting iodine core-level photolines and the photoinduced dissociation after ultraviolet illumination. The developed technique holds promise for tracking the temporal evolution of chemical shifts of atomic markers as local probes for the dynamics of the guest–host interaction.

© 2004 Elsevier B.V. All rights reserved.

**Keywords:** Molecular recognition; Guest–host interaction; Molecular dynamics; Self-assembled monolayer

### 1. Introduction

Molecular recognition is a profound principle of nature providing selectivity in a complex network of chemical reactions. The central mechanism of molecular recognition is a selective interaction between a guest and a host molecule, where the specificity origi-

nates from a combination of chemical and geometrical compatibility between the molecules. The formation of the guest–host complex cannot be regarded as instantaneous, but will follow a temporal evolution, including external and/or internal rearrangement of the geometrical (rotation, isomerization), or electronic (electron transfer) structure of one or both constituents. An observation of the dynamics of such intermolecular processes will reveal detailed information on this biologically as well as biotechnologically relevant mechanism.

\* Corresponding author. Tel.: +49-521-106-5464;  
fax: +49-521-106-6001.  
E-mail address: [siffalov@physik.uni-bielefeld.de](mailto:siffalov@physik.uni-bielefeld.de) (P. Siffalovic).

According to the different processes involved, molecular recognition generally evolves on a wide scale of times. Molecular dynamics on a millisecond to picosecond time-scale can be temporally resolved using techniques like Förster-resonance-transfer (FRET) (Jares-Erijman and Jovin, 2003; Selvin, 2000), or nuclear magnetic resonance (NMR) and electron paramagnetic resonance (EPR) (Clancy et al., 1998; Myers and Oas, 2002). The most fundamental reactions of this molecular interplay, however, occur in extremely short times down to the femtosecond ( $1\text{ fs} = 10^{-15}\text{ s}$ ) regime and their observation requires a detection technique of corresponding speediness. One of the complications for time-resolved studies arises from the statistical nature of molecular recognition: in a living system, one usually cannot predict *when* a bonding will take place. On the other hand, all current techniques capable of resolving dynamics on a femtosecond time-scale rely on a controlled reaction in response to an external trigger. Moreover, the specificity of the studied process should be reflected in local information about the bonding environment. Traditional optical probes, however, are not very specific on an atomic length scale.

In order to gain some degree of control over the guest–host interaction, we consider the use of resorc[4]arenes (Friggeri et al., 1998), a special type of calixarenes, as model systems. The flexible resorc[4]arene cage-type structure (Fig. 1) and the variability of chemical functionalization at the upper rim make these molecules versatile model hosts for *in vitro* studies of molecular recognition (Faull and Gupta, 2001). For a properly conditioned molecular system consisting of a (model) guest embedded in a resorcarene host, an external light pulse may induce a very rapid change of the bonding environment experienced by the guest molecule, which in turn may respond by a rearrangement of its structure or position, or may even leave the complex. This response to an external trigger is now accessible to a temporal tracking using the pump–probe concept, where a pump-light pulse initiates a process whose evolution is then followed using a delayed probe pulse by subsequently varying the temporal delay. The pump–probe technique has proven to be the essential tool for femtochemistry (Zewail, 1994), where the dynamics of photoreactions is followed in the time domain. However, in contrast to the usual visible- or UV-probe utilized in tradi-

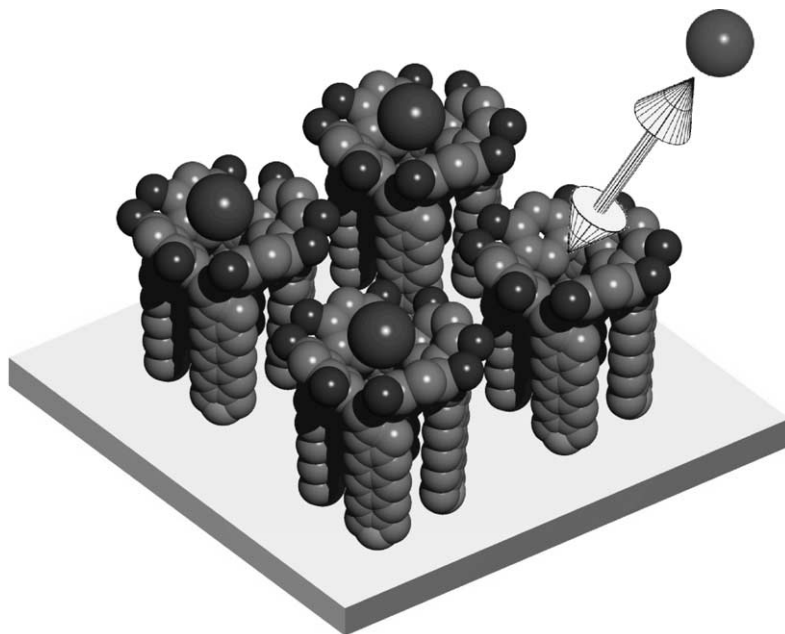


Fig. 1. Schematic drawing of resorc[4]arenes. Their cage-type structure together with a chemically variable upper rim make them versatile model hosts. Self-assembly on a surface provides a dense array of selective bonding sites for guest molecules.

tional femtochemistry, we intend to use probe pulses in the soft X-ray range thus establishing time-resolved X-ray photoelectron spectroscopy (XPS) (Haight and Peale, 1994; Siffalovic et al., 2001; Drescher et al., 2002a) for studies of intermolecular dynamics. XPS, also termed as electron spectroscopy for chemical analysis (ESCA), is a well-established technique for determining (yet hitherto in a static manner) the elemental composition of a molecule as well as the chemical environment of its atomic constituents (Siegahn, 1967). Similar to NMR methods, the latter capability relies on the detection of chemical shifts, i.e. spectral shifts reflecting the local electron density around a specific atom within the molecule. The radio- to microwave frequencies of NMR and EPR, however, ultimately determine the temporal resolution of those methods. ESCA instead relies on X-ray frequencies and correspondingly provides femtosecond (Drescher et al., 2001; Siffalovic et al., 2001) and even sub-femtosecond (Hentschel et al., 2001) temporal resolution.

The experimental preconditions and constraints for time-resolved ESCA in the spirit of the scientific goal outlined above are manifold, the most important ones are:

- (i) Need of a source of femtosecond soft X-ray (probe) pulses well synchronized to equally short visible or ultraviolet (pump) light pulses. Such a light source on the basis of high harmonic generation (Wahlström et al., 1993) has been realized in our laboratory (Siffalovic et al., 2001) and proven its capability of femtosecond XPS (Siffalovic et al., 2002).
- (ii) In ESCA, the information about the process is carried by electrons, which travel only very short distances in solids or liquids before being scattered. Correspondingly, the experiments must be performed at the interface of a molecule with vacuum, which the electrons can escape to.
- (iii) Since X-ray pulses from high harmonic generation generally suffer from small intensities (ca.  $10^6$  photons per second in our case), a high molecular density must be provided. This can be accomplished by preparing the molecular complexes on a solid surface (Davis and Stirling, 1996).
- (iv) The considered photoinduced processes are non-reversible, therefore each molecule can only be pumped and probed once. On the other hand, a sufficient signal-to-noise ratio will require accumulation over many – typically a few tens of thousands – laser shots. After each individual shot, a pristine spot on the target substrate has to be provided. For the realization of our concept, we therefore have to focus both light pulses down to a small spot of a few tens of  $\mu\text{m}$  in diameter and have to cover large (a few  $\text{cm}^2$ ) substrates of minimal microroughness homogeneously with the molecules under study. By raster-scanning, the substrate with the 50 Hz repetition rate of the laser system a continuous data acquisition over more than 1 h can then be sustained.

This article is concerned with the production of such large-scale substrates covered with functionalized resorcarenene hosts. We will first describe the synthesis of resorcarenenes functionalized with iodine marker atoms and their chemical characterization. The second step involves the preparation of the resorc[4]arenes on a gold surface as a self-assembled monolayer (SAM) film and the film characterization with respect to chemical composition, thickness, density and homogeneity. Finally, we will test the utility of the molecular films for ESCA by performing photoelectron spectroscopy on non-illuminated and UV-illuminated substrates. Irradiation with ultraviolet radiation tuned to break the iodine bonds should result in a detectable modification of the surface chemistry.

## 2. Methods

### 2.1. Resorcarenene synthesis

The synthetic strategy is shown in Fig. 2. It starts with the acid-catalyzed condensation of resorcinol and 10-undecylenic aldehyde, forming the cyclic tetramer **1a** in the *rccc* configuration. Subsequently, **1a** was converted into the tetrasulfide **1b** with 1-decanethiol and 9-BBN (Thoden van Velzen et al., 1995a). In the next synthesis step, octaiodide **1c** was prepared. To a suspension of 125 mg (71.9  $\mu\text{mol}$ ) *rccc*-2,8,14,20-tetra-[*n*-decyl(*n*-decylsulphide)]-resorc[4]arene **1b** in

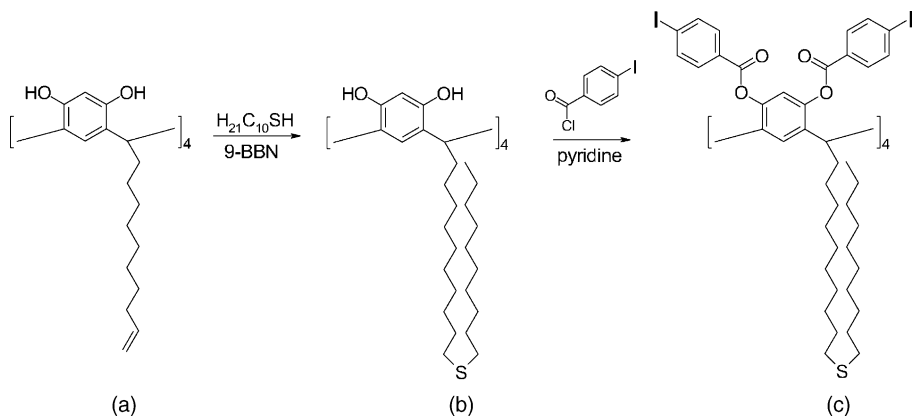


Fig. 2. Synthesis procedure for resor[4]arenes with iodobenzyl functionalization and dialkyl sulfide spacers for attachment to a surface.

900 mg (3.5 mmol) *p*-iodide-benzoic-acid-chloride, 3 mL pyridine was added. This mixture was heated at 80 °C for 2 h. The solution was cooled, carefully quenched with water and three times washed with dichloromethane. The combined organic layers were washed with diluted HCl and water. After drying over MgSO<sub>4</sub>, the solvent was removed under reduced pressure. The product (156 mg, 43.6 mmol, 61%) was isolated by HPLC (Si-100, cyclohexane/ethyl acetate, 97:3) as a colourless solid.

## 2.2. Self-assembled monolayer preparation

Silicon substrates cut from a polished wafer were coated using DC-plasma sputtering. A 40 nm thick titanium layer was deposited at a rate of 0.24 nm/s for improved sticking of the subsequently deposited gold film. Best film qualities were achieved by decreasing the gold deposition rate (Elbel et al., 1995; Wang et al., 1993) in three steps (128 nm at 4.4 nm/s; 75 nm at 1.25 nm/s; 70 nm at 0.37 nm/s). During the whole coating process, the substrate temperature was held at 150 °C. AFM-scans revealed an rms-surface roughness of about 0.9 nm. Self-assembled monolayers of the functionalized resorc[4]arenes on gold were prepared by immersing the substrates directly after evaporation into a 1 mM solution of **1c** in ethanol/chloroform (7/3). Self-assembly was achieved by keeping the adsorbate solution containing the gold substrate for 16 h at 60 °C and subsequent slow (3 h) cooling down to room temperature.

followed by several rinsings with ethyl alcohol and argon.

### *2.3. XPS, AFM and ellipsometry*

X-ray photoelectron spectroscopy (PHI model 5600ci) was performed using the Al<sub>K</sub>-line at 1487 eV photon energy to excite inner shells of SAM molecular templates under high-vacuum ( $10^{-8}$  mbar) conditions. An atomic force microscopy (AFM) capable of covering scan areas of  $50 \mu\text{m} \times 50 \mu\text{m}$  (Nanoscope) was used in air to determine the height of assembled resorc[4]arene films. In order to obtain steps between areas with and without SAM, the covered substrates were illuminated with ultraviolet radiation ( $\lambda = 172 \text{ nm}$ ) from an excimer-lamp (Ushio) through an etched nickel mesh with  $25 \mu\text{m}$  period. Attack from the UV radiation removed the molecular film within 15 min in the uncovered square areas (Brechling et al., 2004). The UV-microstructured templates were also studied with an imaging nulling ellipsometer (Nanofilm) with  $3 \mu\text{m}$  lateral and  $0.1 \text{ nm}$  vertical resolution at a wavelength of 658 nm and an angle of incidence of  $60^\circ$ .

#### *2.4. Pulsed soft X-ray source and ESCA apparatus*

A home-built titanium-sapphire laser system provides intense (200 GW peak power) light pulses of 50 fs duration at a wavelength of 800 nm and a repetition rate of 50 Hz. Focusing into neon gas at in-

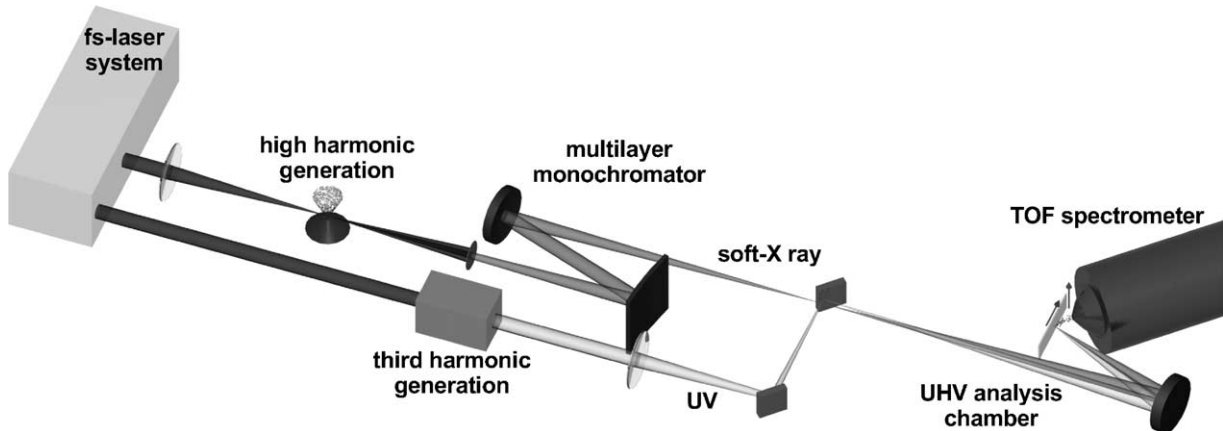


Fig. 3. Apparatus for time-resolved ESCA. Ultrashort soft X-ray pulses are generated as high harmonics of 50 fs laser pulses by focusing into a gas target. After monochromatization the pulses are refocused into a 25  $\mu\text{m}$  (FWHM) spot onto a surface together with dissociating UV radiation. The photoemitted electrons are energy-analyzed in a time-of-flight spectrometer.

tensities of  $\sim 10^{15} \text{ W/cm}^2$  gives rise to the generation of high harmonic orders of the laser fundamental (Fig. 3). A monochromator based on metal-multilayer Bragg-reflectors (Lim et al., 2001) selects the 45th order corresponding to a photon energy of 70 eV (17.7 nm wavelength) while preserving the femtosecond time-structure, as has been demonstrated in previous studies on metallic (Siffalovic et al., 2001) or semiconductor surfaces (Siffalovic et al., 2002). This radiation is refocused to a spot of 25  $\mu\text{m}$  (FWHM) diameter onto the target under study being located in a ultrahigh-vacuum chamber. Photoemitted electrons from the target are energy-analyzed in a time-of-flight (TOF) spectrometer (Drescher et al., 2002b). Frequency tripling of the 800 nm radiation yields femtosecond ultraviolet pulses at 266 nm, which are spatially overlapped with the soft X-rays.

### 3. Results

#### 3.1. Characterization of functionalized resorc[4]arenes in solution

rccc-2,8,14,20-Tetra-[*n*-decyl-(*n*-decylsulphide)]-4,6,10,12,16,18,22,24-octa-*O*-(*p*-iodide-benzoyl)-resorc[4]arene **1c** was characterized by  $^1\text{H}$  and  $^{13}\text{C}$  NMR spectroscopy, ESI-MS spectrometry and UV-vis spectroscopy. In solution the molecule exists

in the boat conformation, which could be confirmed by  $^1\text{H}$  and  $^{13}\text{C}$  NMR spectra showing a perfect  $C_{2v}$ -symmetry. In solution, this conformation is typical for resorcarenes with huge *O*-substituents (Timmermann et al., 1996).

#### 3.2. Self-assembled monolayer characterization

XPS provides a quantitative measure of the elemental composition of a surface. The XPS spectrum of the iodine-functionalized resorc[4]arene SAM is shown in Fig. 4. Analysis of the peak areas and consideration of the ionization cross section for the different elements yields a relative abundance of the elements C:O:I of 1:0.15:0.07. This compares to a ratio of 1:0.10:0.05 from the molecular stoichiometry of the film. Sulfur from the thioether group constituting the bonding to the surface was also found in the XPS spectrum, but too faint for a quantitative analysis. Prolonged illumination with X-rays at 1487 eV resulted in a deformation of the peak forms, indicating a deterioration of the film due to bond fission or cross-linking (Jäger et al., 1997).

In order to obtain information about the film height from atomic force microscopy, a step between the film surface and the substrate must be provided. To this end, the SAM film was patterned following the procedure described in 2.3. The AFM image (Fig. 5a) was analyzed by selecting 51 separated sub-areas, each

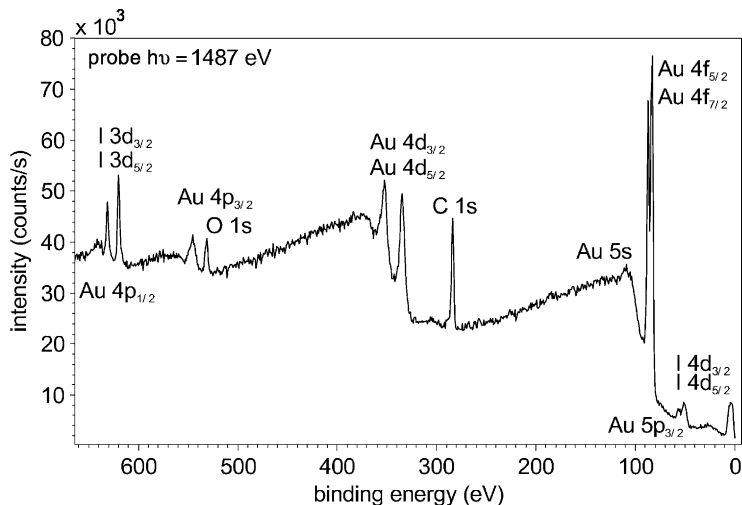


Fig. 4. The stoichiometry of the self-assembled monolayer films of **1c** is extracted from the peak areas of X-ray photoelectron spectra after excitation of the molecular films with 1487 eV radiation.

0.42  $\mu\text{m}$   $\times$  21.5  $\mu\text{m}$  wide and containing a step between a SAM-covered and an uncovered part. After averaging of line-scans perpendicular to the step a mean step height was determined for each sub-area. The histogram of these values, shown in Fig. 5b, leads to a height of the SAM film of  $2.7 \pm 0.5$  nm. Taking into account the height of about 0.4 nm for the iodobenzyl groups, this is in accordance with literature values (Thoden van Velzen et al., 1995b) from surface plasmon resonance measurements ranging between 2.0 and 2.8 nm for similar resorc[4]arene tetrasulfides.

Imaging ellipsometry of the UV-patterned films also reveals the lateral structure (Fig. 6), but here the contrast results from a combination of thickness and refractive index. On the basis of the rigid surface binding geometry of a single molecule, we expect a growth model where each molecule forming the SAM has already the height of the closed monolayer. Correspondingly, we can calculate from the measured ellipsometric angles the effective index of refraction, being a function of the film density (Smith, 1968). Combining the thickness information from the AFM measurement with the ellipsometry data yields an effective refractive index of 1.45. This corresponds to a value previously considered for densely packed calixarene monolayers on gold (Thoden van Velzen et al., 1995b).

In spite of the unique capabilities of X-ray sources based on high harmonic generation in terms of temporal resolution (Hentschel et al., 2001) they generally suffer from low average intensity. Our laser based source provides approximately  $10^6$  photons per second; this is to be compared with typically  $10^{10}$  photons per second for a conventional X-ray tube or even  $10^{13}$  photons per second for beamlines at third-generation synchrotron storage rings. In order to test the feasibility of time-resolved ESCA studies on our model host system, we therefore have to demonstrate that the iodine markers of the resorc[4]arene SAM film are visible in the ESCA spectra obtained with this source. An additional challenge is connected with the low photon energy of 70 eV: while providing larger excitation cross-section as compared to hard X-rays, the corresponding low kinetic energies of approximately 15 eV for the N-shell photoelectrons from iodine overlap with an appreciable background from inelastically scattered electrons originating from the organic film and the gold substrate. In spite of the low relative abundance of iodine atoms in the film, the spectrum in Fig. 7 clearly reveals as atomic fingerprints the two fine-structure components of iodine at 50.6 eV ( $4d_{3/2}$ ) and 48.9 eV ( $4d_{5/2}$ ) binding energy. No features from the gold substrate are evident in the spectrum, thus supporting a closed molecular film (Alloway et al., 2003). According to gas phase studies (Frietas et al.,

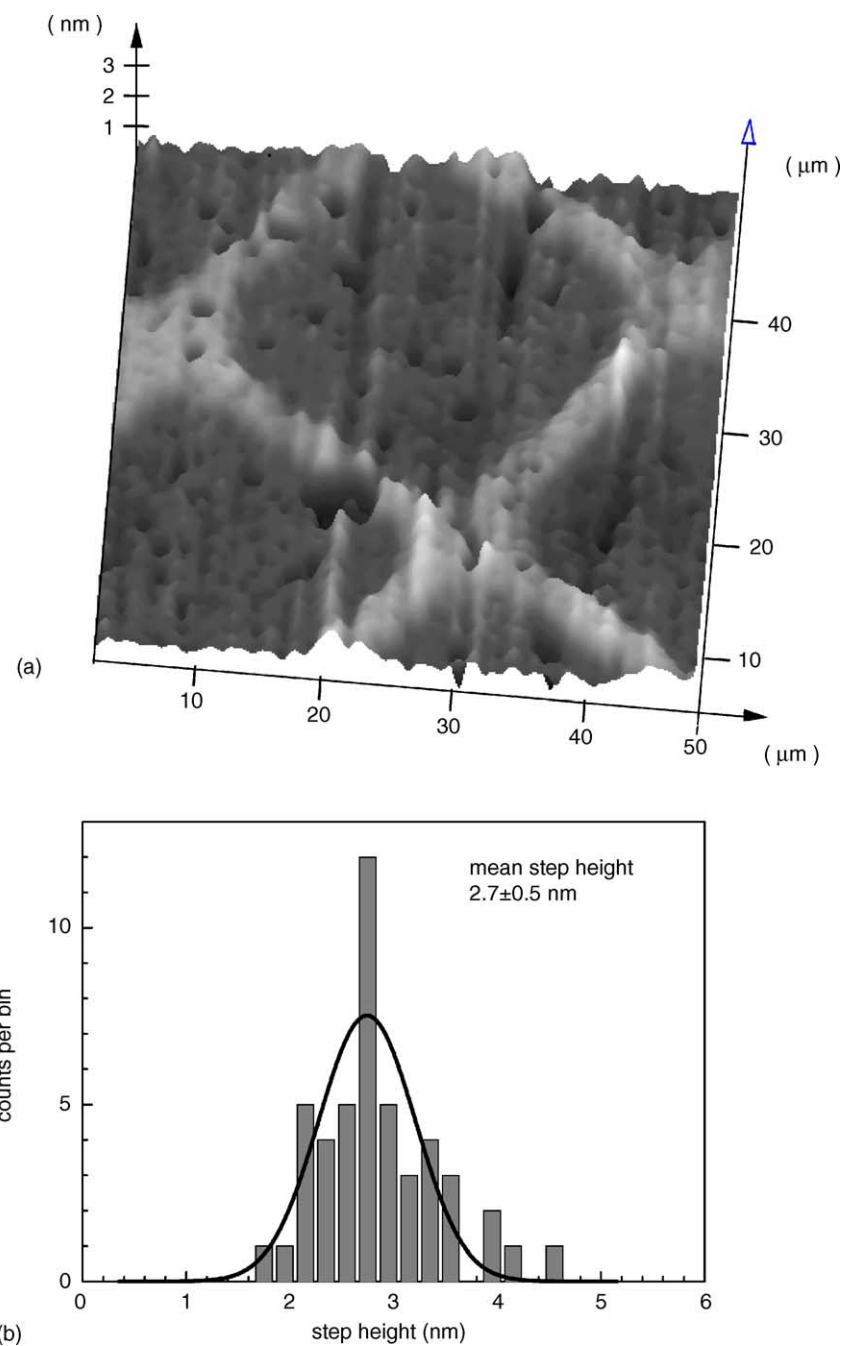


Fig. 5. (a) Atomic force microscopy of a UV-patterned iodine-functionalized resorc[4]arene self-assembled monolayer film yields a height of the molecular film of 2.7 nm. (b) Histogram of measured step heights in 51 sub-areas of (a).

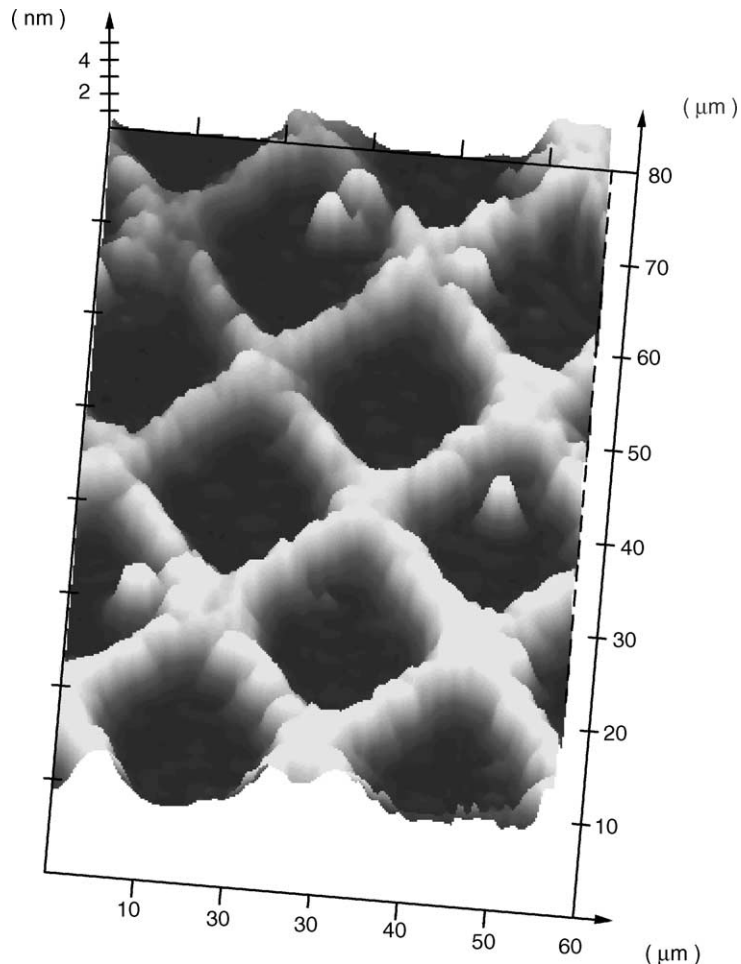


Fig. 6. Imaging ellipsometry of a UV-patterned iodine-functionalized resorc[4]arene self-assembled monolayer film yields an index of refraction of 1.45, if the film height from the AFM study in Fig. 5 is taken into account.

1993; Cheng et al., 1995; Freedman et al., 1980; Kawasaki et al., 1977), illumination of the same spot on the substrate with ultraviolet radiation at 266 nm wavelength should induce the fission of bonds between the iodine and the benzene group. This behaviour is verified in Fig. 7 also for the iodobenzyl groups being attached to our SAM film. The difference spectrum in Fig. 7 does not show any changes in the valence region thus proving the full integrity of the residual molecular film after iodine photodissociation. The integral under the I 4d peaks as a function of the deposited light energy is plotted in Fig. 8. The iodine signal  $I_S$  decreases exponentially towards the background  $I_B$  with

the characteristic decay constant  $\alpha = 2.7 \pm 0.4 \mu\text{J}$ .  $\alpha$  was found independent of the ultraviolet pulse intensity and thus confirms the linear character of the photodissociation even for intensities of the order of  $10^{10} \text{ W/cm}^2$ . After depositing a dose of  $0.28 \text{ J/cm}^2$ , the iodine signal almost completely disappears. Assuming a surface density of  $7 \times 10^{13} \text{ molecules/cm}^2$  corresponding to a densely packed film, this results in a photodissociation cross section of  $2.5 \text{ Mbarn}$  closely reproducing the previously published  $\text{C}_6\text{H}_6\text{I}$  extinction coefficient (Kavita and Puspandu, 2002). This is a further indication of a closed SAM films with the iodobenzyl groups pointing away from the surface.

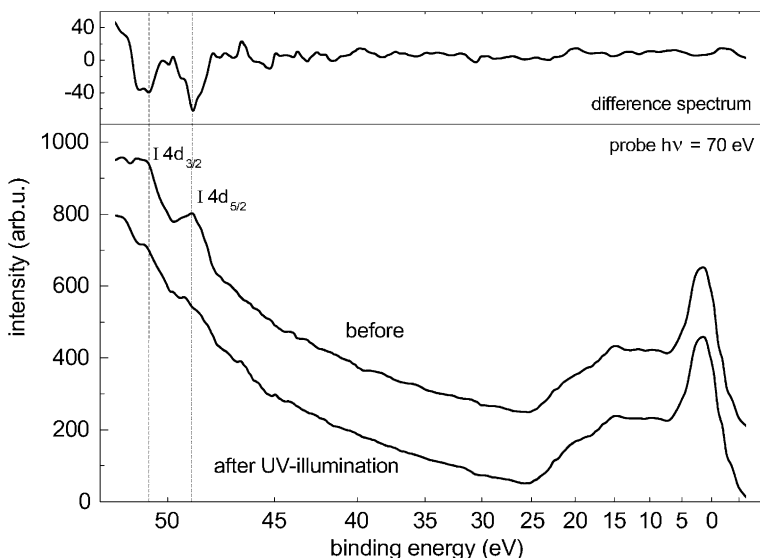


Fig. 7. Photoelectron spectra of a iodine-functionalized resorc[4]arene self-assembled monolayer film obtained with the apparatus from Fig. 3 before (lower panel, top) and after (lower panel, bottom) illumination with ultraviolet radiation at 266 nm. The difference spectrum (upper panel) clearly reveals the disappearance of the iodine atoms from the film while the integrity of the residual molecular layer is preserved.

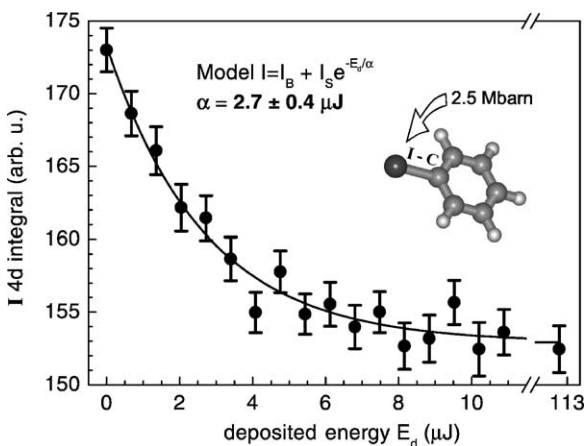


Fig. 8. The iodine signal in ESCA spectra exhibits an exponential dependence on the UV-dose, thus indicating a chemically selective linear photodissociation process.

#### 4. Discussion

Resorc[4]arene molecules can be synthesized which carry iodobenzoyloxy functional groups on their upper rim and dialkyl sulfide spacers on their lower rim. Incubation of highly flat gold substrates

under suitable conditions gives rise to the formation of self-assembled monolayer films. The stoichiometry is basically preserved upon layer assembly as measured with XPS; an excess oxygen content may be indicative of a water layer on top of the film. AFM studies on UV-patterned films reveal a film thickness close to the expected value for an upright orientation of the molecules and support a proper formation of the film. The films refractive index measured with ellipsometry implies a closed molecular monolayer. ESCA on the prepared molecular templates using a laboratory source for 70 eV, 50 fs soft-X-ray pulses is feasible and provides sufficient statistical accuracy already after 10 min of data accumulation. Data acquired on different positions of the substrate do not reveal any changes and thus support the homogeneous preparation over several  $\text{cm}^2$ . Raster scanning of large substrates with laser pump- and X-ray probe pulses focused to microscopic spot size therefore becomes feasible and will enable time-resolved studies of complex molecular systems undergoing non-reversible changes. The spectral signature of the iodine marker atoms attached to the resorc[4]arene is clearly discernible and completely vanishes upon illumination of the film with ultraviolet radiation. The

spectral signature of selected marker atoms attached to the host (or guest) molecules can now be used to study chemical shifts as a transient probe of the local environment at the guest–host interface when a bond to a guest molecule is formed, breaks apart or transforms in other ways in response to a photoexcitation event.

## Acknowledgements

We are indebted to A. Brechling and U. Kleineberg for supporting us in the UV-patterning and ellipsometry measurements. We gratefully acknowledge the support by the Deutsche Forschungsgemeinschaft.

## References

- Alloway, D.M., Hofmann, M., Smith, D.L., Gruhn, N.E., Graham, A.L., Colorado, R., Wysocki, V.H., Lee, T.R., Lee, P.A., Armstrong, N.R., 2003. Interface dipoles arising from self-assembled monolayers on gold: UV-photoemission studies of alkanethiols and partially fluorinated alkanethiols. *J. Phys. Chem. B* 107, 11690–11699.
- Brechling, A., Pohl, M., Kleineberg, U., Heinzmann, U., 2004. Structural organization of DMPC lipid layers on chemically micropatterned self-assembled monolayers as biomimetic systems. *J. Biotechnol.* 112, 115–125.
- Cheng, P.Y., Zhong, D., Zewail, A.H., 1995. Kinetic-energy, femtosecond resolved reaction dynamics. Modes of dissociation (in iodobenzene) from time-velocity correlations. *Chem. Phys. Lett.* 237, 399–405.
- Clancy, C.M.R., Tarasov, V.F., Forbes, M.D.E., 1998. Time-resolved electron paramagnetic resonance studies in organic photochemistry. *Electron. Paramagn. Reson.* 16, 50–78.
- Davis, F., Stirling, C.J.M., 1996. Calix-4-resorcinarene monolayers and multilayers: formation, structure, and differential adsorption. *Langmuir* 12, 5365–5374.
- Drescher, M., Siffalovic, P., Spieweck, M., Heinzmann, U., 2002a. Applicability of monochromatized high harmonic extended ultraviolet radiation for inner-shell photoelectron spectroscopy. *J. Electron. Spectrosc. Relat. Phenom.* 127, 103–108.
- Drescher, M., Hentschel, M., Kienberger, R., Uiberacker, M., Westerwalbesloh, T., Kleineberg, U., Heinzmann, U., Krausz, F., 2002b. Time-resolved atomic inner-shell spectroscopy. *Nature* 419, 803–807.
- Drescher, M., Hentschel, M., Kienberger, R., Tempea, G., Spielman, C., Reider, G., Corkum, P., Krausz, F., 2001. X-ray pulses approaching the Attosecond Frontier. *Science* 291, 1923–1927.
- Elbel, N., Behner, H., von Seggern, H., 1995. Preparation and characterization of epitaxial gold films deposited on mica by direct current magnetron sputtering. *J. Vac. Sci. Technol. B* 13, 2119–2123.
- Faull, J.D., Gupta, V.K., 2001. Selective guest–host association on self-assembled monolayers of calix[4]resorcinarene. *Langmuir* 17, 1470–1476.
- Freedman, A., Yang, S.C., Kawasaki, M., Bersohn, R., 1980. Photodissociation of aryl and aryl-alkyl halides at 193 nm: fragment translational energy distributions. *J. Chem. Phys.* 72, 1028–1033.
- Frietas, J.E., Hwang, H.J., El-Sayed, M.A., 1993. Molecular rotation clocking of the subpicosecond energy redistribution in molecules falling apart. 2. Excess energy dependence of the rates of energy redistribution in the two photodissociation channels of iodobenzene. *J. Phys. Chem.* 97, 12481–12484.
- Friggeri, A., van Veggel, F.C.J.M., Reinhoudt, D.N., 1998. Self-assembled monolayers of cavitand receptors for the binding of neutral molecules in water. *Langmuir* 14, 5457–5463.
- Haight, R., Peale, D.R., 1994. Tunable photoemission with harmonics of subpicosecond lasers. *Rev. Sci. Instrum.* 65, 1853–1857.
- Hentschel, M., Kienberger, R., Spielmann, C., Reider, G.A., Milosevic, N., Brabec, T., Corkum, P.B., Heinzmann, U., Drescher, M., Krausz, F., 2001. Attosecond metrology. *Nature* 414, 509–513.
- Jäger, B., Schürmann, H., Müller, H.U., Himmel, H.-J., Neumann, M., Grunze, M., Wöll, C., 1997. X-ray and low energy electron induced damage in alkanethiolate monolayers on Au-substrates. *Zeitschrift für Physikalische Chemie* 202, 263–272.
- Jares-Erijman, E.A., Jovin, T.M., 2003. FRET imaging. *Nat. Biotechnol.* 21, 1387–1395.
- Kavita, K., Puspendu, K.D., 2002. Photodissociation of  $C_6H_6I$ ,  $C_6F_5I$ , and related iodides in the ultraviolet. *J. Chem. Phys.* 117, 2038–2044.
- Kawasaki, M., Lee, S.J., Bersohn, R., 1977. Photodissociation of molecular beams of aryl halides: translational energy distribution of the fragments. *J. Chem. Phys.* 66, 2647–2655.
- Lim, Y.C., Westerwalbesloh, T., Aschentrup, A., Wehmeyer, O., Haindl, G., Kleineberg, U., Heinzmann, U., 2001. Fabrication and characterization of EUV multilayer mirrors optimized for small spectral reflection bandwidth. *Appl. Phys. A72*, 121–124.
- Myers, J.K., Oas, T.G., 2002. Mechanisms of fast protein folding. *Annu. Rev. Biochem.* 71, 783–815, and references therein.
- Selvin, P.R., 2000. The renaissance of fluorescence resonance energy transfer. *Nat. Struct. Biol.* 7, 730–734.
- Siegahn, K., 1967. ESCA: Atomic, Molecular and Solid State Structure Studied by Means of Electron Spectroscopy. Almqvist & Wiksell.
- Siffalovic, P., Drescher, M., Heinzmann, U., 2002. Femtosecond time-resolved core-level photoelectron spectroscopy tracking surface photovoltage transients on p-GaAs. *Europhys. Lett.* 60, 924–930.
- Siffalovic, P., Drescher, M., Spieweck, M., Wiesenthal, T., Lim, Y.C., Weidner, R., Elizarov, A., Heinzmann, U., 2001. Laser-based apparatus for extended ultraviolet femtosecond time-resolved photoemission spectroscopy. *Rev. Sci. Instrum.* 72, 30–35.

- Smith, T., 1968. Ellipsometry for measurements at and below monolayer coverage. *J. Opt. Soc. Am.* 58, 1069–1079.
- Thoden van Velzen, E.U., Engbersen, J.F.J., Reinhoudt, D.N., 1995a. Synthesis of self-assembling resorc[4]arene tetrasulfide adsorbates. *Synthesis* 8, 989–997.
- Thoden van Velzen, E.U., Engbersen, J.F.J., de Lange, P.J., Mahy, J.W.G., Reinhoudt, D.N., 1995b. Self-assembled monolayers of resorcin[4]arene tetrasulfides on gold. *J. Am. Chem. Soc.* 117, 6853–6862.
- Timmermann, P., Verboom, W., Reinhoudt, D.N., 1996. Resorcinarenes. *THL* 52, 2663–2704.
- Wahlström, C.-G., Larsson, J., Persson, A., Starczewski, T., Svanberg, S., Salières, P., Balcou, P., L'Huillier, A., 1993. High-order harmonic generation in rare gases with an intense short-pulse laser. *Phys. Rev. A* 48, 4709–4720.
- Wang, H., Jing, J., Chu, H.T., Henriksen, P.N., 1993. Rearrangement of Au(1 1 1) surface as a result of scanning with scanning tunneling/atomic force microscopes. *J. Vac. Sci. Technol. B* 11, 2000–2005.
- Zewail, A. H., 1994. Femtochemistry – Ultrafast Dynamics of The Chemical Bond, vol. I and II. World Scientific, New Jersey, Singapore.

**Calixarenes as Hosts for Ammonium Cations.  
A Quantum Chemical Study**

A.B. Rozhenko, W.W. Schoeller, M.C. Letzel, B. Decker,  
C. Agena, J. Mattay

Fakultät für Chemie der Universität  
Postfach 10 01 31  
33501 Bielefeld  
Germany

Fax: +49 (0) 521 106 6467  
e-mail: [wolfgang.schoeller@uni-bielefeld.de](mailto:wolfgang.schoeller@uni-bielefeld.de)

## Abstract

Host-guest complexes of cavitand with different ammonium cations were investigated with quantum chemical method at the density functional level (BP86, B3LYP). The insertion of the parent  $\text{NH}_4^+$  cation is characterized by high negative binding energy. Increasing methyl substitution at the cation decreases its inclination towards the complex formation. The calculated data are in line with the electrospray ionization mass spectrometry (ESI-MS) experiments. They reveal stable aggregates only for the parent  $\text{NH}_4^{(+)}$  cation and for the primary alkylammonium cations.

**Keywords:** ammonium cations, calculations, DFT, cavitand, mass spectrometry

## Introduction

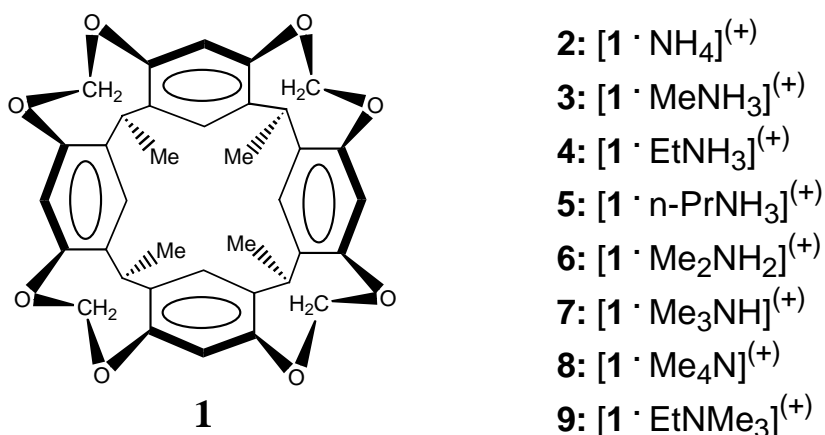
The design of the selectively and effectively bond host-guest aggregates is the challenge of supramolecular chemistry. Calix[4]arenes and structurally similar cavitands are potent and size-selective receptors for a variety of substrates, in particular, for inorganic and organic cations<sup>[1-2]</sup>. A variety of inclusion-complexes of calix[4]arenes with metal cations were investigated experimentally<sup>[3]</sup> as well as theoretically<sup>[4]</sup>. The corresponding aggregates are predominantly bound by electrostatic interactions. The inclusion of alkyl ammonium cations as the cationic guests mimics some bioorganic processes such as, e.g. the recognition of the acetylcholine by acetylcholinesterase, based on the cation-π interaction<sup>[5-6]</sup>. The first detailed experimental study of complexes were reported for the system of tetra-phenolate of resorc[4]arenes with a series of quaternary ammonium cations<sup>[7]</sup>. The structures for some inclusion complexes were also investigated in the solid state<sup>[8-9]</sup>. The cations built with the ligands complexes, which involved solvent molecules as well<sup>[8]</sup>. In the structure of the complex of the anionic sulfonatocalix[4]arene with tetramethylammonium ion published by Atwood et al.,<sup>[9]</sup> the negative charge of the sulfonium groups attracted the positively charged cation. In contrast, the neutral calix[4]arene did not react with quaternary ammonium salts in  $(CDCl_2)_2$  solvent<sup>[10]</sup>. The authors of another paper<sup>[11]</sup> found a significant interaction with a series of ammonium cations only for the phosphate-bridged cavitands that carried at least three P=O groups oriented inside of the cavity.

In contrast to the cavitands, their relatives, calix[4]arene build the stable aggregates with the (alkyl)ammonium cations. In the most cases, the ligands were modified with the  $SO_3^{(-)}$  groups, in order to provide stronger interactions with the positively charged guest. The ammonium cation  $NH_4^+$  did not form stable aggregates with p-sulfonatocalix[4]arene<sup>[12]</sup>. In  $NH_4^+$ , the positive charge is predominantly localized at the hydrogen atoms which is at optimum for a effective cation-π interactions, but it is strongly solvated by the protic solvents. The larger, but less solvated  $Me_4N^+$  cation dived deeply into the cavity and build a stable aggregate. In case of  $Et_4N^+$  cation or  $Pr_4N^+$  cation, the only one alkyl chain was inside the cavity. Interestingly, for the cations  $R_4N^+$  with the long alkyl groups ( $R=Et, n-Pr, n-Bu$ ), the nitrogen atom remained outside the cavity. Only cations with a single alkyl group evidenced ammonium inclusion. The authors<sup>[13]</sup> investigated a series of alkylammonium salts  $RNH_3^+$  ( $R: Me$  to Hept) and found that the enthalpy of binding became more favourable as the length of the alkyl chain increases. The most negative enthalpy (about -20 kJ/mol) was found for  $PentNH_3^+$  and interpreted as an evidence that the pentyl group fitted best into the cavity. For

this case, a conformation with the Me group pointing toward the lower rim of calixarene was assumed. If the aromatic moiety was present in the cation structure, the competitive  $\pi$ - $\pi$  interaction made the aryl inclusion preferable as compared with the cation- $\pi$  interaction model<sup>[14a]</sup>. In these cases the host accepted the conformation *flattened cone*.

The attempts to find out the stable complexes of the neutral cavitands with the (alkyl)ammonium cations failed but it is not an evidence of their overall instability. Up to now, the detailed aspects of the host-guest interactions for this case are not clear. To the best of our knowledge, the complexation of cavitands with the ammonium salts was not investigated with the quantum chemistry methods. The only several molecular dynamics simulations were made for the selected variety of ammonium cations<sup>[12,14]</sup> with calix[4]arenes, with and without anionic groups at the upper rim of the host cyclophanes. While these studies have own merit they suffer from the inaccuracy of the semiempirical force field.

The diversity of the experimental data arose our interest in a further rationale of the complexation process. In the present study we will report on the geometries for various aggregates **2-9** (Scheme 1) which cavitand **1** can build with the different ammonium cations. It will be shown that not only the volume of the cavitand cavity and ammonium cation but also the character of the substitution at nitrogen play a decisive role for complex formation. The O-CH<sub>2</sub>-O bridges in **1** fixed the structure and prevented the necessity to calculate a large diversity of conformations<sup>[16]</sup>. Our study is based on the density functional theory (DFT)<sup>[15]</sup> provides reliable structures and reaction enthalpies. Previous investigations were directed to the inclusion products of calixarenes<sup>[16]</sup> and even their capsules (dimers)<sup>[17]</sup>. In addition to the theoretical investigations mass-spectrometric investigations were performed. The results of these investigations are collected in the last section of the publication.



Scheme 1.

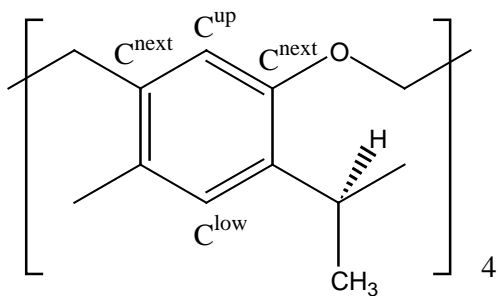
## Details of Calculations

All of the structures, were fully optimized without symmetry constrains, with only exception of **1**, optimized as the C<sub>4</sub> symmetrical structure. We used the BP86 functional<sup>[18 19]</sup> with the Resolution of the Identity (RI)<sup>[20]</sup> algorithm implemented in the TURBOMOLE program packet<sup>[21]</sup>. As split-valence basis set SV(P) implemented in this program package<sup>[22]</sup> was used, (7s4p)/[3s2p] for C, N and O with the contraction {511/31} and (4s)/[2s] for H with the contraction {31}. One set of polarization functions was added for C,N and O. Fine grid value (grid=5) and SCF convergence criterium (scfconv=1.0·10<sup>-8</sup> Hartree) were used for the geometry optimization. For all of the structures vibration analyses were performed, computing analytical first and second order derivatives<sup>[23]</sup>. Some structures were additionally recalculated with the GAUSSIAN-03<sup>[24]</sup> program sets using the standard 6-31G\* basis set<sup>[25]</sup> and the B3LYP hybrid functional<sup>[26 27]</sup>, in order to ascertain that both DFT methods provide comparable structures by geometry optimization. In all cases, the finest grid was used for all calculations (grid=5 for TURBOMOLE and Grid=Ultrafine for GAUSSIAN). No vibration analyses were done for the structures calculated with the B3LYP fuctional. A full account for the optimized geometries is given in the supplementary material of the present publication. The VMD program packet<sup>[28]</sup> was used for the graphical presentation of the calculated structures. The single-point energy calculations were performed at the DFT (RI-BP86) level of approximation and with the TURBOMOLE program, the geometries optimized at the DFT [RI-BP86/SV(P)] level of approximation and using high-quality TZVPP basis set (11s6p)/[5s3p] for C, N and O with the contraction {62111/411} and (5s)/[3s] for H contracted as {311}.<sup>[29]</sup> Three sets of polarization functions were added (2d,1f for C, N and O and 2p,1d for H). The basis set superposition error (BSSE) values were calculated for the TZVPP basis set with the TURBOMOLE packet of program, for different ammonium complexes. First the RI-BP86/TZVPP single point energy calculation was done for the ammonium complex structure introducing the nuclear charges fr the ammonium atoms =0 and the total charge =0. By the second step the total energy was calculated for the free cavitand using the atom coordinates from the equilibrium geometry of the complex. The energy difference was then used to calculate BSSE value. The same procedure was repeated for the ammonium part of the molecule, introducing the zero charges for the cavitand nuclei and the total charge=+1 and then calculating the total energy for the ammonium cation in the conformation found in the complex. The energy differences from these two procedures were comparable rather small and did not play any significant role for the resuts of our calculations.

All obtained BSSE values are listed in Table 1 as the footnotes. The reaction energies were corrected by the zero-point energies calculated at the RI-BP86/SV(P) level without scaling.

## Results and discussions

The plots of the calculated structures are shown in Figure 1. The equilibrium cavitand **1** structure adopted C<sub>4</sub> symmetry. To achieve an effective cation-π interaction one should take into account the following aspects: a) a positive charge should be localized at the atoms or groups which dive into the cavity; b) an optimum distance(s) should be kept between the positive charged centre and the π-system(s) (cation-C<sup>arom</sup>). We will consider here the distances to the carbon atom at the upper (C<sup>up</sup>), the one next to this (C<sup>next</sup>) and that at the lower rim of the cavity (C<sup>low</sup>) (Scheme 2).



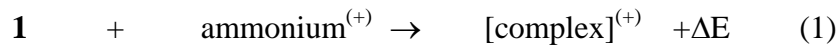
Scheme 2

- Figure 1 -

### Complexation of RNH<sub>3</sub><sup>+</sup> (R=H, Me, Et).

A positive charge in NH<sub>4</sub><sup>+</sup> is localized predominantly at the hydrogen atoms. Two different complexation modes (structures **2a** and **2b**) (Figure 1) were found for the system [cavitand-NH<sub>4</sub>]<sup>+</sup> depending on the number of the hydrogens interacting with the π-systems. Both conformations are characterized by almost the same total energies, calculated either with the BP86 or B3LYP functionals. In the first conformation, three hydrogens are inserted deeply into the cavity whereas the fourth hydrogen does not participate in binding. In the case of **2b**, all four hydrogens are bound. In both cases, the nitrogen is diving deeply into the calixarene cavity. The distance between nitrogen and the carbon atom C<sup>low</sup> (3.2 Å) at the lower rim is even larger than to C<sup>up</sup> (4.0-4.1 Å). The situation does not significantly change by a

substitution of one hydrogen in **2a** with a methyl group (Figure 1, **3a**): the nitrogen atom remains deeply in the cavity (this situation will be further designated as a “ammonium inside” mode of complexation) and the methyl group in **3a** (or the  $\alpha$ -CH<sub>2</sub> group in the cases of **4a** and **5a**) (Figure 2-4) is positioned at the upper rim of the calixarene. The residue of the alkyl substituent (in cases of **4a** and **5a**) is outside the cavity. We also optimized the geometry for the alternative conformations with the alkyl group inserted into the cavity and the ammonium rest pointing outside the calixarene cup (further designated as the “alkyl inside” mode of complexation). Such a conformation for the adduct with MeNH<sub>3</sub><sup>+</sup> as guest remained unstable by energy optimization and relaxed back to **3a**. The reason becomes clear after analysis of the next member of this series, **4b** and **5b** which could be located as minima in energy. Only the Me group remains inside the cavity. The rest of the alkyl chain is oriented in such a way that the NH<sub>3</sub> group at the end of the chain approaches three upper carbon atoms of one of the aromatic rings. The particular short NH-C<sup>up</sup> distances of 2.05 (**4b**) and 2.09 Å (**5b**) and NH-C<sup>next</sup> distances between 2.55 and 2.67 Å indicate practically the  $\eta^3$  coordination for the hydrogen [30]. Such a conformation is not possible for **3b**. In general, the “alkyl inside” inclusion mode can not be excluded on the base of the DFT calculations because they lack the description of electron correlation and, hence, the dispersion component of the interaction energy. On the other hand, the total energy values which we computed refer to the gas phase and can not be taken as a quantitative measure for coordination in solution. Especially polar protic solvents effectively solvate both, the cation and the free cavitand, to a greater extent the former than the latter. The coordination reaction (1) is strongly favoured by introduction of the NH<sub>3</sub> fragment (of an overall RNH<sub>3</sub><sup>+</sup> cation) (Tables 1,2) into the cavity. The alternative structures however could be further stabilized in the presence of polar protic solvent molecules since the NH<sub>3</sub> fragment remains open to solvation from the top. Hence, the alternative coordination, if any, will be favoured in such cases.



- - Tables 1,2 -

### Complexation of $\text{Me}_2\text{NH}_2^+$ , $\text{Me}_3\text{NH}^+$ and $\text{Me}_4\text{N}^+$ .

We have already considered the first two member of this series, which are the complexes with  $\text{NH}_4^+$  (**2**) and  $\text{MeNH}_3^+$  (**3**). Because of the tetrahedral symmetry of  $\text{NH}_4^+$  and the orientation of the single Me group to the outside of the cavitand cavity they are characterized by a nearly central position of nitrogen within the ligand cup. An introduction of additional methyl substituents basically changes the coordination mode. The equilibrium structures of **6** and **7** are shown in Figure 1. In **6** nitrogen is shifted diagonally off the centre of the cavity. By geometry optimization we obtained a  $C_s$  symmetrical equilibrium structure with the symmetry plane going through the cavitand's diagonal. The nitrogen atom lies practically over the centre of the aromatic rings (almost equal N- C<sup>up</sup> and N- C<sup>down</sup> distances (3.40 and 3.82 Å, resp.). Two available NH protons are  $\eta^2$ -connected to the two neighboring aromatic rings [d(NH-C<sup>up</sup>)= 2.35 and d(NH-C<sup>next</sup>)= 2.40 and 2.72 Å]. The  $\Delta E$  energy changes only slightly from **2** to **3** (Table 2) but the reaction (1) becomes significantly less exothermic for  $[\mathbf{1}\cdot\text{NH}_2\text{Me}_2]^{(+)}$  (**6**) and especially for  $[\mathbf{1}\cdot\text{NHMe}_3]^{(+)}$  (**7**). The latter complex reveals the unfavourable “alkyl inside”-type coordination discussed above. In case of **7**, both outside oriented hydrogen atoms are substituted by Me groups, which probably prevent a spontan isomerization found for similar structure **3a**. The equilibrium structure is also of  $C_s$  symmetry (the symmetry plane goes through NH, two C<sup>up</sup> and two C<sup>down</sup> carbon atoms). The nitrogen atom is positioned closer to one of the aromatic rings (d(N-C<sup>up</sup>)= 3.63 and d(N-C<sup>next</sup>)= 4.49 Å) as compared to the three other ones. With increased number of Me groups in **7** nitrogen tends to be closer to the upper rim of the cavitand. The NH hydrogen is  $\eta^1(\eta^3)$ -connected to the upper aromatic carbon (d(NH-C<sup>up</sup>)= 2.60 and d(NH-C<sup>next</sup>)= 2.98 Å). As one can see from these increased distances, the cation- $\pi$  interaction is here weaker than in all other complexes discussed previously. For **7** the calculations predict also a lower negative reaction energy  $\Delta E$ , of only -7.2 kcal/mol.

Does the large tetramethylammonium cation effectively interact with the  $\pi$ -system of cavitand **1**? *A priori*, the positive charge is now delocalized over the 16 atoms of four Me groups and the CH- $\pi$  interactions are weaker than the NH- $\pi$  interaction considered above. The calculations show that in the equilibrium structure (Figure 6), only one Me group is close to the upper rim of the cavitand whereas the residual part of the molecule (including the nitrogen atom) remains outside the cavity. The structure is only nearly  $C_s$  symmetrical, probably, due to the extremely flat potential energy surface for this structure. This is in line with the very low exothermic effect (less than 1 kcal/mol) of reaction (1) forming **8** (calculated with the

larger basis set TZVPP this effect became even slightly endothermic, see Table 1). The attempt to perform optimization for the isomeric structures like tetramethyl-substituted **2b**, failed and the structure relaxed back to **8**. One can conclude that the tetramethylammonium cation can form only very weak, if any, complexes with **1**.

### **Long chain vs. short chain of alkyl substion at the ammonium cation.**

This aspect has been already partially dealt with in the first chapter of the current paper and we have shown that longer alkyl substituents at nitrogen do not improve inclusion compared to the positively charged  $\text{NH}_3^+$  residue. In the present study we consider only a single attempt to modify  $\text{NMe}_4^{(+)}$  in order to check this earlier finding. We compared  $\text{EtNMe}_3^{(+)}$  as substrate building complexes  $[\mathbf{1} \cdot \text{EtNMe}_3]^{(+)}$  by modes “methyl inside” (**9a**) or “ethyl inside” (**9b**) with  $\text{EtNH}_3^{(+)}$  coordinated (**4a** and **4b**, respectively). As already mentioned, the alkyl groups attached to the ammonium centre inside make the former complexation mode less favourable, so we hoped that the latter mode became preferable.

But the “ethyl inside” inclusion complex, **9b**, turned out to possess almost the same total energy as the isomer **9a** and hence, low exothermic reaction energies  $\Delta E$  were found for both isomers. Probably, tetraalkylammonium cations poorly fits into cavitand **1** as guests.

### **Electrospray ionization mass spectrometry of 2-8.**

The complexation of **1** with the ammonium cations was investigated with the EMS spectrometry. First the cavitand was mixed with an equimolar (in relation to every cation) mixture of ammonium-, methylammonium, dimethylammonium-, trimethylammonium- and tetramethylammonium salts. The spectrum resulted is presented in Figure 2. As one can see, only signals corresponding to the complexes with  $\text{NH}_4^{(+)}$  and  $\text{MeNH}_3^{(+)}$  are seen, the former with a higher abundance than the latter. No complexes with  $\text{Me}_2\text{NH}_2^{(+)}$ ,  $\text{Me}_3\text{NH}^{(+)}$  and  $\text{Me}_4\text{N}^{(+)}$  was experimentally detected, in a good agreement with their lower stability predicted by our calculations.

- Figure 2 -

In contrast to, in the spectrum of the mixture of tetramethylcavatand with an equimolar mixture of ammonium-, methylammonium, ethylammonium- and *n*-propylammonium salts (Figure 3), all corresponding signals are visible. This means, in line with our theoretical findings, that the monosubstituted  $\text{RNH}_3^{(+)}$  are able to build stable complexes with tetramethylcavatand. The length of the alkyl chain does not practically affect the ability of the alkylammonium cations to build complexes although their signals are significantly less intensive than that corresponding to complex with  $\text{NH}_4^{(+)}$ .

- Figure 9 -

## Experimental Section

The tetramethylcavatand **1** was prepared as described in the literature.<sup>[31]</sup>

ESI mass spectra were recorded using an Esquire 3000 ion trap mass spectrometer (Bruker Daltonik GmbH, Bremen, Germany) equipped with an offline nano ESI source. Samples were introduced by nanospray needles. Nitrogen served both as the nebulizer gas and the dry gas. Nitrogen was generated by a Bruker nitrogen generator NGM 11. Helium served as cooling gas for the ion trap. The spectra shown here are recorded with the Bruker Daltonik esquireNT 5.1 esquireControl software by the accumulation and averaging of several single spectra. Data Analysis software 3.1 was used for processing the spectra. The tetramethylcavatand **1** was dissolved in chloroform (about 50 pmol/ $\mu\text{L}$ ). This solution was mixed (1:1) with an equimolar mixture of different ammonium salts (100 pmol/ $\mu\text{L}$ , each) in methanol.

## Conclusions

A series of the host-guest complexes for cavatand with the different ammonium cations were investigated theoretically at the DFT (BP86 and B3LYP) level of approximation. The optimized structures reflect different modes of complexation. Only for ammonium cations  $\text{RNH}_3^{(+)}$  ( $\text{R}=\text{H, Alkyl}$ ), nitrogen penetrates deeply into the cavatand cavity (“ammonium inside” complexation mode). The introduction is characterized by high negative reaction energies. They decrease with increasing numbers of methyl groups at nitrogen. For ammonium cations  $\text{NMe}_n\text{H}_{4-n}$  ( $n=2$  to 4) an “alkyl inside” complexation mode is found. The

exothermic complexation energies are small in these cases. The tetramethylammonium cation or other quaternary ammonium cations with larger alkyl substituents probably do not form stable aggregates with the cavitand. We also demonstrated good perspectives of such calculations in the future, for the prediction of stability for interesting host-guest complexes and description of their structure.

### **Acknowledgement**

This work was supported by the Deutsche Forschungsgemeinschaft (SFB 613). Computation time was generously donated by the Rechenzentrum of the Max-Planck Institut at Munich.

**Table 1.** Calculated (RI-BP86/TZVPP//RI-BP86/SV(P)) total energy values and reaction (1) energies for 1-9.

Compound	Guest	Total energy, E, a.u.	ZPE correction, a.u.	E+ZPE, a.u.	Lowest vibration, v, cm <sup>-1</sup>	ΔE, kcal/mol
<b>1</b>	-	-1991.456627	0.597459	-1990.859168	30.3	0.0
<b>1<sup>a</sup></b>	-	-1992.839392	-	-	-	0.0
<b>2a</b>	NH <sub>4</sub> <sup>+</sup>	-2048.347573	0.645203	-2047.702370	31.6	-32.5
<b>2a<sup>a</sup></b>	NH <sub>4</sub> <sup>+</sup>	-2049.779845	-	-	-	-29.2
<b>2b</b>	NH <sub>4</sub> <sup>+</sup>	-2048.347552	0.645855	-2047.701697	33.1	-32.1
<b>2b<sup>a</sup></b>	NH <sub>4</sub> <sup>+</sup>	-2049.781020	-	-	-	-30.0
<b>3a</b>	MeNH <sub>3</sub> <sup>+</sup>	-2087.627832	0.674138	-2086.953705	36.5	-28.1
<b>4a</b>	EtNH <sub>3</sub> <sup>+</sup>	-2126.911434	0.702062	-2126.209435	42.2	-24.3
<b>4a<sup>a</sup></b>	EtNH <sub>3</sub> <sup>+</sup>	-2128.412854	-	-	-	-22.6
<b>4b</b>	EtNH <sub>3</sub> <sup>+</sup>	-2126.886733	0.701354	-2126.185379	30.7	-9.2
<b>4b<sup>a</sup></b>	EtNH <sub>3</sub> <sup>+</sup>	-2128.390028	-	-	-	-8.3
<b>5a</b>	PrNH <sub>3</sub> <sup>+</sup>	-2166.193153	0.729681	-2165.463524	17.6	-23.7
<b>5a<sup>a</sup></b>	PrNH <sub>3</sub> <sup>+</sup>	-2167.727740	-	-	-	-22.1
<b>5b</b>	PrNH <sub>3</sub> <sup>+</sup>	-2166.164251	0.728876	-2165.435375	31.5	-6.1
<b>5b<sup>a</sup></b>	PrNH <sub>3</sub> <sup>+</sup>	-2167.701073	-	-	-	-5.3
<b>6</b>	Me <sub>2</sub> NH <sub>2</sub> <sup>+</sup>	-2126.894979	0.701926	-2126.193053	39.9	-16.6
<b>7</b>	Me <sub>3</sub> NH <sup>+</sup>	-2166.163592	0.729750	-2165.433842	39.3	-6.9
<b>8</b>	Me <sub>4</sub> N <sup>+</sup>	-2205.433465	0.755609	-2204.666665	-4.9	-1.2
<b>9a</b>	EtNMe <sub>3</sub> <sup>+</sup>	-2244.716247	0.783387	-2243.932860	25.7	-0.3
<b>9b</b>	EtNMe <sub>3</sub> <sup>+</sup>	-2244.716066	0.783371	-2243.932695	13.9	-0.2

<sup>a</sup> The structure was optimized at the B3LYP/6-31G\*. No vibrational analysis was performed in this case. No zero-point energy corrections were applied for the ΔE value calculation.

**Table 1. Calculated (RI-BP86/TZVPP//RI-BP86/SV(P)) total energy values and reaction (1) energies for 1-9.**

Compo- und	Guest	Total energy, E, a.u.	ZPE correction, a.u. (BP-86/SV(P))	E+ZPE, a.u.	ΔE, kcal/mol
<b>1</b>	-	-1993.690417	0.597459	-1993.092958	0.0
<b>2a</b>	NH <sub>4</sub> <sup>+</sup>	-2050.666918	0.645203	-2050.666918	-30.2 <sup>b</sup>
<b>2b</b>	NH <sub>4</sub> <sup>+</sup>	-2050.666834	0.645855	-2050.666834	-29.7
<b>3a</b>	MeNH <sub>3</sub> <sup>+</sup>	-2089.988783	0.674138	-2089.314645	-27.8 <sup>c</sup>
<b>4a</b>	EtNH <sub>3</sub> <sup>+</sup>	-2129.318866	0.702062	-2128.616804	-20.6
<b>4b</b>	EtNH <sub>3</sub> <sup>+</sup>	-2129.296627	0.701354	-2128.595273	-6.6
<b>5a</b>	PrNH <sub>3</sub> <sup>+</sup>	-2168.647225	0.729681	-2167.917545	-19.7
<b>5b</b>	PrNH <sub>3</sub> <sup>+</sup>	-2168.621276	0.728876	-2167.892400	-3.4
<b>6</b>	Me <sub>2</sub> NH <sub>2</sub> <sup>+</sup>	-2129.301147	0.701926	-2128.599221	-13.8 <sup>d</sup>
<b>7</b>	Me <sub>3</sub> NH <sup>+</sup>	-2168.614809	0.729750	-2167.885059	-4.5 <sup>e</sup>
<b>8</b>	Me <sub>4</sub> N <sup>+</sup>	-2207.931323	0.755609	-2207.175714	0.4 <sup>f</sup>
<b>9a</b>	EtNMe <sub>3</sub> <sup>+</sup>	-2247.260620	0.783387	-2246.477233	1.5
<b>9b</b>	EtNMe <sub>3</sub> <sup>+</sup>	-2247.260258	0.783371	-2246.476887	1.7

<sup>b</sup> Calculated basis set superposition error (BSSE) 0. kcal/mol

<sup>c</sup> BSSE 0.44 kcal/mol

<sup>d</sup> BSSE 0. kcal/mol

<sup>e</sup> BSSE 0.53 kcal/mol

<sup>f</sup> BSSE 0.35 kcal/mol

## References

- [1] a) C.D. Gutsche, *Calixarenes*, Royal Society of Chemistry, Cambridge, England, **1989**; b) C.D. Gutsche, in *Inclusion Compounds*, Vol. 4 (Eds. J.L. Atwood, J.E.D. Davies, D.D. MacNicol), Oxford University Press, Oxford, **1991**, pp. 27-63; c) C.D. Gutsche, in *Large Ring Molecules* (Ed.: J.A. Semlyen), Wiley, New York, **1996**, pp. 309-343.
- [2] a) *Calixarenes: A Versatile Class of Macroyclic Compounds* (Eds.: J. Vicens; V. Böhmer), Kluwer, Dordrecht, **1991**; b) S. Shinkai, *Tetrahedron* **1993**, *49*, 8933-8968; c) V. Böhmer, *Angew. Chem.* **1995**, *107*, 785-818; *Angew. Chem. Int. Ed. Engl.* **1995**, *34*, 713-745; d) A. Pochini, R. Ungaro, in *Comprehensive Supramolecular Chemistry*; Vol. 2 (Ed.: F. Vögtle) Pergamon, Oxford; **1996**, pp. 103-142; e) A. Ikeda, S. Shinkai, *Chem. Rev.* **1997**, *97*, 1713-1734.
- [3] a) M.T. Blanda, D.B. Farmer, J.S. Brodbelt, B.J. Goolsby, *J. Am. Chem. Soc.* **2000**, *122*, 1486-1491; b) B.J. Goolsby, J.S. Brodbelt, E. Adou, M. Blanda, *Intern. J. Mass. Spectrom.* **1999**, *193*, 197-204; c) F. Allain, H. Virelizier, C. Moulin, C.K. Jankowski, J.F. Dozol, J.C. Tabet, *Spectroscopy*, **2000**, *14*, 127-139; d) J.M.J. Nuutinen, A. Iroco, M. Vincenti, E. Dalcanale, J.M.H. Pakarinen, P. Vainiotalo, *J. Am. Chem. Soc.* **2000**, *122*, 10090-10100; e) M.C. Letzel, C. Agena, J. Mattay, *J. Mass Spectrom.* **2002**, *37*, 63-68.
- [4] M. Mäkinen, P. Vainiotalo, K. Rissanen, *J. Am. Soc. Mass Spectrom.* **2002**, *13*, 851-861; M. Mäkinen, J.-P. Jalkanen, P. Vainiotalo, *Tetrahedron*, **2002**, *58*, 8591-8596.
- [5] See the review on this subject: J.C. Ma, D.A. Dougherty, *Chem. Rev.* **1997**, *97*, 1303-1324.
- [6] a) J.-L. Sussman, M. Harel, F. Frolow, C. Oefner, A. Goldman, L. Toker, I. Silman, *Science*, **1991**, *253*, 872-879; b) A. Casnati, D. Sciotto, G. Arena, in *Calixarenes 2001*; (Eds. Z. Asfari, V. Böhmer, V. Harrowfield, J. Vicens), Kluwer Academic Publishers: Dordrecht, **2001**, Chapter 24 and references therein.
- [7] H.-J. Schneider, D. Güttes, U. Schneider, *J. Am. Chem. Soc.*, **1988**, *110*, 6449-6454.
- [8] J.M. Harrowfield, M.I. Ogden, W.R. Richmond, B.W. Skelton, A.H. White, *J. Chem. Soc. Perkin Trans. 2*, **1993**, 2183-2190.
- [9] J.L. Atwood, L.J. Barbour, P.C. Junk, W. Orr, *Supramol. Chem.*, **1995**, *5*, 105.
- [10] G. Arena, A. Casnati, A. Contino, F.G. Gulino, D. Sciotto, R. Ungaro, *J. Chem. Soc. Perkin Trans. 2*, **2000**, 419-423.
- [11] A. Iroco, M. Vincenti, E. Dalcanale, *Chem. Eur. J.*, **2001**, *7*, 2034-2042.

- [12] A. Ghoufi, C. Bonal, J.P. Morel, N. Morel-Desrosiers, P. Malfreyt, *J. Phys. Chem. B*, **2004**, *108*, 5095-5104.
- [13] F. Perret, J.-P. Morel, N. Morel-Desrosiers, *Supramol. Chem.*, **2003**, *15*, 199-206.
- [14] a) G. Arena, A. Casnati, A. Contino, G.G. Lombardo, D. Sciotto, R. Ungaro, *Chem. Eur. J.*, **1999**, *5*, 738-744; b) A. Mendes, C. Bonal, N. Morel-Desrosiers, J.P. Morel, P. Malfreyt, *J. Phys. Chem.*, **2002**, *106*, 4516-4524.
- [15] W. Koch, M.C. Holthausen, *A Chemist's Guide to Density Functional Theory*, Wiley-VCH, **2001**.
- [16] A.B. Rozhenko, W.W. Schoeller, M. Letzel, B. Decker, C. Agena, J. Mattay, *J. Mol. Struct. (THEOCHEM)*, accepted to publication.
- [17] M.C. Letzel, B. Decker, A.B. Rozhenko, W.W. Schoeller, J. Mattay, *J. Am. Chem. Soc.* **2004**, *126*, 9669-9674.
- [18] A.D. Becke, *Phys. Rev. A*, **1988**, *38*, 3098-3100.
- [19] J.P. Perdew, *Phys. Rev. B*, **1986**, *33*, 8822-8824.
- [20] a) B.I. Dunlap, J.W. Conolly, J.R. Sabin, *J. Chem. Phys.* **1979**, *71*, 339; b) O. Vahtras, J. Almlöf, M.W. Feyereisen, *Chem. Phys. Lett.*, **1993**, *213*, 514; K. Eichkorn, O. Treutler, H. Öhm, M. Häser, R. Ahlich, *Chem. Phys. Lett.* **1995**, *240*, 283-289.
- [21] See <http://www.ipc.uni-karlsruhe.de/tch/tch1/turbomole/index.en.html> and references cited therein.
- [22] A. Schaefer, H. Horn, R. Ahlrichs, *J. Chem. Phys.* **1992**, *97*, 2571-2577.
- [23] P. Deglmann; F. Furche; R. Ahlrichs, *Chem. Phys. Lett.* **2002**, *362*, 511-518; P. Deglmann; F. Furche, *J. Chem. Phys.* **2002**, *117*, 9535.
- [24] *Gaussian 03*, Revision A.1, M. J. Frisch, G. W. Trucks, H. B. Schlegel, G. E. Scuseria, M. A. Robb, J. R. Cheeseman, J. A. Montgomery, Jr., T. Vreven, K. N. Kudin, J. C. Burant, J. M. Millam, S. S. Iyengar, J. Tomasi, V. Barone, B. Mennucci, M. Cossi, G. Scalmani, N. Rega, G. A. Petersson, H. Nakatsuji, M. Hada, M. Ehara, K. Toyota, R. Fukuda, J. Hasegawa, M. Ishida, T. Nakajima, Y. Honda, O. Kitao, H. Nakai, M. Klene, X. Li, J. E. Knox, H. P. Hratchian, J. B. Cross, C. Adamo, J. Jaramillo, R. Gomperts, R. E. Stratmann, O. Yazyev, A. J. Austin, R. Cammi, C. Pomelli, J. W. Ochterski, P. Y. Ayala, K. Morokuma, G. A. Voth, P. Salvador, J. J. Dannenberg, V. G. Zakrzewski, S. Dapprich, A. D. Daniels, M. C. Strain, O. Farkas, D. K. Malick, A. D. Rabuck, K. Raghavachari, J. B. Foresman, J. V. Ortiz, Q. Cui, A. G. Baboul, S. Clifford, J. Cioslowski, B. B. Stefanov, G. Liu, A. Liashenko, P. Piskorz, I. Komaromi, R. L. Martin, D. J. Fox, T. Keith, M. A. Al-Laham, C. Y. Peng, A. Nanayakkara,

M. Challacombe, P. M. W. Gill, B. Johnson, W. Chen, M. W. Wong, C. Gonzalez, and J. A. Pople, *Gaussian, Inc.*, Pittsburgh PA, **2003**.

[25] (a) R. Ditchfield, W.J. Hehre, J.A. Pople, *J. Chem. Phys.* **1971**, *54*, 724; (b) W.J. Hehre, R. Ditchfield, J.A. Pople, *J. Chem. Phys.* **1972**, *56*, 2257; (c) P.C. Hariharan, J.A. Pople, *Mol. Phys.* **1974**, *27*, 209; (d) P.C. Hariharan, J.A. Pople, *Theor. Chim. Acta* **1973**, *28*, 213.

[26] A.D. Becke, *J. Chem. Phys.* **1993**, *98*, 5648-5652.

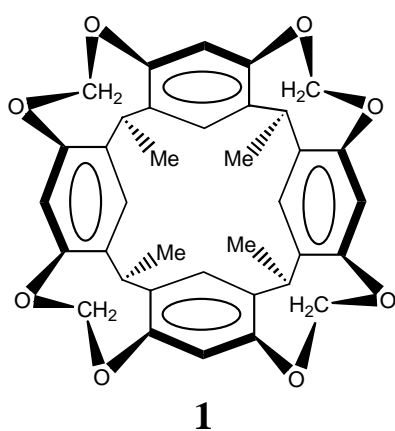
[27] C. Lee, W. Yang, R.G. Parr, *Phys. Rev. B* **1988**, *37*, 785-789.

[28] VMD for WIN-32, Version 1.8.2 (Dezember, 4, 2003): W. Humphrey, A. Dalke, K. Schulten, *J. Mol. Graphics*, **1996**, *14*, 33-38.

<sup>29</sup> A. Schaefer, C. Huber, R. Ahlrichs, *J. Chem. Phys.* **1994**, *100*, 5829-5835.

<sup>30</sup> For this nomenclature see F.A. Cotton, G. Wilkinson, *Advanced Inorganic Chemistry*, John-Wiley & Sons, New York **1988**.

[31] J.R. Moran, S. Karbach, D.J. Cram, *J. Am. Chem. Soc.* **1982**, *104*, 5826-5828.



- 2:**  $[1 \cdot \text{NH}_4]^{(+)}$
- 3:**  $[1 \cdot \text{MeNH}_3]^{(+)}$
- 4:**  $[1 \cdot \text{EtNH}_3]^{(+)}$
- 5:**  $[1 \cdot \text{n-PrNH}_3]^{(+)}$
- 6:**  $[1 \cdot \text{Me}_2\text{NH}_2]^{(+)}$
- 7:**  $[1 \cdot \text{Me}_3\text{NH}]^{(+)}$
- 8:**  $[1 \cdot \text{Me}_4\text{N}]^{(+)}$
- 9:**  $[1 \cdot \text{EtNMe}_3]^{(+)}$

Scheme 1.

Scheme 2. Carbon atom numeration in the aromatic rings of calix[4]arene.

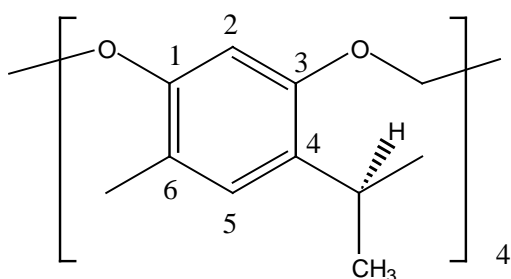


**Figure 1.** Graphic representation of complexes of cavitand 1 with  $\text{NH}_4^+$  (2a and 2b),  $\text{MeNH}_3^+$  (3a),  $\text{EtNH}_3^+$  (4a and 4b), n- $\text{PrNH}_3^+$  (5a and 5b),  $\text{Me}_2\text{NH}_2^+$  (6),  $\text{Me}_3\text{NH}^+$  (7),  $\text{Me}_4\text{N}^+$  (8) and  $\text{EtNMe}_3^+$  (9a and 9b).

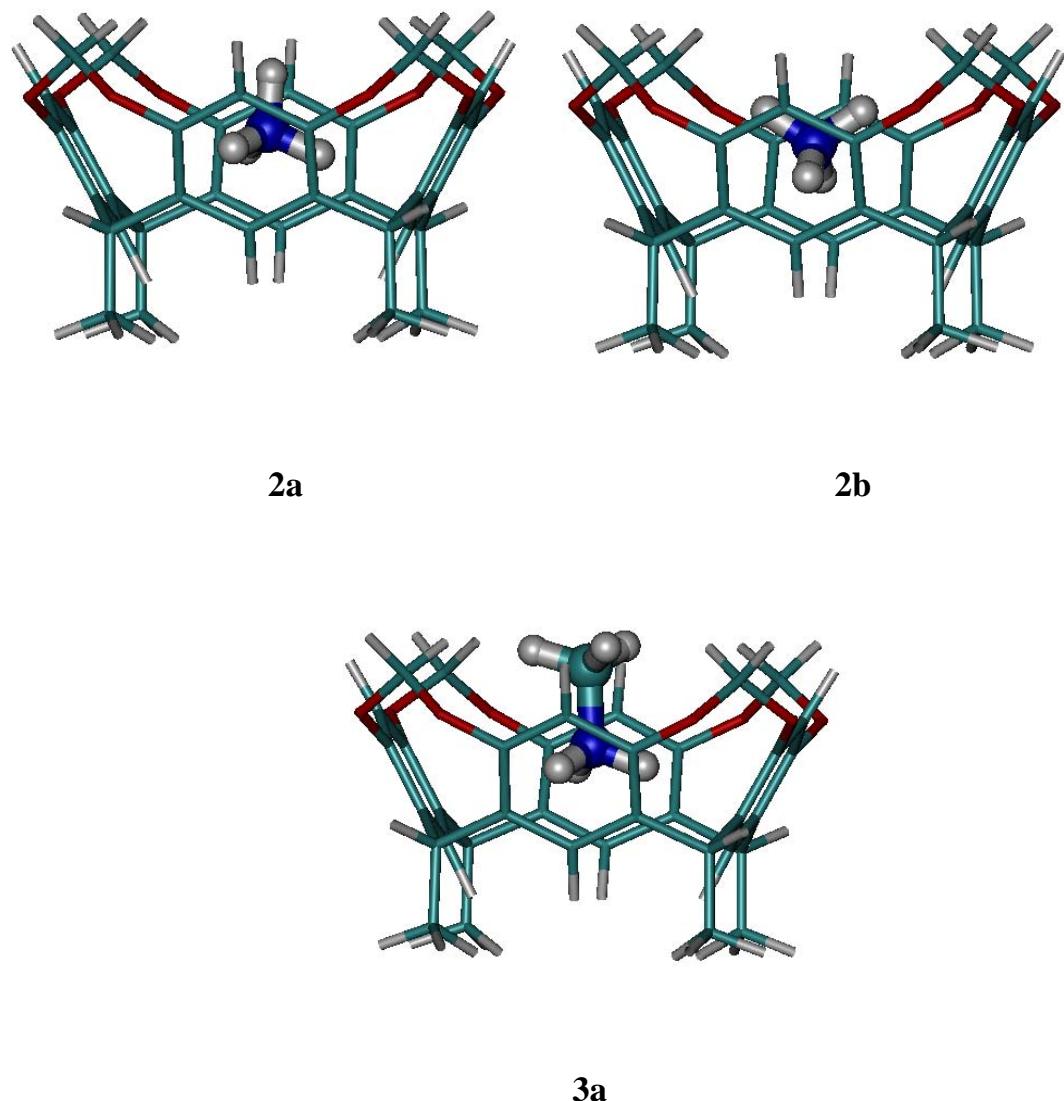


**Figure 1, continue.**

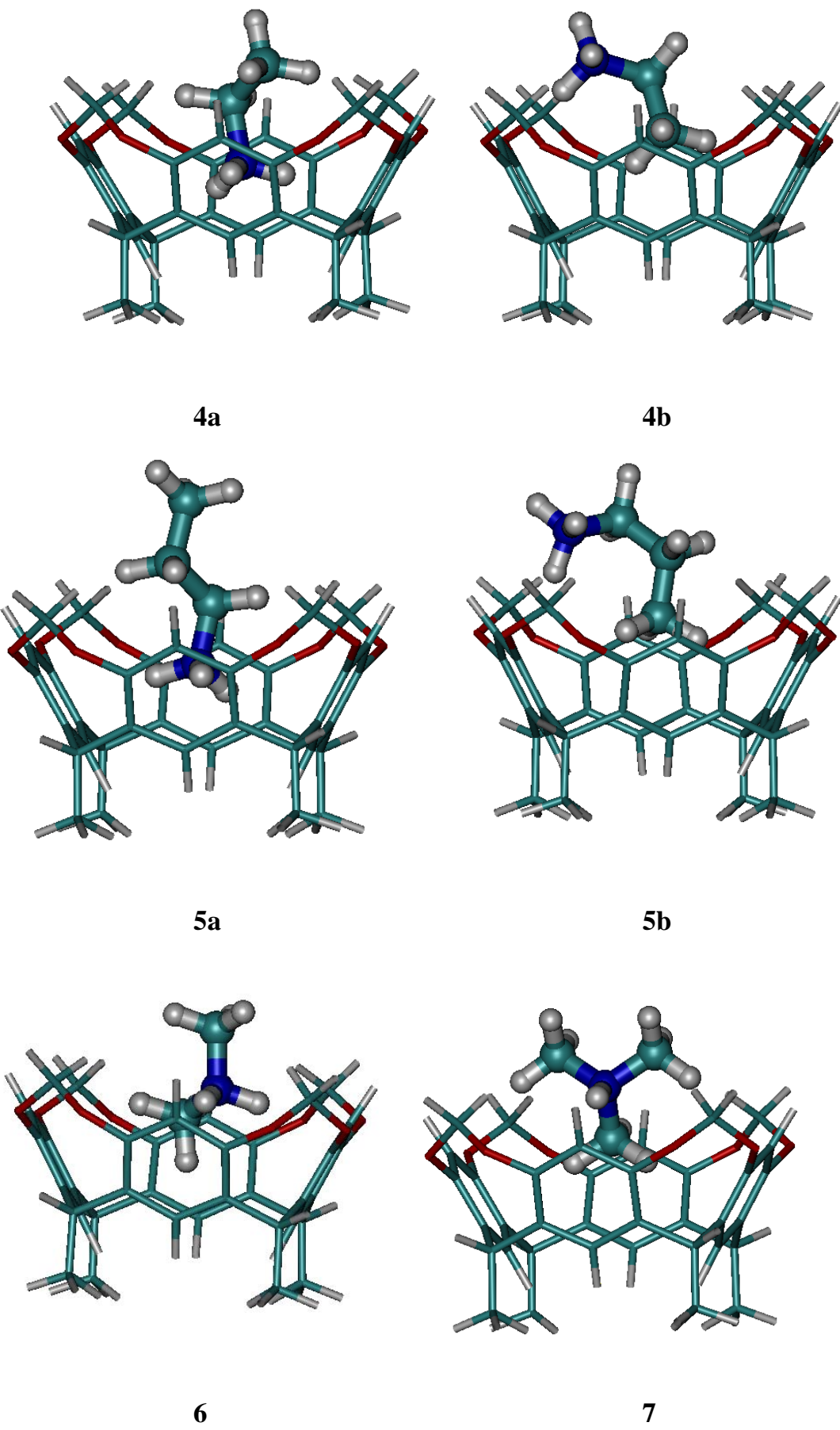
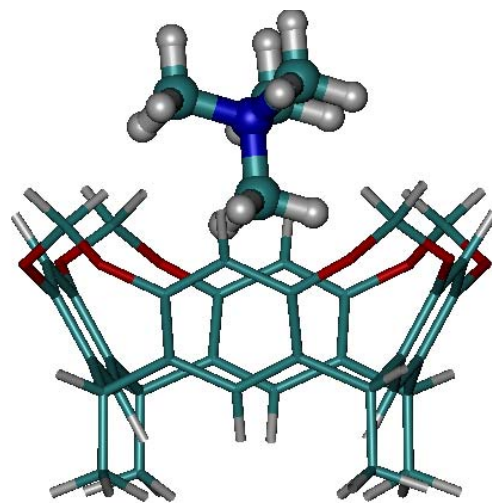


**Figure 1, continue.**



8

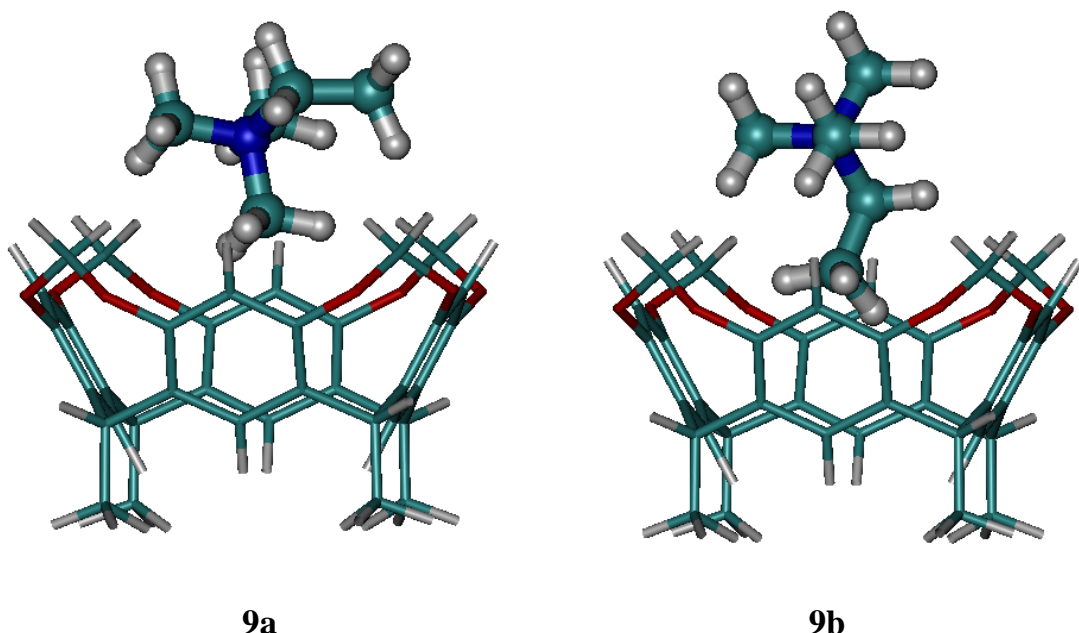


**Figure 8.** EMS spectrum of the mixture of tetramethylcavitand with an equimolar mixture of ammonium-, methylammonium, dimethylammonium-, trimethylammonium- and tetramethylammonium salts. Signals with varying abundances arising from sodium and potassium are due to these ubiquitous alkali metals.

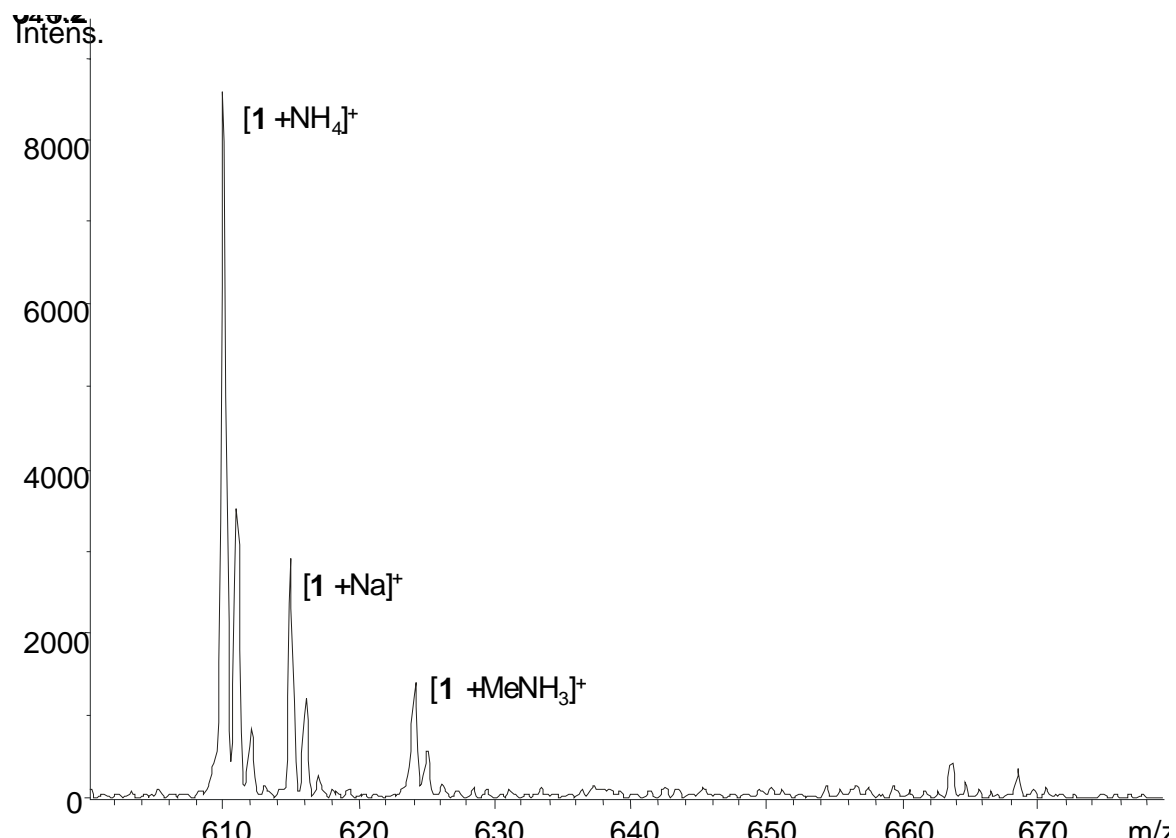
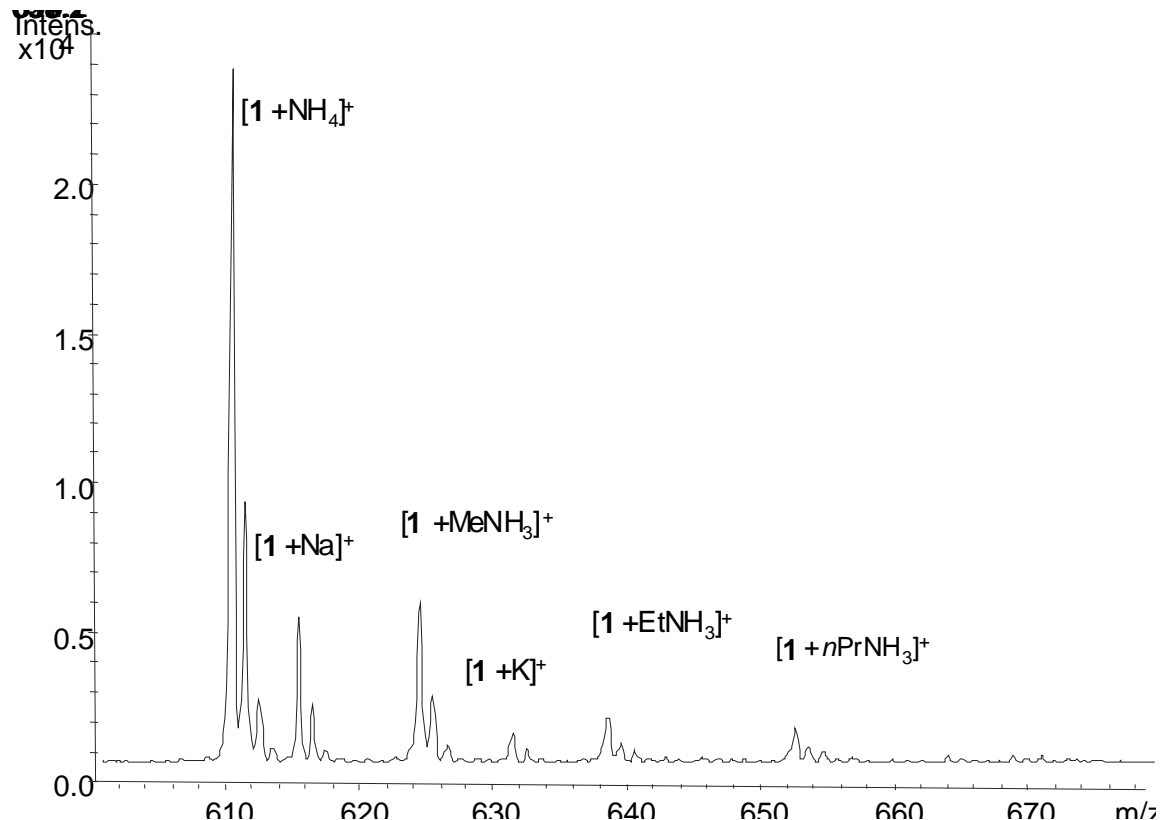


**Figure 8.** EMS spectrum of the mixture of tetramethylcavitand with an equimolar mixture of ammonium-, methylammonium, ethylammonium- and *n*-propylammonium- salts. Signals with varying abundances arising from sodium and potassium are due to these ubiquitous alkali metals.



# Conformational features of calix[4]arenes with alkali metal cations: A quantum chemical investigation with density functional theory

Alexander B. Rozhenko, Wolfgang W. Schoeller\*, Matthias C. Letzel, Björn Decker,  
Ceno Agena, Jochen Mattay

*Fakultät für Chemie, Universität Bielefeld, Postfach 10 01 31, 33501 Bielefeld, Germany*

Received 20 December 2004; revised 16 June 2005; accepted 20 June 2005

Available online 31 August 2005

## Abstract

A variety of conformations for three model calix[4]arenes with 8 or 12 OH groups have been investigated by calculations at density functional (RI-BP86) and RI-MP2 level of approximation. The calixarenes form stable complexes with the alkali metal cations of lithium up to caesium. For the investigations all-valence electron basis sets as well as various effective core potentials were probed. The stabilities of complexes were analysed in comparison with the corresponding benzene complexes,  $M^+ \cdot C_6H_6$ . The formation of the calixarene metal complexes is considered in two steps, (a) in a distortion from the equilibrium conformation of the free calixarenes and (b) subsequent complexation. The distortion energies are small for the ‘crown’ and larger for the ‘boat’ conformations. On the other hand the latter are more stabilized by significant interaction energy of the cation with two adjacent  $\pi$ -systems of the aromatic rings. As a result, these two conformations are of similar stabilities for  $K^+$  to  $Cs^+$  complexes with resorc[4]arenes, with a slight advantage for the ‘boat’ structure. The most stable conformation for the coordination products of these cations with the calix[4]arene with 12 OH groups is a slightly flattened ‘crown’ that is derived by maximum hydrogen bonding of the OH-groups and the most effective cation- $\pi$  interactions. Special cases are complexes of  $Li^+$  and  $Na^+$  which in most instances prefer the coordination on the oxygen atoms of the upper rim of the calixarene cavities and thus form ‘boat’-like structures.

© 2005 Published by Elsevier B.V.

**Keywords:** Calix[4]arenes; Alkali metal cations; Complexes; DFT; BP86; MP2; ECP; Calculation

## 1. Introduction

The reliable prediction of the host-guest interactions is an important goal in supramolecular chemistry. So far, a classic modelling of these aspects is provided in the complex formation of calix[4]arenes with alkali metal cations. These have been investigated in detail with electrospray ionization mass spectrometry (ESI-MS) [1–4]. These measurements refer to investigations in the gas phase. Since experimental structures on the insertion complexes with alkali metal cations are hitherto not known, the choice in favour of the definite conformations was alternatively made in solution on the basis of NMR-spectral information. A thorough

quantum chemical description of these species is still lacking, mainly due to the large size of these structures for ab initio calculations. Up to now the calculations were performed at the Hartree–Fock level of theory with relative small basis sets, with the use of semi-empirical methods or using molecular mechanics or Monte-Carlo simulations. It was shown for the p-tert-butylcalix[4]arene complex with carbon disulfide [5] that the SYBYL force field [6] or the Allinger type force field methods (MM+, MM2, MM3) [7] served a qualitative understanding for complex formation, but these methods were not at all able to describe the geometrical parameters properly. On the other hand, semi-empirical methods such as PM3 geometry optimization provided a wrong chemical structure, host and guest were separated [5], in contradiction to the experiment. Also the molecular mechanics and the Hartree–Fock (RHF/3-21G(d)) investigations for the complexes of resorc[4]arenes with various alkali metal cations gave different structures for the lithium complex [4]. It indicates a strong sensitivity

\* Corresponding author. Fax: +49 0 521 106 6467.

E-mail address: [wolfgang.schoeller@uni-bielefeld.de](mailto:wolfgang.schoeller@uni-bielefeld.de) (W.W. Schoeller).

of the calculational results on the approximation level. It is known that the various density functional theory (DFT) methods yield reliable structures for the most organic and elementorganic species [8], but up to now they were not applied to the relative large calixarene complexes. Thus, Mäkinen et al. analysed recently the complexes of calix[4]arenes with various alkali metal cations combining the theoretical and mass-spectrometric approaches [9,10]. The authors compared the calculated total energies for five extreme conformations of tetraethyl resorc[4]arenes. A mixed basis set was used for the geometry optimization at the Hartree–Fock level of approximation: the 6-31++G(d,p) set for the eight OH-groups and only the 3-21G basis set for the remaining atoms of the molecular skeleton. Moreover, only high symmetrical conformations were investigated without frequency analyses ensuring the resulting structures as local energy minima. The only single point energy calculations were performed at the DFT (B3LYP/6-31++G(d,p)) level of theory. A progress in computers and software allows DFT geometry optimization for the large calixarene structures [11]. Recently a full DFT (B3LYP) investigation on the energetic stabilities of the conformers of the calix[4]arenes with para-substitution in the aromatic rings and their alkali metal complexes was published [12]. However, the authors calculated only inclusion products with  $\text{Li}^+$ ,  $\text{Na}^+$  and  $\text{K}^+$  cations.

## 2. Computational section

All of the quantum chemical calculations were carried out with the TURBOMOLE [13] and in some cases also with the CAUSSIAN-03 [14] suite of program systems. The structures corresponding to various symmetries were fully optimized at the DFT (BP86 [15–17]) level within the RI approximation [18] (RI-DFT) and using the split-valence basis set SV(P) [19]. For the heavy atoms Rb and Cs, the effective core potentials from the Stuttgart group [20] were used with the default basis set (def-SV(P)) for the TURBOMOLE set of programs and with the valence shell contracted as {51131/31/1} for Rb and {31111/411} for Cs (core electrons 28 for Rb and 46 for Cs). For all of the structures vibration analyses were performed, computing analytical first and second order derivatives [21] at the same approximation level as was used for the structure optimizations. The single-point energy calculations at the RI-MP2 level of approximation [22] were performed using the equilibrium geometries and the standard triple-zeta basis sets (TZVP) [23] (again with the implemented ECP basis sets of the same quality for Rb and Cs). The energy values were corrected by addition of the ZPE energy correction values obtained at the RI-BP86/SV(P) level of approximation. The corrected RI-MP2 energies were also used to compare the stabilities of various conformations computed with the other type of basis sets. The TZVP basis set superposition errors for some complexes were estimated

using a standard procedure. A single point energy calculation (at the Hartree–Fock level of theory) was performed for the complex with the alkali metal cation as a ghost atom, setting the nuclear charge of the cation equal zero and keeping all its basis functions. For the same structure another energy calculation was made, but without the cation and cation's basis functions. The differences between both energy values (the basis counterpoise corrections) found with this procedure resulted only to 0.1 to 0.4 kcal/mol. The contribution from the basis expansion of the alkali metal cation (calculated for the cation with all the basis function of the calixarene complex) did not exceed 0.03 kcal/mol and hence could be neglected.

Additionally, free calixarenes and their complexes with  $\text{Li}^+$  and  $\text{Na}^+$  were recalculated using the GAUSSIAN-03 set of programs, B3LYP hybrid functional (Becke's three-parameter exchange functional [24] and the Lee–Yang–Parr correlation functional [25]) and a standard Gaussian 6-31G(d) basis set [26] with 6d functions at the heavy atoms. This gave similar results which will not be discussed here. For the higher element homologues with  $\text{K}^+$  to  $\text{Cs}^+$  two different relativistically corrected effective core potentials were also utilized: (a) the ECP of Stevens, Basch, Krauss, Jasien and Cundari (SBKJC) [27] and (b) the ECP of Hay and Wadt (HW) [28]. In the cases of the SBKJC and HW ECP basis sets, valence orbitals were described by double-zeta sets of Gaussian orbitals, augmented with one set (6d) of polarization functions (at the heavy atoms). The SBKJC seemed to describe incorrectly the electronic structure of complexes involving  $\text{Rb}^+$  and (in some cases)  $\text{Cs}^+$  cations. The results will not be considered here, these data are available on request. The VMD program packet [29] was used for the graphical presentation of the calculated structures.

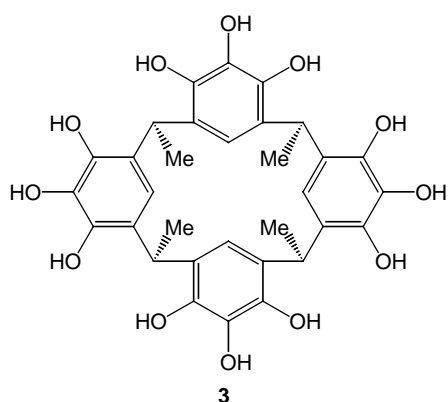
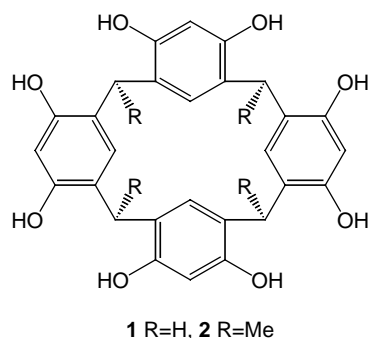
## 3. Results and discussion

We present here the quantum chemical study on resorc[4]arenes **1,2** and calix[4]arenes **3** and their alkali metal complexes at a DFT (RI-BP86) level of approximation.

The calculations of the high-symmetrical structures allow a drastic reduction of the computational labor, but they do not always provide the structure corresponding to the real minima in energy. As we will show below, several different local minima in energy were found for the alkali metal complexes. In this connection we calculated a number of structures with different symmetries and types of coordination in order to find the deepest minimum in energy for every complex of interest.

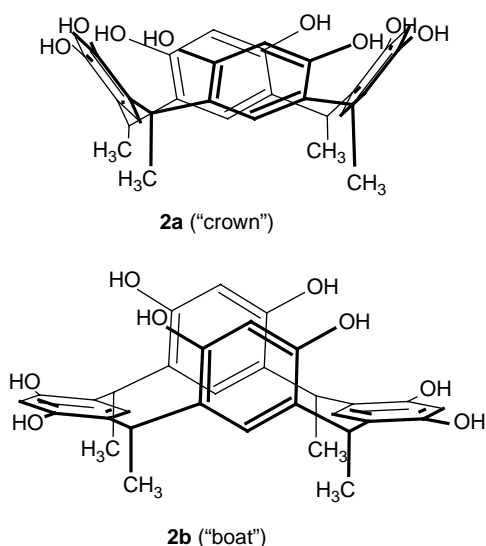
### 3.1. Free calixarenes

As objects for the investigations we have chosen the calix[4]arenes **1–3** (Scheme 1). The structure **1** is a parent



Scheme 1.

resorc[4]arene. The methyl groups introduced at the lower rim of the cavity in **2** mimic the effect of alkyl substitution in the real calixarenes [4]. We will consider here only two main conformations for calix[4]arenes which are most important for complexation: the ‘crown’ (Scheme 2, a) and ‘boat’ (Scheme 2, b) conformations which are close in energy to each other [9]. Other possible isomers (listed for example in [12]) can be formed only with breaking the C–C bond(s). Such an isomerization does not take place



Scheme 2.

spontaneously in solution and hence it will be not considered here.

The DFT calculations indicate that the  $C_4$  symmetrical ‘crown’ conformations of the resorc[4]arenes, **1a** and **2a**, are appr. 4 to 5 kcal/mol lower in energy than the ‘boat’ structures, **1b** and **2b** (the plots for **2a** and **2b** are shown in Fig. 1). Detailed energy data for all isomers are collected in Appendices A–C. An introduction of four additional OH groups into the aromatic rings (Scheme 3) strongly favour the ‘crown’ conformation, **3a**, in comparison with the alternative ‘boat’ conformations, **3b** and **3c**. It is due to the formation of additional hydrogen bonds in **3a**. In **3b** four hydrogen bonds are broken and the other hydrogen bonds are weakened because eight hydrogens form (hydrogen) bonds with only four oxygens attached to the aromatic rings. In **3c** they are connected to different oxygen atoms but our

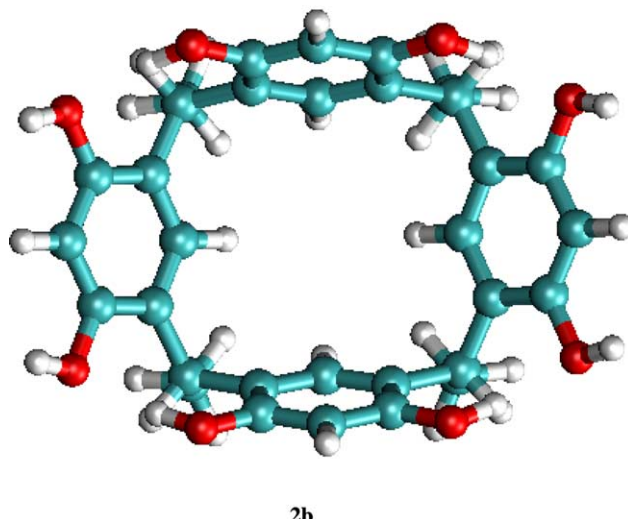
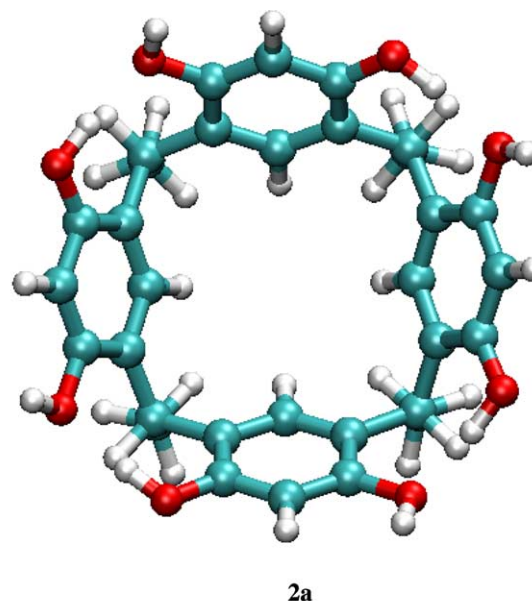
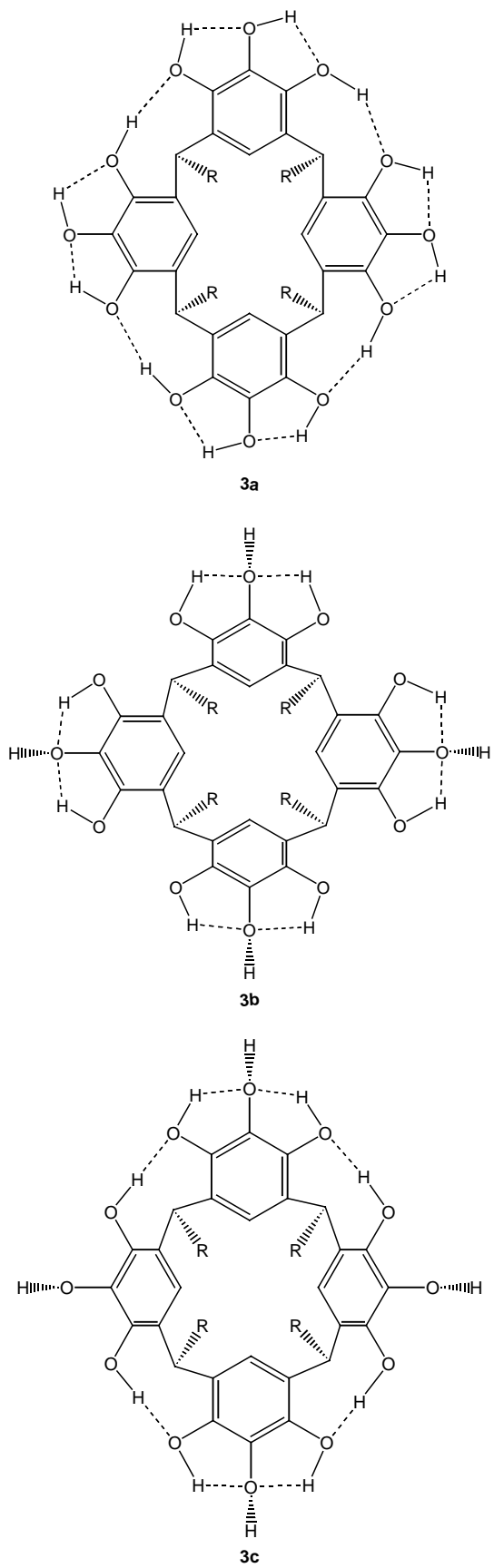


Fig. 1. Plots of the ‘crown’ (top) and ‘boat’ (bottom) conformations of the calix[4]arene **2** (optimized at the RI-BP86/SV(P) level of approximation).



Scheme 3.

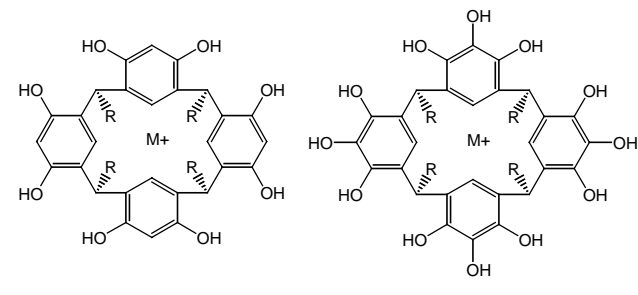
indicate higher total energies than found for **3b**. Moreover, **3c** appears not anymore as a real energy minimum on the potential energy surface.

### 3.2. Alkali metal complexes

Next we consider the conformations which derive from complexation of **1–3** with the alkali metal cations (Scheme 4).

The optimized  $C_4$  symmetrical ‘crown’ structures of complexes of calixarene **1** (Fig. 2, conformation **a**) appear (with only exception of **1Li**) as minima at the potential energy surfaces (PES). In contrast to, for the adducts of **2** which have the same symmetry, one imaginary frequency is found by the frequency analyses (see Appendix B). The imaginary vibrations for all complexes correspond to a symmetry reduction to  $C_2$ . Indeed, reoptimization leads to ‘boat-like’  $C_2$  symmetrical structures (Fig. 2, **e**) with slightly lower total energies and different cation-aromatic ring distances. In contrast to the free resorc[4]arenes, for the complexes of resorc[4]arenes, the ‘boat’-structures ( $C_{2v}$  symmetry) (Fig. 2, conformation **c**) possess similar (for **1M**) or insignificantly lower (for **2M**) total energies than the ‘crown’ conformations ( $C_4$  symmetry).

A special note should be made concerning the  $\text{Li}^+$  and  $\text{Na}^+$  complexes. As it has been mentioned above, the  $C_4$  symmetrical ‘crown’ indicates a well-pronounced trend to lower the total energy by the distortions flattening the calixarene cavity. The reported ab initio calculations [4] predicted a special type of coordination for the lithium complexes, with the  $\text{Li}^+$  cation coordinated to the oxygen atoms. We have probed two possible distortions:  $C_4$  to  $C_1$  symmetry reduction (Fig. 2, conformations **a** and **b**) or  $C_{2v}$  to  $C_s$  distortion (**c** and **d**), with the cation shifted from the middle of the cavity upwards to the ‘boats bow’, keeping the H bonding character inherent to the higher symmetry congener. Two other conformations (Fig. 2, conformations **e**, **f**) found by energy optimization (conformation **e** could not be located for **1**) together with their relative energy values are plotted in Fig. 2 as well. Both products of O-coordination of  $\text{Li}^+$  with calixarenes **1** and **2** (Fig. 2, **b** and **d**) are significantly more stable than the corresponding

**1M**  $\text{R} = \text{H}$ , **2M,3M**  $\text{R} = \text{Me}$ ; **M+**:  $\text{Li}^+$ ,  $\text{Na}^+$ ,  $\text{K}^+$ ,  $\text{Rb}^+$ ,  $\text{Cs}^+$ 

Scheme 4.

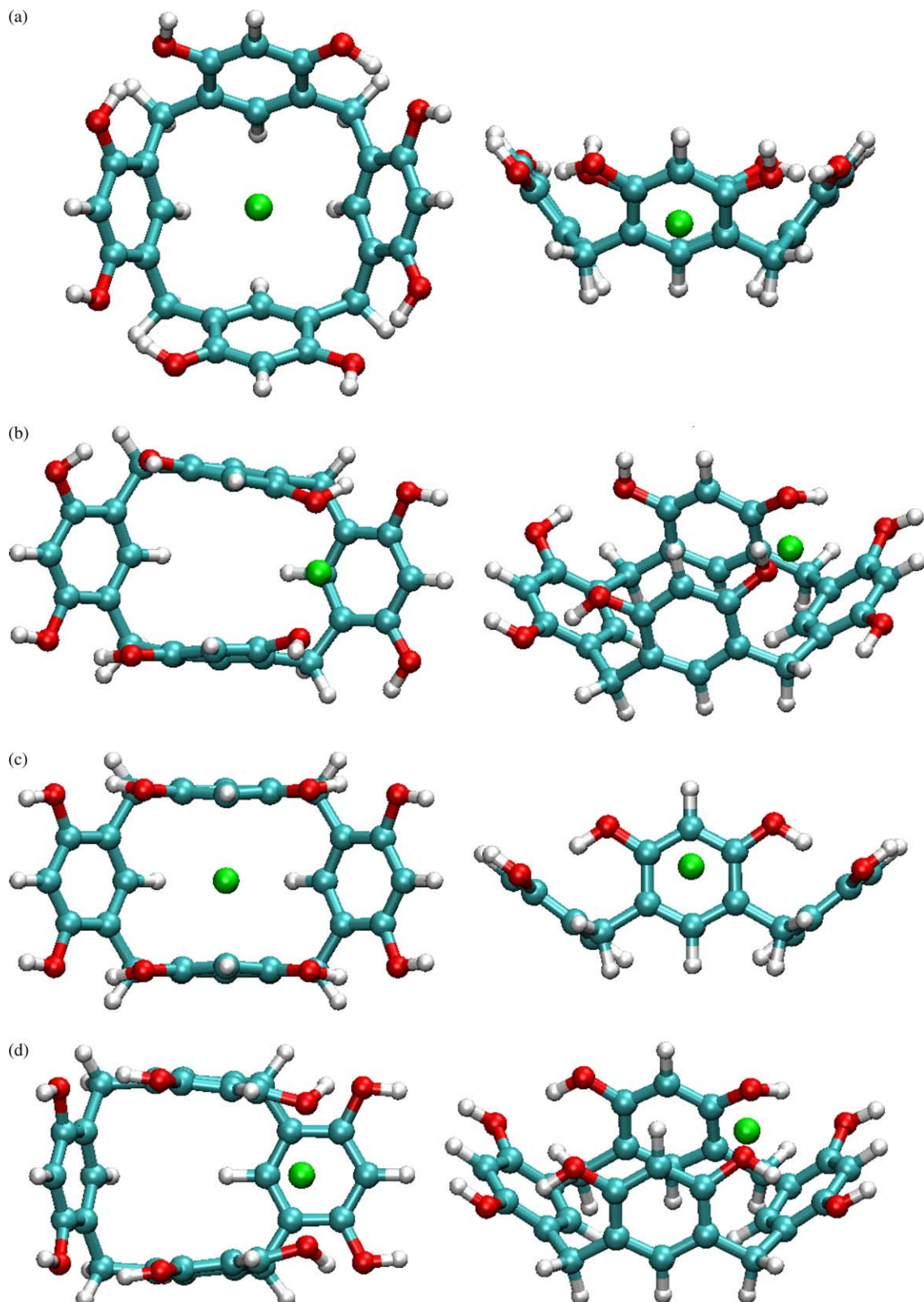


Fig. 2. Plots of various conformations of  $\text{Li}^+$  complexes of resorc[4]arenes (optimized at the RI-BP86/SV(P) level of approximation). (a) **1Li**,  $C_4$  symmetry ('crown') (0.0 kcal/mol). (b) **1Li**,  $C_1$  symmetry (coordination with two oxygen atoms and one aromatic ring) ( $\Delta E = -9.3$  kcal/mol). (c) **1Li**,  $C_{2v}$  symmetry ('boat') ( $\Delta E = -4.6$  kcal/mol). (d) **1Li**,  $C_s$  symmetry (coordination with two oxygen atoms and one aromatic ring) ( $\Delta E = -12.4$  kcal/mol). (e) **2Li**,  $C_2$  symmetry ('flattened crown') ( $\Delta E = -0.3$  kcal/mol compared with the corresponding  $C_4$  symmetrical 'crown' conformation). (f) **1Li**,  $C_2$  symmetry ('flattened crown') ( $\Delta E = +1.7$  kcal/mol).

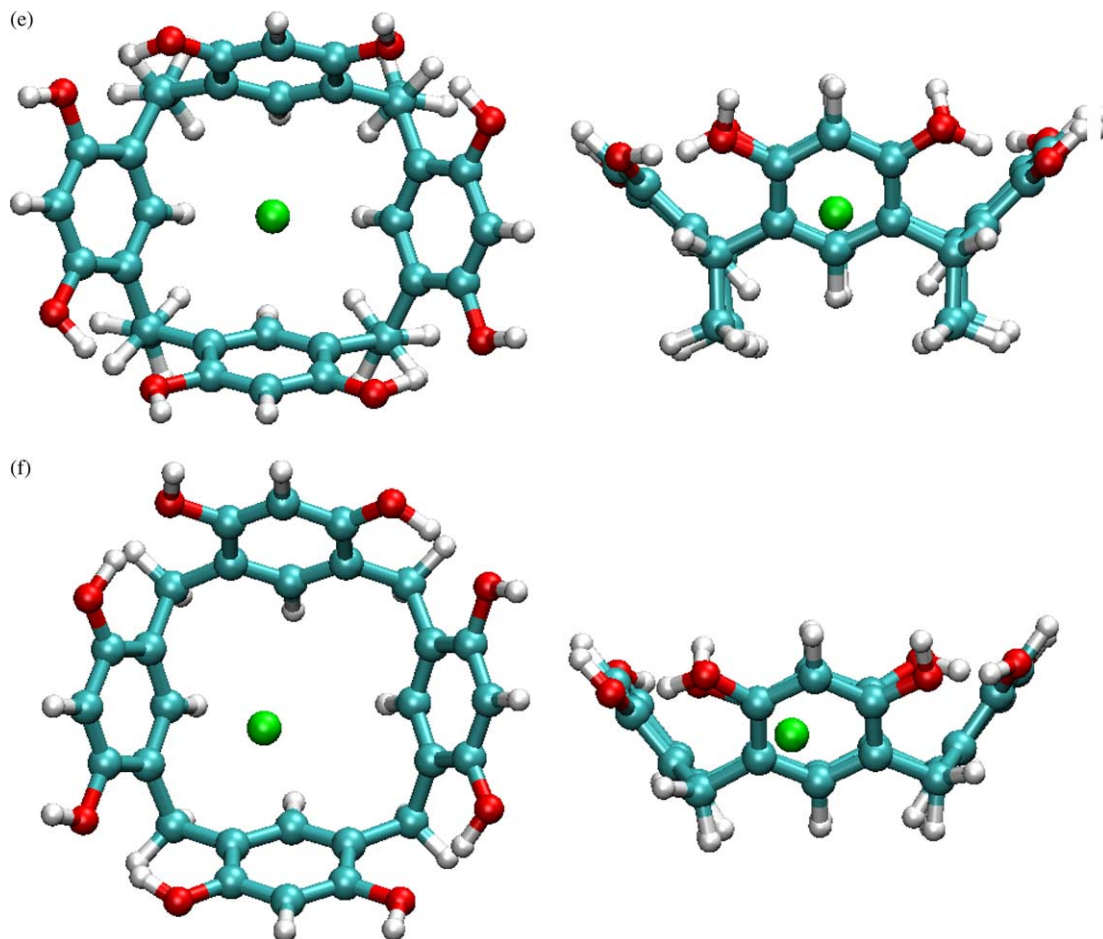


Fig. 2 (continued)

high-symmetrical congeners **a** and **c**, with some advantage for the  $C_s$  symmetrical conformation, **d**. In more detail, the  $\text{Li}^+$  cation is coordinated with two oxygen atoms and the nearest aromatic ring. We note here that other minima could also be found by the geometry optimization of the  $\text{Li}^+$  complexes (for example, structure **f** in Fig. 2). But they possess higher total energies than the structures **b** and **d**.

Similar structures (**b,d**) have been found for **1Na** and **2Na** as the most stable conformations. All other cations ( $\text{K}^+$  to  $\text{Cs}^+$ ) prefer  $C_{2v}$  symmetrical ‘boat’ structures with coordination of the cation with the aromatic rings (C-coordination) inside of the calixarene cavity of **1** or **2**. No significant  $\text{M}^+-\text{O}$  (metal–oxygen) overlap interaction has been found in these cases, even if the metal cation is positioned closer to the upper rim of the calix[4]arene cavity. For instance the shortest  $\text{M}^+-\text{O}$  distance in **2Cs** ( $C_{2v}$  symmetry) is 4.17 Å whereas the shortest  $\text{Cs}^+-\text{C}^{\text{arom}}$  distance is 3.49 Å.

The  $C_{2v}$  symmetrical ‘boat’ conformations **3M** are characterized by noticeably higher total energies (see Appendix C) as compared with the corresponding ‘crown’ structures. Hence they play no significant role for the description of the real calixarene complexes and we will not

consider these conformations in more detail. The geometry optimization for **3K** to **3Cs**, with the symmetry reduction from  $C_4$  to  $C_2$ , leads to the ‘boat-like’  $C_2$  symmetrical structures (Fig. 3, **c**) without any significant lowering in the total energy. The structures with the lithium cation coordinated at oxygen and simultaneously at one of the aromatic rings were located as well. Depending on the hydrogen coordination order, they belong to  $C_1$  (Fig. 3, **a**) or  $C_s$  symmetry (**b**). In contrast to **1M** or **2M**,  $C_s$  symmetrical structures (**b**) could be found for all complexes of **3**. But this conformation possesses a slightly lower total energy only for **3Li**. The  $C_4$  symmetrical ‘crown’ conformation remains most favorable for **3Na** and slightly flattened  $C_2$  symmetrical structures (Fig. 3, **c**) were obtained only slightly lower in energy for **3K** to **3Cs**.

### 3.3. Relative stabilities of calix[4]arene complexes

A method for the direct theoretical estimation of the relative stabilities of the calixarene complexes with the alkali metal cations is not feasible. The calculated energies of reaction (1) smoothly decrease in the order  $\text{M}^+=\text{Li}^+$  to  $\text{Cs}^+$ , but in the experiment this trend can be mediated by

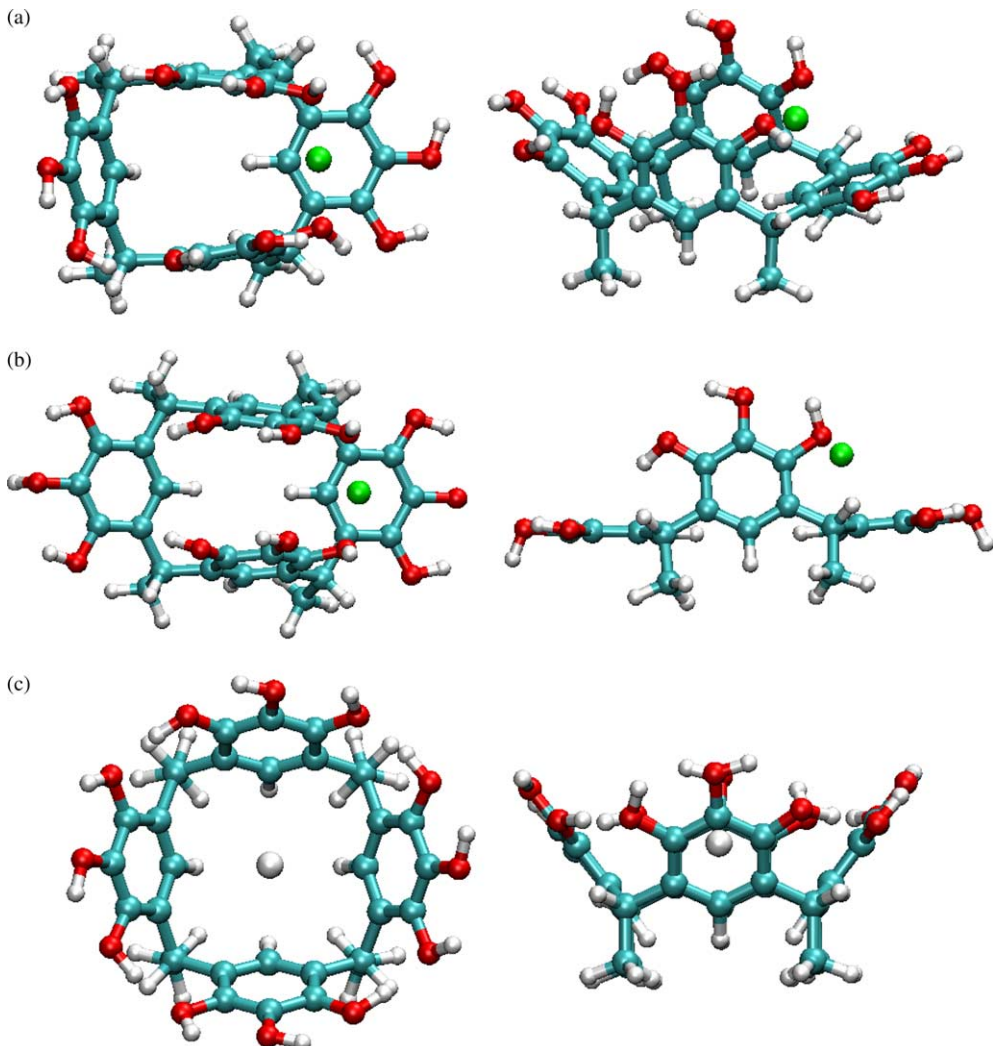


Fig. 3. Plots of  $C_1$  (a) and  $C_s$  (b) symmetrical conformations of **3Li** (a,b) and  $C_2$  symmetrical conformation **3K** (c) and relative total energies ( $\Delta E$ ) compared with corresponding  $C_4$  symmetrical ‘crown’ conformation (optimized at the RI-BP86/SV(P) level of approximation). (a) **3Li**,  $C_1$  symmetry ( $\Delta E = -2.7$  kcal/mol). (b) **3Li**,  $C_s$  symmetry ( $\Delta E = -6.2$  kcal/mol). (c) **3Li**,  $C_2$  symmetry ( $\Delta E = -0.2$  kcal/mol).

the different ability of the alkali metal cations to undergo solvation (it decreases in the same order) [30]. The energies  $\Delta E^{(1)}$  for the ‘crown’ conformations are recorded in Table 1 together with the values for the other (most stable) conformation.

Table 1  
Calculated  $\Delta E^{(1)}$  values (reaction (1)) for complexes **1M–3M** (RI-MP2/TZVP//RI-BP86/SV(P) level of approximation,  $C_4$  symmetrical ‘crown’ conformations)

M	$\Delta E^{(1)}$ , kcal/mol		
	1	2	3
$\text{Li}^+$	-54.4 (-68.0 <sup>a</sup> )	-57.1 (-71.7 <sup>a</sup> )	-60.1 (-66.2 <sup>a</sup> )
$\text{Na}^+$	-46.5 (-51.3 <sup>a</sup> )	-48.8 (-54.5 <sup>a</sup> )	-50.5
$\text{K}^+$	-35.7 (-38.5 <sup>b</sup> )	-37.8 (-41.7 <sup>b</sup> )	-38.3 (-38.4 <sup>c</sup> )
$\text{Rb}^+$	-33.7 (-35.7 <sup>b</sup> )	-35.9 (-38.1 <sup>b</sup> )	-36.5 (-36.7 <sup>c</sup> )
$\text{Cs}^+$	-32.0 (-32.8 <sup>b</sup> )	-34.4 (-35.9 <sup>b</sup> )	-35.0 (-35.1 <sup>c</sup> )

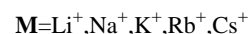
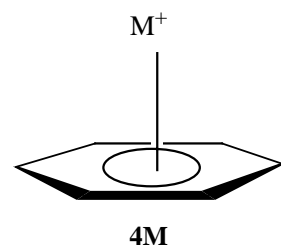
<sup>a</sup> Calculated for  $C_s$  symmetrical structure.

<sup>b</sup> Calculated for  $C_{2v}$  symmetrical structure.

<sup>c</sup> Calculated for  $C_2$  symmetrical structure.



We will examine here some indirect estimation procedures for the analysis of stability. Since in the calixarene complexes the cation interactions with the  $\pi$ -system (of the aromatic rings) are of importance [31], we have compared



Scheme 5.

Table 2

Calculated (RI-MP2/TZVP//RI-BP86/SV(P) level of approximation)  $\Delta E^{(2)}$  values [reaction (2)], M<sup>+</sup>-C distances in **2M**, as compared with cation–benzene complexes, **4M**

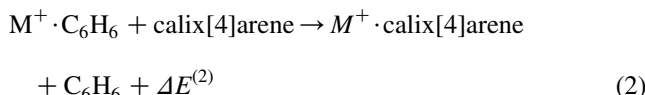
Complex	$\Delta E^{(2)a}$	The shortest calculated M <sup>+</sup> -C distances				
		C <sup>4</sup> -M <sup>+</sup> , Å	C <sup>3</sup> -M <sup>+</sup> , Å	C <sup>2</sup> -M <sup>+</sup> , Å	C <sup>1</sup> -M <sup>+</sup> , Å	C-M <sup>+</sup> in C <sub>6</sub> H <sub>6</sub> ·M <sup>+</sup> , Å
<b>2Li</b>	−19.1 (−32.7)	2.72 (2.69 <sup>b</sup> )	3.26 (2.81)	4.13 (2.98)	4.53 (3.08)	2.41
<b>2Na</b>	−25.4 (−30.2)	2.86 (2.91 <sup>c</sup> )	3.31 (3.05)	4.07 (3.25)	4.43 (3.36)	2.83
<b>2K</b>	−21.7 (−24.5)	3.19 (3.34)	3.49 (3.34)	4.02 (3.29)	4.31 (3.25)	3.28
<b>2Rb</b>	−21.2 (−23.2)	3.39 (3.53)	3.62 (3.50)	4.04 (3.41)	4.28 (3.36)	3.47
<b>2Cs</b>	−21.1 (−21.9)	3.59 (3.75)	3.76 (3.70)	4.08 (3.55)	4.29 (3.49)	3.70

<sup>a</sup> Data for C<sub>4</sub> symmetrical structures. In parentheses are the values calculated for the deepest minima in energy: C<sub>s</sub> for **2Li** and **2Na** and C<sub>2v</sub> for **2K** to **2Cs**. The carbon atom positioned between two OH groups is numerated as C<sup>1</sup> (**Scheme 6**).

<sup>b</sup> The shortest Li–O distance is 2.00 Å.

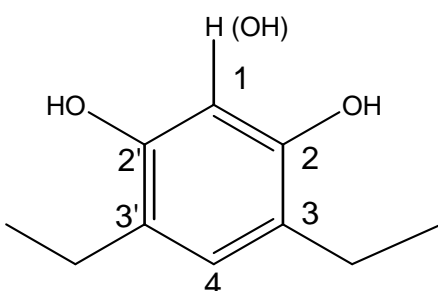
<sup>c</sup> The shortest Na–O distance is 2.42 Å.

the stabilities of the considered inclusion models with the corresponding arene complexes **4M** (**Scheme 5**), using the same approximation level [reaction (2)].



All the optimized structures **4M** reveal C<sub>6v</sub> symmetry with identical C–M<sup>+</sup> distances (**Table 2**). These increase continuously from Li<sup>+</sup> to Cs<sup>+</sup>.

Because of the similar type of interactions in **4M** and **2M**, the reaction (2) energies can be considered as a measure of the ‘cavity effect’ of the calixarene. The cation interacts simultaneously with two or more aromatic π-systems inside of the calixarene cavity. The complexation energies  $\Delta E^{(2)}$  for the series of complexes **2M** together with the most relevant bonding parameters are listed in **Table 2**. We may compare the M–C<sup>arom</sup> distances with the corresponding distances in the benzene complexes **4M**. The depth of the cation diving into the calixarene cavity is determined by the shortest M–C contacts. For the C<sub>4</sub> symmetrical ‘crown’ conformations, four equivalent M–C<sup>4</sup> interactions play the most important role. But the corresponding distances in **2Li** (2.72 Å) are too long compared with the ‘desired’ value calculated for the Li<sup>+</sup>-benzene adduct, **4Li** (2.41 Å). Hence, this species has the lowest  $\Delta E^{(2)}$  exothermic energy value within the series of interest. In general, ‘crown’ complexes **2M** tend to be distorted to the more flattened ‘boat-like’ structures.



Scheme 6.

The most favorable alternative for **2Li** is the mixed coordination with two ‘hard’ oxygens and one of the aromatic rings (**Fig. 2, b, d**). A similar equilibrium structure as the deepest energy minimum was found for **2Na** as well. More heavy cations do not tend to coordinate with oxygens and adopt the C<sub>2v</sub> symmetrical conformation. For instance, **2K** possesses ten almost equal M–C distances (3.25–3.34 Å) with two aromatic rings building ‘boat sides’. All of them are comparable in length to that found for the benzene complex of K<sup>+</sup> (3.28 Å). For the equilibrium conformations corresponding to the deepest energy minima, exothermic energies of reaction (2) (**Table 2**, values in parentheses) decrease smoothly from Li<sup>+</sup> to Cs<sup>+</sup>.

Another important aspect for consideration are the relative stabilities of the complexes **1** to **3** with respect to coordination of the same metal cation in the calix[4]arene cavity. Experimentally this was investigated with electrospray ionization mass spectrometry [4], a procedure for gas phase experiments. Theoretically a relative measure can be estimated via the following gas phase reactions:



Table 3  
Calculated (RI-MP2/TZVP//RI-BP86/SV(P)) reaction energies  $\Delta E^{(3a)}$ ,  $\Delta E^{(3b)}$  and  $\Delta E^{(3c)}$  (reactions (3a)–(3c))<sup>a</sup>

M	$\Delta E$ , kcal/mol			
	$\Delta E^{(3a)}$	$\Delta E^{(3b)}$	$\Delta E^{(3c)}$	$\Delta E^{(3c)a,b}$
Li <sup>+</sup>	−3.6 (−2.7)	1.8 (−11.9)	5.4 (−2.4)	(−3.0)
Na <sup>+</sup>	−3.2 (−2.3)	0.8 (−4.0)	4.0 (−1.2)	(−1.7)
K <sup>+</sup>	−3.1 (−2.1)	0.2 (−2.6)	3.3 (0.9)	(−0.5)
Rb <sup>+</sup>	−2.4 (−2.2)	−1.0 (−2.7)	1.4 (0.6)	(−0.5)
Cs <sup>+</sup>	−3.2 (−2.4)	−2.3 (−3.0)	0.9 (0.1)	(−0.6)

<sup>a</sup> The values calculated for the C<sub>4</sub> symmetrical conformations are listed in parentheses.

<sup>b</sup> Calculated at the RI-BP86/SV(P) level of theory.

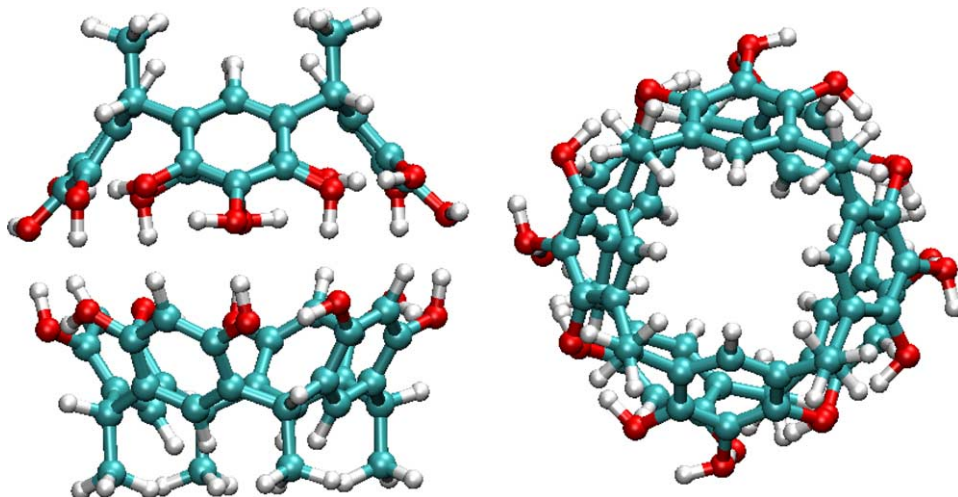
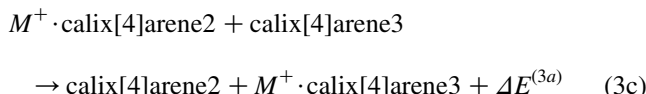


Fig. 4. Structural plots of the capsel involving calixarenes **2** and **3** (optimized at the RI-BP86/SV(P) level of approximation without symmetry restriction).



The results of our calculations show that the ligand change exerts only a minor effect, it does not exceed a few kcal/mol (Table 3). However, it is strongly basis set and approximation level dependent. Exothermic enthalpies for reactions (3a) reflect the fact that the alkyl substitution at the lower rim of the calixarene makes the complexation more favourable, probably due to destabilization of the equilibrium structure of **2**. A more detailed discussion on this aspect is presented in the following section.

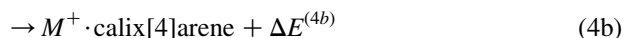
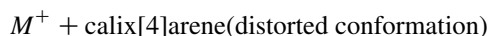
Surprisingly, the introduction of additional OH groups from **2** to **3** impedes complexation, presumably due to a more pronounced conformational flexibility of resor[4]-arene **2** as compared with calixarene **3**. At a first glance, our assertion is in contradiction with the results of the ESI-MS experiment [4]. There, it was found by fragmentation of the metal complexes of the mixed dimer capsule generated from two different calixarenes of type **2** and **3**, that the complexation of  $\text{Li}^+$  and  $\text{Na}^+$  with **3** were definitely favoured compared to **2**. Other cations ( $\text{K}^+$  to  $\text{Cs}^+$ ) showed no pronounced selectivity towards the type of calixarenes. Our calculations explain this as follows: in the capsule both calixarenes are in the ‘crown’ conformation (Fig. 4). By the experimentally observed fragmentation of the dimer, so called kinetic methods developed by Cooks and Wong [32] were used. This means that the structure of the fragments were not significantly changed during the reaction. Hence, by the above mentioned fragmentation, the complexes should be compared in their ‘crown’ form. In this case, the  $\text{Li}^+$  and  $\text{Na}^+$  complexes with the calixarene **3** are more favoured (Table 3, in parentheses). The energies for reaction (3c) for  $\text{K}^+$  to  $\text{Cs}^+$  are fairly small. However these are endothermic which indicate only an insignificant preference for **2M** complexes. It qualitatively agrees with

the experiment [4]. We note however that the calculated reaction energies are obviously depending on the basis set and the approximation level used (see for example the data obtained at the RI-BP86/SV(P) level of approximation in Table 3). The detailed investigation of complexation of alkali metal cations with various capsules is beyond of the subject of this paper, due to the large size of the corresponding species. Additionally, it would be necessary to evaluate a large number of isomers.

### 3.4. Preparation energies

In this section we analyze the different aspects which contribute to the total exothermic energy of formation of **1M–3M**. We have divided the reaction (1) into two steps: the first part of the total energy [equation (4a),  $\Delta E^{(4a)}$ ] is related to a ‘preparation energy’ which is necessary to bring the calixarene into the equilibrium conformation inherent to the corresponding complex. This energy contribution is positive (endothermic). The second part ( $\Delta E^{(4b)}$ ) should be negative (exothermic). This provides an overall exothermic effect for reaction (1) and makes the complex stable. We note again that such a picture is still restricted to gas phase reactions because it neglects for instance the cations solvation effects.

#### calix[4]arene



A similar analysis is well established in the analysis of preparation energies for transition metal complexation [33]. The preparation energies ( $\Delta E^{(4a)}$ ) values for alkali metal

Table 4

Preparation energies  $\Delta E^{(4a)}$ , in kcal/mol for the calculated complexes **1M–3M** [RI-BP86/SV(P) level of approximation]<sup>a</sup>

M	$\Delta E^{(4a)}$			<b>2</b>			<b>3</b>		
	<b>1</b>			<b>2</b>			<b>3</b>		
	$C_4$	$C_{2v}$	Absolute minimum	$C_4$	$C_{2v}$	Absolute minimum	$C_4$	$C_{2v}$	Absolute minimum
$\text{Li}^+$	2.5	18.0	26.7 ( $C_s$ )	2.5	15.5	23.3 ( $C_s$ )	3.7	42.6	34.7 ( $C_s$ )
$\text{Na}^+$	1.8	11.3	18.5 ( $C_s$ )	1.8	10.1	15.6 ( $C_s$ )	2.4	41.7	2.4 ( $C_4$ )
$\text{K}^+$	1.4	9.2	9.2 ( $C_{2v}$ )	1.4	7.8	7.8 ( $C_{2v}$ )	1.8	42.1	1.9 ( $C_2$ )
$\text{Rb}^+$	1.4	8.5	8.5 ( $C_{2v}$ )	1.4	7.3	7.3 ( $C_{2v}$ )	2.6	42.9	2.8 ( $C_2$ )
$\text{Cs}^+$	1.5	8.1	8.1 ( $C_{2v}$ )	1.5	7.2	7.2 ( $C_{2v}$ )	1.9	43.7	2.3 ( $C_2$ )

<sup>a</sup> All preparation energies were calculated relative to the most stable ‘crown’ conformation of the free calixarene.

cation complexation with calixarenes are collected in Table 4. A complete list of data can be found in Appendices A–C.

In the cases of the complexes **1M** and **2M**, the preparation energies are fairly small for the ‘crown’ conformations. Interestingly, they are identical for the same cation complexes of these two series. The  $C_{2v}$  symmetrical structures, while more favourable for the  $\text{K}^+$  to  $\text{Cs}^+$  complexes of **1**, **2**, require in overall larger energies to obtain the ‘prepared’ conformations. In addition, these energies are slightly less in magnitude for **2** than for **1**. This led us suggest that the alkyl substitution favours complexation, due to destabilization of the ground state of the free calixarene **2** and makes its equilibrium structure more ‘prepared’ for the cation addition. Large preparation energies are required for formation of the  $C_{2v}$  symmetrical complexes involving the smallest cation  $\text{Li}^+$  (**1Li** and **2Li**). Both  $\text{Li}^+$  and  $\text{Na}^+$  ‘boat’ conformations are further stabilized by reducing the symmetry from  $C_{2v}$  to  $C_s$ . The latter conformations are characterized by especially high preparation energy values. This implies very large  $\Delta E^{(4b)}$  binding energies as well. The distortions of the calixarene geometry (and respectively,  $\Delta E^{(4a)}$ ) are smaller for the  $C_{2v}$  symmetrical ‘boat’ conformations of the complexes **1**, **2** with the heavy cations  $\text{K}^+$  to  $\text{Cs}^+$ , which become the deepest minima at the PES.

Especially high preparation energies are obtained for the ‘boat’ conformations of **3**, due to the H-bonding which have to be broken by a  $C_4$  to  $C_{2v}$  or  $C_4$  to  $C_s$  symmetry distortion. Nevertheless, the  $C_s$  symmetrical conformation is still the most favourable for **3Li**, while it is not so pronounced as has been found for **1Li** and **2Li**.

#### 4. Conclusions

Various conformations of three calix[4]arenes have been investigated by quantum chemical calculations. The results of our investigations can be summarized as follows:

- (1) The ‘crown’ ( $C_4$  symmetrical) and ‘boat’ ( $C_{2v}$  symmetrical) conformations have similar energies for the two resorc[4]arenes, **1** and **2** with the slightly more stable ‘crown’ structure. This becomes more pronounced for calix[4]arene **3** with 12 OH-group in the aromatic rings.

- (2) The two main factors causing the stabilities of the alkali metal complexes deduce from the minimal distortion of the equilibrium conformation of the free calixarene and the achievement of maximum interactions of the alkali metal cation with the  $\pi$ -systems of the aromatic rings or, in the cases of  $\text{Li}^+$  and  $\text{Na}^+$ , with oxygens as donors. Sometimes a subtle relationship results between two main conformations (‘crown’ and ‘boat’) results, they are then very close in total energy. The former, the ‘crown’ conformation is characterized by a very low preparation energy which is required to change the conformation of the free calix[4]arene to that in the equilibrium structure of the complex. But as a further consequence, a weak binding energy towards the cation results. In contrast to, the ‘boat’ conformation requires more energy to be distorted to the equilibrium structure in the complex but it is simultaneously more stabilized, due to the significantly larger interaction energy with the donor fragments in the calixarene molecule. For the  $\text{Li}^+$  und  $\text{Na}^+$  complexes of resorc[4]arenes a special type of coordination is found to be of advantage. The cation interacts with only one  $\pi$ -system and two oxygen atoms. Thus, the side coordination on the upper rim of the calixarene cavity is found to be most favorable in these cases.
- (3) The (slightly flattened) ‘crown’ conformation is the most stable structure for the metal complexes of **3**. The 12 effective hydrogen bonds make **3** less conformationally flexible but the side coordination of  $\text{Li}^+$  in **3Li** is still most favourable.
- (4) All estimates of the relative stabilities of the various complexes indicate larger complexation energies for the light alkali metals ( $\text{Li}^+$ ,  $\text{Na}^+$ ), as compared with their heavier congeners ( $\text{K}^+$  to  $\text{Cs}^+$ ).

#### Acknowledgements

This work has been supported by the Deutsche Forschungsgemeinschaft (SFB 613). The calculations were performed on an IBM Regatta and the computation time was generously allocated by the Max-Planck Institut at Munich.

## Appendix A

Calculated total energy values ( $E$ ), zero-point energy correction values (ZPE), lowest vibrational frequency ( $\nu$ ) and preparation energies ( $E^{(4a)}$ ) for complexes of calixarene **1**

Structure (symmetry)	Cation	$E$ , a.u. <sup>a</sup>	ZPE, a.u. <sup>a</sup>	$E+ZPE$ , a.u. <sup>a</sup>	$\nu$ , cm <sup>-1</sup>	$\Delta E$ , kcal/mol <sup>a,b</sup>	$E$ , a.u. <sup>c</sup>	$E+ZPE$ , a.u. <sup>c</sup>	$\Delta E$ , kcal/mol <sup>b,c</sup>	$E_{\text{prep.}}$ a.u. <sup>a,d</sup>	$E^{(4a)}$ , kcal/mol <sup>a</sup>
<b>1</b> ( $C_4$ )	–	−1682.063034	0.458049	−1681.604986	19.3	–	−1679.181422	−1678.723373	–	–	–
<b>1Li</b> ( $C_4$ )	Li +	−1689.425265	0.458250	−1688.967016	−25.2	–	−1686.517123	−1686.058874	–	−1682.059032	2.5
<b>1Na</b> ( $C_4$ )	Na +	−1844.175992	0.458894	−1843.717099	15.8	–	−1840.999275	−1840.540381	–	−1682.060122	1.8
<b>1K</b> ( $C_4$ )	K +	−2281.850676	0.458711	−2281.391965	15.5	–	−2278.272747	−2277.814036	–	−1682.060779	1.4
<b>1Rb</b> ( $C_4$ )	Rb +	−1706.079928	0.458586	−1705.621342	11.4	–	−1702.910879	−1702.452293	–	−1682.060725	1.4
<b>1Cs</b> ( $C_4$ )	Cs +	−1702.148904	0.458521	−1701.690383	14.5	–	−1698.967230	−1698.508709	–	−1682.060712	1.5
<b>1Li</b> ( $C_1$ )	Li +	−1689.428039	0.458931	−1688.969107	42.1	−1.3	−1686.532677	−1686.073746	−9.3	– <sup>e</sup>	– <sup>e</sup>
<b>1Na</b> ( $C_1$ )	Na +	−1844.165189	0.458193	−1843.706996	35.2	6.3	−1840.997998	−1840.539805	0.4	– <sup>e</sup>	– <sup>e</sup>
<b>1</b> ( $C_{2v}$ )	–	−1682.052944	0.457686	−1681.595258	18.1	6.1	−1679.173063	−1678.715378	5.0	–	–
<b>1Li</b> ( $C_{2v}$ )	Li +	−1689.423156	0.459317	−1688.963839	30.1	2.0	−1686.525470	−1686.066153	−4.6	−1682.034413	18.0
<b>1Na</b> ( $C_{2v}$ )	Na +	−1844.174508	0.459023	−1843.715485	29.7	1.0	−1841.003800	−1840.544777	−2.8	−1682.045018	11.3
<b>1K</b> ( $C_{2v}$ )	K +	−2281.850678	0.459045	−2281.391632	39.1	0.2	−2278.277250	−2277.818204	−2.6	−1682.048399	9.2
<b>1Rb</b> ( $C_{2v}$ )	Rb +	−1706.080171	0.458876	−1705.621296	25.6	0.0	−1702.913996	−1702.455120	−1.8	−1682.049464	8.5
<b>1Cs</b> ( $C_{2v}$ )	Cs +	−1702.147479	0.458580	−1701.688899	12.1	0.9	−1698.968416	−1698.509836	−0.7	−1682.050100	8.1
<b>1Li</b> ( $C_s$ )	Li +	−1846.544648	0.567658	−1845.976990	23.0	−5.4	−1843.339427	−1842.771769	−11.5	−1682.020550	26.7
<b>1Na</b> ( $C_s$ )	Na +	−2001.280098	0.567145	−2000.712953	30.3	3.2	−1997.803827	−1997.236682	−1.7	−1682.033604	18.5

<sup>a</sup> Calculated at the BP86/SV(P) level of approximation.

<sup>b</sup> Calculated relative to the corresponding  $C_4$  symmetrical ‘crown’ conformation.

<sup>c</sup> Calculated at the RIMP2/TZVP//BP86/SV(P) level of approximation.

<sup>d</sup> Single point calculation for the calixarene with the conformation in the corresponding complex.

<sup>e</sup> The value was not determined.

## Appendix B

Calculated total energy values ( $E$ ), zero-point energy correction values (ZPE), lowest vibrational frequency ( $\nu$ ) and preparation energy ( $E_{(4a)}$ ) for complexes of calixarene **2**

Structure (symmetry)	Cation	$E$ , a.u. <sup>a</sup>	ZPE, a.u. <sup>a</sup>	$E + ZPE$ , a.u. <sup>a</sup>	$\nu$ , cm <sup>-1</sup>	$\Delta E$ , kcal/mol <sup>a,b</sup>	$E$ , a.u. <sup>c</sup>	$E + ZPE$ , a.u. <sup>c</sup>	$\Delta E$ , kcal/mol <sup>b,c</sup>	$E_{\text{prep.}}$ , a.u. <sup>a,d</sup>	$E^{(4a)}$ , kcal/mol <sup>a</sup>
<b>2</b> ( $C_4$ )	–	–1839.170041	0.566815	–1838.603226	7.0	–	–1835.980467	–1835.413653	–	–	–
<b>2Li</b> ( $C_4$ )	Li+	–1846.535473	0.567040	–1845.968433	–116.2	–	–1843.320514	–1842.753474	–	–1839.166028	2.5
<b>2Na</b> ( $C_4$ )	Na+	–2001.285924	0.567932	–2000.717991	–5.4	–	–1997.801958	–1997.234026	–	–1839.167128	1.8
<b>2K</b> ( $C_4$ )	K+	–2438.960317	0.567806	–2438.392511	–12.1	–	–2435.075145	–2434.507339	–	–1839.167798	1.4
<b>2Rb</b> ( $C_4$ )	Rb+	–1863.189475	0.567498	–1862.621977	–15.3	–	–1859.713385	–1859.145887	–	–1839.167754	1.4
<b>2Cs</b> ( $C_4$ )	Cs+	–1859.258317	0.567250	–1858.691067	–13.8	–	–1855.770096	–1855.202846	–	–1839.167715	1.5
<b>2Li</b> ( $C_2$ )	Li+	–1846.535694	0.567410	–1845.968284	–115.3	0.1	–1843.321432	–1842.754023	–0.3	– <sup>e</sup>	– <sup>c</sup>
<b>2Na</b> ( $C_2$ )	Na+	–2001.285888	0.567759	–2000.718128	11.2	–0.1	–1997.802841	–1997.235081	–0.7	– <sup>e</sup>	– <sup>c</sup>
<b>2K</b> ( $C_2$ )	K+	–2438.960664	0.567367	–2438.393298	19.1	–0.5	–2435.077462	–2434.510095	–1.7	– <sup>e</sup>	– <sup>c</sup>
<b>2Rb</b> ( $C_2$ )	Rb+	–1863.190078	0.567356	–1862.622722	23.2	–0.5	–1859.715550	–1859.148194	–1.4	– <sup>e</sup>	– <sup>c</sup>
<b>2Cs</b> ( $C_2$ )	Cs+	–1859.258529	0.567177	–1858.691352	19.2	–0.2	–1855.771262	–1855.204085	–0.8	– <sup>e</sup>	– <sup>c</sup>
<b>2Li</b> ( $C_1$ )	Li+	–1846.544648	0.567658	–1845.976990	23.0	–5.4	–1843.339427	–1842.771769	–11.5	– <sup>e</sup>	– <sup>c</sup>
<b>2Na</b> ( $C_1$ )	Na+	–2001.280098	0.567145	–2000.712953	30.3	3.2	–1997.803827	–1997.236682	–1.7	– <sup>e</sup>	– <sup>c</sup>
<b>2</b> ( $C_{2v}$ )	–	–1839.160887	0.566805	–1838.594082	22.5	5.7	–1835.973617	–1835.406812	4.3	–	–
<b>2Li</b> ( $C_{2v}$ )	Li+	–1846.538495	0.568117	–1845.970378	35.0	–1.2	–1843.331170	–1842.763052	–6.0	–1839.145302	15.5
<b>2Na</b> ( $C_{2v}$ )	Na+	–2001.288193	0.567985	–2000.720208	25.9	–1.4	–1997.809416	–1997.241431	–4.6	–1839.153888	10.1
<b>2K</b> ( $C_{2v}$ )	K+	–2438.963037	0.568120	–2438.394917	36.7	–1.5	–2435.081285	–2434.513165	–3.7	–1839.157588	7.8
<b>2Rb</b> ( $C_{2v}$ )	Rb+	–1863.191874	0.567947	–1862.623927	25.1	–1.2	–1859.716835	–1859.148889	–1.9	–1839.158342	7.3
<b>2Cs</b> ( $C_{2v}$ )	Cs+	–1859.258641	0.567657	–1858.690984	26.7	0.1	–1855.772511	–1855.204854	–1.3	–1839.158609	7.2
<b>2Li</b> ( $C_s$ )	Li+	–1846.551326	0.569284	–1845.982041	38.5	–8.5	–1843.343737	–1842.774453	–13.2	–1839.132895	23.3
<b>2Na</b> ( $C_s$ )	Na+	–2001.288993	0.568484	–2000.720509	36.3	–1.6	–1997.811111	–1997.242627	–5.4	–1839.145169	15.6
<b>2K</b> ( $C_s$ )	K+	–2438.960389	0.568202	–2438.392187	–20.4	0.2	–2435.080504	–2434.512302	–3.1	– <sup>e</sup>	– <sup>e</sup>

<sup>a</sup> Calculated at the BP86/SV(P) level of approximation.

<sup>b</sup> Calculated relative to the corresponding  $C_4$  symmetrical ‘crown’ conformation.

<sup>c</sup> Calculated at the RIMP2/TZVP//BP86/SV(P) level of approximation.

<sup>d</sup> Single point calculation for the calixarene with the conformation in the corresponding complex.

<sup>e</sup> The value was not determined.

## Appendix C

Calculated total energy values (E), zero-point energy correction values (ZPE), lowest vibrational frequency ( $\nu$ ) and preparation energy ( $E^{(4a)}$ ) for complexes of calixarene **3**

Structure (symmetry)	Cation	E, a.u. <sup>a</sup>	ZPE, a.u. <sup>a</sup>	E+ZPE, a.u. <sup>a</sup>	$\nu$ , cm <sup>-1</sup>	$\Delta E$ , kcal/mol <sup>a,b</sup>	E, a.u. <sup>c</sup>	E+ZPE, a.u. <sup>c</sup>	$\Delta E$ , kcal/mol <sup>b,c</sup>	$E_{\text{prep.}}$ a.u. <sup>a,d</sup>	$E^{(4a)}$ , kcal/mol <sup>a</sup>
<b>3</b> ( $C_4$ )	–	–2139.864380	0.582602	–2139.281778	14.0	–	–2136.342384	–2135.759783	–	–	–
<b>3Li</b> ( $C_4$ )	Li +	–2147.237000	0.582918	–2146.654082	10.0	–	–2143.687196	–2143.104278	–	–2139.858493	3.7
<b>3Na</b> ( $C_4$ )	Na +	–2301.985467	0.583412	–2301.402055	13.1	–	–2298.166655	–2297.583243	–	–2139.860523	2.4
<b>3K</b> ( $C_4$ )	K +	–2739.656626	0.583317	–2739.073309	13.5	–	–2735.437880	–2734.854563	–	–2139.861500	1.8
<b>3Rb</b> ( $C_4$ )	Rb +	–2163.884510	0.583154	–2163.301355	6.6	–	–2160.076152	–2159.492998	–	–2139.860308	2.6
<b>3Cs</b> ( $C_4$ )	Cs +	–2159.953960	0.582968	–2159.370992	8.6	–	–2156.132925	–2155.549957	–	–2139.861281	1.9
<b>3K</b> ( $C_2$ )	K +	–2739.656524	0.583004	–2739.073520	9.9	–0.1	–2735.437926	–2734.854922	–1.7	–2139.861320	–0.2
<b>3Rb</b> ( $C_2$ )	Rb +	–2163.885710	0.582693	–2163.303017	16.9	–1.0	–2160.076580	–2159.493887	–1.4	–2139.859982	–0.6
<b>3Cs</b> ( $C_2$ )	Cs +	–2159.953736	0.582691	–2159.371046	13.9	0.0	–2156.133023	–2155.550332	–0.8	–2139.860779	–0.2
<b>3Li</b> ( $C_1$ )	Li +	–2147.234059	0.583911	–2146.650148	17.2	2.5	–2143.692418	–2143.108507	–2.7	– <sup>e</sup>	– <sup>e</sup>
<b>3Na</b> ( $C_1$ )	Na +	–2301.972662	0.583749	–2301.388913	31.6	8.2	–2298.159344	–2297.575595	4.8	– <sup>e</sup>	– <sup>e</sup>
<b>3</b> ( $C_{2v}$ )	–	–2139.804162	0.579692	–2139.224469	11.5	36.0	–2136.294246	–2135.714554	28.4	–	–
<b>3Li</b> ( $C_{2v}$ )	Li +	–2147.184957	0.580436	–2146.604521	–64.3	31.1	–2143.648294	–2143.067858	22.9	–2139.796485	42.6
<b>3Na</b> ( $C_{2v}$ )	Na +	–2301.929343	0.579983	–2301.349360	–27.0	33.1	–2298.122218	–2297.542234	25.7	–2139.797954	41.7
<b>3K</b> ( $C_{2v}$ )	K +	–2739.599908	0.580299	–2739.019609	18.8	33.7	–2735.389581	–2734.809282	28.4	–2139.797279	42.1
<b>3Rb</b> ( $C_{2v}$ )	Rb +	–2163.828149	0.580588	–2163.247561	20.7	33.8	–2160.025562	–2159.444973	30.1	–2139.796013	42.9
<b>3Cs</b> ( $C_{2v}$ )	Cs +	–2159.894588	0.580659	–2159.313929	15.4	35.8	–2156.079909	–2155.499250	31.8	–2139.794713	43.7
<b>3Li</b> ( $C_s$ )	Li +	–2147.234008	0.583462	–2146.650546	27.1	2.2	–2143.697002	–2143.697002	–6.2	–2139.809020	34.7
<b>3Na</b> ( $C_s$ )	Na +	–2301.962732	0.581958	–2301.380774	25.7	13.4	–2298.156799	–2297.574841	5.3	– <sup>e</sup>	– <sup>e</sup>
<b>3K</b> ( $C_s$ )	K +	–2739.622987	0.580982	–2739.042005	13.1	19.6	–2735.418165	–2734.837184	10.9	– <sup>e</sup>	– <sup>e</sup>
<b>3Rb</b> ( $C_s$ )	Rb +	–2163.849767	0.580974	–2163.268793	13.6	20.4	–2160.052635	–2159.471661	13.4	– <sup>e</sup>	– <sup>e</sup>
<b>3Cs</b> ( $C_s$ )	Cs +	–2159.925111	0.582320	–2159.342790	–3.6	17.7	–2156.111216	–2155.528896	13.6	– <sup>e</sup>	– <sup>e</sup>

<sup>a</sup> Calculated at the BP86/SV(P) level of approximation.

<sup>b</sup> Calculated relative to the corresponding  $C_4$  symmetrical ‘crown’ conformation.

<sup>c</sup> Calculated at the RIMP2/TZVP//BP86/SV(P) level of approximation.

<sup>d</sup> Single point calculation for the calixarene with the conformation in the corresponding complex.

<sup>e</sup> The value was not determined.

## References

- [1] M.T. Blanda, D.B. Farmer, J.S. Brodbelt, B.J. Coolsby, *J. Am. Chem. Soc.* 122 (2000) 1486; B.J. Goolsby, J.S. Brodbelt, E. Adou, M. Blanda, *Int. J. Mass. Spectrom.* 193 (1999) 197.
- [2] F. Allain, H. Virelizier, C. Moulin, C.K. Jankowski, J.F. Dozol, J.C. Tabet, *Spectroscopy* 14 (2000) 127.
- [3] J.M.J. Nuutinen, A. Irico, M. Vincenti, E. Dalcanale, J.M.H. Pakarinen, P. Vainiotalo, *J. Am. Chem. Soc.* 122 (2000) 10090.
- [4] M.C. Letzel, C. Agena, J. Mattay, *J. Mass Spectrom.* 37 (2002) 63.
- [5] J. Schatz, A.C. Backes, H.-U. Siehl, *J. Chem. Soc., Perkin Trans. 2* (2000) 609.
- [6] W. Hehre, SPARTAN, Ver. 5.0.3, Wavefunction Inc., 180401 Von Karman Avenue, Suite 370, Irvine, CA 92612, USA, 1997.
- [7] N.L. Allinger, Y.H. Yuh, J.H. Lii, *J. Am. Chem. Soc.* 111 (1989) 8551.
- [8] W. Koch, M.C. Holthausen, *A Chemist's Guide to Density Functional Theory*, Wiley, Weinheim, 2001.
- [9] M. Mäkinen, P. Vainiotalo, K. Rissanen, *J. Am. Soc. Mass Spectrom.* 13 (2002) 851.
- [10] M. Mäkinen, J.-P. Jalkanen, P. Vainiotalo, *Tetrahedron* 58 (2002) 8591.
- [11] R.J. Bernardino, B.J.C. Cabral, *J. Phys. Chem. A* 103 (1999) 9080; R.J. Bernardino, B.J.C. Cabral, *Supramol. Chem.* 14 (2002) 57; R.J. Bernardino, B.J.C. Cabral, *J. Mol. Struct.: Theochem.* 549 (2001) 253; B.P. Hay, J.B. Nicolas, D. Feller, *J. Am. Chem. Soc.* 122 (2000) 10083.
- [12] A.T. Macias, J.E. Norton, J.D. Evanseck, *J. Am. Chem. Soc.* 125 (2003) 2351.
- [13] See <http://www.ipc.uni-karlsruhe.de/tch/tch1/turbomole/index.en.html> and references cited therein.
- [14] M.J. Frisch, G.W. Trucks, H.B. Schlegel, G.E. Scuseria, M.A. Robb, J.R. Cheeseman, J.A. Montgomery, Jr., T. Vreven, K.N. Kudin, J.C. Burant, J.M. Millam, S.S. Iyengar, J. Tomasi, V. Barone, B. Mennucci, M. Cossi, G. Scalmani, N. Rega, G.A. Petersson, H. Nakatsuji, M. Hada, M. Ehara, K. Toyota, R. Fukuda, J. Hasegawa, M. Ishida, T. Nakajima, Y. Honda, O. Kitao, H. Nakai, M. Klene, X. Li, J.E. Knox, H.P. Hratchian, J.B. Cross, C. Adamo, J. Jaramillo, R. Gomperts, R.E. Stratmann, O. Yazyev, A.J. Austin, R. Cammi, C. Pomelli, J.W. Ochterski, P.Y. Ayala, K. Morokuma, G.A. Voth, P. Salvador, J.J. Dannenberg, V.G. Zakrzewski, S. Dapprich, A.D. Daniels, M.C. Strain, O. Farkas, D.K. Malick, A.D. Rabuck, K. Raghavachari, J.B. Foresman, J.V. Ortiz, Q. Cui, A.G. Baboul, S. Clifford, J. Cioslowski, B.B. Stefanov, G. Liu, A. Liashenko, P. Piskorz, I. Komaromi, R.L. Martin, D.J. Fox, T. Keith, M.A. Al-Laham, C.Y. Peng, A. Nanayakkara, M. Challacombe, P.M.W. Gill, B. Johnson, W. Chen, M.W. Wong, C. Gonzalez, J.A. Pople, Gaussian 03, Revision A.1, Gaussian, Inc., Pittsburgh PA, 2003.
- [15] S.H. Vosko, L. Wilk, M. Nusair, *Can. J. Phys.* 58 (1980) 1200.
- [16] A.D. Becke, *Phys. Rev. A* 38 (1988) 3098.
- [17] J.P. Perdew, *Phys. Rev. B* 33 (1986) 8822.
- [18] B.I. Dunlap, J.W. Conolly, J.R. Sabin, *J. Chem. Phys.* 71 (1979) 339; O. Vahtras, J. Almlöf, M.W. Feyereisen, *Chem. Phys. Lett.* 213 (1993) 514; K. Eichhorn, O. Treutler, H. Öhm, M. Häser, R. Ahlrichs, *Chem. Phys. Lett.* 240 (1995) 283.
- [19] A. Schäfer, H. Horn, R. Ahlrichs, *J. Chem. Phys.* 97 (1992) 2571.
- [20] Stuttgart RSC 1997 ECP. For more detailed information see for example <http://www.emsl.pnl.gov/forms/basisform.html>.
- [21] P. Deglmann, F. Furche, R. Ahlrichs, *Chem. Phys. Lett.* 362 (2002) 511; P. Deglmann, F. Furche, *J. Chem. Phys.* 117 (2002) 9535.
- [22] F. Weigend, M. Häser, *Theor. Chem. Acc.* 97 (1997) 331; F. Weigend, M. Häser, H. Patzelt, R. Ahlrichs, *Chem. Phys. Lett.* 294 (1998) 143.
- [23] A. Schäfer, C. Hüber, R. Ahlrichs, *J. Chem. Phys.* 100 (1994) 5829.
- [24] A.D. Becke, *J. Chem. Phys.* 98 (1993) 5648.
- [25] C. Lee, W. Yang, R.G. Parr, *Phys. Rev. B* 37 (1988) 785.
- [26] R. Ditchfield, W.J. Hehre, J.A. Pople, *J. Chem. Phys.* 54 (1971) 724; W.J. Hehre, R. Ditchfield, J.A. Pople, *J. Chem. Phys.* 56 (1972) 2257; P.C. Hariharan, J.A. Pople, *Mol. Phys.* 27 (1974) 209; P.C. Hariharan, J.A. Pople, *Theor. Chim. Acta* 28 (1973) 213.
- [27] W.J. Stevens, H. Basch, J. Krauss, *J. Chem. Phys.* 81 (1984) 6026; W. Stevens, M. Krauss, H. Basch, P.G. Jasien, *Can. J. Chem.* 70 (1992) 612; T.R. Cundari, W.J. Stevens, *J. Chem. Phys.* 98 (1993) 5555.
- [28] P.J. Hay, W.R. Wadt, *J. Chem. Phys.* 82 (1985) 270; W.R. Wadt, P.J. Hay, *J. Chem. Phys.* 82 (1985) 284; P.J. Hay, W.R. Wadt, *J. Chem. Phys.* 82 (1985) 299.
- [29] VMD for WIN-32, Version 1.8.2 (Dezember, 4, 2003) W. Humphrey, A. Dalke, K. Schulten, *J. Mol. Graphics* 14 (1996) 33.
- [30] For a theoretical investigation of the solvation problem see for example: E.M. Cabaleiro-Lago, J. Rodriguez-Otero, *J. Phys. Chem. A* 106 (2002) 7195; S. Abirami, N.L. Ma, N.K. Goh, *Chem. Phys. Lett.* 359 (2002) 500.
- [31] J.B. Nicholas, B.P. Hay, D.A. Dixon, *J. Phys. Chem. A* 103 (1999) 1394; J.B. Nicholas, B.P. Hay, *J. Phys. Chem. A* 103 (1999) 9815; D. Feller, D.A. Dixon, J.B. Nicholas, *J. Phys. Chem. A* 104 (2000) 11414; J.C. Amicangelo, P.B. Armentrout, *J. Phys. Chem. A* 104 (2000) 11420.
- [32] R.G. Cooks, P.S.H. Wong, *Acc. Chem. Res.* (1998) 379.
- [33] W.W. Schoeller, D. Eisner, S. Grigoleit, A.B. Rozhenko, A. Alijah, *J. Am. Chem. Soc.* 122 (2000) 10115 and references therein.

**Einzmolekül-Untersuchungen****Supramolekulare Chemie mit einzelnen Molekülen\*\***

Rainer Eckel, Robert Ros, Björn Decker, Jochen Mattay\* und Dario Anselmetti\*

Die supramolekulare Chemie<sup>[1]</sup> beschäftigt sich mit der Synthese und den Eigenschaften von Verbindungen mit gerichteten und spezifischen nichtkovalenten Wechselwirkungen zwischen maßgeschneiderten organischen Bausteinen. Große Bedeutung kommt hierbei synthetischen Wirt-Gast-Systemen zu, die supramolekulare Strukturen von hoher Komplexität bilden können. Supramolekulare Systeme sind hinsichtlich Spezifität und Funktionalität („molekulare Schalter“) plan- und optimierbar, woraus sich Konzepte für die Entwicklung von neuen Materialien für molekulare Erkennung, molekulare Überstrukturen und Selbstorganisation ableiten. Mithilfe mechanischer Einzmolekül-Kraftspektroskopie untersuchten wir die Bindung von einzelnen Wirt-Gast-Komplexen aus Resorc[4]arenen als Rezeptoren und Ammoniumderivaten als Liganden. Durch die Verwendung von verdünnten Proben des Wirtmoleküls und von Gastmolekülen, die durch einen langen Polymerlinker an einer AFM-Spitze immobilisiert waren, ließ sich Mehrfachbindung vermeiden, sodass erstmalig einzelne Wirt-Gast-Dissociationsereignisse in einem supramolekularen System beobachtet werden konnten. Die molekularen Bindungskräfte, ihre Abhängigkeit von der äußeren Beladung, die Dissociationsgeschwindigkeit und die molekulare Reaktionslänge hängen direkt mit den molekularen Eigenschaften des supramolekularen Systems zusammen und sind in Einklang mit einem aktivierten Zerfall eines metastabilen gebundenen Zustands; ähnliche Ergebnisse wurden auch für biologische Rezeptor-Ligand-Systeme erhalten. Die Resultate geben Aufschluss über Mechanismen, Kinetik und Thermodynamik der intermolekularen Assoziation in Chemie und Biologie und zeigen neue Konzepte für die Entwicklung synthetischer Rezeptorsysteme auf.

Calixarene sind gut untersuchte Modellsysteme für Rezeptoren, die synthetische Hohlräume für den Einschluss kleiner kationischer Gäste wie Alkalimetall- oder Ammoniumionen bereitstellen.<sup>[2-5]</sup> Organische Kationen wie Ammoniumionen spielen eine wichtige Rolle bei molekularen Erkennungsprozessen in der Natur (z. B. in Proteineinseitenketten). Calix[n]arene sind eine Klasse makrocyclischer Verbindungen, die durch basenkatalysierte Kondensation von *n* Phenolderivaten und Formaldehyd gebildet werden.<sup>[2,3]</sup> Die hier verwendeten Resorc[4]arene<sup>[6,7]</sup> bestehen aus vier Resorcin-Bausteinen, die über Methingruppen verbrückt sind. Dieses Strukturprinzip lässt Freiheitsgrade für Rotationen um die Methin-C-C-Bindungen zu, sodass sich fünf mögliche Konformationen ergeben: Krone ( $C_{4v}$ ), Boot ( $C_{2v}$ ), Sessel ( $C_{2h}$ ), Diamant ( $C_s$ ) und Sattel ( $D_{2d}$ ). Um die konformative Flexibilität in Resorc[4]arenen einzuschränken, können z. B. die Hydroxygruppen am oberen Rand des Moleküls durch Kondensation verknüpft werden, wodurch das Molekül in der Kronen-Konformation fixiert wird. Die neue Verbindung wird als Cavitand<sup>[8]</sup> bezeichnet, und der starre Hohlraum des Wirtes dient nun als Templat für den Einschluss kleiner Gast-Ionen. Die Bindung kleiner Kationen an den Resorc[4]aren-Cavitanen wird durch Ion-Dipol-Wechselwirkungen ermöglicht, wobei Wasserstoffbrücken und Kation-π-Wechselwirkungen zwischen dem positiv geladenen Ion und dem aromatischen Ringsystem des Cavitanen von großer Bedeutung sind.<sup>[9]</sup> Die Spezifität der Bindung ist durch die sterische Komplementarität von Wirt und Gast gegeben: Nur Kationen, die klein genug sind, um in den Hohlraum zu passen, werden durch den Resorc[4]aren-Rezeptor erkannt. In unserem Experiment wurde ein 2,8,14,20-Tetra[10-(decylthio)decyl]-Cavitand mit einer berechneten Hohlraumweite von 0.7 nm auf die spezifische Erkennung von Ammoniumionen und Ammoniumderivaten untersucht (Abbildung 1).<sup>[9]</sup>

Zur Untersuchung dieser Wechselwirkungen verwenden wir die Einzmolekül-Kraftspektroskopie. Bei dieser Methode wird die Verbiegung des Kraftsensors („cantilever“) eines Rasterkraftmikroskops (AFM) detektiert. Die Technik ermöglicht die Messung sehr kleiner Kräfte (Pikonewton) unter physiologischen Bedingungen. Zusammen mit ihrer räumlichen Auflösung bis in den Subnanometerbereich bietet die Einzmolekül-Kraftspektroskopie einzigartige Möglichkeiten zur Untersuchung und Manipulation einzelner Moleküle.

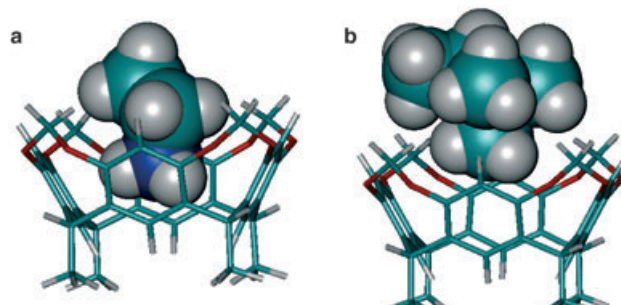


**Abbildung 1.** Gasphasenstruktur des Wirt-Gast-Komplexes aus dem Cavitanden und einem Ethylammoniumion (a) oder einem Trimethyl-ethylammoniumion (b). Die Struktur wurde auf dem B3LYP/3-21G\*-Niveau optimiert.

[\*] Dipl.-Chem. R. Eckel, Priv.-Doz. Dr. R. Ros, Prof. Dr. D. Anselmetti  
Experimentelle Biophysik und Angewandte Nanowissenschaften  
Universität Bielefeld  
Universitätsstraße 25, 33615 Bielefeld (Deutschland)  
Fax: (+49) 521-106-2959  
E-mail: dario.anselmetti@physik.uni-bielefeld.de

Dipl.-Chem. B. Decker, Prof. Dr. J. Mattay

Organische Chemie  
Universität Bielefeld  
Universitätsstraße 25, 33615 Bielefeld (Deutschland)  
Fax: (+49) 521-106-6417  
E-mail: mattay@uni-bielefeld.de

[\*\*] Die Autoren danken der Deutschen Forschungsgemeinschaft (SFB613) für finanzielle Unterstützung.

Hintergrundinformationen zu diesem Beitrag sind im WWW unter <http://www.angewandte.de> zu finden oder können beim Autor angefordert werden.

küle und zur Bestimmung von Kräften in und zwischen individuellen Molekülen, wodurch Informationen über die molekulare Energielandschaft zugänglich werden. Die Rasterkraftmikroskopie und verwandte Einzelmolekültechniken mit ultraempfindlichen Kraftsensoren wurden zur Untersuchung der molekularen Erkennung und spezifischen Bindung bei einer Vielzahl von Systemen eingesetzt. Beispiele sind Biotin-Streptavidin/Avidin-,<sup>[10,11]</sup> Antikörper-Antigen-,<sup>[12-15]</sup> Selectin-Ligand,<sup>[16]</sup> und DNA-Protein-Komplexe<sup>[17]</sup> sowie Komplexe aus DNA-Strängen<sup>[18,19]</sup> und Zelladhäsionsproteoglycanen.<sup>[20]</sup>

Untersucht wurden auch Wirt-Gast-Wechselwirkungen bei  $\beta$ -Cyclodextrin-Ferrocen<sup>[21-23]</sup> und 18-Krone[6]-Ammonium.<sup>[24,25]</sup> In beiden Fällen wurde die Wirt-Gast-Wechselwirkung zwischen Einzelmolekülen nur anhand einer statistischen Analyse der Kräfthistogramme identifiziert. Es wurde kein von der Beladungsrate abhängiges Kraftspektrum erhalten, das auf eine thermisch aktivierte Dissoziation hätte hinweisen können oder Informationen zur Energielandschaft der Wechselwirkung geliefert hätte. Im Unterschied zu diesen Experimenten nutzten wir verdünnte Cavitand-Monolagen auf einer Goldoberfläche in einem 1:40-Gemisch mit Didecylsulfid. Die Gast-Ionen (Ammonium, Trimethylammonium und Triethylammonium; jedes mit einem weiteren Rest funktionalisiert) wurden über einen flexiblen Polyethylenglycol(PEG)-Linker kovalent an die AFM-Spitze gebunden (Abbildung 2). Diese Immobilisierungsmethode erhöht die sterische Flexibilität, was die Komplexbildung sowie die Bindung eines einzelnen Wirt-Gast-Paars und dessen Identifizierung erleichtert. Die funktionalisierte AFM-Spitze wurde mit einer regulierbaren konstanten Geschwindigkeit periodisch an die mit dem Cavitanden bedeckte Oberfläche (in Ethanol) angenähert und wieder zurückgezogen.

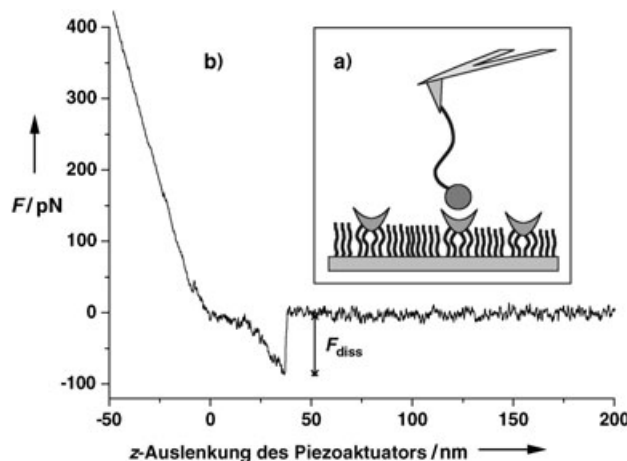


**Abbildung 2.** a) Prinzip der AFM-Experimente: Der Cavitand wird zusammen mit Didecylsulfid im molaren Verhältnis 1:40 auf einem Goldsubstrat immobilisiert. Der (Tetraorganyl)ammoniumrest (schattierter Kreis) wird über einen flexiblen Polymerlinker an eine AFM-Spitze aus Siliciumnitrid gebunden. b) Typische Kraft-Distanz-Kurve (nur retraktiver Teil gezeigt); die Dehnung des PEG-Linkers über eine bestimmte Strecke vor dem Bruch der Bindung (Abriss der Spitze von der Oberfläche und Relaxation des Kraftsensors) zeigt ein spezifisches Bindungs- und anschließendes Dissoziationsereignis an.

Molekulare Dissoziationsereignisse konnten durch Auftragung der Kraftantwort des Kraftsensors gegen die z-Position des Piezoaktuators identifiziert werden (Abbildung 2). Die elastische Dehnung des PEG-Linkers vor dem Abriss, die eine Elastizitätskurve nach dem „worm-like chain“-Modell beschreibt, diente als Kriterium zur Unterscheidung zwischen echten Bindungsereignissen und unspezifischer Adhäsion. Da die Kraftwerte der molekularen Dissoziationsereignisse stochastisch verteilt sind, wurden die Abrisskräfte von typischerweise 200 Abrissen in einem Kräfthistogramm aufgetragen. Durch Gauß-Regression wurde das Maximum der Verteilung als die wahrscheinlichste Dissoziationskraft bestimmt. Der experimentelle Fehler beruht auf dem statistischen Fehler (Standardabweichung) und der Unsicherheit in der effektiven Federkonstanten; die Fehler, die im Folgenden für die Geschwindigkeit der thermischen Dissoziation bei verschwindender äußerer Kraft und für die Weite der Bindungstasche angegeben sind, wurden aus diesen Werten durch Fehlerfortpflanzung berechnet.

In Abbildung 3 sind die erhaltenen Kräfthistogramme für die Bindung des Cavitanden an die Ammonium-, Trimethylammonium- und Triethylammoniumreste zusammen mit Kompositionsexperimenten in Lösungen der freien Ionen gezeigt. Die Gesamtdissoziationswahrscheinlichkeiten (die Zahl der identifizierten Abrisse geteilt durch die Zahl der Kraftspektroskopiezzyklen insgesamt) für die Ammonium- und Trimethylammoniumreste liegen bei etwa 25 %. Um die Spezifität der Wirt-Gast-Wechselwirkung zu überprüfen, wurden in Kontrollexperimenten freie Ammonium- oder Tetramethylammoniumionen dem Lösungsmittel als konkurrierende Liganden zugesetzt, woraufhin in beiden Fällen die Gesamtdissoziationswahrscheinlichkeit signifikant sank. Der Effekt war bei Sättigung mit Tetramethylammoniumionen stärker ausgeprägt (Abbildung 3b,e). Durch Waschen der Spitze und der Probe mit reinem Ethanol wurde die Bindungsfunktionalität der Systeme vollständig reaktiviert (Abbildung 3c,f). Dieser starke Einfluss der freien Ionen, die mit den an der Spitze funktionalisierten Resten konkurrieren, dient als eindeutiger Beleg für die Spezifität der molekularen Erkennung zwischen Wirt und Gast.

Im Falle des Triethylammoniumrestes findet sich ein anderes Ergebnis. Aus Abbildung 3 ist ersichtlich, dass die Gesamtdissoziationswahrscheinlichkeit viel niedriger ist als bei Ammonium- oder Tetramethylammoniumionen, während die Abrisskraft von ähnlicher Größenordnung ist. Darüber hinaus sinkt die Gesamtdissoziationswahrscheinlichkeit nur unwesentlich, wenn das Lösungsmittel durch Ethanol ausgetauscht wird, das mit dem Kompetitor gesättigt ist (Abbildung 3h). Das Waschen mit reinem Ethanol blieb ebenfalls ohne Effekt (Abbildung 3i). Diese Ergebnisse sind mit der Tatsache in Einklang, dass der Triethylammoniumrest mit einem berechneten Durchmesser von 0.8 nm den Durchmesser des Rezeptorhohlraums des Resorc[4]aren-Cavitanden klar überschreitet: Unsere Einzelmolekülexperimente liefern also deutliche Belege für eine spezifische und selektive Wirt-Gast-Wechselwirkung.

Nach der Theorie des thermisch aktivierten Zerfalls eines metastabilen gebundenen Zustands<sup>[26,27]</sup> sind die gemessenen Kräfte nicht konstant, sondern hängen von der zeitlichen

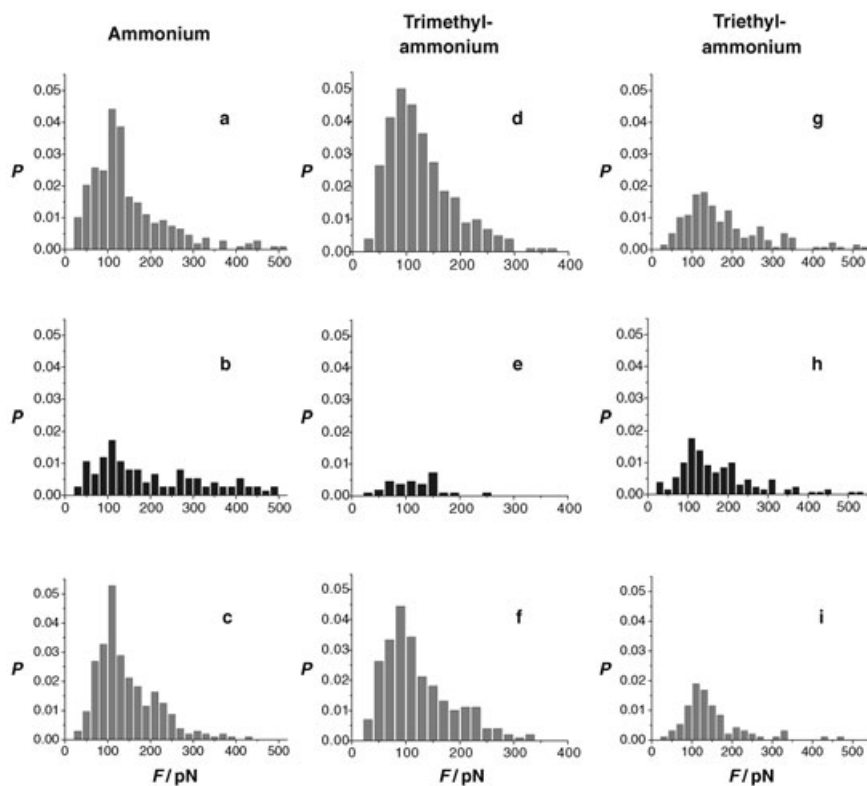


**Abbildung 3.** Ergebnisse der AFM-Experimente in Ethanol (a, d, g) und der Kompositionsexperimente in gesättigten ethanolischen Lösungen der freien Ionen (b, e, h). Durch Waschen mit Ethanol wurden die ursprünglichen Dissoziationswahrscheinlichkeiten ( $P$ ) wiederhergestellt (c, f, i).

Kraftentwicklung auf den molekularen Komplex ab, die man als Beladungsrate („loading rate“) bezeichnet. Die Beladungsrate errechnet sich aus dem Produkt der experimentellen Geschwindigkeit und der molekularen Elastizität. Die Elastizität des molekularen Systems wurde aus der Steigung der Kraft-Distanz-Kurve (korrigiert auf die molekulare Ausdehnung) auf den letzten 20 Datenpunkten vor dem Abriss erhalten und die Beladungsrate dann als Produkt aus Elastizität und Rückziehgeschwindigkeit berechnet.

Mithilfe der dynamischen Kraftspektroskopie wurden Details der Bindungskinetik und Informationen über die Längenskala der Wechselwirkung erhalten. Die Ergebnisse für die Geschwindigkeiten der natürlichen thermischen Dissoziation sind in Abbildung 4 gezeigt; man erhält  $k_{\text{off}} = (0.99 \pm 0.81) \text{ s}^{-1}$  für den Ammoniumrest und  $k_{\text{off}} = (1.87 \pm 0.75) \times 10^{-2} \text{ s}^{-1}$  für den Trimethylammoniumrest, was Lebensdauern der Bindungen von  $\tau = 1.01 \text{ s}$  bzw.  $\tau = 53.5 \text{ s}$  entspricht. Dieses Ergebnis deutet ebenso wie die Resultate der Kompositionsexperimente darauf hin, dass sich der Trimethylammoniumrest besser, d.h. mit höherer Bindungsaffinität in den Rezeptorhohlraum einfügt als der Ammoniumrest. Bei Rezeptor-Ligand-Bindungen wird die Affinität der Wechselwirkung (Gleichgewichtskonstante der Dissoziation  $K_{\text{diss}} = k_{\text{off}}/k_{\text{on}}$ ) durch die Dissoziationsgeschwindigkeitskonstante  $k_{\text{off}}$  dominiert (und variiert), während die Assoziationsgeschwindigkeitskonstanten  $k_{\text{on}}$  weniger stark variieren.<sup>[13]</sup> Unter der Annahme diffusionskontrollierter Assoziation mit einer typischen Assoziationsgeschwindigkeit von  $k_{\text{on}} =$

$10^5 \text{ M}^{-1} \text{ s}^{-1}$ <sup>[13,28]</sup> für die Bindung eines Liganden in die Bindungstasche des Rezeptors lassen sich Gleichgewichtskonstanten von  $K_{\text{diss}} = 0.99 \text{ s}^{-1}/10^5 \text{ M}^{-1} \text{ s}^{-1} \approx 10^{-5} \text{ M}$  für Ammonium und  $K_{\text{diss}} = 2 \times 10^{-2} \text{ s}^{-1}/10^5 \text{ M}^{-1} \text{ s}^{-1} = 2 \times 10^{-7} \text{ M}$  für Trimethylammonium angeben. Aus den Gleichgewichtskonstanten leiten sich die Differenzen der freien Reaktionsenthalpien (Gibbs-Energien) gemäß  $\Delta G = RT \ln K_{\text{diss}}$  ab. Es ergeben sich ungefähre Werte von  $\Delta G \approx -28 \text{ kJ mol}^{-1}$  (Ammonium) und  $\Delta G \approx -38 \text{ kJ mol}^{-1}$  (Trimethylammonium). Diese  $\Delta G$ -Werte stimmen gut mit kalorimetrisch und NMR-spektroskopisch ermittelten Werten für ähnliche supramolekulare Systeme wie Cyclodextrine<sup>[23,29]</sup> und wasserlösliche Cavitanden<sup>[30]</sup> überein. Dieser Befund ist aus zwei Gründen von Bedeutung: 1) Es wurde belegt, dass die Rasterkraftspektroskopie für die Untersuchung von Wechselwirkungen zwischen Einzelmolekülen mit einer zehn Größenordnungen umfassenden Bandbreite der Affinität anwendbar ist ( $10^{-15} \text{ M}$  (Biotin-Streptavidin) bis  $10^{-5} \text{ M}$  (diese Arbeit)). 2) Durch Anwendung dieser Technik ist es nun möglich, Gleichgewichtskonstanten

und Bindungsenergien einzelner (supra)molekularer Komplexe abzuschätzen. Dies ist von allgemeinem Interesse, da z.B. in NMR-Experimenten die Bestimmung von Gleichgewichtskonstanten und den zugehörigen Bindungsenergien für ionische Bindungspartner mit stark unterschiedlichen Löslichkeitseigenschaften sehr schwierig ist (so sind uns für das hier betrachtete System keine Werte bekannt).

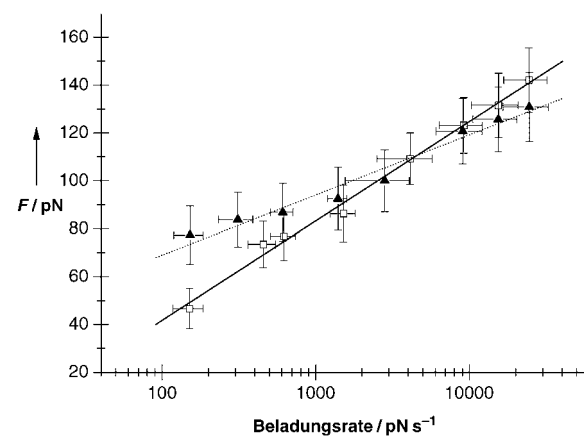


**Abbildung 4.** Halblogarithmische Auftragung der Dissoziationskraft gegen die Beladungsrate für die Bindung des Ammonium- und des Trimethylammoniumrestes an den Resorc[4]aren-Cavitanen. □: Ammoniumrest ( $k_{\text{off}} = 0.99 \text{ s}^{-1}$ ,  $x_\beta = 0.22 \text{ nm}$ ), ▲: Trimethylammoniumrest ( $k_{\text{off}} = 0.0187 \text{ s}^{-1}$ ,  $x_\beta = 0.38 \text{ nm}$ ).

Aus der inversen Steigung der Auftragung der Kraft gegen die Beladungsrate erhält man molekulare Reaktionslängen von  $x_\beta = (0.22 \pm 0.04)$  nm für den Ammoniumrest und  $x_\beta = (0.38 \pm 0.06)$  nm für den Trimethylammoniumrest. Diese Werte sind vergleichbar mit den berechneten Van-der-Waals-Durchmessern von 0.3 nm für den Ammonium- und 0.6 nm für den Trimethylammoniumrest.<sup>[9]</sup> Es lässt sich also schließen, dass der Passgenauigkeit (sterischen Komplementarität), mit der sich das Gastmolekül in den Rezeptorhohlraum einfügt, eine große Bedeutung bei der Wechselwirkung zukommt, wobei Kation- $\pi$ -Wechselwirkungen beträchtlich zum molekularen Bindungsmechanismus beitragen. Dieser Sachverhalt trifft auch für den Trimethylammoniumrest zu, da gezeigt werden konnte, dass an den Wasserstoffatomen der Methylgruppen eine positive Partialladung vorliegt.<sup>[31,32]</sup>

Wir haben gezeigt, dass die spezifische Wechselwirkung einzelner Gastmoleküle mit ihren Rezeptoren wie auch ihre Dissoziation mit dem Mechanismus des aktivierte Zerfalls eines metastabilen Zustandes in Einklang sind. Die Dissoziation ist thermisch aktiviert, wie es bereits theoretisch vorhergesagt und an biologischen Ligand-Rezeptor-Systemen experimentell verifiziert worden ist. Die gemessenen Reaktionslängen entsprechen den berechneten Van-der-Waals-Durchmessern der Gastliganden und ermöglichen eine Abschätzung, wie tief ein Ligand in den Rezeptorhohlraum des Calixaren-Cavitanen eindringt. Die gemessenen Reaktionsgeschwindigkeiten stimmen mit den für eine niederaffine Wirt-Gast-Wechselwirkung erwarteten Werten überein. Mit Hilfe der Einzelmolekül-Kraftspektroskopie konnten schließlich erstmals die untersuchten Liganden bezüglich ihrer Affinität zum Rezeptor klassifiziert und abgestuft werden.

Eingegangen am 21. Juli 2004

**Stichwörter:** Calixarene · Einzelmolekül-Untersuchungen · Kraftspektroskopie · Supramolekulare Chemie · Wirt-Gast-Systeme

- [1] a) J.-M. Lehn, *Supramolecular Chemistry*, VCH, Weinheim, 1995; b) F. Vögtle, *Supramolecular Chemistry*, Wiley, Chichester, 1991; c) J. L. Atwood, J. E. D. Davies, D. D. Macnicol, F. Vögtle, J.-M. Lehn, *Comprehensive Supramolecular Chemistry*, Pergamon, New York, 1996; d) J. W. Steed, J. L. Atwood, *Supramolecular Chemistry*, Wiley, Chichester, 2000; e) E. Fischer, *Ber. Dtsch. Chem. Ges.* **1894**, 27, 2985–2993; f) P. Ehrlich, *Klin. Jahrb.* **1897**, 6, 299–326; g) A. Werner, *Ber. Dtsch. Chem. Ges.* **1907**, 40, 15–69.
- [2] C. D. Gutsche, *Calixarenes*, Royal Society of Chemistry, Cambridge, 1989.
- [3] C. D. Gutsche, *Calixarenes Revisited*, Royal Society of Chemistry, Cambridge, 1998.
- [4] J. Vicens, V. Böhmer, *Calixarenes. A Versatile Class of Macroyclic Compounds*, Kluwer, Dordrecht, 1991.
- [5] L. Mandolini, R. Ungaro, *Calixarenes in Action*, Imperial College Press, London, 2000.
- [6] V. Böhmer, *Angew. Chem.* **1995**, 107, 785–818; *Angew. Chem. Int. Ed. Engl.* **1995**, 34, 713–745.
- [7] P. Timmerman, W. Verboom, D. N. Reinhoudt, *Tetrahedron* **1996**, 52, 2663–2704.
- [8] D. J. Cram, S. Karbach, H. E. Kim, C. B. Knobler, E. F. Mavrick, J. L. Ericson, R. C. Helgeson, *J. Am. Chem. Soc.* **1988**, 110, 2229–2237.
- [9] A. B. Rozhenko, W. W. Schoeller, M. C. Letzel, B. Decker, C. Agena, J. Mattay, unveröffentlichte Ergebnisse.
- [10] G. U. Lee, D. A. Kidwell, R. J. Colton, *Langmuir* **1994**, 10, 354–357.
- [11] E.-L. Florin, V. T. Moy, H. E. Gaub, *Science* **1994**, 264, 415–417.
- [12] P. Hinterdorfer, W. Baumgartner, H. Gruber, K. Schilcher, H. Schindler, *Proc. Natl. Acad. Sci. USA* **1996**, 93, 3477–3481.
- [13] F. Schwesinger, R. Ros, T. Strunz, D. Anselmetti, H.-J. Güntherodt, A. Honegger, L. Jermutus, L. Tiefenauer, A. Plückthun, *Proc. Natl. Acad. Sci. USA* **2000**, 97, 9972–9977.
- [14] U. Dammer, M. Hegner, D. Anselmetti, P. Wagner, M. Dreier, W. Huber, H.-J. Güntherodt, *Biophys. J.* **1996**, 70, 2437–2441.
- [15] R. Ros, F. Schwesinger, D. Anselmetti, M. Kubon, R. Schäfer, A. Plückthun, L. Tiefenauer, *Proc. Natl. Acad. Sci. USA* **1998**, 95, 7402–7405.
- [16] J. Fritz, A. G. Katopodis, F. Kolbinger, D. Anselmetti, *Proc. Natl. Acad. Sci. USA* **1998**, 95, 12283–12288.
- [17] F. W. Bartels, B. Baumgarth, D. Anselmetti, R. Ros, A. Becker, *J. Struct. Biol.* **2003**, 143, 145–152.
- [18] G. U. Lee, L. A. Chrisey, R. J. Colton, *Science* **1994**, 266, 771–773.
- [19] T. Strunz, K. Oroszlan, R. Schäfer, H.-J. Güntherodt, *Proc. Natl. Acad. Sci. USA* **1999**, 96, 11277–11282.
- [20] U. Dammer, O. Popescu, P. Wagner, D. Anselmetti, H.-J. Güntherodt, G. N. Misevic, *Science* **1995**, 267, 1173–1175.
- [21] H. Schönher, M. W. J. Beulen, J. Bügler, J. Huskens, F. C. J. M. van Veggel, D. N. Reinhoudt, G. J. Vancso, *J. Am. Chem. Soc.* **2000**, 122, 4963–4967.
- [22] S. Zapotoczny, T. Auletta, M. R. de Jong, H. Schönher, J. Huskens, F. C. J. M. van Veggel, D. N. Reinhoudt, G. J. Vancso, *Langmuir* **2002**, 18, 6988–6994.
- [23] T. Auletta, M. R. de Jong, A. Mulder, F. C. J. M. van Veggel, J. Huskens, D. N. Reinhoudt, S. Zou, S. Zapotoczny, H. Schönher, G. J. Vancso, L. Kuipers, *J. Am. Chem. Soc.* **2004**, 126, 1577–1584.
- [24] S. Kado, K. Kimura, *J. Am. Chem. Soc.* **2003**, 125, 4560–4564.
- [25] S. Kado, K. Yamada, K. Kimura, *Langmuir* **2004**, 20, 3259–3263.
- [26] G. I. Bell, *Science* **1978**, 200, 618–627.
- [27] E. Evans, K. Ritchie, *Biophys. J.* **1997**, 72, 1541–1555.
- [28] M. Schlosshauer, D. Baker, *Protein Sci.* **2004**, 13, 1660–1669.
- [29] L. A. Godínez, L. Schwartz, C. M. Criss, A. E. Kaifer, *J. Phys. Chem. B* **1997**, 101, 3376–3380.
- [30] T. Haino, D. M. Rudkevich, A. Shivanayuk, K. Rissanen, J. Rebek, Jr., *Chem. Eur. J.* **2000**, 6, 3797–3805.
- [31] C. A. Deakyne, M. Meot-Ner (Mautner), *J. Am. Chem. Soc.* **1985**, 107, 474–479.
- [32] H. J. Schneider, T. Schiestel, P. Zimmermann, *J. Am. Chem. Soc.* **1992**, 114, 7698–7703.

**Supramolecular Chemistry at the Single-Molecule Level\*\***

Rainer Eckel, Robert Ros, Björn Decker,  
Jochen Mattay,\* and Dario Anselmetti\*

In supramolecular chemistry<sup>[1]</sup> synthetically designed organic constituents interact noncovalently, in a directed and specific way to form host–guest complexes of higher complexity. The ability to tailor the molecular interplay with respect of chemical design, specificity, and molecular switching opens up the development of new molecular materials for artificial molecular recognition, molecular organization, and self-assembly. We have used mechanical single-molecule force spectroscopy to investigate the binding of individual resorc[4]arene-ligand host–guest complexes. By using diluted samples of the host and guest molecules that are modified with a long linker which is attached to an atomic force microscope (AFM) tip, we were able to prevent multiple binding and to observe single host–guest unbinding events in a supramolecular system for the first time. The molecular binding forces, their dependence on external loading rates, the rate of dissociation, and the molecular cavity length directly relate to the molecular properties of the supramolecular species and are consistent with an activated decay of a metastable bound state, a finding already established for biological receptor–ligand complexes. This result allows new insights into the mechanisms, kinetics, and thermodynamics of intermolecular association in chemistry and biology, and opens new possibilities in the investigation, design, and development of synthetic receptor systems.

Calixarenes are model receptor systems providing synthetic receptor cavities for the inclusion of small cationic guests, such as alkali-metal or ammonium ions.<sup>[2–5]</sup> Organic cations, such as ammonium ions, play a significant role in molecular recognition processes in nature (e.g. in protein side chains). Calix[n]arenes, generally, are a class of macrocyclic compounds formed by the base-catalyzed condensation of *n*-phenol derivatives and formaldehyde.<sup>[2,3]</sup> The resorc[4]arenes<sup>[6,7]</sup> considered herein are calixarenes formed from four

[\*] Dipl.-Chem. R. Eckel, Priv.-Doz. Dr. R. Ros, Prof. Dr. D. Anselmetti  
Experimental Biophysics and Applied Nanoscience  
Bielefeld University  
Universitätsstrasse 25, 33615 Bielefeld (Germany)  
Fax: (+49) 521-106-2959  
E-mail: dario.anselmetti@physik.uni-bielefeld.de  
Dipl.-Chem. B. Decker, Prof. Dr. J. Mattay  
Organic Chemistry  
Bielefeld University  
Universitätsstrasse 25, 33615 Bielefeld (Germany)  
Fax: (+49) 521-106-6417  
E-mail: mattay@uni-bielefeld.de

[\*\*] Financial support from the Deutsche Forschungsgemeinschaft (SFB 613) is gratefully acknowledged.

 Supporting information for this article is available on the WWW under <http://www.angewandte.org> or from the author.

resorcinol building blocks linked by methine groups. This structure leaves degrees of freedom for rotation around the methine C–C bonds, which results in five discernible conformations: crown ( $C_{4v}$ ), boat ( $C_{2v}$ ), chair ( $C_{2h}$ ), diamond ( $C_s$ ), and saddle ( $D_{2d}$ ). A means to constrain this conformational flexibility in resorc[4]arenes is to link the hydroxy groups at the upper rim of the molecule, to form ether bridges. In this way, the molecule is fixed in the crown conformation, a so-called cavitand,<sup>[8]</sup> and the rigid cavity of this host serves as a template for the inclusion of small guest ions. The binding of cations to the resorc[4]arene cavitand is facilitated by ion-dipole interactions, although hydrogen bonds and cation- $\pi$  interactions between the positive charge of the ion and the cavitand with the aromatic rings also have considerable influence.<sup>[9]</sup> The specificity of the binding is governed by the steric complementarity of the host and guest: only cations small enough to fit into the tailored cavity are recognized by the resorc[4]arene cavitand receptor. In our experiments the 2,8,14,20-tetra-(10-(decylthio)decyl) cavitand, which has a calculated cavity width of 0.7 nm, serves as a host and its specific recognition of ammonium ions and ammonium-ion derivatives is tested (Figure 1).<sup>[9]</sup>

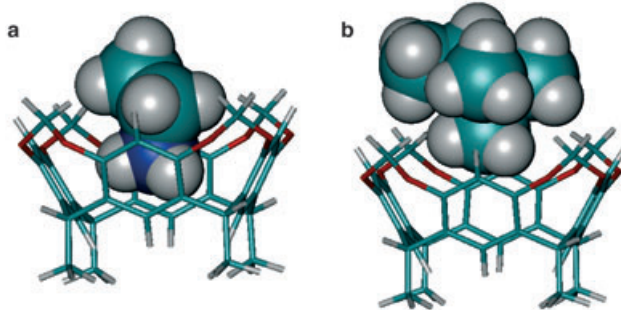


**Figure 1.** Gas-phase structure for the complex formed by the cavitand with a) an ethyl ammonium ion and b) an ethyl trimethyl ammonium ion. Structure optimized at the B3LPY/3-21G\* level.

To investigate these interactions we applied single-molecule force spectroscopy, a method which uses the deflection of an AFM cantilever to measure minute forces in the pico-Newton (pN) range under physiological conditions. In combination with its sub-nanometer spatial resolution, single-molecule force spectroscopy provides, in contrast to standard ensemble experiments, a potent tool to address and manipulate single molecules and investigate forces within and between individual molecules, to yield information about the molecular energy landscape. During the last fifteen years, AFM spectroscopy and related single-molecule techniques based on ultra-sensitive force probes have found applications in the study of molecular recognition and of the specific bond formation in a variety of systems, such as biotin–streptavidin/avidin,<sup>[10,11]</sup> antibody–antigen,<sup>[12–15]</sup> selectin–ligand,<sup>[16]</sup> DNA–protein,<sup>[17]</sup> between individual strands of DNA,<sup>[18,19]</sup> and cell-adhesion proteoglycans.<sup>[20]</sup>

Similarly, host–guest interactions in supramolecular systems have been investigated on  $\beta$ -cyclodextrin–ferrocene<sup>[21–23]</sup> and [18]crown-6–ammonium systems.<sup>[24,25]</sup> In both cases

single-molecule host–guest interaction could only be identified by a statistical analysis of the measured force distribution histograms, however, with no evidence of a loading-rate-dependent force spectrum, which could account for a thermally driven unbinding and give access to the energy landscape of this interaction. In contrast to these experiments, we used diluted cavitand monolayers on a gold surface in a 1:40 mixture with didecylsulfide. The guest ions (ammonium, trimethyl ammonium, and triethyl ammonium, each carrying one additional functional group) were covalently attached to the AFM tip with a flexible poly(ethylene glycol) (PEG) linker (Figure 2). This method introduces more steric flexi-

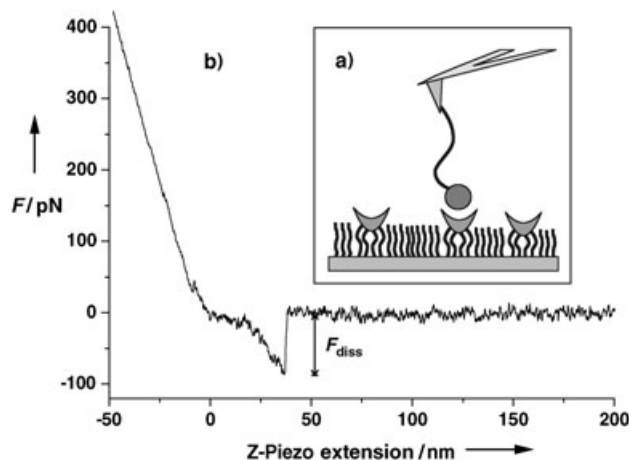


**Figure 2.** Force spectroscopy: a) schematic setup. The cavitand is immobilized together with didecylsulfide in a 1:40 mixture on a gold substrate. The (tetraorganyl) ammonium residue (shaded circle), is attached to an  $\text{Si}_3\text{N}_4$  AFM tip by a flexible polymer linker. b) Typical force–distance curve (only retractive trace shown). The stretching of the PEG linker over a certain distance prior to bond rupture (tip detachment and relaxation of the cantilever) indicates an unbinding event.

bility which facilitates complex formation and supports binding of a single host–guest pair and its proper identification. The functionalized AFM tip was repetitively approached to and retracted from the cavitand surface (in ethanol) at an adjustable but constant velocity.

Molecular unbinding events could be identified by plotting the force response of the AFM cantilever against the z-position of the piezo actuator (of the cavitand surface; Figure 2). The elastic stretching of the PEG spacer before the point of detachment, which shows an elasticity curve in accordance with the wormlike-chain polymer-elasticity model, served as the criterion to discriminate real single-binding events from unspecific adhesion. Since the molecular unbinding process is of stochastic nature, rupture forces from many rupture events (typically 200) were compiled in a force histogram. The mean value resulting from a single-nodal Gaussian fit to the histogram distribution is the most probable unbinding force. The experimental error is based on the statistical error (standard variation) and the uncertainty in the effective spring constant of the cantilever; the errors given

below for the thermal dissociation (off rate) at zero force and the width of the binding pocket are derived from these values by error propagation.

Figure 3 shows three force histograms for the binding of the cavitand to ammonium, trimethyl ammonium, and

triethyl ammonium residues. The histograms show the unbinding probability  $P$  versus force  $F$  in pN. The histograms for ammonium (a,c,e) show a broad distribution with a peak around 100 pN. The histograms for trimethyl ammonium (d,f) show a narrower distribution with a peak around 100 pN. The histograms for triethyl ammonium (g,i) show a very narrow distribution with a peak around 100 pN. The histograms for ammonium in ethanol (a,d,g) show a higher unbinding probability than the histograms for ammonium in ethanol saturated with free ions (b,e,h). The histograms for triethyl ammonium in ethanol (g) show a lower unbinding probability than the histograms for triethyl ammonium in ethanol saturated with free ions (i).

According to the thermally driven unbinding theory of an activated decay of a metastable bound state<sup>[26,27]</sup> the measured forces are not constant and depend on the temporal force evolution on the molecular complex, which is referred to as the loading rate, and can be calculated from the experimental velocity multiplied by the molecular elasticity. The elasticity of the molecular system was obtained from the slope of the force–distance curves (corrected for molecular extension) for the last 20 data points prior to detachment of the cantilever. The loading rate then was given by the system elasticity multiplied by the retract velocity.

With dynamic force spectroscopy (force-loading-rate plots) details about the kinetics of the binding and information concerning the length scale of the interaction can be extracted. The results for the natural thermal off-rates are presented in Figure 4, yielding  $k_{\text{off}} = (0.99 \pm 0.81) \text{ s}^{-1}$  for the ammonium and  $k_{\text{off}} = (1.87 \pm 0.75) \times 10^{-2} \text{ s}^{-1}$  for the trimethyl ammonium residue, resulting in a bond lifetime of  $\tau = 1.01 \text{ s}$  (for the ammonium residue) and  $\tau = 53.5 \text{ s}$  (trimethyl ammonium residue). This finding,

together with the results of the competition experiments, indicate that the trimethyl ammonium residue fits more

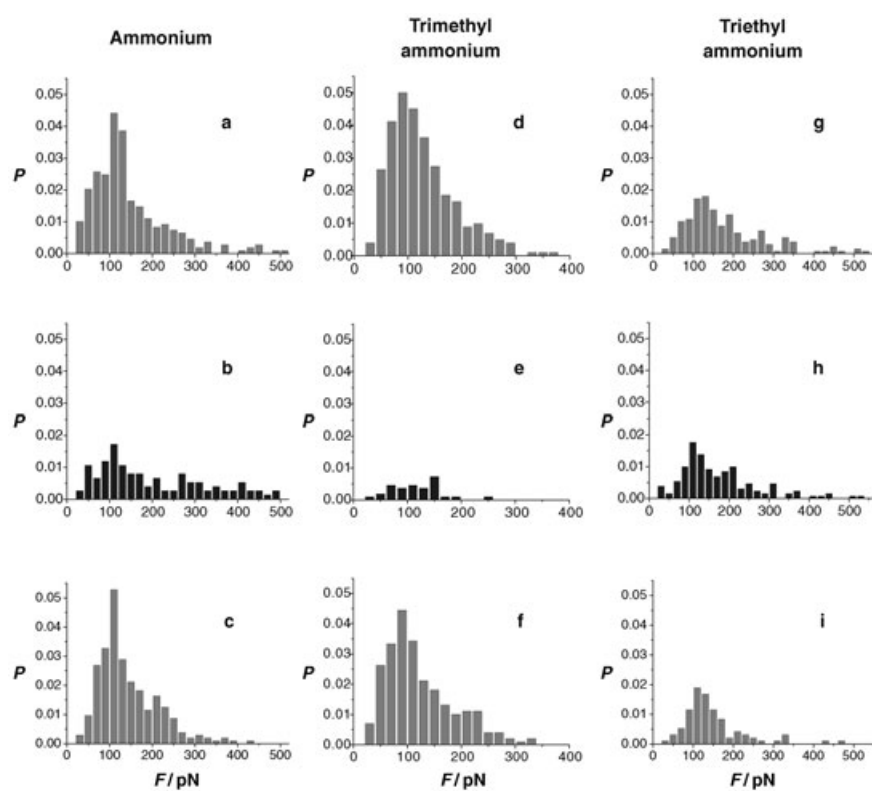


**Figure 3.** Force spectroscopy experiments in ethanol (a,d,g), in ethanol saturated with the respective free ions (b,e,h), washing with ethanol restored the original unbinding probability  $P$  (c,f,i).

triethyl ammonium residues and the corresponding competition experiments. The total unbinding probability (that is, the total number of identified rupture events divided by the number of approach–retract cycles) for the ammonium and trimethyl ammonium residues both amount to approximately 25 %. As a control experiment for validating the specificity of the host–guest interaction, free ammonium or tetramethyl ammonium ions were added to the solvent as competing ligands. In both cases the total (integrated) unbinding probability was significantly reduced. The effect was stronger for solvent saturated with the tetramethyl ammonium ion (Figure 3 b,e). After washing tip and sample again with the original solvent (ethanol without competitor), the systems could be reactivated to their full former unbinding functionality (Figure 3 c,f). This effect of the free ions competing with the modified ions linked to the AFM tip demonstrates the specificity of the molecular recognition between the host and guest.

For the triethyl ammonium residue, the results are different. From Figure 3, it can be seen that the integrated unbinding probability is much lower for this system than for the ammonium or tetramethyl ammonium ions, whereas the

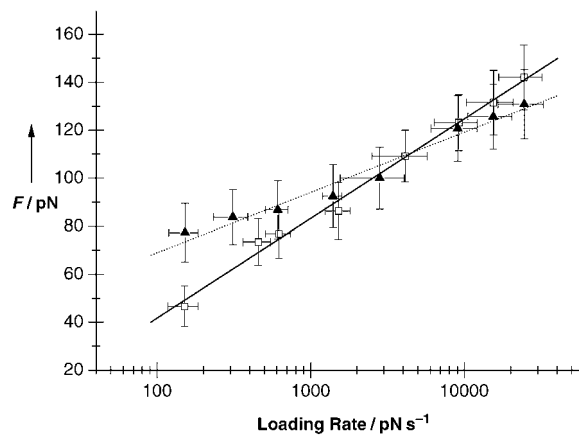


**Figure 4.** The unbinding forces, plotted logarithmically against the corresponding loading rates, for the binding of the ammonium ( $\square$ ) and trimethyl ammonium ( $\blacktriangle$ ) residues to the resorc[4]arene cavitand. For details see text.

tightly into the receptor cavity, that is, its complexation is accompanied by a greater rise in binding affinity than for ammonium. In receptor–ligand interactions, the interaction affinity (equilibrium constant of dissociation  $K_{\text{diss}} = k_{\text{off}}/k_{\text{on}}$ ) is mostly dominated (and varied) by the reaction off-rate  $k_{\text{off}}$ , whereas the values for the reaction on-rate  $k_{\text{on}}$  do not exhibit such a drastic variation.<sup>[13]</sup> Assuming a diffusion-limited association with a typical on-rate for a ligand binding to a receptor pocket of  $k_{\text{on}} = 10^5 \text{ M}^{-1} \text{s}^{-1}$ ,<sup>[13,28]</sup> we can deduce equilibrium constants of  $K_{\text{diss}} = 0.99 \text{ s}^{-1}/10^5 \text{ M}^{-1} \text{s}^{-1} \approx 10^{-5} \text{ M}$  for ammonium ions and  $K_{\text{diss}} = 2 \times 10^{-2} \text{ s}^{-1}/10^5 \text{ M}^{-1} \text{s}^{-1} = 2 \times 10^{-7} \text{ M}$  for trimethyl ammonium ions. From the equilibrium constants for these host–guest systems the Gibbs' free energy difference  $\Delta G = RT \ln K_{\text{diss}}$  can be derived, which gives a rough estimate of the related binding energies of  $\Delta G \approx -28 \text{ kJ mol}^{-1}$  (ammonium) and  $\Delta G \approx -38 \text{ kJ mol}^{-1}$  (trimethyl ammonium). These values for  $\Delta G$  correspond well with calorimetric or NMR spectroscopic data obtained for related supramolecular systems, such as cyclodextrins<sup>[23,29]</sup> and water-soluble cavitands.<sup>[30]</sup> This aspect is important for two reasons: 1) it shows that AFM force spectroscopy can be used to investigate single-molecule affinity interactions in a broad affinity range of ten orders of magnitude ( $10^{-15} \text{ M}$  (biotin-streptavidin) to  $10^{-5} \text{ M}$  (this work)), and 2) that this technique allows the estimation of equilibration constants and related binding energies of single (supra)molecular complexes. This factor is of broad interest, since a determination of reaction equilibrium constants and associated binding energies of ionic binding partners with a wide variation in solubility, for example, by NMR spectroscopic titration experiments, is extremely difficult to accomplish, and no corresponding values for our system are known to us.

From the inverse slope of the loading-rate dependency the molecular reaction lengths (width of binding pocket) can be extracted yielding  $x_\beta = (0.22 \pm 0.04) \text{ nm}$  for ammonium, and  $x_\beta = (0.38 \pm 0.06) \text{ nm}$  for the trimethyl ammonium ions. These values are qualitatively comparable with calculated van der Waals diameters of 0.3 nm for ammonium and 0.6 nm for trimethyl ammonium.<sup>[9]</sup> Therefore we can conclude that the steric complementarity of the host and guest plays an important role in the interaction, with cation–π interactions contributing considerably to the molecular binding mechanism. This finding is also consistent for the interaction of the trimethyl ammonium residue with the cavitand because a the positive-charge distribution has been shown to reside on the hydrogen atoms of the methyl groups.<sup>[31,31]</sup>

In summary, we could show that the specific interaction and dissociation of single guest molecules and their host receptors in supramolecular systems are consistent with an activated decay of a metastable bound state and obey the laws of thermally driven unbinding, as predicted theoretically and verified in biological ligand–receptor systems. The measured reaction lengths were compatible with the calculated van der Waals diameters of the corresponding guest ligands, and give a rough estimate of how deep a ligand enters the receptor site of a calixarene cavitand. The measured single-molecule kinetic reaction rates are consistent with the expected nature of a moderate-affinity host–guest interaction, whereas a clear affinity ranking between the probed host ligands by

single-molecule force spectroscopy was possible for the first time.

Received: July 21, 2004

**Keywords:** atomic force microscopy · calixarenes · host–guest systems · single molecules · supramolecular chemistry

- [1] a) J.-M. Lehn, *Supramolecular Chemistry*, VCH, Weinheim, 1995; b) F. Vögtle, *Supramolecular Chemistry*, Wiley, Chichester, 1991; c) J. L. Atwood, J. E. D. Davies, D. D. Macnicol, F. Vögtle, J.-M. Lehn, *Comprehensive Supramolecular Chemistry*, Pergamon, New York, 1996; d) J. W. Steed, J. L. Atwood, *Supramolecular Chemistry*, Wiley, Chichester, 2000; e) E. Fischer, *Ber. Dtsch. Chem. Ges.* **1894**, 27, 2985–2993; f) P. Ehrlich, *Klin. Jahrb.* **1897**, 6, 299–326; g) A. Werner, *Ber. Dtsch. Chem. Ges.* **1907**, 40, 15–69.
- [2] C. D. Gutsche, *Calixarenes*, Royal Society of Chemistry, Cambridge, 1989.
- [3] C. D. Gutsche, *Calixarenes Revisited*, Royal Society of Chemistry, Cambridge, 1998.
- [4] J. Vicens, V. Böhmer, *Calixarenes. A Versatile Class of Macroyclic Compounds*, Kluwer, Dordrecht, 1991.
- [5] L. Mandolini, R. Ungaro, *Calixarenes in Action*, Imperial College Press, London, 2000.
- [6] V. Böhmer, *Angew. Chem.* **1995**, 107, 785–818; *Angew. Chem. Int. Ed. Engl.* **1995**, 34, 713–745.
- [7] P. Timmerman, W. Verboom, D. N. Reinhoudt, *Tetrahedron* **1996**, 52, 2663–2704.
- [8] D. J. Cram, S. Karbach, H. E. Kim, C. B. Knobler, E. F. Maverick, J. L. Ericson, R. C. Helgeson, *J. Am. Chem. Soc.* **1988**, 110, 2229–2237.
- [9] A. B. Rozhenko, W. W. Schoeller, M. C. Letzel, B. Decker, C. Agena, J. Mattay, unpublished results.
- [10] G. U. Lee, D. A. Kidwell, R. J. Colton, *Langmuir* **1994**, 10, 354–357.
- [11] E.-L. Florin, V. T. Moy, H. E. Gaub, *Science* **1994**, 264, 415–417.
- [12] P. Hinterdorfer, W. Baumgartner, H. Gruber, K. Schilcher, H. Schindler, *Proc. Natl. Acad. Sci. USA* **1996**, 93, 3477–3481.
- [13] F. Schwesinger, R. Ros, T. Strunz, D. Anselmetti, H.-J. Güntherodt, A. Honegger, L. Jermutus, L. Tiefenauer, A. Plückthun, *Proc. Natl. Acad. Sci. USA* **2000**, 97, 9972–9977.
- [14] U. Dammer, M. Hegner, D. Anselmetti, P. Wagner, M. Dreier, W. Huber, H.-J. Güntherodt, *Biophys. J.* **1996**, 70, 2437–2441.
- [15] R. Ros, F. Schwesinger, D. Anselmetti, M. Kubon, R. Schäfer, A. Plückthun, L. Tiefenauer, *Proc. Natl. Acad. Sci. USA* **1998**, 95, 7402–7405.
- [16] J. Fritz, A. G. Katopodis, F. Kolbinger, D. Anselmetti, *Proc. Natl. Acad. Sci. USA* **1998**, 95, 12283–12288.
- [17] F. W. Bartels, B. Baumgarth, D. Anselmetti, R. Ros, A. Becker, *J. Struct. Biol.* **2003**, 143, 145–152.
- [18] G. U. Lee, L. A. Chrisey, R. J. Colton, *Science* **1994**, 266, 771–773.
- [19] T. Strunz, K. Oroszlan, R. Schäfer, H.-J. Güntherodt, *Proc. Natl. Acad. Sci. USA* **1999**, 96, 11277–11282.
- [20] U. Dammer, O. Popescu, P. Wagner, D. Anselmetti, H.-J. Güntherodt, G. N. Misevic, *Science* **1995**, 267, 1173–1175.
- [21] H. Schönherr, M. W. J. Beulen, J. Bügler, J. Huskens, F. C. J. M. van Veggel, D. N. Reinhoudt, G. J. Vancso, *J. Am. Chem. Soc.* **2000**, 122, 4963–4967.
- [22] S. Zapotoczny, T. Auletta, M. R. de Jong, H. Schönherr, J. Huskens, F. C. J. M. van Veggel, D. N. Reinhoudt, G. J. Vancso, *Langmuir* **2002**, 18, 6988–6994.
- [23] T. Auletta, M. R. de Jong, A. Mulder, F. C. J. M. van Veggel, J. Huskens, D. N. Reinhoudt, S. Zou, S. Zapotoczny, H. Schönherr,

- G. J. Vancso, L. Kuipers, *J. Am. Chem. Soc.* **2004**, *126*, 1577–1584.
- [24] S. Kado, K. Kimura, *J. Am. Chem. Soc.* **2003**, *125*, 4560–4564.
- [25] S. Kado, K. Yamada, K. Kimura, *Langmuir* **2004**, *20*, 3259–3263.
- [26] G. I. Bell, *Science* **1978**, *200*, 618–627.
- [27] E. Evans, K. Ritchie, *Biophys. J.* **1997**, *72*, 1541–1555.
- [28] M. Schlosshauer, D. Baker, *Protein Sci.* **2004**, *13*, 1660–1669.
- [29] L. A. Godínez, L. Schwartz, C. M. Criss, A. E. Kaifer, *J. Phys. Chem. B* **1997**, *101*, 3376–3380.
- [30] T. Haino, D. M. Rudkevich, A. Shivanuk, K. Rissanen, J. Rebek, Jr., *Chem. Eur. J.* **2000**, *6*, 3797–3805.
- [31] C. A. Deakyne, M. Meot-Ner (Mautner), *J. Am. Chem. Soc.* **1985**, *107*, 474–479.
- [32] H. J. Schneider, T. Schiestel, P. Zimmermann, *J. Am. Chem. Soc.* **1992**, *114*, 7698–7703.